UNIVERSIDADE FEDERAL DE ITAJUBÁ

PROGRAMA DE PÓS-GRADUAÇÃO EM ENGENHARIA ELÉTRICA

Rondineli Rodrigues Pereira

ALGORITMOS ADAPTATIVOS PARA FILTROS ATIVOS DE POTÊNCIA

Tese submetida ao Programa de Pós-Graduação em Engenharia Elétrica como parte dos requisitos para obtenção do Título de Doutor em Ciências em Engenharia Elétrica.

Área de Concentração:
Automação e Sistemas Elétricos Industriais.

Orientador:
Luiz Eduardo Borges da Silva

Co-orientador:
Carlos Henrique da Silva

Maio de 2011

Itajubá - MG

Agradecimentos

Agradeço a Deus por ter me permitido realizar meus sonhos, que a anos atrás pareciam tão impossíveis. E que a cada dia me abençoa com suas graças em minha vida.

A minha esposa Danielle e ao meu filho Arthur pelo carinho, amor e compreensão nas horas de ausência em que tive que me dedicar a este trabalho. E que são a fonte de inspiração para minha vida.

A minha mãe Ivony que sempre orou, torceu, realizou grandes esforços para que eu pudesse continuar na minha caminhada em busca dos meus sonhos. A meu grande irmão Ramon, que às vezes me tira do sério, mas a quem tenho um grande amor e dedicação.

Agradeço meus avós, Carmelita e Valdete (in memorian), Iracema (in memorian) e Sebastião, aos meus tios, tias, primas e primos que sempre me incentivam na luta diária por meus objetivos.

Ao povo brasileiro e a CAPES pelo apoio financeiro, neste dois anos de pesquisa.

Um agradecimento especial ao professor Luiz Eduardo pela atenção, apoio, amizade, confiança e estímulo. Ao professor Carlos Henrique pela grande ajuda e observações construtivas sobre o trabalho.

Resumo

Este trabalho apresenta uma nova estratégia para melhorar a aplicação de Filtros Adaptativos para detecção de harmônicos em um Filtro Ativo de Potência *Shunt.*

O objetivo final da estratégia é melhorar a velocidade de convergência do Filtro Adaptativo e reduzir o erro em regime permanente. Dois casos são apresentados e discutidos, utilizando um Filtro Adaptativo Sintonizado. Em um caso é utilizando o algoritmo de adaptação *Least Mean Square* (*LMS*) para o ajuste dos coeficientes e no outro caso o algoritmo *Recursive Least Square* (*RLS*).

A estratégia proposta não faz uso de um *Phased Looked Loop* (*PLL*) para gerar os sinais ortogonais de entrada do Filtro Adaptativo Sintonizado. Estes sinais são gerados através da transformada de *Clarke* dos sinais da corrente da carga e posterior filtragem. Com isto, é obtida uma velocidade de convergência inferior a um ciclo da componente fundamental.

Simulações utilizando o *Matlab/Simulink* são apresentadas para esclarecer o algoritmo. Implementações práticas também são realizadas usando o Processador Digital de Sinais da *Texas Instruments* TMS320F2812, sendo os resultados apresentados.

Abstract

This work presents a new strategy to improve the applicability of Adaptive Filters for harmonic detection in Shunt Active Power Filters (SAPF).

The final objective of the strategy is improving the speed of convergence of the Adaptive Filter and reduces the steady-state error. Two main cases are presented and discussed, using an Adaptive Notch Filter. In one case the Least Mean Square (LMS) algorithm was used to adjust the coefficients and in the other case the Recursive Least Square (RLS) algorithm.

The new strategy proposed doesn't use a *Phased Looked Loop* (*PLL*) to generate the orthogonal input signals for the adaptive notch filter. These two signals are generated with Clarke transformation of the load current and then the two orthogonal signals are filtered. With this, the total transient response drops below one cycle of the fundamental frequency (60Hz).

Simulations using Matlab/Simulink are presented to clarify the algorithm. Also practical implementation is performed using the DSP Texas Instruments TMS320F2812 and the results depicted.

Índice

Lista de Figuras

Lista de Tabelas

Lista de Abreviaturas

Abreviaturas	Significado
FAP	Filtro Ativo de Potência
FAPP	Filtro Ativo de Potência Paralelo
DSP	Digital Signal Processor
MSE	Mean-Square Error
LMS	Least Mean Square
RLS	Recursive Least Square
THDi	Current Total Harmonic Distortion
CA	Corrente Alternada
CC	Corrente Contínua
VSI	Voltage Source Inverter
CSI	Current Source Inverter
V_S	Tensão da Fonte
I_L	Corrente da Carga
I_C	Corrente de Compensação
I_S	Corrente da Fonte
Ta	Tempo de Adaptação

1 Introdução

A proliferação de conversores de potência estáticos, tais como retificadores monofásicos e trifásicos, conversores tiristorizados e outras aplicações da eletrônica de potência vêm causando alguns efeitos colaterais nos sistemas elétricos. Tais efeitos se devem a não linearidade característica destas cargas que provocam sérios distúrbios nas fontes CA.

Estes distúrbios têm como causa principal os harmônicos de corrente que provocam o aquecimento adicional dos elementos do sistema, como transformadores e condutores, reduzem a estabilidade do sistema e diminuem as margens seguras de operação. Contribuindo para uma crescente piora na qualidade da energia elétrica fornecida.

Em geral, o conteúdo harmônico das correntes nas fontes está constantemente mudando em virtude das necessidades da corrente nas cargas. Neste contexto os Filtros Ativos de Potência (FAP) [1-5] aparecem como uma solução adequada ao problema exposto.

Neste trabalho, será utilizada a topologia do Filtro Ativo de Potência Paralelo (FAPP). O FAPP tem como função principal o fornecimento de todo o conteúdo harmônico presente na corrente da carga. Deste modo, a função da concessionária de energia elétrica se restringe a fornecer a corrente fundamental.

Atualmente, os algoritmos denominados na literatura de Referência Síncrona [6] e Teoria da Potência Instantânea p-q [7] são as duas técnicas mais utilizadas para extrair o conteúdo harmônico da corrente da carga no Filtro Ativo de Potência Paralelo.

O método de detecção de harmônicos com Filtragem Adaptativa vem, nos últimos anos, sendo aplicado na tarefa de extrair o conteúdo harmônico da corrente da carga utilizado no algoritmo de controle dos FAPP. Entretanto, é necessária a aplicação de técnicas para melhorar a velocidade de convergência do algoritmo de adaptação do Filtro Adaptativo com vistas à melhoria do comportamento dinâmico do FAPP.

Neste trabalho foi desenvolvida uma nova estratégia para melhorar a aplicação de Filtros Adaptativos na detecção de harmônicos em um Filtro Ativo de Potência Paralelo. O objetivo principal da técnica desenvolvida é melhorar o tempo de convergência do Filtro Adaptativo e reduzir o erro em regime permanente.

Os conceitos teóricos e a metodologia aplicada no trabalho foram apresentados e comprovados pelas simulações e resultados experimentais. As simulações foram realizadas no programa *Matlab/Simulink* com o Filtro Adaptativo Sintonizado (do inglês, *Adaptive Notch Filter*). Os resultados experimentais foram implementados no Processador Digital de Sinais TMS320F2812 para o controle de FAPP utilizando a linguagem de programação C.

O Filtro Ativo de Potência Paralelo é composto por 3 inversores fonte de tensão de 35kVA, trabalhando em uma freqüência de chaveamento de 40kHz. A tensão do *link DC* foi ajustada em 400V. Foi usado um indutor de 5mH para conectar o FAPP no sistema de potência, sendo a tensão do sistema de 220V.

A carga não-linear utilizada foi um retificador de 6 pulsos, tipo *CSI* (do inglês, *Current Source Inverter*), de 100kVA.

No teste em regime permanente foi utilizada uma corrente com amplitude de 19,2A *RMS*. No o teste com transitório na amplitude da corrente da carga foi aplicado um transitório de 6,5A para 12,8A, ou seja, uma variação de aproximadamente 100%. Também foi realizado outro teste, em que tanto a amplitude como o conteúdo harmônico da corrente da carga foram alterados simultaneamente. Em todos estes casos o tempo de convergência da estratégia proposta foi inferior a um ciclo da componente fundamental, resultado este superior ao encontrado na literatura de filtros adaptativos aplicados a detecção de harmônicos.

Este texto está organizado conforme os capítulos descritos a seguir:

No Capítulo 2, **Aplicação de Filtros Adaptativos em Filtros Ativos de Potência,** é realizada uma breve revisão da literatura sobre este tema.

O Capítulo 3, **Filtros Adaptativos,** aborda a teoria geral da Filtragem Adaptativa, o funcionamento dos algoritmos de adaptação *Least Mean Square* e *Recursive Least Square*. Ilustrando a aplicação de filtros adaptativos na detecção de harmônicos.

O Capítulo 4, **Resultados de Simulação,** apresenta os resultados das simulações realizadas no *Matlab/Simulink* para o Filtro Adaptativo Sintonizado. Comprovando a eficiência da estratégia desenvolvida.

No Capítulo 5, **Resultados Experimentais,** são mostrados os resultados da implementação, no DSP TMS320F2812, da detecção de harmônicos, com Filtro Adaptativo Sintonizado, no controle de um FAPP.

E no Capítulo 6, ***Conclusão***, as conclusões pertinentes e as possibilidades de trabalhos futuros são apresentadas.

2 Aplicação de Filtros Adaptativos em Filtros Ativos de Potência

A compensação de correntes harmônicas, geradas por equipamentos de eletrônica de potência, tem se tornado cada vez mais importante devido ao uso crescente desses equipamentos em aplicações industriais. Neste contexto, cada vez mais, novas técnicas são desenvolvidas com o intuito de melhorar a eficiência dos Filtros Ativos de Potência na mitigação de harmônicos. O desempenho de um Filtro Ativo de Potência depende, basicamente, do algoritmo de extração de harmônicos para geração da corrente de referência, o método de controle para geração da corrente harmônica de compensação e da característica dinâmica do Filtro Ativo como um todo [12].

No sistema elétrico de potência a corrente pode ser descrita como

$$i(t) = \sum_{n=1}^{N} A_n \sin(n\omega t + \theta_n) \tag{2.1}$$

A corrente fundamental é definida como $i_1(t)$ e a corrente harmônica por

$$i_h(t) = \sum_{n=2}^{N} A_n \sin(n\omega t + \theta_n) \tag{2.2}$$

A corrente harmônica pode ser obtida com a eliminação da componente fundamental em $i(t)$. Com isto, o problema em questão passa a ser como extrair a componente fundamental separando as componentes harmônicas. Neste contexto, a utilização de Filtros Adaptativos, nos últimos anos, vem demonstrando ser uma técnica eficaz na realização desta tarefa.

Lou e *Hou* (1995) desenvolveram um método para detecção de correntes harmônicas e reativas baseado no conceito do cancelamento de ruído adaptativo [13]. O método visava à implementação através de circuitos digitais, demonstrando a viabilidade da técnica através de resultados experimentais. Mas o método desenvolvido apresentou uma convergência lenta em situações de variação no valor da corrente da carga.

O trabalho de *Karimi* et al. (2003) resultou em uma melhora na velocidade de convergência e no erro em regime permanente [14]. Os resultados foram alcançados com a modificação da estrutura desenvolvida por *Lou* e *Hou* (1995), buscando reduzir as oscilações causadas pelo aumento do valor do parâmetro μ.

Os trabalhos de *Mu Longhua* e *Jiangzi* (2005), Li et al. (2006) e Qu et al. (2007) utilizaram o método *variable step-size* [15] para obter um tempo de convergência menor. Resultados de simulação e experimentais comprovaram a viabilidade destas estratégias [16-18]. Apresentando um tempo de convergência equivalente a dois ciclos da freqüência fundamental.

Pereira et al. (2009) obtiveram uma melhora no tempo de convergência para o algoritmo *LMS* utilizando o método *variable step-size* e uma técnica para a detecção de transitórios na amplitude da corrente da carga [19-21]. Esta técnica foi baseada no oscilador de *Coulon* [28]. Apresentando, desta maneira, um tempo de convergência equivalente a um ciclo e meio da freqüência fundamental.

Recentemente, novos trabalhos vêm sendo publicados utilizando filtros adaptativos sintonizados apresentando um tempo de convergência da ordem de um ciclo da freqüência fundamental [22-25].

Outra aplicação com Filtros Adaptativos é a predição de amostras futuras para compensar algum tipo de atraso no processo de geração da corrente de compensação nos Filtros Ativos de Potência. Esta aplicação foi demonstrada inicialmente no trabalho de *Fukuda* e *Sugawa* (1996) em um sistema contendo um filtro passivo paralelo e um filtro ativo paralelo [25], em que a predição de amostras foi realizada para o sinal com o conteúdo harmônico da carga. *Väliviita* e *Ovaska* (1996) e *Han* et al. (2005) implementaram esta estratégia em um filtro ativo paralelo para compensar o atraso de fase, devido ao filtro passa-baixas utilizado para extração da componente fundamental [11][27].

No próximo capítulo deste trabalho, a teoria sobre Filtros Adaptativos e a sua aplicação em Filtros Ativos de Potência será abordada em detalhe.

3 Filtros Adaptativos

3.1 O Filtro Adaptativo

Um Filtro Adaptativo é um dispositivo computacional que procura modelar a relação entre dois sinais em tempo real de maneira iterativa [8]. Um Filtro Adaptativo pode ser implementado como um conjunto de instruções executadas por um Microprocessador de Propósito Geral ou um Processador Digital de Sinais (*DSP*), como um conjunto de operações lógicas numa *Field-Programmable Gate Array* (*FPGA*) ou ainda em um circuito integrado *VLSI* personalizado.

Um Filtro Adaptativo pode ser definido por quatro aspectos:

1. Os sinais processados pelo filtro;
2. A estrutura que define como o sinal de saída do filtro é calculado a partir do sinal de entrada;
3. Os parâmetros da estrutura que podem ser alterados iterativamente mudando a relação entre a entrada e a saída do filtro;
4. O algoritmo de adaptação que descreve como os parâmetros serão ajustados de um instante para o próximo.

Ao escolher uma estrutura de Filtro Adaptativo em particular, deve ser especificado o número e tipo de parâmetros que podem ser ajustados. O algoritmo de adaptação usado para atualizar os valores dos parâmetros do sistema pode ser obtido entre uma grande quantidade de algoritmos existentes e comumente é formulado através de um procedimento de otimização para minimizar um erro.

Como notação matemática utilizada, neste texto, quantidades escalares serão representadas por letras minúsculas e quantidades vetoriais por letras maiúsculas em negrito. Então, seqüências ou sinais escalares e vetoriais serão representados como $x(n)$ e $\boldsymbol{X}(n)$, respectivamente.

3.2 A Filtragem Adaptativa

A Figura 3.1 mostra um diagrama em bloco no qual uma amostra do sinal digital de entrada $x(n)$ é processada por um Filtro Adaptativo, que calcula a amostra do sinal de saída $y(n)$. O sinal de saída é comparado com um segundo sinal $d(n)$, chamado de resposta desejada, pela subtração das duas amostras no instante *n*. Este sinal gerado pela subtração é conhecido como sinal de erro $e(n)$, como pode ser observado na Equação 3.1.

$$e(n) = d(n) - y(n) \qquad (3.1)$$

O sinal de erro é usado no procedimento de adaptação dos coeficientes do filtro do instante *n* para o instante *n+1* de uma forma bem definida. Este processo de adaptação é representado pela seta que atravessa o bloco do Filtro Adaptativo na Figura 3.1. Com o passar do processo de adaptação é esperado que a saída do Filtro Adaptativo torne-se mais próxima possível da resposta desejada e a magnitude de $e(n)$ decaia.
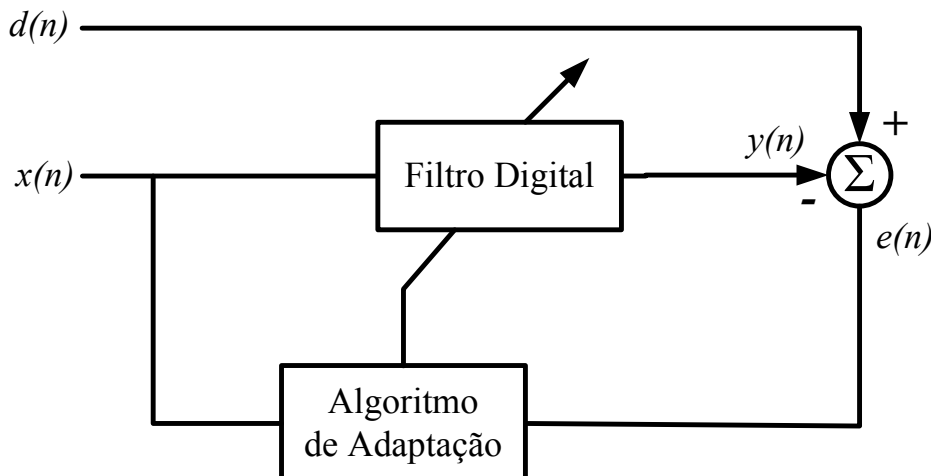
Figura 3.1: Estrutura geral de um Filtro Adaptativo.

Em filtragem adaptativa o termo adaptação refere-se ao método em que os parâmetros do sistema são alterados do instante *n* para o instante *n+1*. O número e tipo de parâmetros dentro do sistema dependem da estrutura computacional escolhida para o sistema.

Uma pergunta comum numa primeira análise da ação do Filtro Adaptativo diz respeito a qual seria sua utilidade em obter um sinal igual à resposta desejada $d(n)$ sendo o sinal $d(n)$ já conhecido. Na realidade o conceito de obter $y(n)$ a partir de $d(n)$ em alguns sistemas não permite a visualização das sutilezas da filtragem adaptativa. Para tanto é citado abaixo duas situações que podem responder a questão levantada.

- Na prática, a quantidade de interesse nem sempre é $d(n)$. A necessidade pode ser representar em $y(n)$ um componente específico de $d(n)$ contido em $x(n)$, ou isolar um componente de $d(n)$ que não está contido em $x(n)$ através do erro $e(n)$. Alternativamente, o interesse pode ser unicamente nos valores dos parâmetros do sistema não havendo preocupação com $x(n)$, $y(n)$ ou $d(n)$.

- Existem algumas situações nas quais $d(n)$ não está disponível em nenhum momento. Então, nestes casos deve-se utilizar a estimativa mais recente para calcular $y(n)$ na tentativa de estimar a resposta desejada $d(n)$.

3.3 Estruturas para o Filtro

Em geral, qualquer sistema com um número de parâmetros finito que afete o valor $y(n)$ calculado a partir de $x(n)$ pode ser utilizado como Filtro Adaptativo.

Definindo, então, o vetor de coeficientes ou *kernel* $\boldsymbol{W}(n)$ na Equação 3.2. Em que $\{w_i(n)\}$, com $0 \leq i \leq L\text{-}1$, são os coeficientes do sistema no instante *n*.

$$\boldsymbol{W}(n) = [w_0(n)\, w_1(n)\, w_2(n) \dots w_{L-1}(n)]^T \tag{3.2}$$

Com esta definição pode-se obter um relacionamento geral de entrada e saída para o Filtro Adaptativo como na Equação 3.3.

$$y(n) = f\big(\boldsymbol{W}(n), y(n-1), \dots, y(n-N), x(n), x(n-1), \dots, x(n-M+1)\big) \tag{3.3}$$

Onde:
$f(.)$: representa qualquer função linear ou não-linear;
M e *N*: são inteiros positivos.

Embora a Equação 3.3 represente a descrição mais geral da estrutura de um Filtro Adaptativo, existe um interesse em determinar o melhor relacionamento linear entre a entrada e a resposta desejada para muitos problemas. Este relacionamento tipicamente toma a forma de um filtro *Finite-Impulse-Response* (*FIR*) ou *Infinite-Impulse-Response* (*IIR*) [9]. A Figura 3.2 exibe a estrutura de um filtro *FIR*, em que z^{-1} denota uma unidade de atraso e cada $w_i(n)$ é um ganho multiplicativo dentro do sistema. Neste caso, os coeficientes em $\boldsymbol{W}(n)$ correspondem ao valor da resposta ao impulso do filtro no instante *n*. O sinal de saída $y(n)$ pode ser escrito como na Equação 3.4.
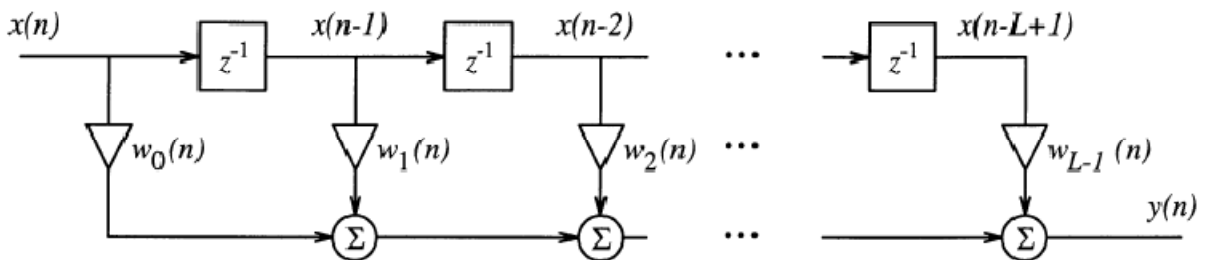
Figura 3.2: Estrutura de um filtro FIR.

$$y(n) = \sum_{i=0}^{L-1} w_i(n)\, x(n-i) = \boldsymbol{W}^T(n)\boldsymbol{X}(n) \qquad (3.4)$$

Onde:

$\boldsymbol{X}(n) = [x(n)\ x(n-1)\ ...\ x(n-L+1)]^T$: denota o vetor do sinal de entrada;

$.^T$: representa o vetor transposto.

Este sistema requer *L* multiplicações e *L-1* adições, estes cálculos podem ser realizados por um processador ou circuito, contanto que *L* não seja grande demais e nem o período de amostragem do sinal pequeno. Para alocar *L* amostras do sinal de entrada e *L* coeficientes é necessário um total de 2*L* posições de memória.

A estrutura de um filtro *IIR* é mostrada na Figura 3.3 e sua representação matemática encontra-se na Equação 3.5.
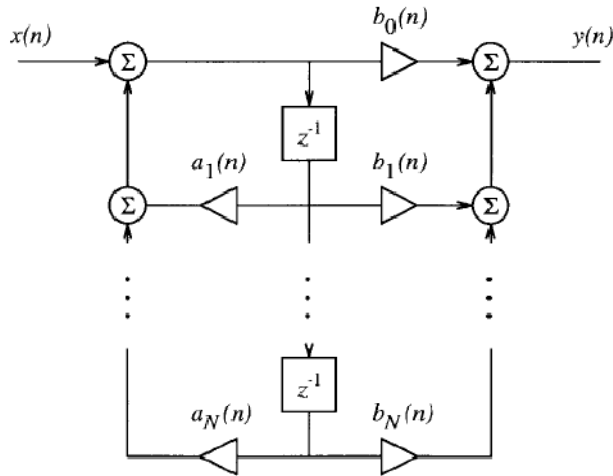
Figura 3.3: Estrutura de um filtro *IIR*.

$$y(n) = \sum_{i=1}^{N} a_i(n)\, y(n-i) + \sum_{j=0}^{N} b_j(n)\, x(n-j) \qquad (3.5)$$

Embora o diagrama em blocos não demonstre de forma clara o sistema, a Equação 3.5 pode ser facilmente escrita em notação vetorial como é apresentado na Equação 3.6.

$$y(n) = \boldsymbol{W}^T(n)\boldsymbol{U}(n) \qquad (3.6)$$

Onde:

$$\boldsymbol{W}(n) = [a_1(n)\, a_2(n) \ldots a_N(n)\, b_0(n)\, b_1(n) \ldots b_N(n)]^T$$
$$\boldsymbol{U}(n) = [y(n-1)\, y(n-2) \ldots y(n-N)\, x(n)\, x(n-1) \ldots x(n-N)]^T$$

Diferentemente de um filtro *FIR*, o cálculo do sinal de saída $y(n)$ para um filtro *IIR* envolve um número fixo de multiplicações, adições e posições de memória.

Uma questão crítica na escolha da estrutura do Filtro Adaptativo é a sua complexidade computacional. Como a operação do Filtro Adaptativo ocorre tipicamente em tempo real, todos os cálculos do sistema devem ocorrer durante o tempo de um período de amostragem. Neste sentido, as estruturas descritas anteriormente são muito úteis, pois é possível calcular $y(n)$ em uma quantidade de tempo finita utilizando operações aritméticas e quantidades de memória finitas.

3.4 Algoritmos de Adaptação Baseados no Gradiente

Um algoritmo adaptativo é um procedimento para o ajuste dos coeficientes do Filtro Adaptativo com o intuito de minimizar uma função de custo $J(\boldsymbol{W})$, escolhida para a tarefa em questão. A definição da função de custo deve ser tal que meça o quanto o processo de ajuste está sendo incapaz de reduzir o erro $e(n)$ entre $d(n)$ e $y(n)$.

Desta maneira é importante a definição da estrutura do Filtro Adaptativo, *FIR* ou *IIR*, pois assim pode-se determinar qual será o algoritmo de adaptação. Na maioria dos casos a estrutura escolhida é a de um filtro *FIR*, pois a estabilidade entre entrada e saída de um filtro *FIR* é garantida para qualquer conjunto de coeficientes fixos e os algoritmos de adaptação para os filtros *FIR* em geral são mais simples.

3.4.1 Forma Geral do Algoritmo

A forma geral do algoritmo de adaptação para os coeficientes de um Filtro Adaptativo *FIR* é apresentada na Equação 3.7.

$$\boldsymbol{W}(n+1) = \boldsymbol{W}(n) + \mu(n)\boldsymbol{G}\big(e(n), \boldsymbol{X}(n), \boldsymbol{\Phi}(n)\big) \tag{3.7}$$

Onde:

$\boldsymbol{G}(.)$: vetor dos valores de uma função não-linear;

$\mu(n)$: passo de adaptação;

$e(n)$: sinal de erro;

$\boldsymbol{X}(n)$: vetor do sinal de entrada;

$\boldsymbol{\Phi}(n)$: vetor que armazena informações pertinentes sobre as características do sinal de entrada, do sinal de erro e dos coeficientes dos instantes anteriores.

Nos algoritmos mais simples, $\boldsymbol{\Phi}(n)$ não é usado, e as únicas informações necessárias para o ajuste dos coeficientes no instante *n* são o sinal de erro, o vetor do sinal de entrada e o passo de adaptação.

O termo passo de adaptação é utilizado para μ, pois este parâmetro define a magnitude das mudanças ou "passo" em que o algoritmo iterativamente determina o vetor de coeficientes mais adequado. Freqüentemente, o sucesso ou falha em uma

aplicação de filtragem adaptativa depende da forma que o valor de μ foi escolhido ou calculado para obter o melhor desempenho de um Filtro Adaptativo.

3.4.2 Função de Custo *MSE* (*Mean-Square Error*)

Uma particular função de custo que produz um popular algoritmo adaptativo é a função de custo $J_{MSE}(n)$ (*Mean-Square Error*), apresentada na Equação 3.8.

$$J_{MSE}(n) = \frac{1}{2}\int_{-\infty}^{\infty} e^2(n)p_n\big(e(n)\big)\,de(n) = \frac{1}{2}E\{e^2(n)\} \tag{3.8}$$

Onde:

$p_n(e)$: representa função da densidade de probabilidade do erro no instante *n*.

$E\{.\}$: é a esperança matemática ou valor médio.

Para demonstrar a utilidade da função de custo *MSE* para Filtros Adaptativos *FIR* alguns fatores podem ser citados:

- $J_{MSE}(n)$ possui um mínimo bem definido em relação aos coeficientes de $\boldsymbol{W}(n)$;
- Os valores dos coeficientes obtidos, neste mínimo, são os únicos que minimizam o sinal de erro, indicando que $y(n)$ aproximou-se de $d(n)$;
- A derivada de $J_{MSE}(n)$ pode ser calculada em relação a cada coeficiente de $\boldsymbol{W}(n)$.

O último aspecto citado possui uma grande importância, pois através dele é possível determinar os valores dos coeficientes ideais tendo conhecimento da estatística de $d(n)$ e $x(n)$, bem como, definir um simples procedimento iterativo para adaptação dos coeficientes do filtro *FIR*.

3.4.3 A Solução de Wiener

Para o filtro *FIR*, os valores dos coeficientes de $\boldsymbol{W}(n)$ que minimizam $J_{MSE}(n)$ são definidos se a estatística do sinal de entrada e da resposta desejada for conhecida. A formulação deste problema para sinais em tempo contínuo e a solução resultante foram primeiramente desenvolvidas por *Wiener* em 1949. Desta maneira, este vetor com os coeficientes ideais $\boldsymbol{W}_{MSE}(n)$ é denominado *solução de Wiener* para o problema da

filtragem adaptativa. Como já mencionado anteriormente $J_{MSE}(n)$ é uma função quadrática em relação aos coeficientes de $W(n)$. Sendo assim, pode-se utilizar do resultado da teoria de otimização, o qual afirma ser a derivada da função de custo igual a zero no ponto de minimização da superfície de erro. O vetor $W_{MSE}(n)$ pode ser encontrado com a solução das equações do sistema pela Equação 3.9.

$$\frac{\partial J_{MSE}(n)}{\partial w_i(n)} = 0, \ \ 0 \leq i \leq L\text{-}1. \tag{3.9}$$

Tomando a derivada de $J_{MSE}(n)$ na Equação 3.8 e obtendo $e(n)$ e $y(n)$ das Equações 3.1 e 3.4, respectivamente, tem-se:

$$\frac{\partial J_{MSE}(n)}{\partial w_i(n)} = E\left\{e(n)\frac{\partial e(n)}{\partial w_i(n)}\right\} = -E\left\{e(n)\frac{\partial y(n)}{\partial w_i(n)}\right\} = -E\{e(n)x(n-i)\} \tag{3.10}$$

$$\frac{\partial J_{MSE}(n)}{\partial w_i(n)} = -\left(E\{d(n)x(n-i)\} - \sum_{j=0}^{L-1} E\{x(n-i)x(n-j)\}w_j(n)\right) \tag{3.11}$$

Para a expansão da Equação 3.10 obtendo a Equação 3.11 foram usadas as definições de $e(n)$ e $y(n)$ para a estrutura de um filtro *FIR*.

O sistema de equações para definição de $W_{MSE}(n)$ pode ser representado na forma vetorial. Para tanto é necessário definir a matriz $R_{XX}(n)$ e o vetor $P_{dX}(n)$ na Equação 3.12. E combinando as Equações 3.9 e 3.11 obtém-se a Equação 3.13 que é a representação vetorial para o sistema de equações.

$$R_{XX}(n) = E\{X(n)X^T(n)\} \text{ e } P_{dX}(n) = E\{d(n)X(n)\} \tag{3.12}$$

Onde:

$R_{XX}(n)$: matriz de correlação da entrada.

$P_{dX}(n)$: vetor de correlação cruzada entre a resposta desejada e sinal de entrada.

$$R_{XX}(n)W_{MSE}(n) - P_{dX}(n) = \mathbf{0} \tag{3.13}$$

Onde:

$\mathbf{0}$: é o vetor zero.

Contanto que a matriz $R_{XX}(n)$ possua inversa, o vetor da solução de *Wiener* para este problema será:

$$W_{MSE}(n) = R_{XX}^{-1}(n)P_{dX}(n) \qquad (3.14)$$

3.4.4 Método *Steepest Descent*

O método *Steepest Descent* é um conhecido procedimento para a minimização do valor da função de custo $J(n)$ em relação a um conjunto de coeficientes ajustáveis $W(n)$. Este procedimento ajusta cada coeficiente do sistema de acordo com a Equação 3.15, em que o n-ésimo coeficiente do sistema é alterado de acordo com a derivada da função de custo em relação ao n-ésimo coeficiente. Já a forma vetorial encontra-se na Equação 3.16.

$$w_i(n+1) = w_i(n) - \mu(n)\frac{\partial J(n)}{\partial w_i(n)} \qquad (3.15)$$

$$W(n+1) = W(n) - \mu(n)\frac{\partial J(n)}{\partial W(n)} \qquad (3.16)$$

Para o Filtro Adaptativo *FIR*, que minimiza a função de custo *MSE*, pode-se usar o resultado da Equação 3.11 para representar explicitamente a forma do método *Steepest Descent*. Com a substituição destes resultados na Equação 3.15 tem-se:

$$W(n+1) = W(n) + \mu(n)\big(P_{dX}(n) - R_{XX}(n)W_{MSE}(n)\big) \qquad (3.17)$$

Porém, o método *Steepest Descent* depende das quantidades estatísticas $E\{d(n)x(n-i)\}$ e $E\{x(n-i)x(n-j)\}$ contidos em $P_{dX}(n)$ e $R_{XX}(n)$, respectivamente. E na prática têm-se apenas as medidas de $d(n)$ e $x(n)$ para serem utilizadas no procedimento de adaptação. Apesar de ser possível determinar estimativas adequadas para as quantidades estatísticas necessárias na Equação 3.17, uma versão aproximada do método *Steepest Descent*, que depende apenas dos valores dos próprios sinais, foi desenvolvida. Este procedimento é conhecido com algoritmo *LMS* (*Least Mean Square*).

3.4.5 O Algoritmo *LMS* (*Least Mean Square*)

A função de custo $J(n)$ escolhida para o algoritmo *Steepest Descent* determina os coeficientes para o Filtro Adaptativo. Se a função de custo *MSE* na Equação 3.8 for escolhida, então o algoritmo resultante dependerá da estatística de $x(n)$ e $d(n)$ devido às operações contidas nesta função de custo. Como tipicamente têm-se apenas as medidas de $x(n)$ e $d(n)$, substitui-se a função de custo por uma alternativa que depende somente destas medidas. Uma função de custo alternativa usada pode ser a dos Mínimos Quadrados (*LS – Least Square*), apresentada a seguir.

$$J_{LS}(n) = \sum_{k=0}^{n} \alpha(k) \big(d(k) - W^T(n)X(k) \big)^2 \tag{3.18}$$

Onde:

$\alpha(k)$: é uma seqüência de pesos para os termos do somatório.

Entretanto, esta função de custo requer um grande número de cálculos para obtenção do resultado final e das derivadas em relação a cada $w_i(n)$. Buscando uma maior simplificação nos cálculos foi proposta a função de custo Média dos Mínimos Quadrados (*LMS – Least Mean Square*):

$$J_{LMS}(n) = \frac{1}{2} e^2(n) \tag{3.19}$$

Esta função de custo pode ser entendida como uma estimativa instantânea da função de custo *MSE*, $J_{MSE}(n) = E\{J_{LMS}(n)\}$. Embora isto não pareça útil, o algoritmo resultante obtido quando $J_{LMS}(n)$ é usado como $J(n)$ é extremamente eficaz em aplicações práticas.

Realizando as derivadas de $J_{LMS}(n)$ em relação aos elementos de $\boldsymbol{W}(n)$ e substituindo o resultado na Equação 3.15 obtém-se o algoritmo adaptativo *LMS*, apresentado na Equação 3.20. Estando este algoritmo compatível com a forma geral descrita na Equação 3.7.

$$\boldsymbol{W}(n+1) = \boldsymbol{W}(n) + \mu(n)e(n)\boldsymbol{X}(n) \tag{3.20}$$

Este algoritmo apenas requer multiplicações e adições para ser implementado. De fato, o número e o tipo das operações necessárias para o algoritmo *LMS* são aproximadamente os mesmos para um filtro *FIR* com coeficientes fixos, o que é uma das razões para a popularidade deste algoritmo.

Um fator importante na demonstração do comportamento eficaz do algoritmo *LMS* está no fato de sua solução, obtida nas proximidades do ponto de convergência, estar relacionada à solução de *Wiener*. Analisando o algoritmo com certas suposições estatísticas sobre o sinal de entrada e a resposta desejada obtém-se a Equação 3.21, sendo $\boldsymbol{W}_{MSE}(n)$ um vetor fixo.

$$\lim_{n \to \infty} E\{\boldsymbol{W}(n)\} = \boldsymbol{W}_{MSE} \tag{3.21}$$

Além disso, o comportamento do algoritmo *LMS* é similar ao método *Steepest Descent* que depende explicitamente da estatística do sinal de entrada e da resposta desejada.

3.5 Método *LS* (*Least Square*)

Nos métodos de filtragem adaptativa discutidos anteriormente, foram considerados algoritmos baseados no gradiente para minimizar a função de custo $J_{MSE}(n)$ (*Mean-Square Error*). A dificuldade destes métodos está no fato da necessidade do conhecimento das quantidades estatísticas $E\{d(n)x(n-i)\}$ e $E\{x(n-i)x(n-j)\}$. Quando esta informação estatística é desconhecida, é necessário a estimação destes valores estatísticos. Uma alternativa é considerar medidas do valor do erro que não inclua expectativa matemática e que possa ser calculada diretamente dos dados. Como por exemplo, no método dos Mínimos Quadrados (*LS – Least Square*), apresentada anteriormente.

O filtro de *Wiener* e sua versão adaptativa o algoritmo *LMS* são formulados através do ponto de vista estatístico. Pois o desenvolvimento destas soluções está baseado na minimização da quantidade estatística, *Mean-Square Error*. Por outro lado, a classe de métodos baseados no método *Least Square* são formulados seguindo o ponto

de vista determinístico. De tal forma que os parâmetros do filtro adaptativo são calculados para que a quantidade expressa na Equação (3.22) seja minimizada.

$$\mathcal{E}(n) = \sum_{i=0}^{n} \lambda^{n-i} |e(i)|^2 \tag{3.22}$$

Onde:

$0 \leq \lambda \leq 1$: é o denominado peso exponencial ou fator de esquecimento.

A escolha de $\lambda < 1$ resulta em um método que coloca maior importância nas amostras mais recentes dos valores observados e menor importância nas amostras menos recentes.

3.5.1 O Algoritmo *RLS* (*Recursive Least Square*)

Para calcular os coeficientes que minimizam $\mathcal{E}(n)$ deve-se proceder como anteriormente igualando a zero a derivada de $\mathcal{E}(n)$ em relação a $\omega_n(k)$ para *k = 0, 1, ..., p* .

$$\frac{\partial \mathcal{E}(n)}{\partial w_n(k)} = 2 \sum_{i=0}^{n} \lambda^{n-i} e(i) \frac{\partial e(i)}{\partial w_n(k)} = -\sum_{i=0}^{n} \lambda^{n-i} e(i) x(i-k) = 0 \tag{3.23}$$

Sabendo que:

$$e(i) = d(i) - y(i) = d(i) - \boldsymbol{W}_n^T \boldsymbol{X}(i) \tag{3.24}$$

Substituindo (3.24) em (3.23):

$$\sum_{i=0}^{n} \lambda^{n-i} \big[d(i) - \sum_{l=0}^{p} w_n(l) x(i-l) \big] x(i-k) = 0 \tag{3.25}$$

Invertendo a ordem dos somatórios e rearranjando os termos:

$$\sum_{l=0}^{p} w_n(l) \big[\sum_{i=0}^{n} \lambda^{n-i} x(i-l)\, x(i-k) \big] = \sum_{i=0}^{n} \lambda^{n-i} d(i) x(i-k) \tag{3.26}$$

A Equação 3.26 pode ser expressa na forma matricial da seguinte maneira:

$$R_x(n)W_n = r_{dx}(n) \tag{3.27}$$

Onde:

$R_x(n)$: matriz de correlação da entrada determinística com pesos exponenciais.

$r_{dx}(n)$: vetor de correlação cruzada entre a resposta desejada e sinal de entrada determinístico.

Uma solução recursiva pode ser desenvolvida para o cálculo dos coeficientes da seguinte maneira:

$$W_n = W_{n-1} + \Delta W_{n-1} \tag{3.28}$$

Onde:

ΔW_{n-1}: é a correção aplicada à solução no instante *n–1*.

O vetor de coeficientes que minimizam $\mathcal{E}(n)$ pode ser expresso pela Equação 3.29.

$$W_n = R_x^{-1}(n)r_{dx}(n) \tag{3.29}$$

Então, a fórmula recursiva deve ser desenvolvida expressando $r_{dx}(n)$ em termos de $r_{dx}(n-1)$, $R_x^{-1}(n)$ em termos de $R_x^{-1}(n-1)$ e do vetor de entrada $X(n)$. Ficando estas equações da seguinte maneira:

$$r_{dx}(n) = \lambda r_{dx}(n-1) + d(n)X(n) \tag{3.30}$$

$$R_x(n) = \lambda R_x(n-1) + X(n)X^T(n) \tag{3.31}$$

Mas como o interesse está em encontrar uma equação recursiva para $R_x^{-1}(n)$, a identidade de *Woodbury's* deve ser aplicada. Esta identidade é apresentada na Equação 3.32.

$$(A + uv^T)^{-1} = A^{-1} - \frac{A^{-1}uv^TA^{-1}}{1+v^TA^{-1}u} \tag{3.32}$$

Fazendo $A = \lambda^{-1}R_x^{-1}(n)$ e $u = v = X(n)$ a seguinte equação recursiva para o inverso de $R_x(n)$ é encontrada:

$$R_x^{-1}(n) = \lambda^{-1}R_x^{-1}(n-1) - \frac{\lambda^{-2}R_x^{-1}(n-1)X(n)X^T(n)R_x^{-1}(n-1)}{1+\lambda^{-1}X^T(n)R_x^{-1}(n-1)X(n)} \quad (3.33)$$

Para simplificar a notação, $R_x^{-1}(n)$ será representado por $P(n)$ e o vetor de ganho $g(n)$ será definido como:

$$g(n) = \frac{\lambda^{-1}P(n-1)X(n)}{1+\lambda^{-1}X^T(n)P(n-1)X(n)} \quad (3.34)$$

Incorporando estas definições na Equação (3.33), obtém-se:

$$P(n) = \lambda^{-1}[P(n-1) - g(n)X^T(n)P(n-1)] \quad (3.35)$$

Para completar a equação recursiva é necessário desenvolver a equação de atualização dos coeficientes do vetor W_n. Com $W_n = P(n)r_{dx}(n)$ e substituindo $r_{dx}(n)$ pela Equação 3.30:

$$W_n = \lambda P(n)r_{dx}(n-1) + d(n)P(n)X(n) \quad (3.36)$$

Incorporando $P(n)$ dado pela Equação (3.35) no primeiro termo do lado direito da Equação 3.36 e fazendo $P(n)X(n) = g(n)$:

$$W_n = [P(n-1) - g(n)X(n)P(n-1)]r_{dx}(n-1) + d(n)g(n) \quad (3.37)$$

Considerando $W_{n-1} = P(n-1)r_{dx}(n-1)$:

$$W_n = W_{n-1} + g(n)[d(n) - W_{n-1}^T X(n)] \quad (3.38)$$

Que pode ser reescrito, da seguinte forma:

$$W_n = W_{n-1} + e(n) g(n) \quad (3.39)$$

$e(n) = d(n) - W_{n-1}^T X(n)$ é a diferença entre $d(n)$ e a saída do filtro formada pela aplicação dos coeficientes calculados previamente, W_{n-1}, pelo vetor de entrada $X(n)$. Sendo denominada de erro a *priori*.

Como o algoritmo *RLS* envolve uma atualização recursiva do vetor $\boldsymbol{W}_n$ e da matriz inversa de correlação $\boldsymbol{P}(n)$, desta maneira, são requeridas condições iniciais para estes termos. Uma aproximação comumente utilizada na inicialização na matriz de correlação é a seguinte:

$$\boldsymbol{R}_x(0) = \delta\boldsymbol{I} \qquad (3.40)$$

Onde δ é uma constante positiva de pequeno valor, com isto, $\boldsymbol{P}(0) = \delta^{-1}\boldsymbol{I}$. Já o vetor de coeficientes deve ser iniciado como um vetor nulo.

$$\boldsymbol{W}_n = \boldsymbol{0} \qquad (3.41)$$

A implementação do algoritmo *Recursive Least Square* pode ser dividida em cinco etapas:

Etapa 01 (Inicialização):

$$\boldsymbol{P}(0) = \delta^{-1}\boldsymbol{I} \qquad (3.42)$$
$$\boldsymbol{W}_n = \boldsymbol{0} \qquad (3.43)$$

Etapa 02 (Cálculo do vetor ganho):

$$\boldsymbol{g}(n) = \frac{\lambda^{-1}P(n-1)X(n)}{1+\lambda^{-1}X^T(n)P(n-1)X(n)} \qquad (3.44)$$

Etapa 03 (Filtragem e cálculo do erro):

$$y(\boldsymbol{n}) = \boldsymbol{W}_{n-1}^T\boldsymbol{X}(n) \qquad (3.45)$$
$$e(n) = d(n) - y(n) \qquad (3.46)$$

Etapa 04 (Adaptação dos coeficientes):

$$\boldsymbol{W}_n = \boldsymbol{W}_{n-1} + e(n)\,\boldsymbol{g}(n) \qquad (3.47)$$

Etapa 05 (Cálculo da matriz inversa de correlação de entrada):

$$\boldsymbol{P}(n) = \lambda^{-1}[\boldsymbol{P}(n-1) - \boldsymbol{g}(n)\boldsymbol{X}^T(n)\boldsymbol{P}(n-1)] \tag{3.48}$$

3.6 Aplicações

Certamente uma grande parcela dos estudos e desenvolvimentos realizados com os Filtros Adaptativos deve-se as várias aplicações em que estes sistemas são utilizados. Neste texto serão descritas duas aplicações de filtragem adaptativa: o Cancelamento de Ruído Adaptativo e Predição Linear. Com estes dois exemplos espera-se demonstrar a aplicabilidade e importância desta tecnologia.

3.6.1 Cancelamento de Ruído Adaptativo

Quando medidas de certos sinais e processos estão sendo coletadas, limitações físicas freqüentemente não permitem que medidas precisas das quantidades de interesse sejam obtidas. Tipicamente, o sinal de interesse é linearmente somado com outros ruídos estranhos no processo de medida, introduzindo erros inaceitáveis nas medidas. Porém, caso alguma medida deste ruído possa ser obtida em alguma parte do sistema, um Filtro Adaptativo poderá ser utilizado para determinar a relação entre o ruído $x(n)$ e a componente deste ruído contida no sinal de interesse $d(n)$. Pois, o Filtro Adaptativo processa o sinal $x(n)$ produzindo o sinal de saída $y(n)$, que por sua vez, acompanha as características do ruído contido em $d(n)$. Desta maneira, o sinal de erro gerado $e(n)$ é o próprio sinal de interesse sem o indesejável ruído.

A Figura 3.4 demonstra a estrutura base para o Cancelamento de Ruído Adaptativo.
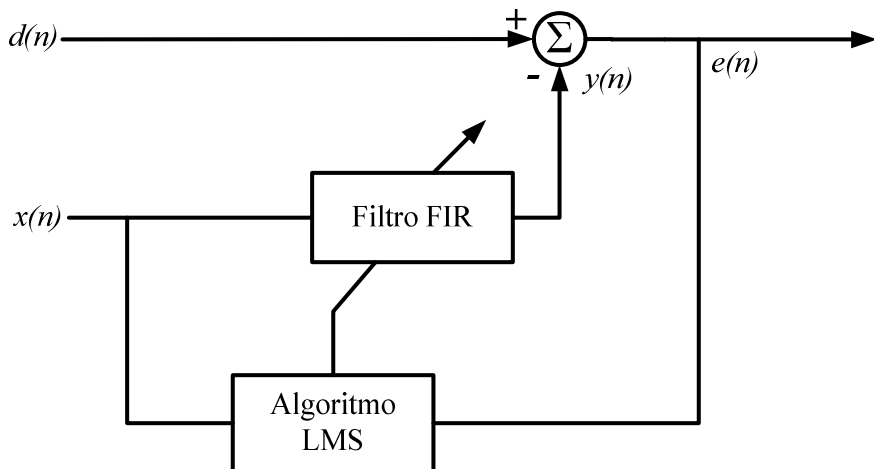
Figura 3.4: Estrutura geral para o Cancelamento de Ruído Adaptativo.

Uma das primeiras aplicações de Cancelamento de Ruído Adaptativo [10] foi na área médica, o que possibilitou a realização do exame de Eletrocardiograma (ECG) das batidas do coração de um bebê ainda na barriga da mãe. Em que o ECG das batidas do coração do bebê é extraído através do ECG da mãe.

3.6.2 Predição Linear com Filtro Adaptativo

O termo Predição Linear deve-se a utilização de um Filtro Adaptativo Linear para predizer valores futuros de um sinal de entrada. Neste filtro o sinal de entrada $x(n)$ é a própria resposta desejada $d(n)$ atrasada um número específico de amostras.

É importante observar que nesta aplicação a resposta desejada $d(n)$ sempre estará disponível, pois ela é o próprio sinal de entrada do sistema.

Para predizer amostras futuras é necessário utilizar uma cópia do Filtro *FIR* da Figura 3.5, com os coeficientes já adaptados para predição, tendo na entrada a amostra atual do sinal de entrada do sistema. Desta forma um número definido de amostras poderá ser predito. Este número de amostra predito depende, é claro, de quantas amostras do sinal de entrada do sistema foram atrasadas no processo de adaptação dos coeficientes.

A Figura 3.5 demonstra a estrutura base para a Predição Linear com Filtro Adaptativo.
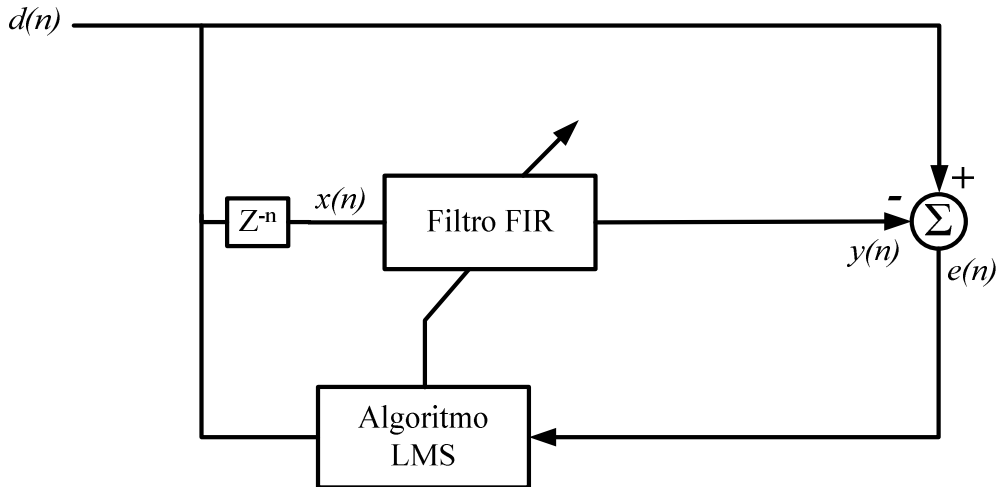
Figura 3.5: Estrutura geral para predição linear.

Uma das aplicações da Predição Linear com Filtro Adaptativo é a solução de problemas envolvendo o atraso de sinais [11]. Podendo ser, por exemplo, o atraso causado pela filtragem de sinais em filtros digitais, pelo processo de amostragem, etc.

3.7 Filtro Adaptativo Sintonizado (*Adaptive Notch Filter*)

Em algumas situações o sinal de interesse $d(n)$ pode conter alguma interferência senoidal indesejável. Um dos métodos convencionais para o cancelamento desta interferência é passar o sinal por um filtro digital sintonizado, cuja característica é possuir ganho unitário em todas as freqüências exceto na freqüência da interferência senoidal, em que o ganho deve ser zero. Quando a interferência senoidal estiver disponível *Widrow* et al. [10] propuseram uma solução alternativa constituída de um deslocador de fase de 90° e um filtro adaptativo com dois coeficientes. A estrutura geral para o cancelamento de uma interferência senoidal com um Filtro Adaptativo Sintonizado é apresenta na Figura 3.6.
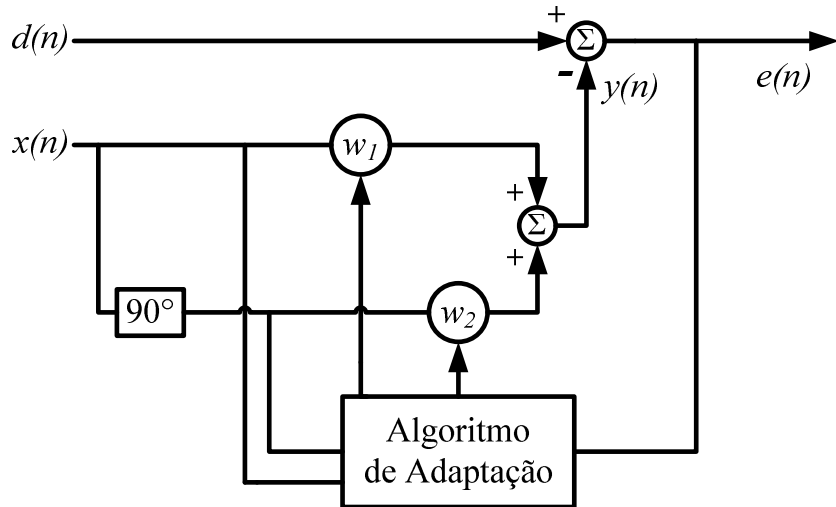
Figura 3.6: Estrutura para o Filtro Adaptativo Sintonizado.

Como observado na estrutura dois sinais ortogonais senoidais são utilizados como entrada, um para a entrada $x(n)$ e outro defasado 90º de $x(n)$. O sinal de saída $y(n)$ é obtido com a soma dos dois sinais de entrada multiplicados por seus respectivos coeficientes. O sinal de saída $y(n)$ reproduz o sinal de interferência senoidal contido em $d(n)$, desta forma, o sinal sem a interferência será o próprio erro $e(n)$.

Os algoritmos *Least Mean Square* e *Recursive Least Square* podem ser utilizados como algoritmos de adaptação em um Filtro Adaptativo Sintonizado.

Os coeficientes do filtro adaptativo sintonizado são ajustados através do algoritmo *LMS* da seguinte maneira:

$$w_1(n + 1) = w_1(n) + \mu(n)e(n)x(n) \tag{3.49}$$

$$w_2(n + 1) = w_2(n) + \mu(n)e(n)x_{90°}(n) \tag{3.50}$$

Em que:

$x(n)$: sinal senoidal com mesma freqüência que a interferência.

$x_{90°}(n)$: $x(n)$ com deslocamento de fase de 90°.

Já a implementação do algoritmo *RLS*, aplicado a um filtro adaptativo sintonizado, é apresentado em cinco etapas:

Etapa 01 (Initialização):

$$P_{\lambda 1}(0) = P_{\lambda 2}(0) = \delta \tag{3.51}$$

$$w_1(0) = w_2(0) = 0 \tag{3.52}$$

Etapa 02 (Cálculo do ganho):

$$g_1(n) = \frac{P_{\lambda 1}(n-1)x(n)}{\lambda + x^2(n)P_{\lambda 1}(n-1)} \tag{3.53}$$

$$g_2(n) = \frac{P_{\lambda 2}(n-1)x_{90°}(n)}{\lambda + x_{90°}^2(n)P_{\lambda 2}(n-1)} \tag{3.54}$$

Etapa 03 (Filtragem e cálculo do erro):

$$y(n) = w_1(n-1)x(n) + w_2(n-1)x_{90°}(n) \tag{3.55}$$

$$e(n) = d(n) - y(n) \tag{3.56}$$

Etapa 04 (Adaptação dos coeficientes):

$$w_1(n) = w_1(n-1) + g_1(n)e(n) \tag{3.57}$$

$$w_2(n) = w_2(n-1) + g_2(n)e(n) \tag{3.58}$$

Etapa 05 (Cálculo dos coeficientes de correlação inversa):

$$P_{\lambda 1}(n) = \lambda^{-1}P_{\lambda 1}(n-1) - \lambda^{-1}g_1(n)x(n)P_{\lambda 1}(n-1) \tag{3.59}$$

$$P_{\lambda 2}(n) = \lambda^{-1}P_{\lambda 2}(n-1) - \lambda^{-1}g_2(n)x_{90°}(n)P_{\lambda 2}(n-1) \tag{3.60}$$

Como demonstrado pelas equações, no caso do filtro adaptativo sintonizado, o vetor de ganho $\boldsymbol{g}(n)$ é transformado nos ganhos $g_1(n)$ and $g_2(n)$, calculados na Etapa 02. A matriz inversa de correlação $\boldsymbol{P}(n)$ é transformada nos dois valores escalares $P_{\lambda 1}(n)$ e $P_{\lambda 2}(n)$, calculados na Etapa 05. Isto torna a implementação do algoritmo mais simples em termos de consumo computacional, pois não é necessário o cálculo da matriz inversa $\boldsymbol{P}(n)$.

A principal aplicação de Filtros Adaptativos Sintonizados está no cancelamento de interferência senoidal comum em áreas como telecomunicações e biomédica. Mas, nos últimos anos, a aplicação desta técnica vem sendo estendida a área Detecção de Harmônicos, com aplicação nos algoritmos de controle de Filtros Ativos de Potência.

3.8 Detecção de Harmônicos com Filtro Adaptativo

A técnica de cancelamento de ruído adaptativo vem sendo utilizada em várias aplicações de processamento de sinal. Este método mantém o sistema em seu melhor modo de operação auto-ajustando continuamente seus parâmetros. De acordo com a teoria do cancelamento de ruído adaptativo, o princípio da detecção de harmônicos com filtragem adaptativa é ilustrado através da Figura 3.7. Nesta estrutura básica de um Filtro Adaptativo aplicado à detecção da corrente harmônica, $d(n)$ representa a corrente $i(t)$ poluída com harmônicos (corrente da carga) e $x(n)$ representa a forma de onda senoidal $v_{sin}(t)$ em fase com a tensão da fonte. O sinal de referência $x(n)$ processado pelo Filtro Adaptativo produz o sinal de saída $y(n)$ que acompanha a variação da componente fundamental de $i(t)$. O objetivo do Filtro Adaptativo é aproximar $y(n)$, em amplitude e fase, a componente fundamental $i_1(n)$. Então, o conteúdo harmônico $i_h(n)$ pode ser diretamente obtido pelo sinal de erro $e(n)$, subtraindo $y(n)$ de $d(n)$. Os coeficientes do Filtro Adaptativo são ajustados através do algoritmo *Least Mean Square* (*LMS*) ou *Recursive Least Square* (*RLS*).
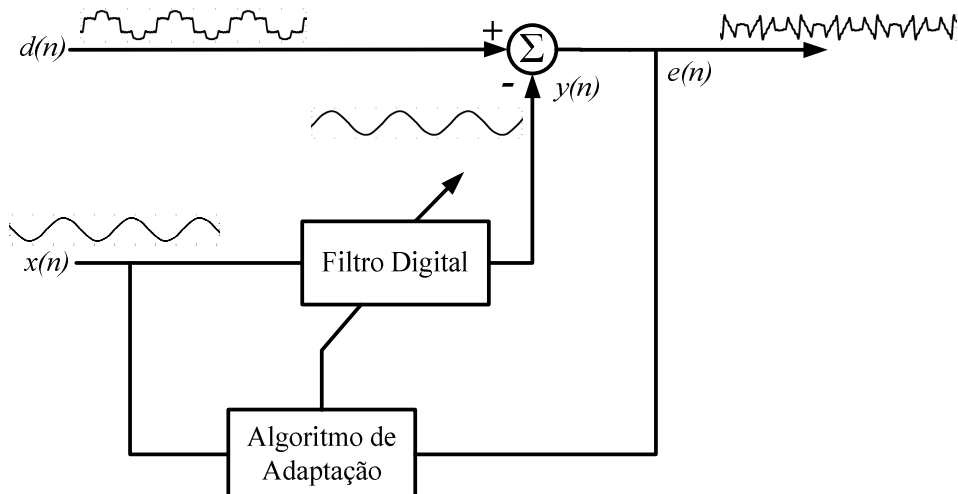
Figura 3.7: Princípio da detecção de harmônicos com Filtro Adaptativo.

A estrutura para o Filtro Adaptativo Sintonizado, apresentada na Figura 3.8, é um pouco diferente. No Filtro Adaptativo Sintonizado, como mencionado anteriormente, dois sinais ortogonais são utilizados como entrada, um para a entrada $x(n)$ (em fase com a tensão da fonte) e outro adiantado 90º de $x(n)$. Com isto, é

necessária a adaptação, com o algoritmo *LMS* ou *RLS*, de apenas dois coeficientes, um para cada entrada. O sinal de saída $y(n)$ é obtido com a soma dos dois sinais de entrada multiplicados por seus respectivos coeficientes. O conteúdo harmônico $i_h(n)$, como mencionado anteriormente, é diretamente obtido pelo sinal de erro $e(n)$.
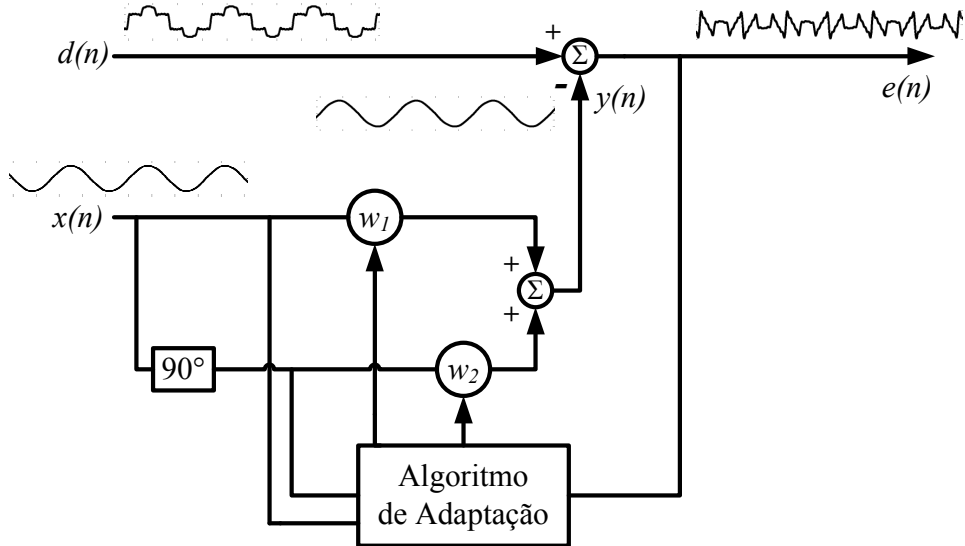
Figura 3.8: Princípio da detecção de harmônicos com Filtro Adaptativo Sintonizado.

3.9 Geração dos Sinais Ortogonais com a Transformada de Clarke

Como apresentado nos parágrafos anteriores $x(n)$ é um sinal senoidal em fase com a tensão da fonte. Este sinal é obtido tradicionalmente com utilização de *PLL* (*Phased Locked Loop*) aplicado na tensão da fonte [28].

Neste trabalho, uma nova abordagem foi utilizada para gerar os sinais ortogonais de entrada para o Filtro Adaptativo Sintonizado. Estes sinais são gerados através da Transformada de *Clarke*, aplicada à corrente da carga, como ilustrado na Figura 3.9. Como observado na Equação 3.61, a Transformada de Clarke gera dois sinais ortogonais $I_{L\alpha}$ e $I_{L\beta}$. Estes sinais ortogonais possuem um conteúdo harmônico, que é eliminado através de um Filtro Passa-Baixa *Butterworth* de terceira ordem com uma freqüência de corte de 100Hz.

$$\begin{bmatrix} I_{L0} \\ I_{L\alpha} \\ I_{L\beta} \end{bmatrix} = \sqrt{\frac{2}{3}} \cdot \begin{bmatrix} \frac{1}{\sqrt{2}} & \frac{1}{\sqrt{2}} & \frac{1}{\sqrt{2}} \\ 1 & -\frac{1}{2} & -\frac{1}{2} \\ 0 & \frac{\sqrt{3}}{2} & -\frac{\sqrt{3}}{2} \end{bmatrix} \cdot \begin{bmatrix} I_{LA} \\ I_{LB} \\ I_{LC} \end{bmatrix} \tag{3.61}$$
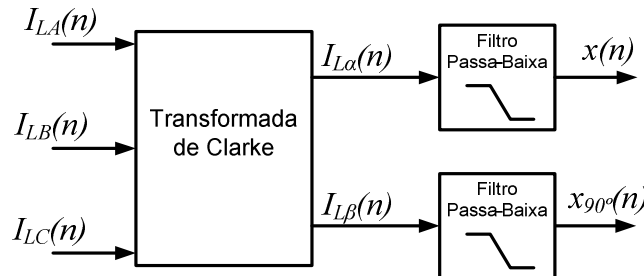
Figura 3.9: Geração dos sinais ortogonais de entrada para o Filtro Adaptativo Sintonizado.

Desta forma, dois sinais ortogonais, $x(n)$ e $x_{90°}(n)$, com uma freqüência de 60Hz são obtidos sem a utilização de um *PLL*. A Figura 3.10 mostra esses sinais.
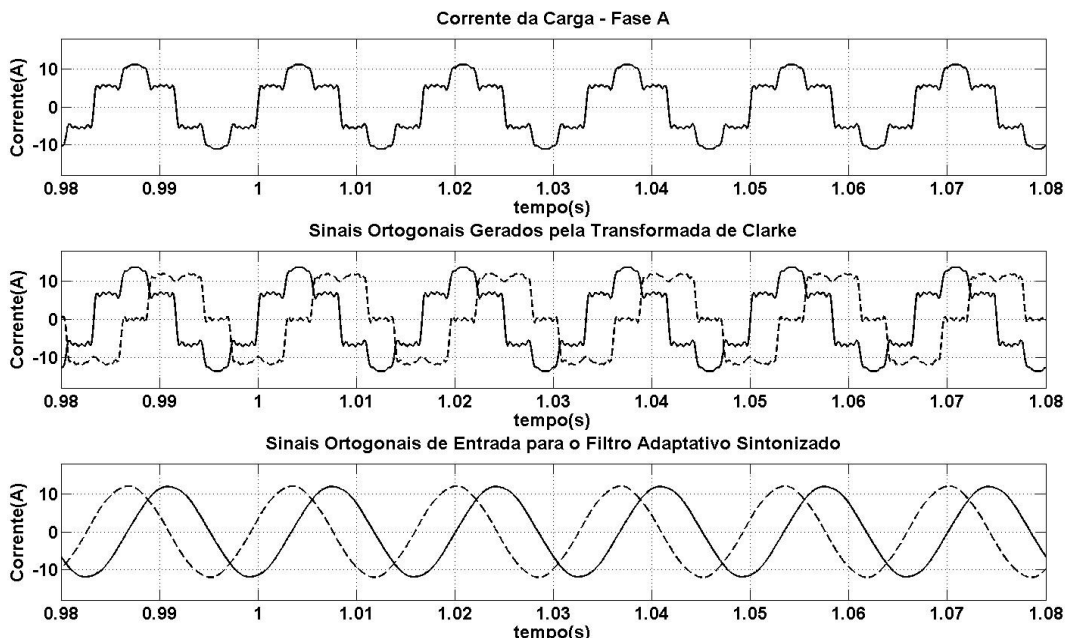
Figura 3.10: Corrente da carga na fase A, sinais ortogonais obtidos com a transformada de Clarke e sinais ortogonais de entrada para o Filtro Adaptativo Sintonizado.

Com a ausência de um *PLL*, o sinal $x(n)$ não se encontra mais em fase com a tensão da fonte. Fato este, que não é problemático, pois o próprio Filtro Adaptativo realiza o ajuste de fase.

A utilização da Transformada de *Clarke* diretamente na corrente da carga e posterior filtragem dos sinais ortogonais $I_{L\alpha}$ e $I_{L\beta}$ permite que os sinais $x(n)$ e $x_{90°}(n)$ sigam a variação de amplitude da corrente da carga. Desta maneira, a velocidade de convergência do algoritmo é significativamente melhorada. O tempo de convergência obtido com esta técnica é inferior a um ciclo da freqüência fundamental.

3.10 Conclusões do Capítulo

A extração do conteúdo harmônico da corrente da carga usando Filtros Adaptativos demonstra ser uma técnica viável e eficaz. O que é demonstrado pelas recentes publicações em periódicos e em congressos apresentadas no Capítulo 2, bem como, pela teoria exposta neste capítulo.

Mesmo assim, o tempo de convergência e o erro em regime permanente do Filtro Adaptativo devem ser melhorados buscando uma resposta mais precisa do algoritmo e adequada em comparação ao desempenho dos algoritmos Referência Síncrona e Teoria da Potência Instantânea p-q. Desta forma, a geração dos sinais ortogonais utilizando a transformada de Clarke melhora de forma significativa o tempo de convergência. Já a contribuição quanto ao erro em regime permanente é detalhada no Apêndice B.

Nos próximos capítulos serão apresentados os resultados das simulações e das implementações experimentais em um Filtro Ativo Paralelo para aplicação da detecção de harmônicos com Filtros Adaptativos.

4 Resultados de Simulação

Nos capítulos anteriores, os principais conceitos necessários para implementação da técnica de detecção de harmônicos com filtragem adaptativa foram apresentados. Desta maneira, é necessário a simulação da técnica para a verificação e validação dos resultados, para uma posterior implementação no Processador Digital de Sinais TMS320F2812.

O objetivo destas simulações é observar o comportamento do algoritmo para a geração do conteúdo harmônico, com base nos sinais utilizados pelo mesmo.

Tanto a velocidade de convergência do algoritmo como a resposta em regime permanente serão analisados com maior detalhe. Pois, estes são os dois principais aspectos a serem levados em consideração para a aplicação da técnica proposta em um Filtro Ativo de Potência.

As simulações foram realizadas no programa *Matlab/Simulink*. As principais características dos sinais encontrados neste tipo de aplicação foram simuladas, com ênfase nos dois aspectos citados no parágrafo anterior.

Nas próximas páginas serão apresentadas as simulações da técnica de detecção de harmônicos com Filtros Adaptativos Sintonizados usando os algoritmos de adaptação *Least Mean Square* (*LMS*) e *Recursive Least Square (RLS)*.

4.1 Filtro Adaptativo Sintonizado com Algoritmo *LMS*

No Filtro Adaptativo Sintonizado dois sinais ortogonais são utilizados como sinais de entrada e apenas dois coeficientes são utilizados, um para cada sinal de entrada. O algoritmo de adaptação dos coeficientes usado nesta primeira simulação é o *Least Mean Square* (*LMS*).

O valor *RMS* de cada componente harmônico da corrente da carga utilizado na simulação está disponível na Tabela 4.1.

Tabela 4.1: Valor *RMS* de cada componente harmônico da corrente da carga para simulação.

	RMS
Fundamental	7,071 A
5° Harmônico	1,677 A
7° Harmônico	0,693 A
11° Harmônico	0,614 A
13° Harmônico	0,411 A
17° Harmônico	0,376 A
19° Harmônico	0,276 A
23° Harmônico	0,260 A
25° Harmônico	0,195 A

A Figura 4.1 apresenta os sinais gerados pelo Filtro Adaptativo Sintonizado para detecção dos harmônicos da corrente da carga. Como já mencionado no capítulo anterior, a corrente da carga é usada como sinal desejado $d(n)$ e dois sinais ortogonais, $x(n)$ e $x_{90°}(n)$, são utilizados como entrada. A saída do Filtro Adaptativo é indicada por $y(n)$, em fase e com a mesma amplitude da componente fundamental da corrente da carga. A subtração de $d(n) - y(n)$ gera o sinal de erro $e(n)$ que contém o conteúdo harmônico necessário para a compensação.
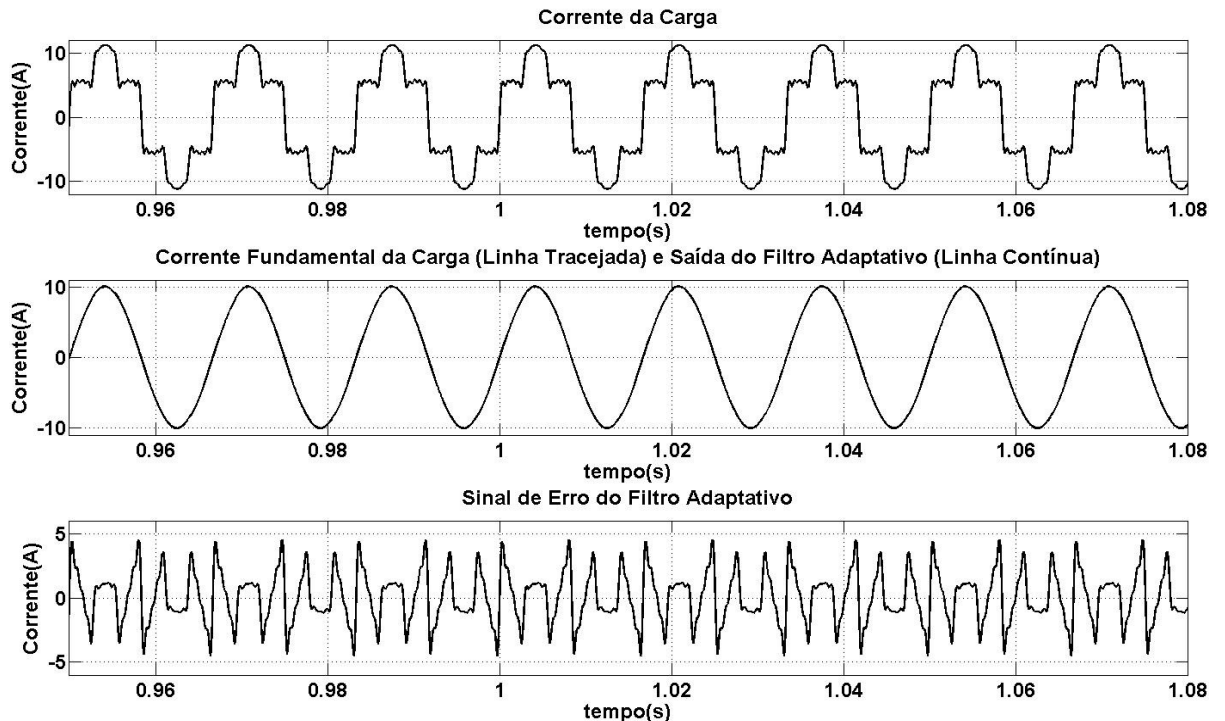
Figura 4.1: Sinal desejado, sinal de saída e sinal de erro do Filtro Adaptativo Sintonizado *LMS* em regime permanente.

A seguir são apresentados os principais sinais utilizados nestas simulações com Filtro Adaptativo Sintonizado ajustado pelo algoritmo *LMS*, em que o valor $\mu = 0,00000125$ foi utilizado para o passo de adaptação.

A Figura 4.2 demonstra a correta geração da corrente fundamental da carga pelo Filtro Adaptativo Sintonizado. A corrente fundamental da carga é reproduzida em sua totalidade pelo algoritmo.
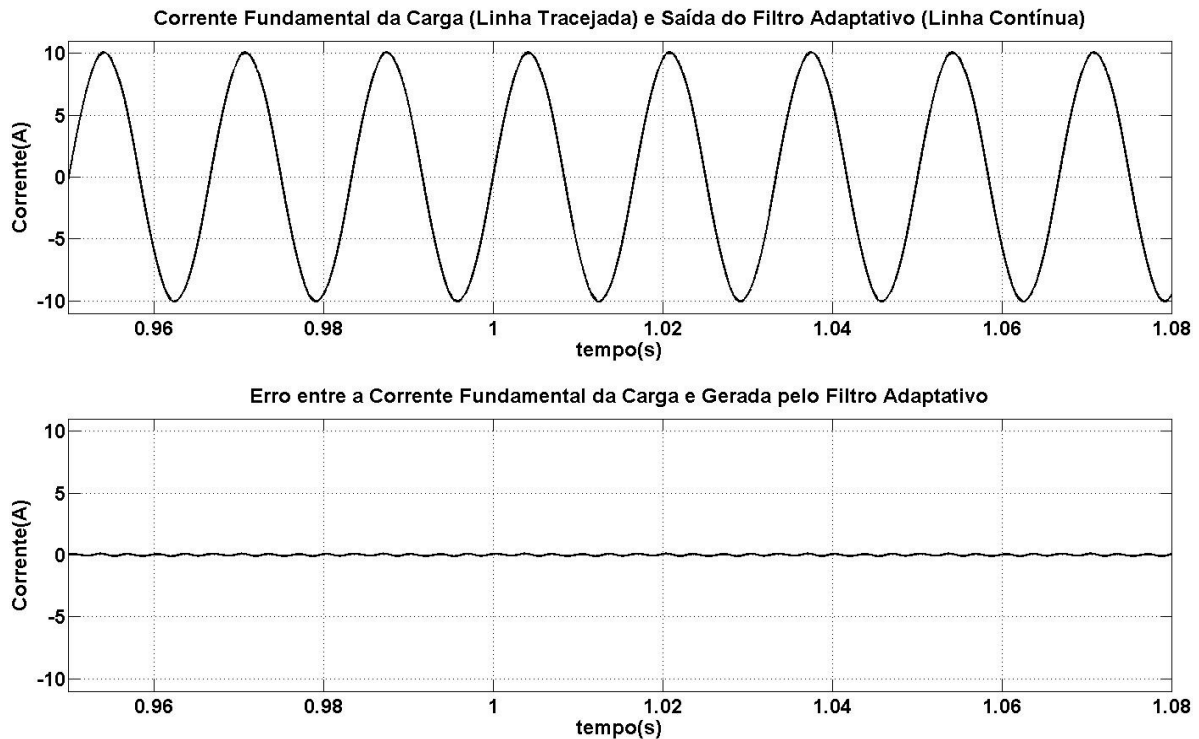
Figura 4.2: Comparação entre a corrente fundamental da carga e a gerada pelo Filtro Adaptativo Sintonizado *LMS* em regime permanente.

A demonstração da compensação do conteúdo harmônico e os espectros harmônicos da corrente da carga e compensada são mostrados pelas Figuras Figura 4.3 e Figura 4.4, respectivamente.
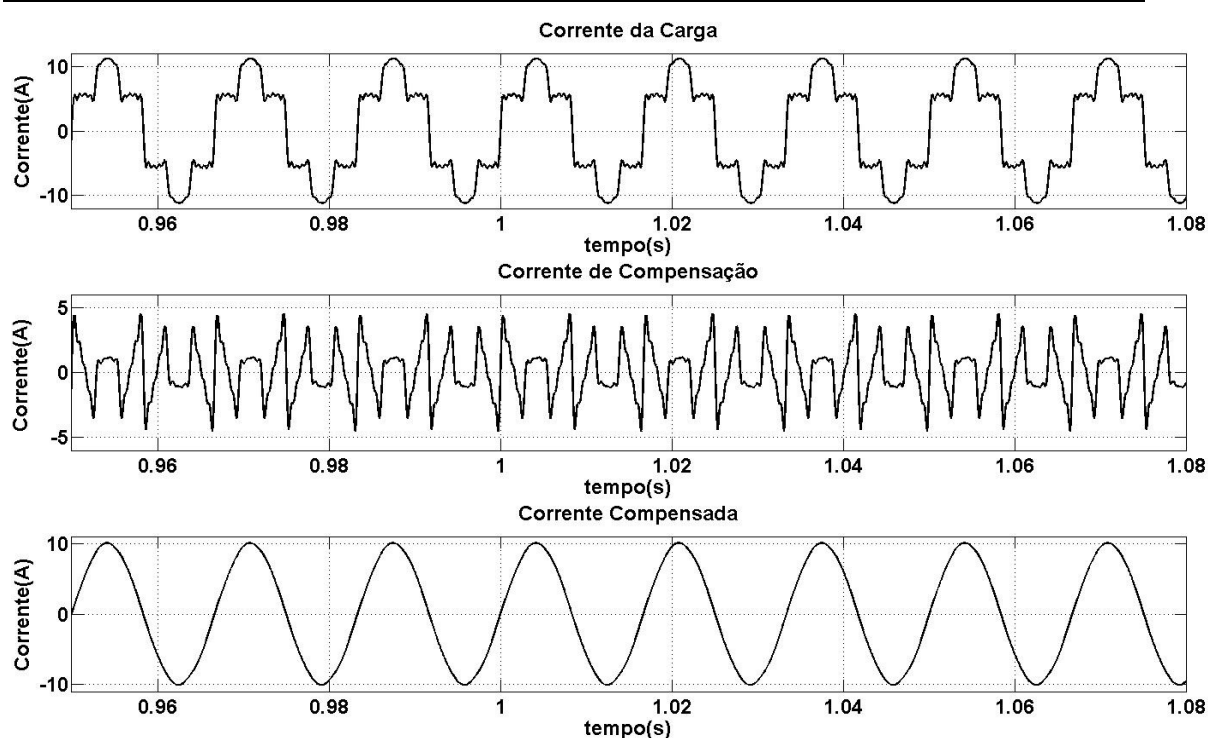
Figura 4.3: Resultado da compensação em regime permanente com Filtro Adaptativo Sintonizado *LMS*.
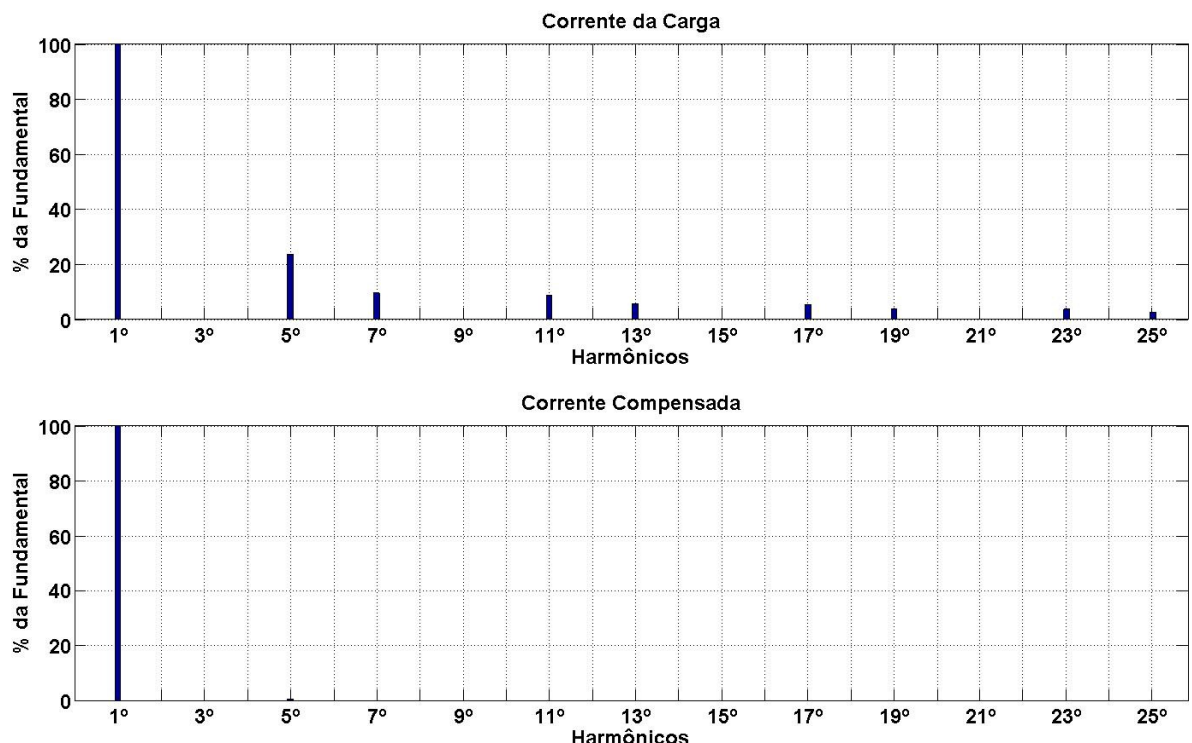
Figura 4.4: Espectro harmônico da corrente da carga e corrente compensada com Filtro Adaptativo Sintonizado *LMS*.

A seguir são apresentadas as simulações com alteração do valor da amplitude da corrente da carga. Nestas simulações, foi aplicada à amplitude da corrente da carga um aumento de 100% de seu valor e em seguida um decréscimo de 25%.

A Figura 4.5 mostra a corrente da carga, a corrente fundamental da carga juntamente com o sinal de saída do Filtro Adaptativo Sintonizado e o sinal de erro. Como pode ser observado, com a utilização da nova técnica para gerar os sinais ortogonais de entrada, o tempo gasto para o ajuste dos coeficientes do filtro após o transitório na amplitude da carga é inferior a meio ciclo da fundamental.
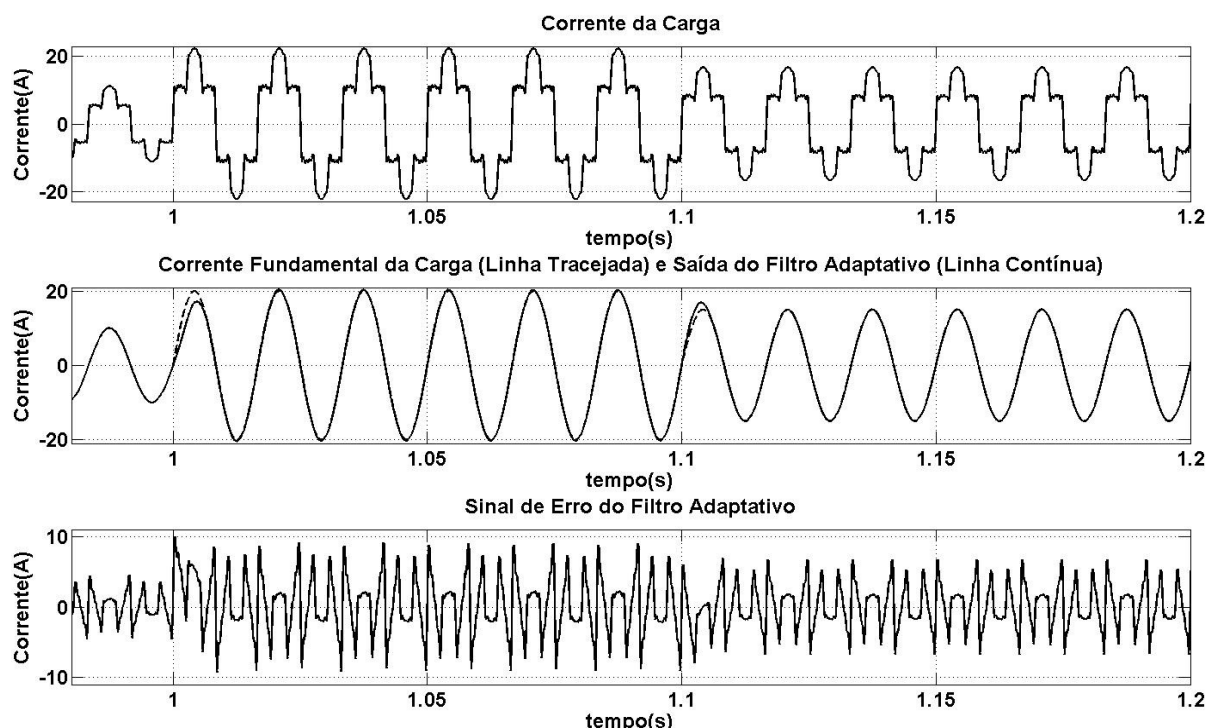
Figura 4.5: Sinal desejado, sinal de saída e sinal de erro do Filtro Adaptativo Sintonizado *LMS* com transitório.

A Figura 4.6 apresenta a comparação entre a corrente fundamental da carga e a corrente fundamental gerada pelo Filtro Adaptativo, juntamente com o erro entre estes dois sinais. Já a Figura 4.7 demonstra o resultado da compensação com a corrente harmônica gerada.
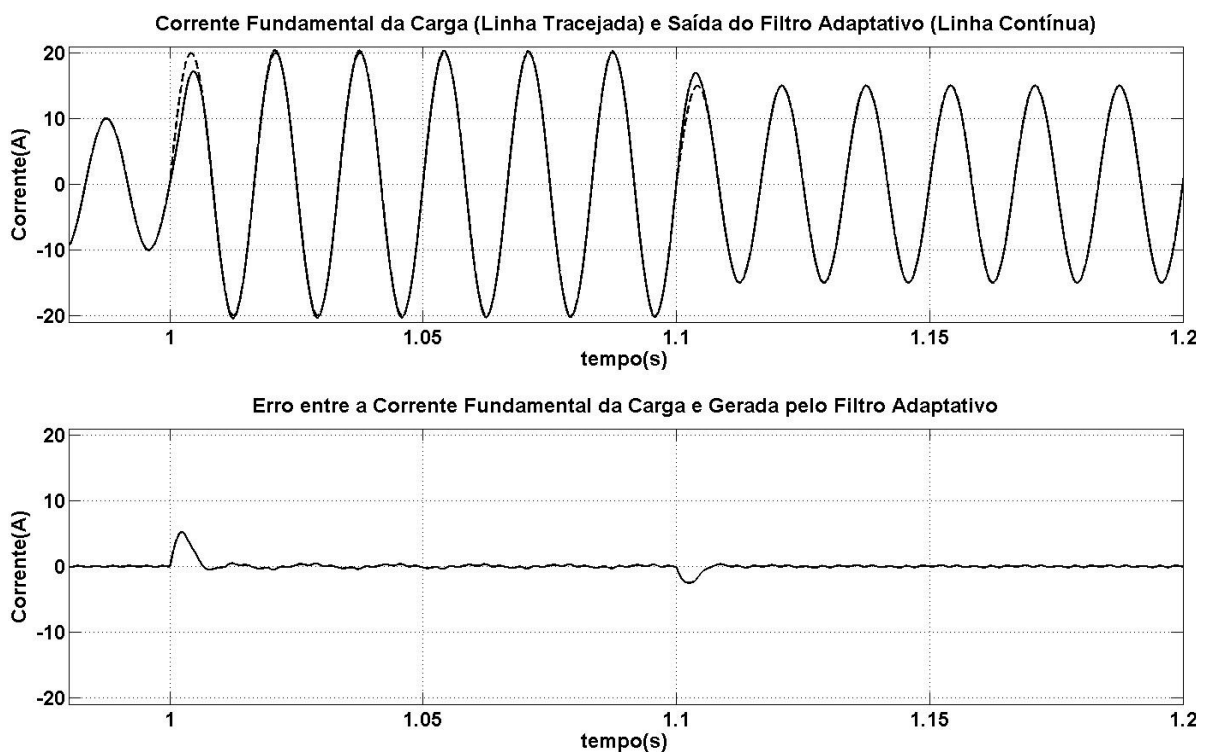
Figura 4.6: Comparação entre a corrente fundamental da carga e a gerada pelo Filtro Adaptativo Sintonizado *LMS* com transitório.
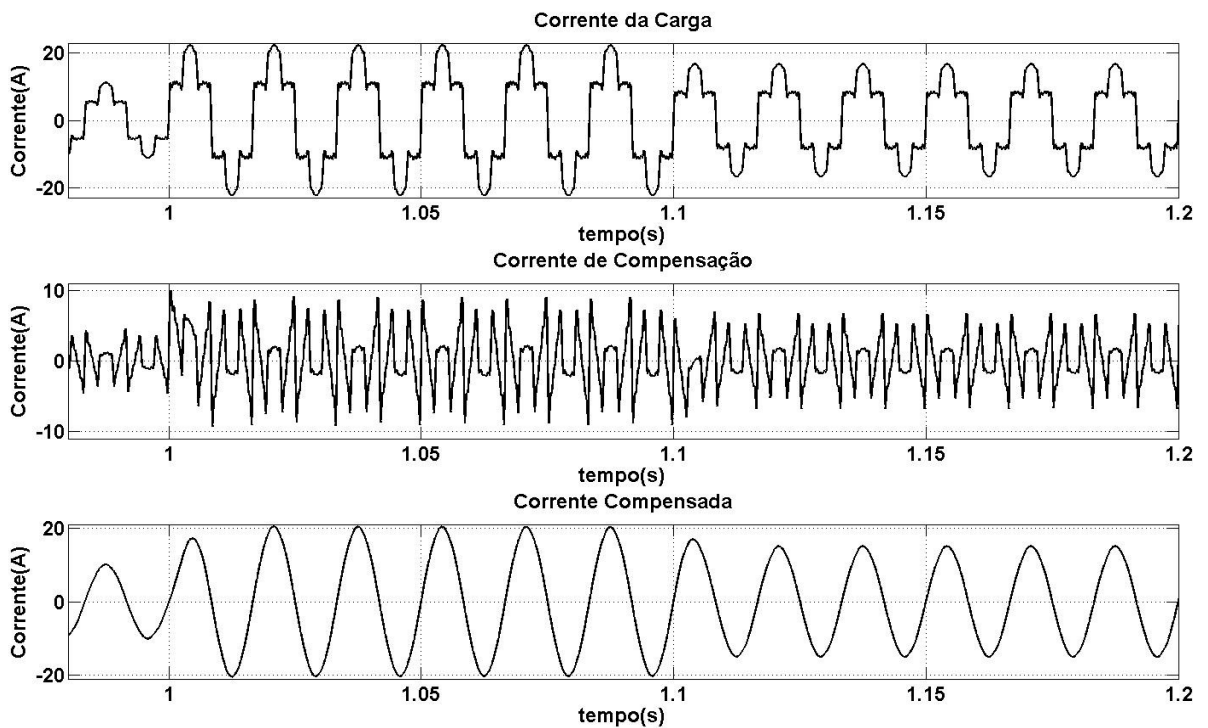
Figura 4.7: Resultado da compensação com transitório utilizando o Filtro Adaptativo Sintonizado *LMS*.

As próximas figuras apresentam uma alteração simultânea na amplitude e no conteúdo harmônico da corrente da carga, através da simulação do transitório de uma

carga linear para uma não-linear e vice-versa. As Figuras Figura 4.8, Figura 4.9 e Figura 4.10 ilustram o comportamento do algoritmo quando ocorre a transição de um sinal apenas com a componente fundamental para um sinal com a componente fundamental (com aumento de 100% na sua amplitude) e componentes harmônicos na corrente da carga.
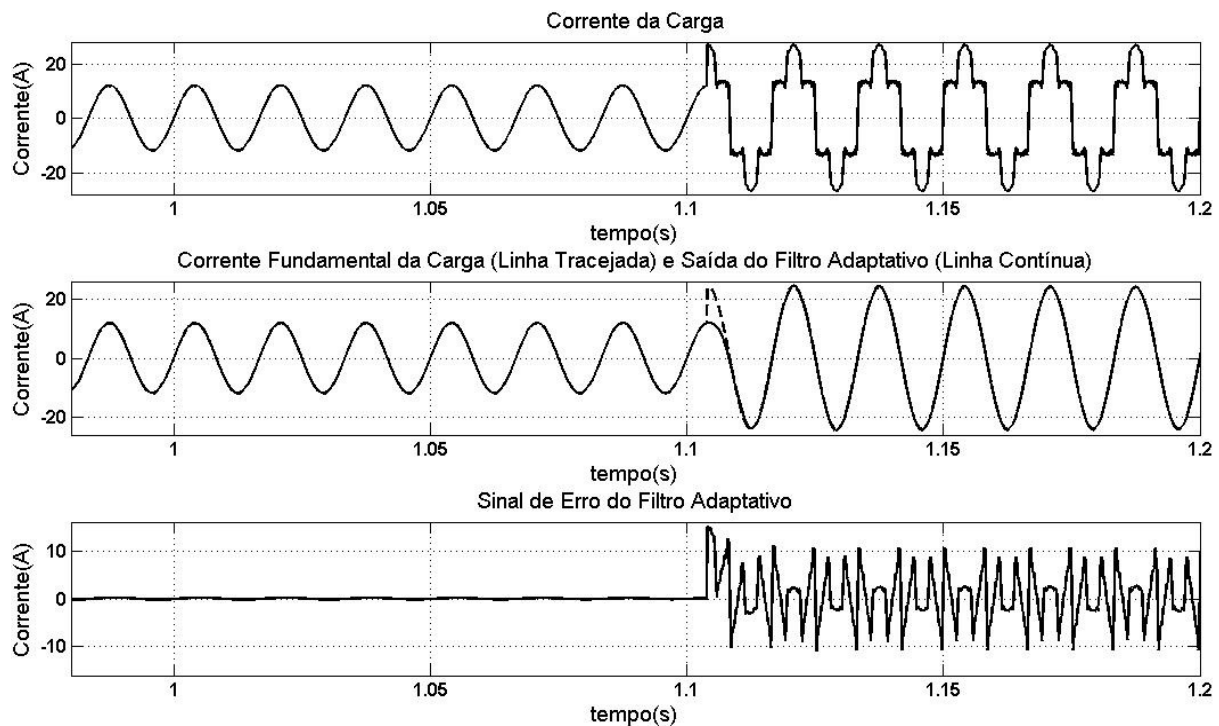
Figura 4.8: Sinal desejado, sinal de saída e sinal de erro do Filtro Adaptativo Sintonizado *LMS* com uma alteração na corrente da carga de linear para não-linear.
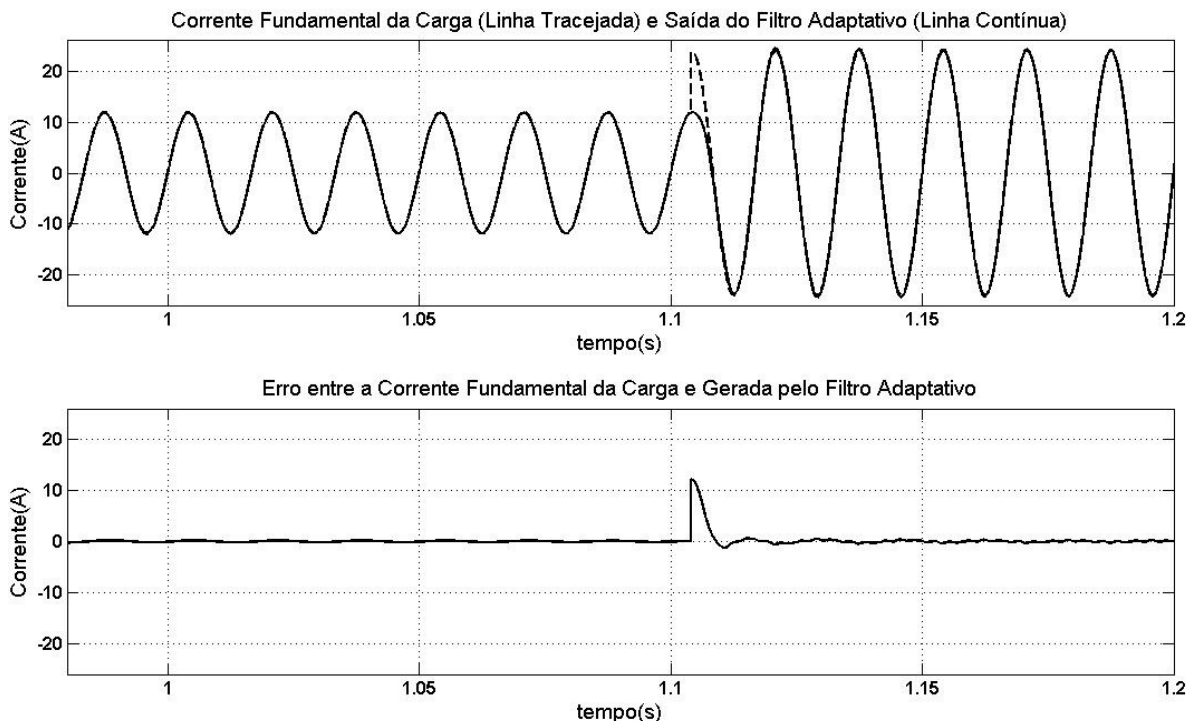
Figura 4.9: Comparação entre a corrente fundamental da carga e a gerada pelo Filtro Adaptativo Sintonizado *LMS* com uma alteração na corrente da carga de linear para não-linear.
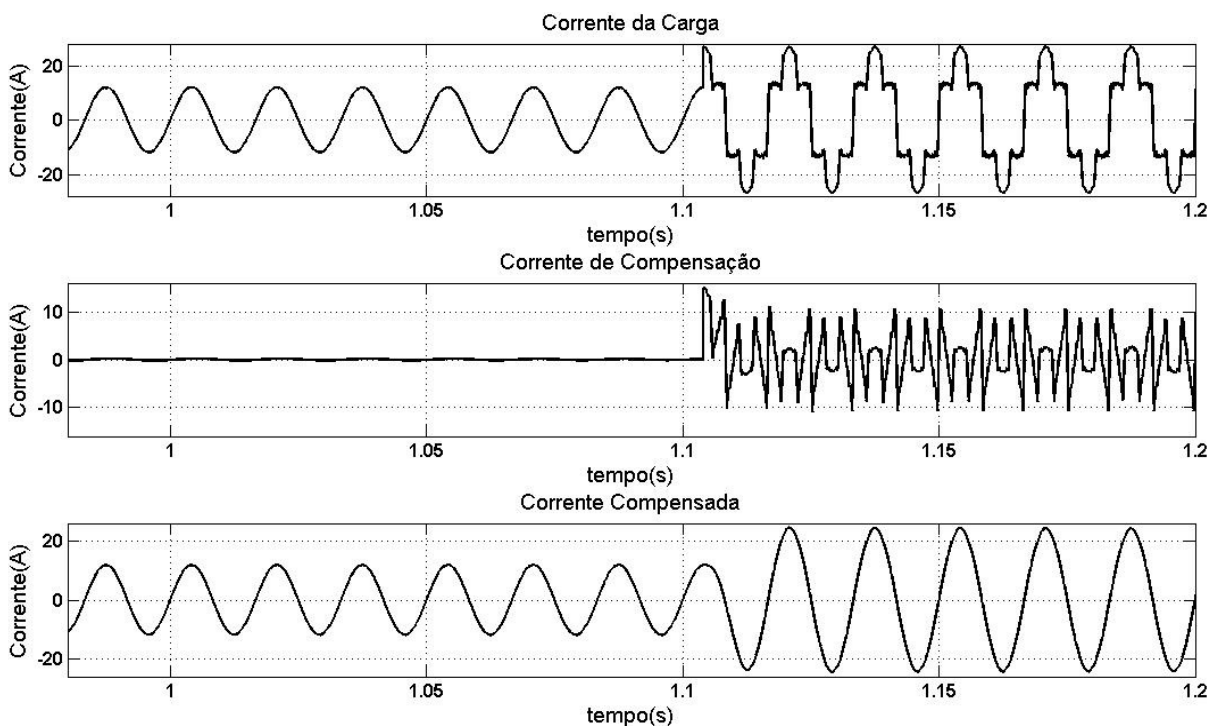
Figura 4.10: Resultado da compensação com transitório utilizando o Filtro Adaptativo Sintonizado *LMS* com uma alteração na corrente da carga de linear para não-linear.

As Figuras Figura 4.11,Figura 4.12 e Figura 4.13 ilustram o comportamento do algoritmo quando ocorre a transição oposta a apresentada anteriormente na corrente da

carga, um sinal com a componente fundamental e componentes harmônicos para um sinal apenas com a componente fundamental (com aumento de 100% na sua amplitude).
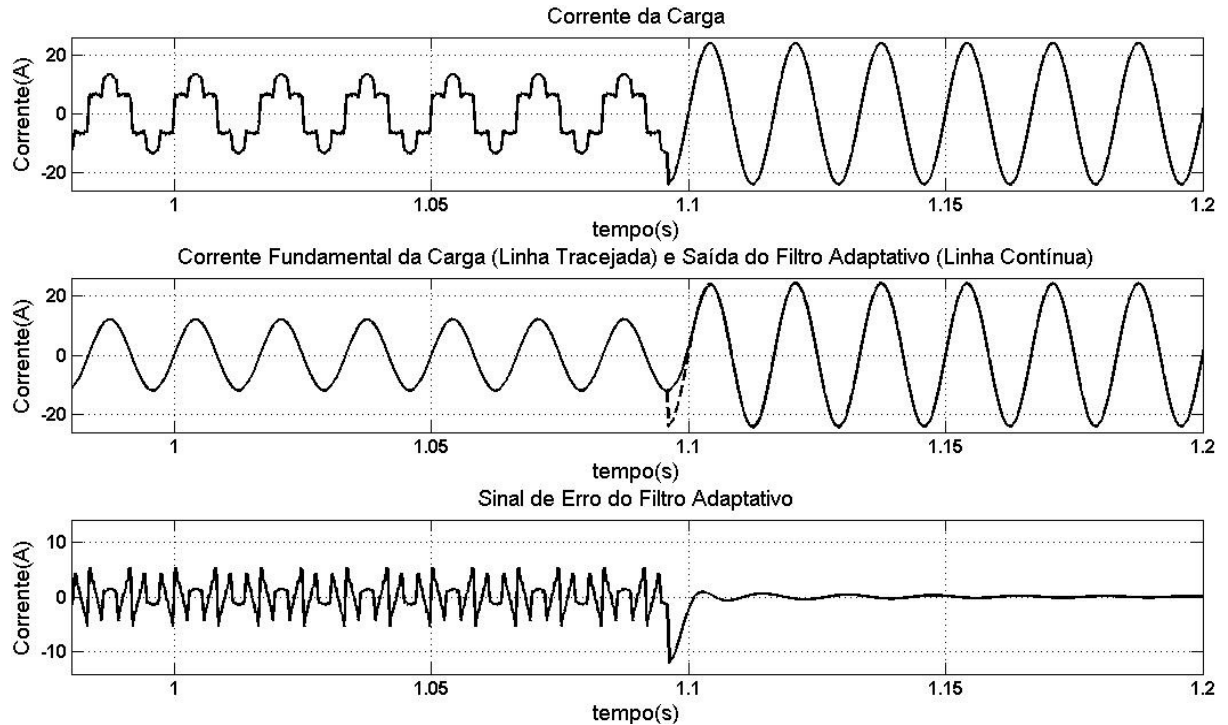
Figura 4.11: Sinal desejado, sinal de saída e sinal de erro do Filtro Adaptativo Sintonizado *LMS* com uma alteração na corrente da carga de não-linear para linear.
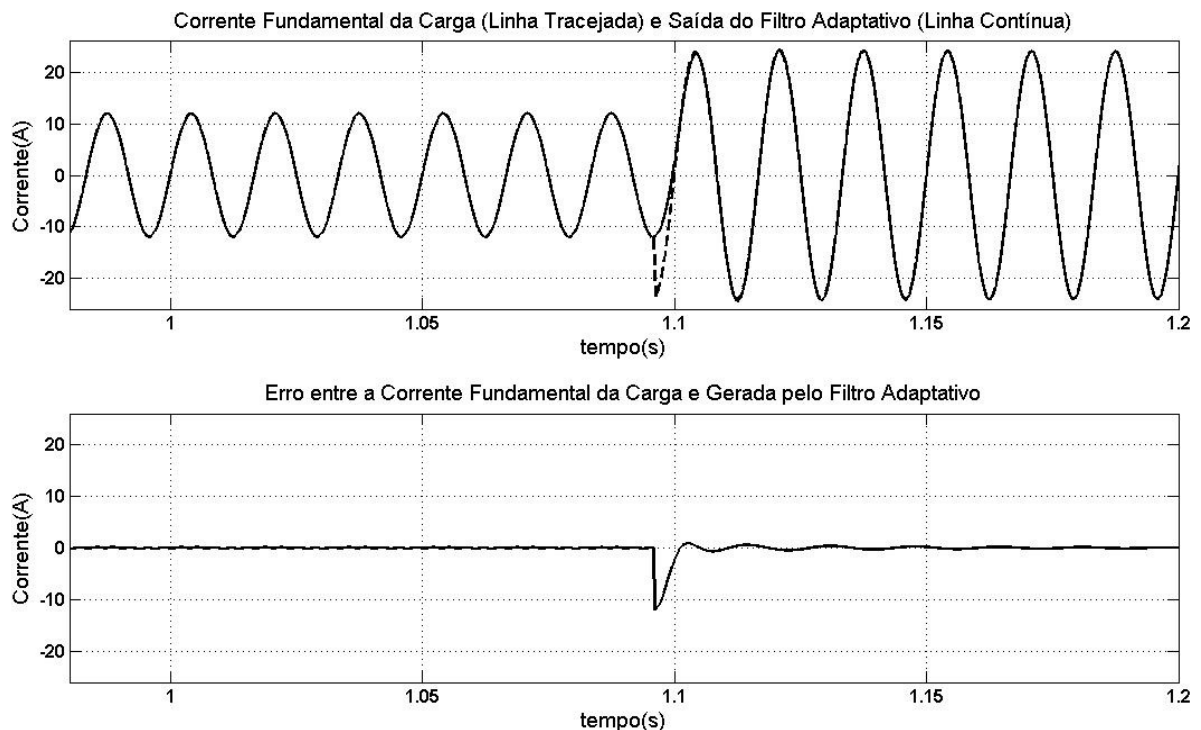
**Figura 4.12: Comparação entre a corrente fundamental da carga e a gerada pelo Filtro Adaptativo Sintonizado *LMS* com uma alteração na corrente da carga de não-linear para linear.**
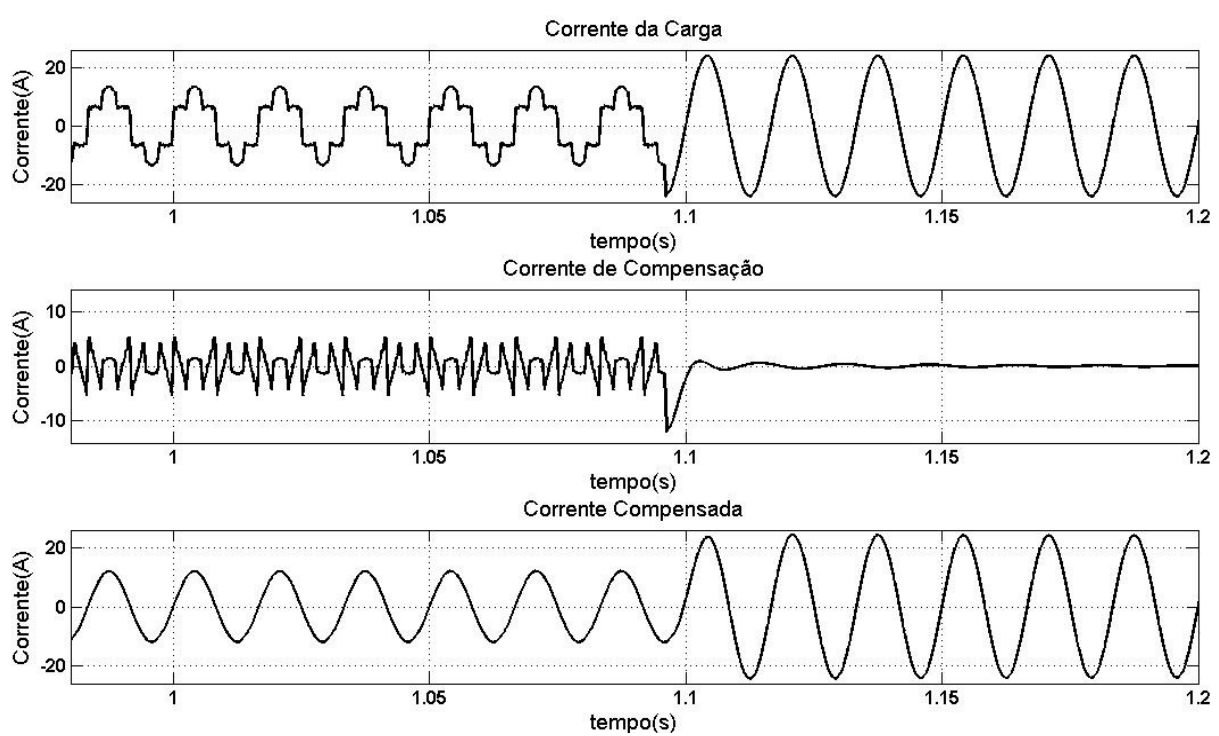
Figura 4.13: Resultado da compensação com transitório utilizando o Filtro Adaptativo Sintonizado *LMS* com uma alteração na corrente da carga de não-linear para linear.

4.2 Filtro Adaptativo Sintonizado com Algoritmo *RLS*

Os resultados apresentados nas próximas páginas deste capítulo são referentes à implementação do algoritmo da adaptação *Recursive Least Square* (*RLS*). Na Figura 4.14 estão contidos os sinais da corrente da carga, da componente fundamental da corrente da carga juntamente com a saída do Filtro Adaptativo e o sinal de erro do Filtro Adaptativo.

A comparação entre a componente fundamental da corrente da carga com a gerada pelo filtro adaptativo está na Figura 4.15.

Nas Figuras Figura 4.16 e Figura 4.17, a forma de onda e espectro harmônico da corrente compensada, demonstram a correta compensação do conteúdo harmônico da corrente da carga.
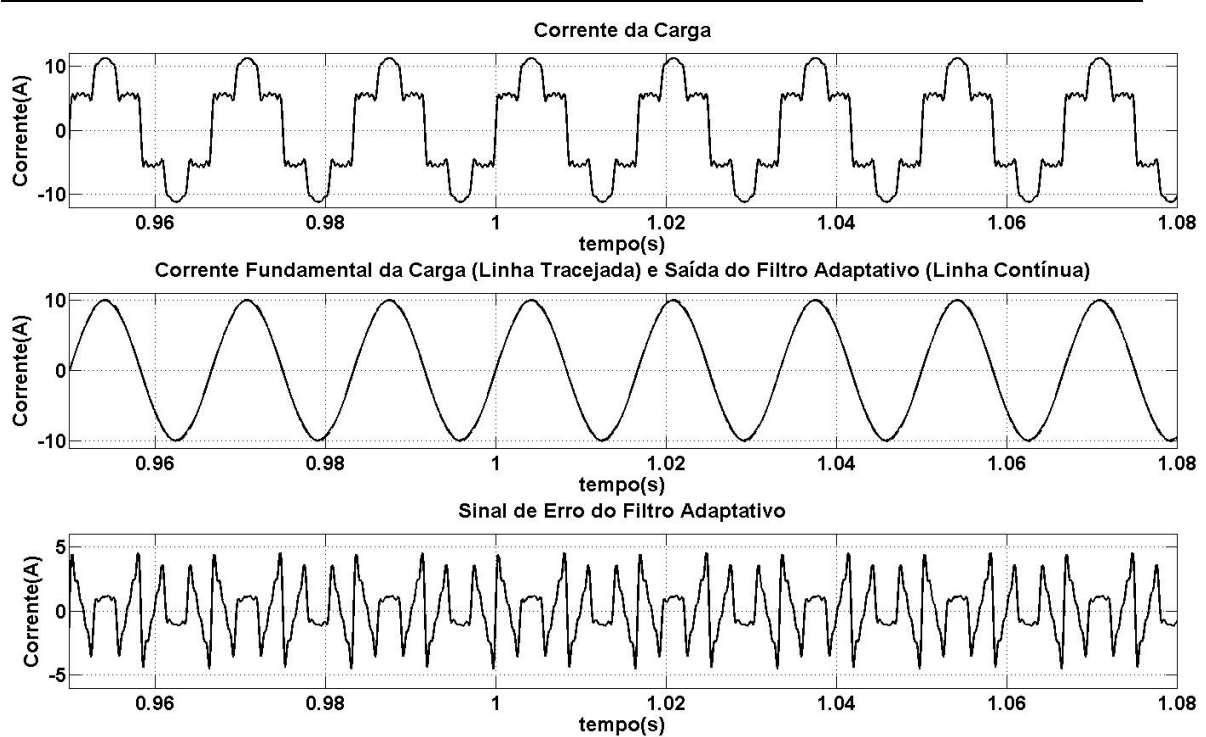
Figura 4.14: Sinal desejado, sinal de saída e sinal de erro do Filtro Adaptativo Sintonizado *RLS* em regime permanente.
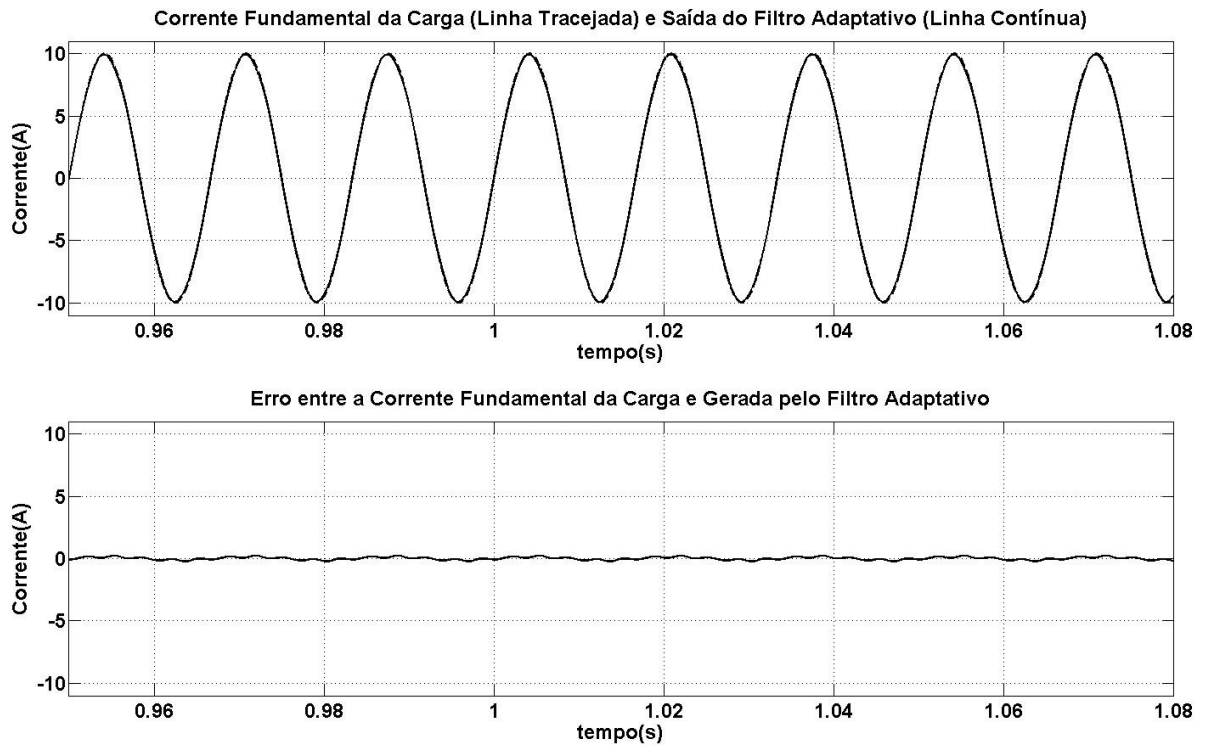
Figura 4.15: Comparação entre a corrente da fundamental da carga e a gerada pelo Filtro Adaptativo Sintonizado *RLS* em regime permanente.
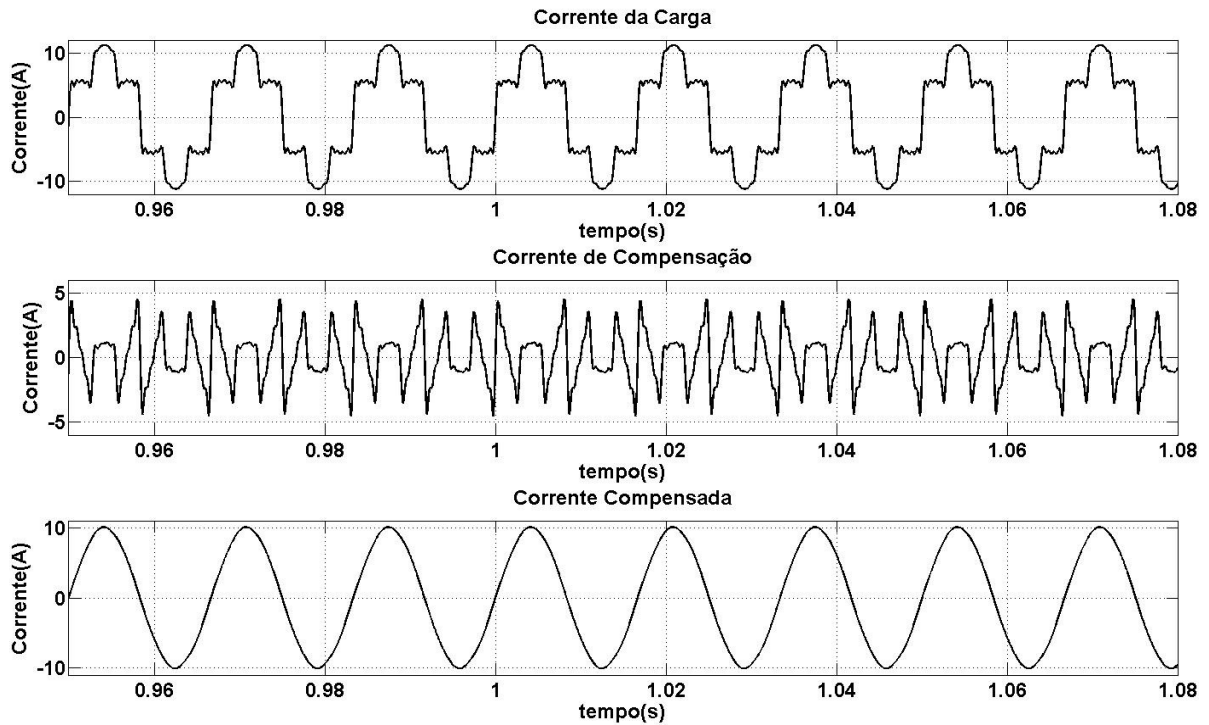
Figura 4.16: Resultado da compensação em regime permanente com Filtro Adaptativo Sintonizado *RLS*.
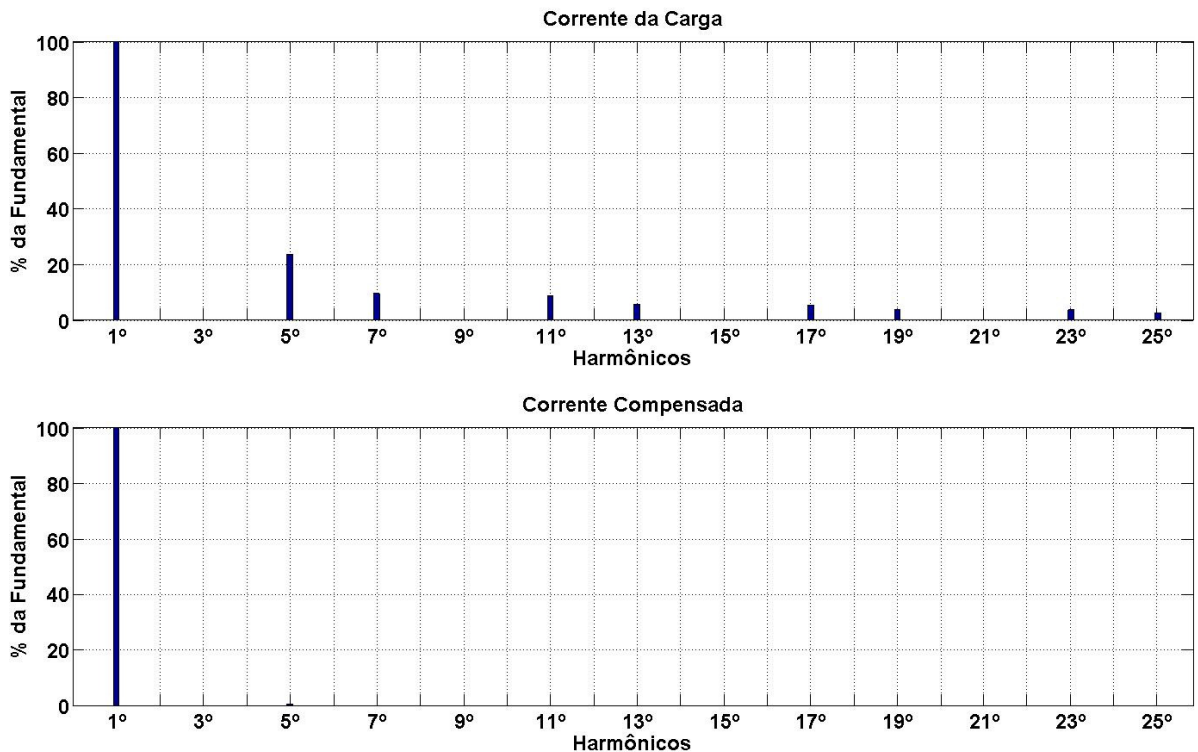
Figura 4.17: Espectro harmônico da corrente da carga e corrente compensada com Filtro Adaptativo Sintonizado *RLS*.

As próximas simulações apresentam transitórios no valor da amplitude da corrente da carga. Nestas simulações, foi aplicado à amplitude da corrente da carga um aumento de 100% de seu valor e em seguida um decréscimo de 25%.

A Figura 4.18 mostra a corrente da carga, a corrente fundamental da carga juntamente com o sinal de saída do Filtro Adaptativo Sintonizado e o sinal de erro. Após o transitório na amplitude da corrente da carga o tempo gasto para o ajuste dos coeficientes do filtro foi inferior a meio ciclo da fundamental.

A Figura 4.19 apresenta a comparação entre a corrente fundamental da carga e a corrente fundamental gerada pelo Filtro Adaptativo, juntamente com o erro entre estes dois sinais. Já a Figura 4.20 demonstra o resultado da compensação com a corrente harmônica gerada.
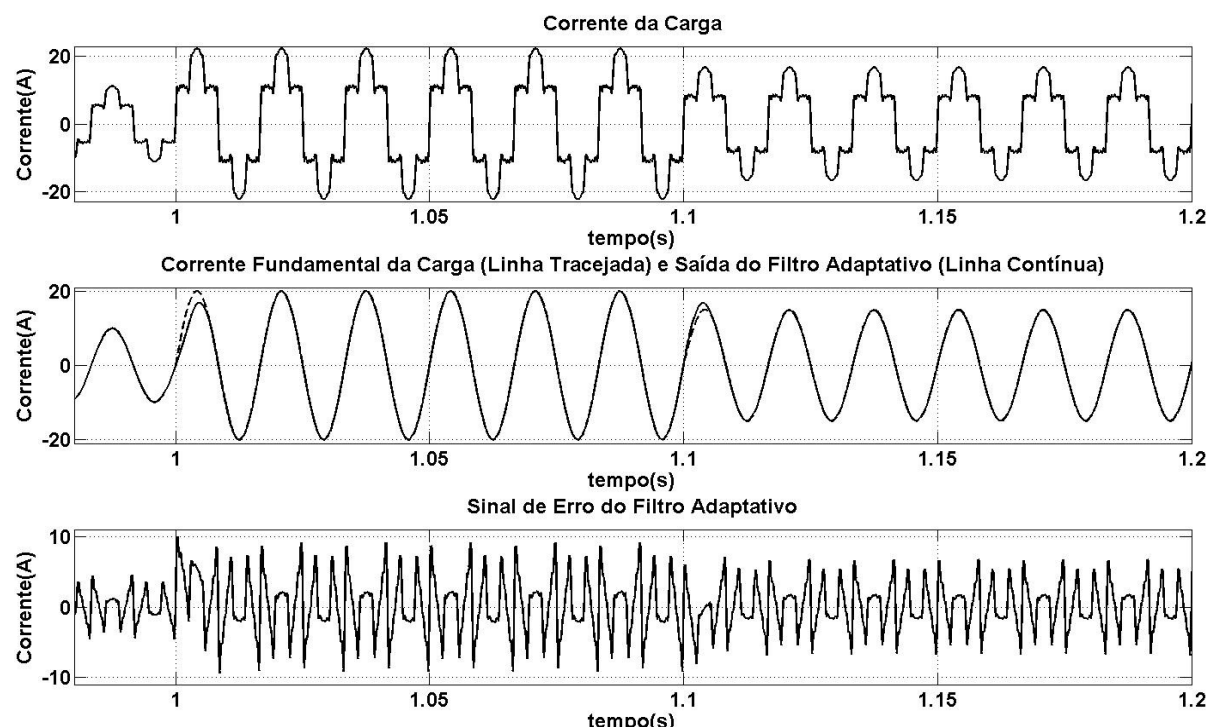
**Figura 4.18: Sinal desejado, sinal de saída e sinal de erro do Filtro Adaptativo Sintonizado *RLS* com transitório.**
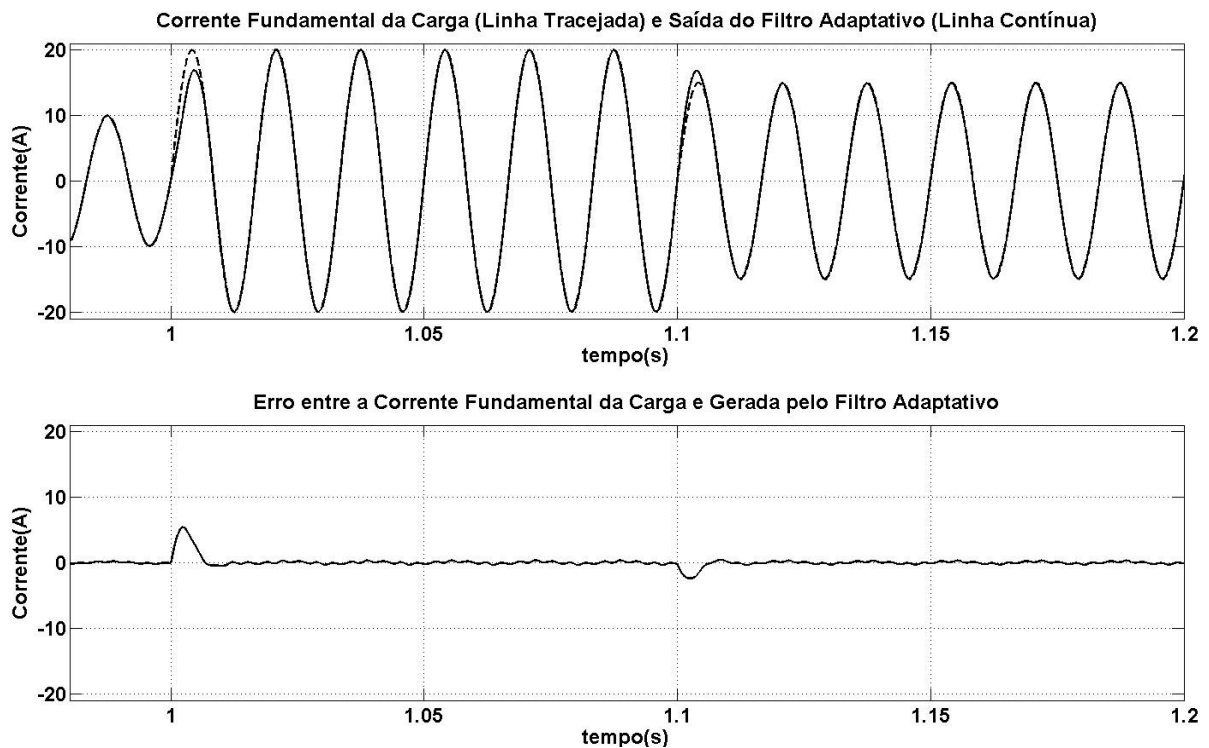
Figura 4.19: Comparação entre a corrente fundamental da carga e a gerada pelo Filtro Adaptativo Sintonizado *RLS* com transitório.
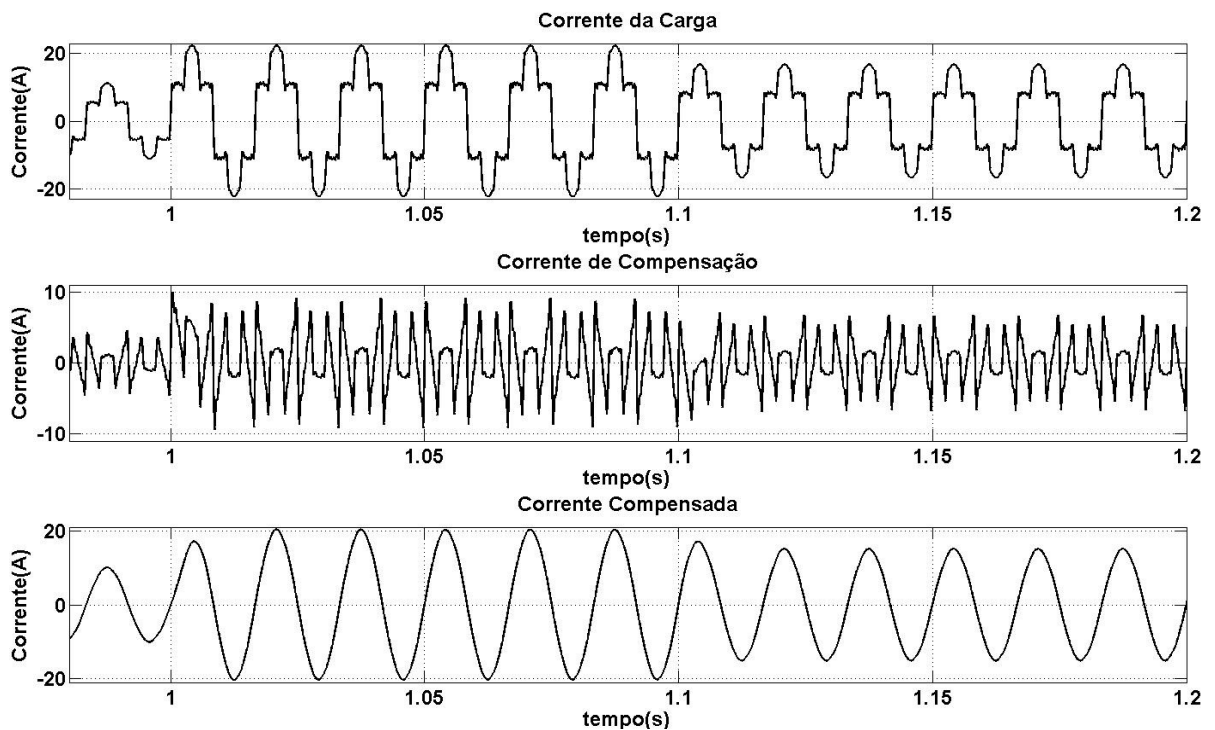

Figura 4.20: Resultado da compensação com transitório utilizando o Filtro Adaptativo Sintonizado *RLS*.

As próximas figuras apresentam uma alteração simultânea na amplitude e no conteúdo harmônico da corrente da carga, como demonstrado para o Filtro Adaptativo utilizando o algoritmo *LMS*. As Figuras Figura 4.21, Figura 4.22 e Figura 4.23 ilustram o comportamento do algoritmo quando ocorre a transição de um sinal apenas com a componente fundamental para um sinal com a componente fundamental (com aumento de 100% na sua amplitude) e componentes harmônicos na corrente da carga.
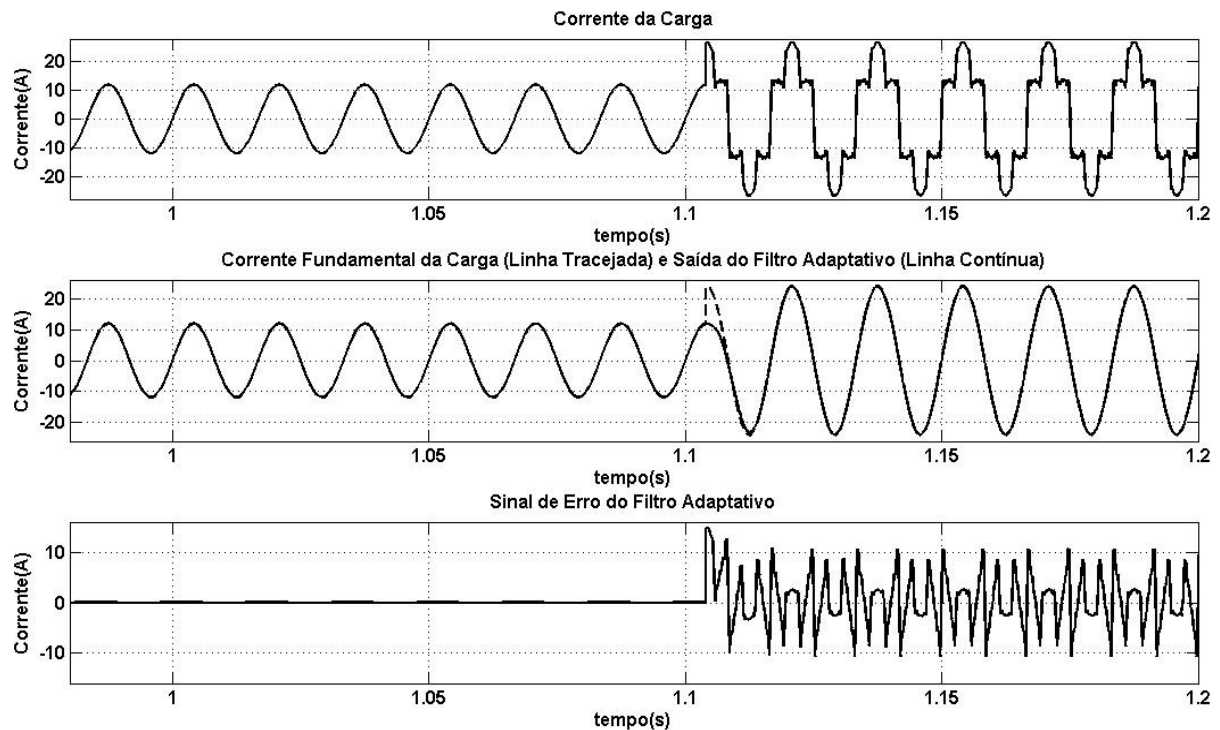

Figura 4.21: Sinal desejado, sinal de saída e sinal de erro do Filtro Adaptativo Sintonizado *RLS* com uma alteração na corrente da carga de linear para não-linear.
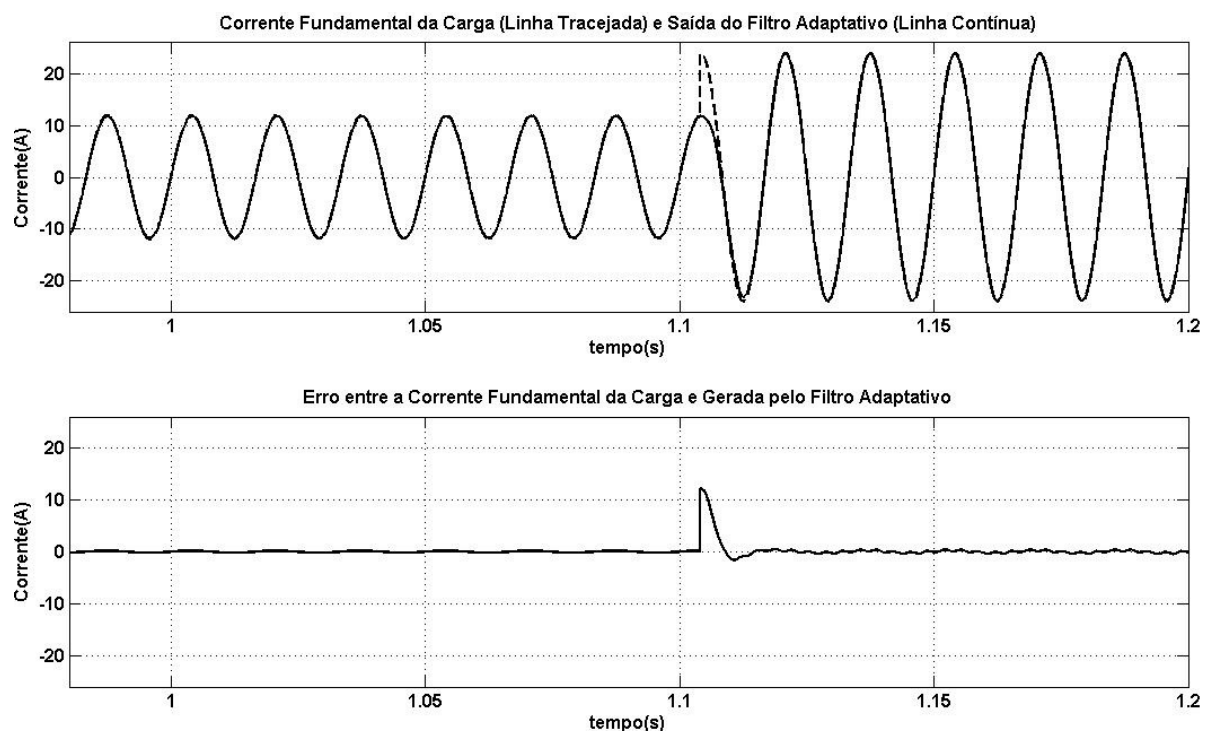
Figura 4.22: Comparação entre a corrente fundamental da carga e a gerada pelo Filtro Adaptativo Sintonizado *RLS* com uma alteração na corrente da carga de linear para não-linear.
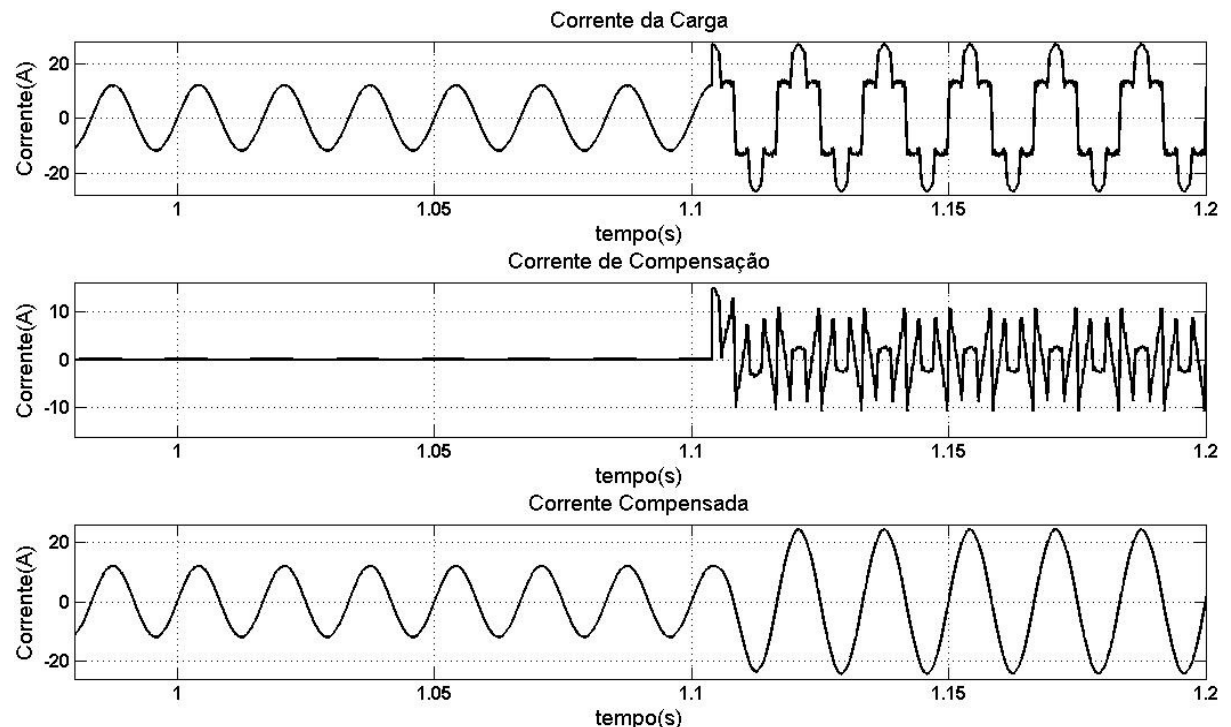

Figura 4.23: Resultado da compensação com transitório utilizando o Filtro Adaptativo Sintonizado *RLS* com uma alteração na corrente da carga de linear para não-linear.

As Figuras Figura 4.24, Figura 4.25 e Figura 4.26 ilustram o comportamento do algoritmo *RLS* quando ocorre um transitório de uma carga não-linear para uma carga linear. Ou seja, uma variação do conteúdo harmônico.
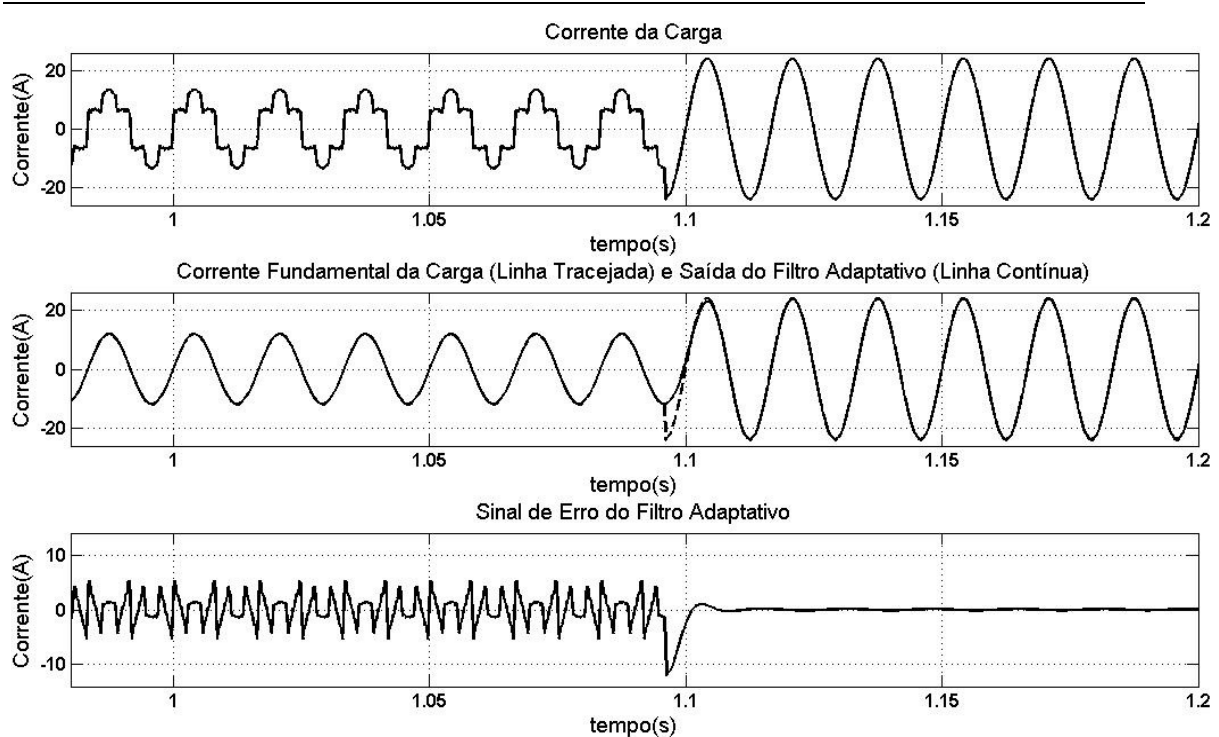
Figura 4.24: Sinal desejado, sinal de saída e sinal de erro do Filtro Adaptativo Sintonizado *RLS* com uma alteração na corrente da carga de não-linear para linear.
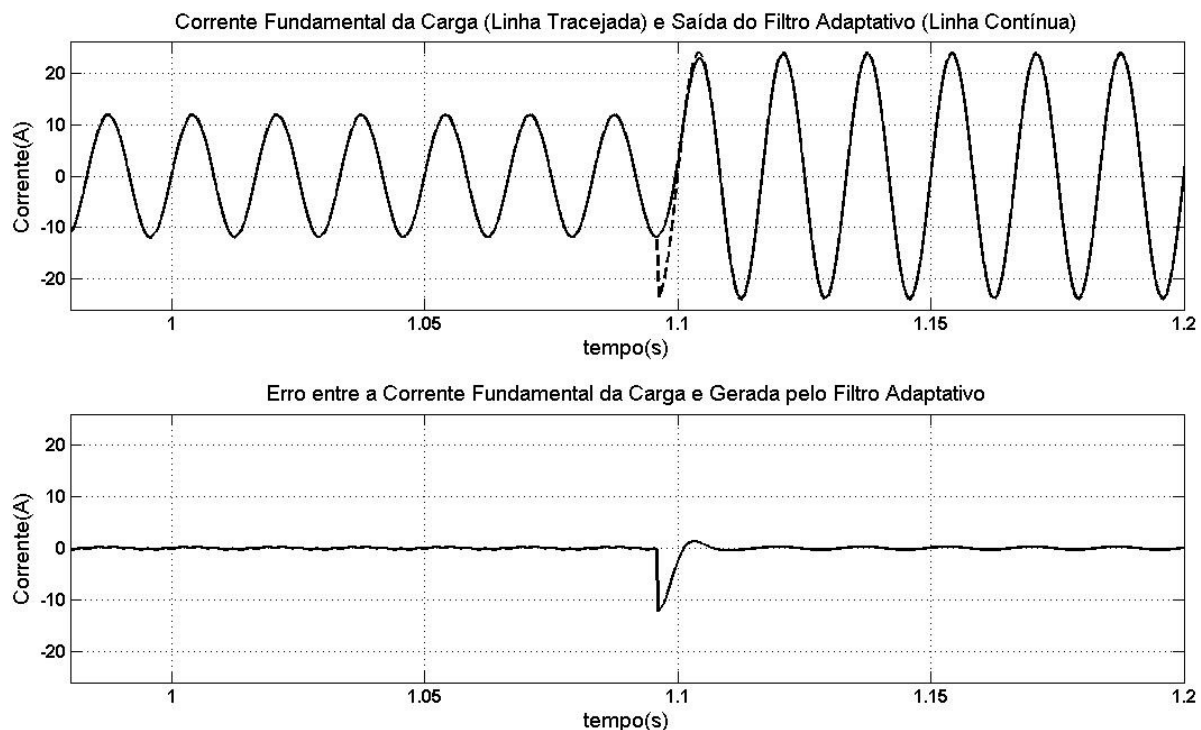

Figura 4.25: Comparação entre a corrente fundamental da carga e a gerada pelo Filtro Adaptativo Sintonizado *RLS* com uma alteração na corrente da carga de não-linear para linear.

46
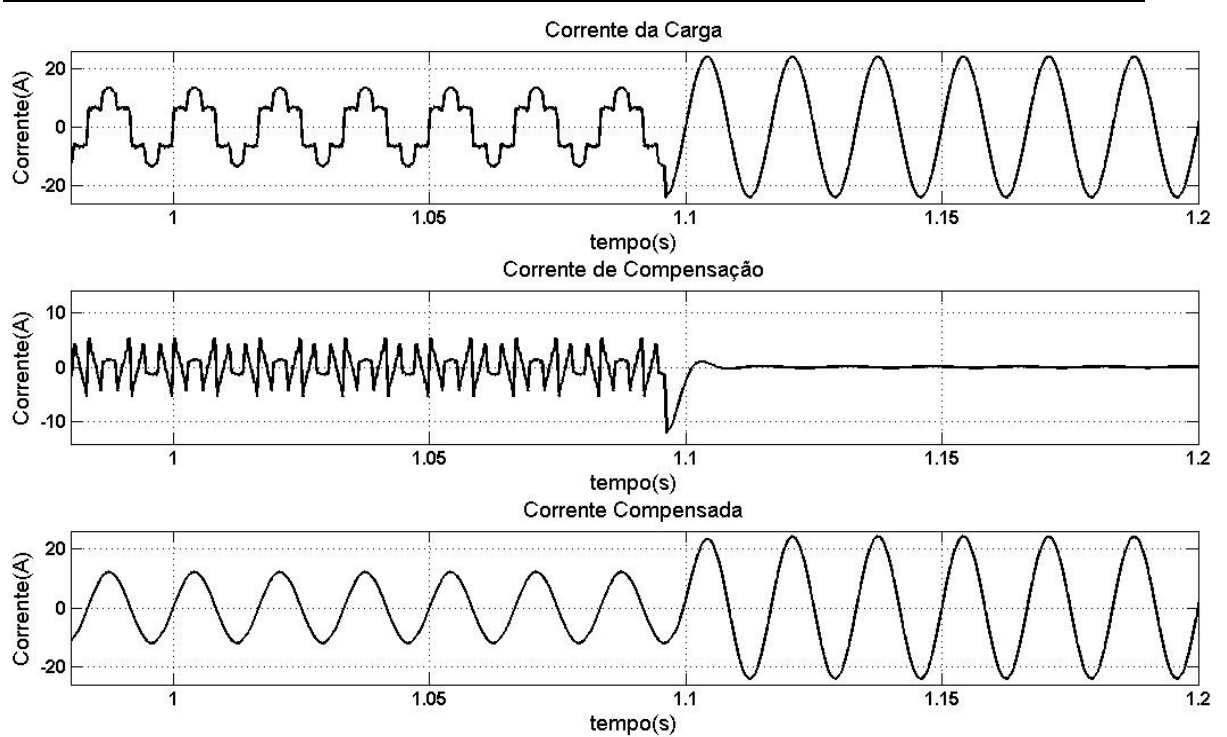
**Figura 4.26: Resultado da compensação com transitório utilizando o Filtro Adaptativo Sintonizado
RLS com uma alteração na corrente da carga de não- linear para linear.**

As simulações realizadas com o Filtro Adaptativo Sintonizado demonstraram uma resposta em regime permanente aceitável e uma adaptação dos coeficientes do Filtro Adaptativo inferior a meio ciclo da fundamental. Este tempo de convergência foi alcançado com os dois tipos de algoritmos de adaptação, tanto o *Least Mean Square* como o *Recursive Least Square*.

As expectativas iniciais com o uso da transformada de *Clarke* para gerar os sinais ortogonais de entrada foram confirmadas através destas simulações. Pois, os sinais ortogonais senoidais provenientes da filtragem dos sinais $I_{L\alpha}$ e $I_{L\beta}$ conseguem seguir a variação de amplitude da corrente da carga. Assim, uma significativa melhora na resposta transitória do algoritmo é obtida.

4.3 Conclusões do Capítulo

Tanto o algoritmo *LMS* quanto o *RLS* apresentaram resultados idênticos e condizentes com o proposto inicialmente neste trabalho, um tempo de convergência inferior a um ciclo da componente fundamental. Nestas simulações, que levaram em

consideração apenas o comportamento do algoritmo (desprezando tempo gasto na amostragem, os circuitos de condicionamento de sinal e o inversor de freqüência), o tempo de convergência foi de aproximadamente 8ms.

O algoritmo *RLS* apresenta uma resposta em regime permanente um pouco superior comparada a do algoritmo *LMS*. Mas como o gasto computacional do algoritmo *LMS* é inferior, este algoritmo demonstra ser a escolha mais adequada como algoritmo de adaptação para os dois coeficientes do Filtro Adaptativo Sintonizado.

Outro aspecto relevante, mencionado neste trabalho e não encontrado na literatura, é sobre o erro em regime permanente entre o sinal gerado pelo Filtro Adaptativo e o sinal da componente fundamental na corrente da carga. Os resultados de simulação deste capítulo apresentam este erro, que é de aproximadamente 1% da amplitude da componente fundamental.

Buscando uma atenuação no valor deste erro, foi proposto o algoritmo descrito no Apêndice B em que o valor do erro caiu para 0,1% da amplitude da componente fundamental da corrente da carga.

No próximo capítulo, serão apresentados os resultados experimentais da aplicação da técnica de detecção de harmônicos com o Filtro Adaptativo Sintonizado em um Filtro Ativo Paralelo Trifásico. Em que o conteúdo harmônico extraído pela técnica com Filtros Adaptativos foi utilizado como referência para a corrente de compensação.

5 Resultados Experimentais

Neste capítulo serão apresentados os resultados da aplicação da técnica de detecção de harmônicos com Filtros Adaptativos no controle de um Filtro Ativo de Potência Paralelo (FAPP). O sistema de controle implementado no *DSP* TMS320F2812 é ilustrado na Figura 5.1, constituído por cinco blocos: Controle Harmônico, *MSRF-PLL*, Controle do *Link DC*, Sinal de Referência do FAP e *PWM*.
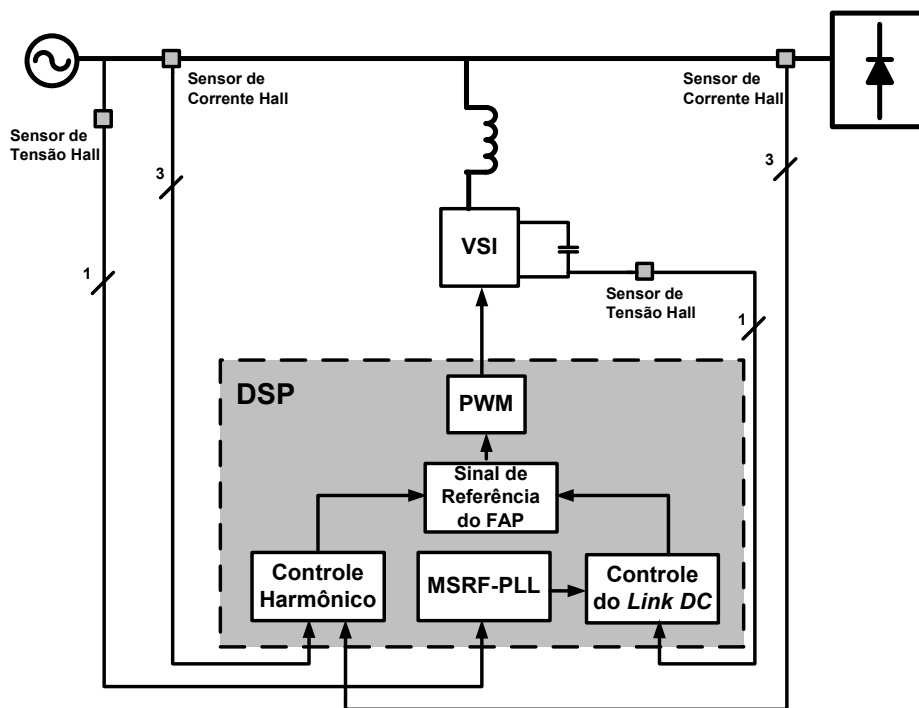
Figura 5.1: Estrutura geral de um Filtro Ativo de Potência Paralelo.

O bloco Controle Harmônico é a parte deste sistema de controle em que é gerada a referência harmônica utilizada como corrente de compensação. Portanto, é nesta parte do sistema em que a técnica de detecção de harmônicos com Filtros Adaptativos é utilizada.

O bloco *MSRF-PLL* (*Modified Synchronous Reference Frame – Phase Locked Loop*) é responsável por gerar o sincronismo do FAP com a tensão da fonte. Os sinais em fase com a tensão da fonte gerados por este bloco são utilizados no bloco Controle do *Link DC*.

Para manter o valor da tensão contínua, armazenada nos capacitores do inversor de freqüência em um valor pré-estabelecido, é necessário realizar um controle sobre a mesma, sendo esta a função do bloco Controle do *Link DC*.

A soma dos sinais gerados nos blocos Controle Harmônico e Controle do *Link DC* é realizada no bloco Sinal de Referência do FAP, que por sua vez envia este sinal resultante para o bloco PWM. No bloco PWM são produzidos os pulsos para o controle dos semicondutores no inversor de freqüência, gerando assim a corrente harmônica para compensação.

O algoritmo de controle do FAAP foi implementado no Processador Digital de Sinal TMS320F2812 utilizando a linguagem de programação C, sendo o *DSP* configurado para trabalhar com uma freqüência de amostragem de 40kHz.

A Figura 5.2 apresenta uma fotografia do FAPP utilizado nos experimentos. O Filtro Ativo Paralelo ou *Shunt* é composto por 3 inversores fonte de tensão (do inglês *Voltage Source Inverter – VSI*) de 35kVA, trabalhando em uma freqüência de chaveamento de 40kHz. A tensão do *link DC* foi ajustada em 400V. Foi usado um indutor de 5mH para conectar o FAPP no sistema de potência, sendo a tensão do sistema de 220V.

A carga não-linear utilizada foi um retificador de 6 pulsos, tipo *CSI* (do inglês, *Current Source Inverter*), de 100kVA. A Figura 5.3 ilustra a fotografia da carga trifásica não-linear.

Os sensores *Hall* de tensão e corrente e a parte frontal do Filtro Ativo *Shunt* com as placas de condicionamento de sinal, inversor *VSI* e *DSP* TMS320F2812 estão presentes nas fotografias das Figuras Figura 5.4 e Figura 5.5.

Figura 5.2: Foto frontal do FAPP utilizado nos testes experimentais.

Figura 5.3: Carga não-linear utilizada no experimento.
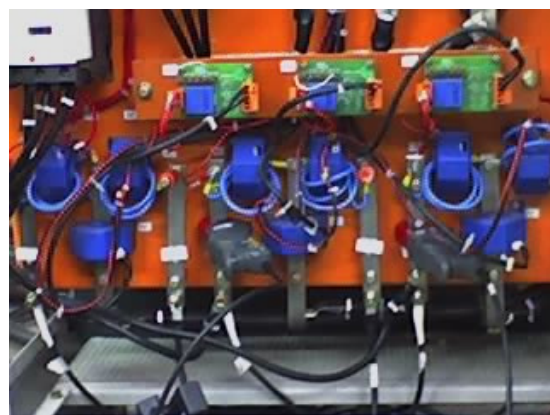
Figura 5.4: Sensores *Hall* de tensão e corrente utilizados no FAPP.
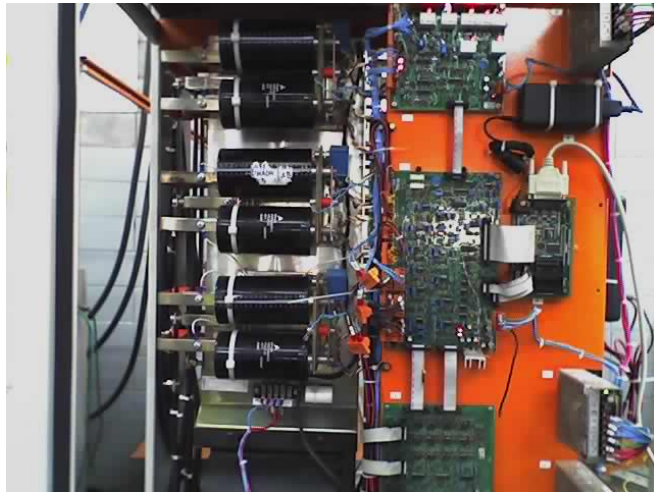
Figura 5.5: Placas de condicionamento de sinal, inversor VSI e placa com o DSP TMS320F2812.

Nas próximas páginas, deste capítulo, serão apresentados os resultados da aplicação da técnica de detecção de harmônicos, com Filtros Adaptativos, no algoritmo de controle do FAPP descrito acima.

A medida utilizada para avaliar o conteúdo harmônico em um sinal de corrente é a Distorção Harmônica Total da Corrente, *THDi*, medida esta relativa ao valor da corrente fundamental do sistema, e expressa por:

$$THDi = \frac{\sqrt{\sum_{h=2}^{\infty} I_h{}^2}}{I_f} \cdot 100\% \qquad (5.1)$$

Ao ocorrer a compensação do conteúdo harmônico, conseqüentemente, o valor desta medida diminui. Sendo assim, a *THDi* da corrente da fonte é utilizado como parâmetro na avaliação do desempenho do Filtro Ativo de Potência.

Os testes foram realizados para uma amplitude da corrente da carga de 19,2A RMS.

Inicialmente serão apresentados os resultados obtidos com um Filtro Adaptativo Sintonizado com algoritmo *LMS* e posteriormente os resultados com o Filtro Adaptativo Sintonizado com algoritmo *RLS*. Um transitório da amplitude da corrente da carga de 6,5A para 12,8A, ou seja, uma variação de aproximadamente 100% é utilizada para validação do tempo de convergência obtido na simulação. Uma alteração no conteúdo harmônico com uma transição entre uma carga linear para uma não-linear também é utilizada para verificação do tempo de convergência com o algoritmo *LMS*.

5.1 Filtro Adaptativo Sintonizado *LMS*

Os resultados da implementação da extração de harmônicos utilizando o Filtro Adaptativo Sintonizado com o algoritmo *LMS* serão abordados nesta seção. Como mencionado no Capítulo 3, para o Filtro Adaptativo Sintonizado são necessárias duas entradas ortogonais e apenas dois coeficientes. Desta maneira, foi necessário gerar dois sinais senoidais com deslocamento de fase de 90°, um em relação ao outro.

Esta tarefa pode ser realizada de uma maneira simples com o uso da transformada de *Clarke* e posterior filtragem dos sinais ortogonais de saída, $I_{L\alpha}$ e $I_{L\beta}$, gerados pela transformada. A utilização da Transformada de *Clarke* diretamente na corrente da carga e posterior filtragem dos sinais ortogonais permite que os sinais $x(n)$ e $x_{90°}(n)$ sigam a variação de amplitude da corrente da carga. Desta maneira, a velocidade de convergência do algoritmo é significativamente melhorada.

A seguir serão apresentados os resultados dos testes para uma corrente da carga de 19,2A, um caso de transitório na amplitude da corrente da carga e variação do conteúdo harmônico.

A corrente da carga para as três fases é apresentada na Figura 5.6. A corrente da carga, a corrente de compensação e a corrente da fonte, na fase A, são mostradas na Figura 5.7. Já na Figura 5.8 são apresentadas as correntes da fonte nas três fases com a compensação harmônica.

O espectro harmônico da corrente da fonte, com e sem o FAPP, é ilustrado pela Figura 5.9. O espectro mostra a amplitude de cada componente harmônico em relação a amplitude da fundamental e também a *THDi*. Demonstrando o correto decréscimo do conteúdo harmônico da corrente da fonte. Os valores numéricos deste decréscimo podem ser encontrados na Tabela 5.1.
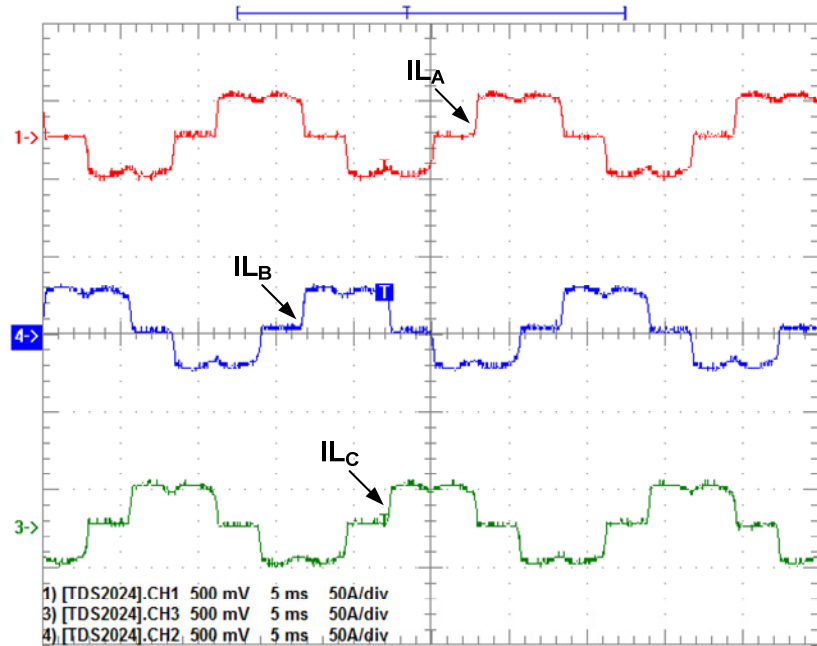
Figura 5.6: Corrente da carga de 19,2A *RMS* para fases as A, B e C.
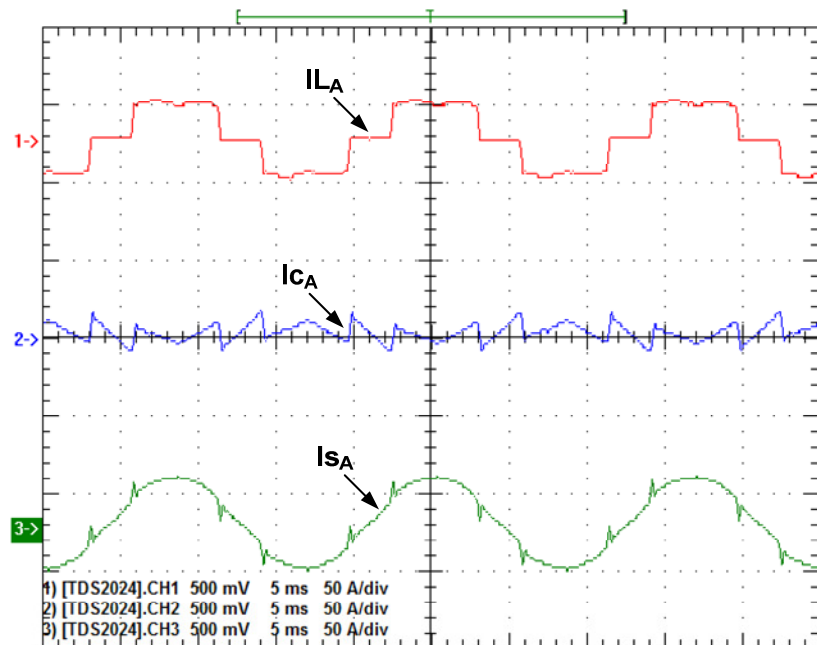
Figura 5.7: Corrente da carga, de compensação e da fonte, para I$_L$ com 19,2A *RMS*.
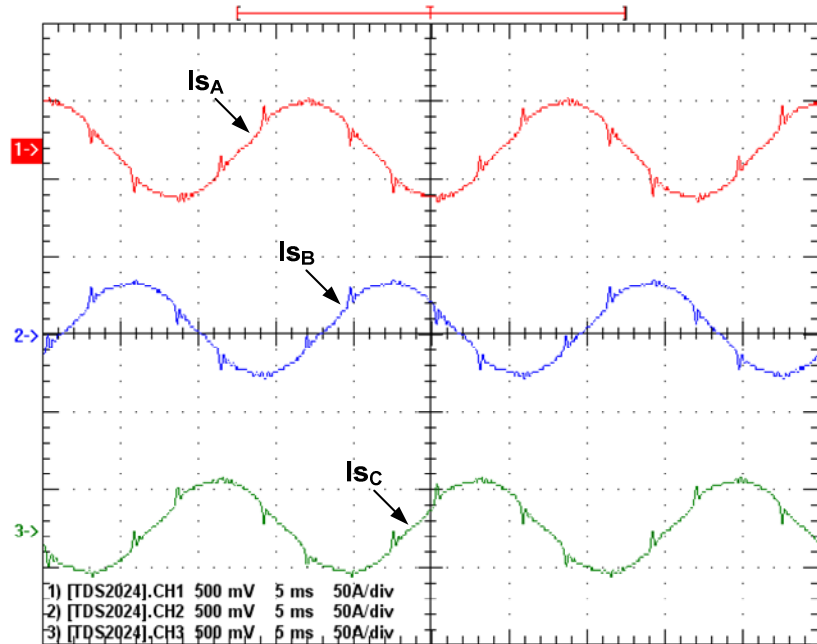
Figura 5.8: Corrente da fonte nas fases as A, B e C, para I$_L$ com 19,2A *RMS*.
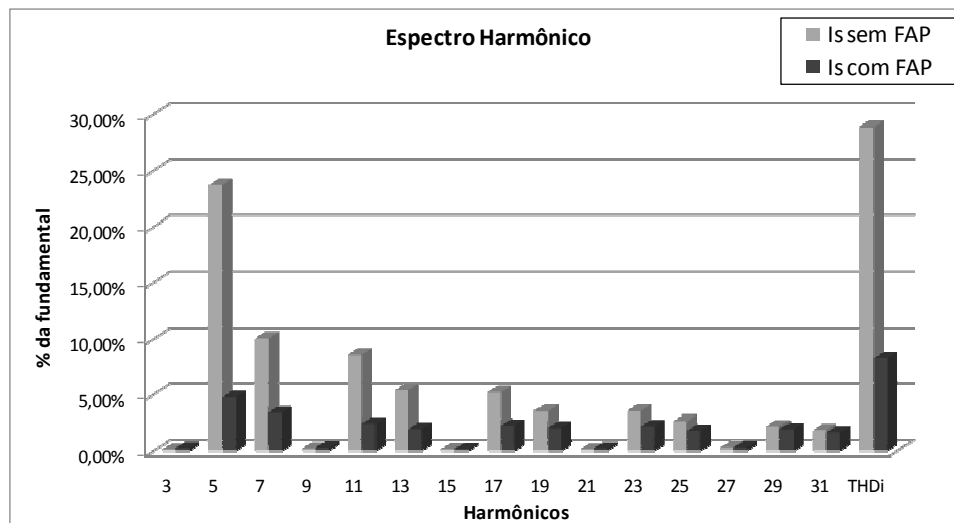
Figura 5.9: Espectro Harmônico da corrente da fonte para I$_L$ com 19,2A *RMS*.

Os valores na Tabela 5.1 mostram que a amplitude do 5° harmônico decresceu de 23,73% para 4,78% uma queda de 79,86%. A amplitude do 7° harmônico decresceu 66,60%, a do 11° harmônico decresceu 71,59%, a do 13° harmônico decresceu 63,45%, a do 17° harmônico decresceu 56,24%, a do 19° harmônico decresceu 41,36%, a do 23° harmônico decresceu 37,39% e a do 25° harmônico decresceu 31,95%.

Tabela 5.1: Corrente de cada componente harmônico, sem e com FAP, para I$_L$ com 19,2A *RMS*.

	I$_s$ sem FAP		I$_s$ com FAP	
	A *RMS*	% da fundamental	A *RMS*	% da fundamental
3º Harmônico	0,02601	0,14%	0,05722	0,27%
5º Harmônico	4,53210	23,73%	1,00430	4,78%
7º Harmônico	1,92760	10,09%	0,70764	3,37%
9º Harmônico	0,04132	0,22%	0,06249	0,30%
11º Harmônico	1,64100	8,59%	0,51339	2,44%
13º Harmônico	1,02860	5,39%	0,41352	1,97%
15º Harmônico	0,03070	0,16%	0,04082	0,19%
17º Harmônico	0,99549	5,21%	0,47868	2,28%
19º Harmônico	0,67343	3,53%	0,43519	2,07%
21º Harmônico	0,03000	0,16%	0,04956	0,24%
23º Harmônico	0,67426	3,53%	0,46507	2,21%
25º Harmônico	0,50876	2,66%	0,38036	1,81%
27º Harmônico	0,06112	0,32%	0,07100	0,34%
29º Harmônico	0,42160	2,21%	0,40947	1,95%
31º Harmônico	0,35883	1,88%	0,34877	1,66%

O *THDi* foi alterado de 28,9% para 8,29%, um decréscimo de 71,31%.

A queda no valor de *THDi* após a inserção do Filtro Ativo de Potência Paralelo demonstra a correta ação do mesmo. Comprovando a exatidão da referência harmônica produzida pelo método de detecção de harmônicos utilizando um Filtro Adaptativo Sintonizado.

➢ **Transitório na Amplitude da Corrente da Carga de 6,5A para 12,8A**

Os resultados anteriores demonstraram o correto funcionamento do Filtro Ativo de Potência Paralelo na compensação do conteúdo harmônico da corrente da fonte nas fases A, B e C. Comprovando assim, a eficiência da técnica de detecção de harmônicos com o uso de um Filtro Adaptativo Sintonizado, na geração do conteúdo harmônico da corrente de compensação produzida pelo FAPP.

Mas, como abordado nos capítulos anteriores, a velocidade de convergência do algoritmo de adaptação deve ser compatível com a necessidade do tipo de aplicação. Em um Filtro Ativo de Potência essa convergência deve ocorrer no menor tempo possível.

A utilização da Transformada de *Clarke* diretamente na corrente da carga e posterior filtragem dos sinais ortogonais permite que os sinais $x(n)$ e $x_{90°}(n)$ sigam a variação de amplitude da corrente da carga. Sendo assim, a velocidade de convergência do algoritmo é significativamente melhorada. O tempo de convergência obtido com esta técnica é inferior a um ciclo da freqüência fundamental.

A Figura 5.10 apresenta o resultado com uma variação de aproximadamente 100% na amplitude da corrente da carga, com a utilização da transformada de Clarke para gerar dois sinais ortogonais de entrada. Com isto, a corrente de compensação consegue acompanhar a alteração na corrente da carga com um tempo de adaptação **Ta** inferior a um ciclo da fundamental. Estando este resultado de acordo com o proposto inicialmente neste trabalho.
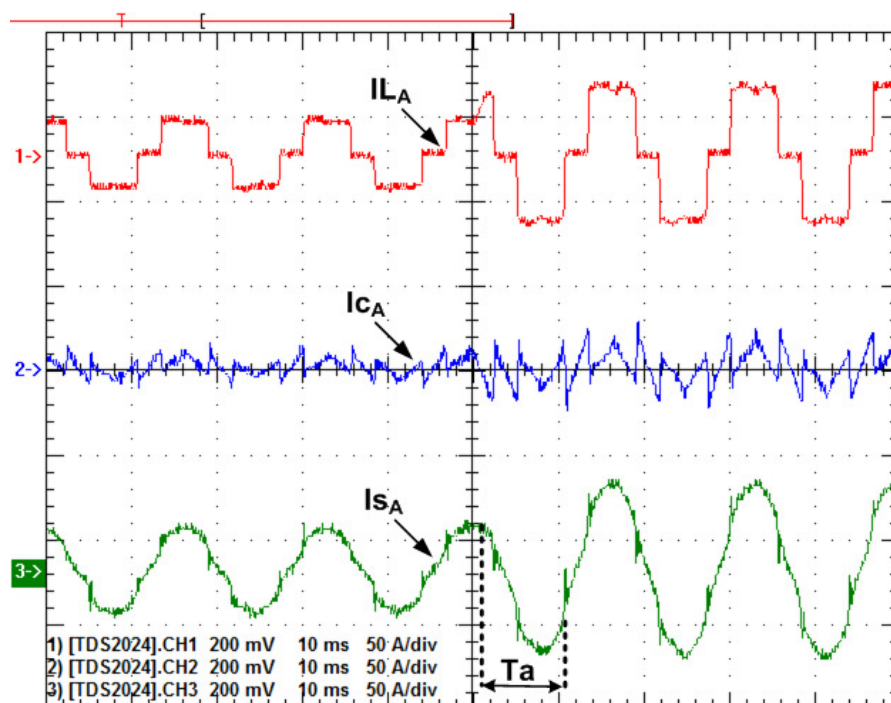
Figura 5.10: Variação de 100% da amplitude da corrente da carga utilizando o algoritmo *LMS*.

➢ **Transitório na Amplitude e no Conteúdo Harmônico da Corrente da Carga.**

Para comprovar o comportamento do algoritmo quando ocorre uma alteração no conteúdo harmônico foi realizado um experimento prático alterando a corrente da carga entre uma carga linear (sem conteúdo harmônico) e uma não-linear (com conteúdo harmônico).

A Figura 5.11 apresenta o comportamento do algoritmo diante de uma mudança no tipo da carga de linear para não-linear. Nesta alteração do conteúdo harmônico juntamente com o valor da amplitude da corrente da carga o tempo de adaptação **Ta** é inferior a um ciclo da freqüência fundamental.
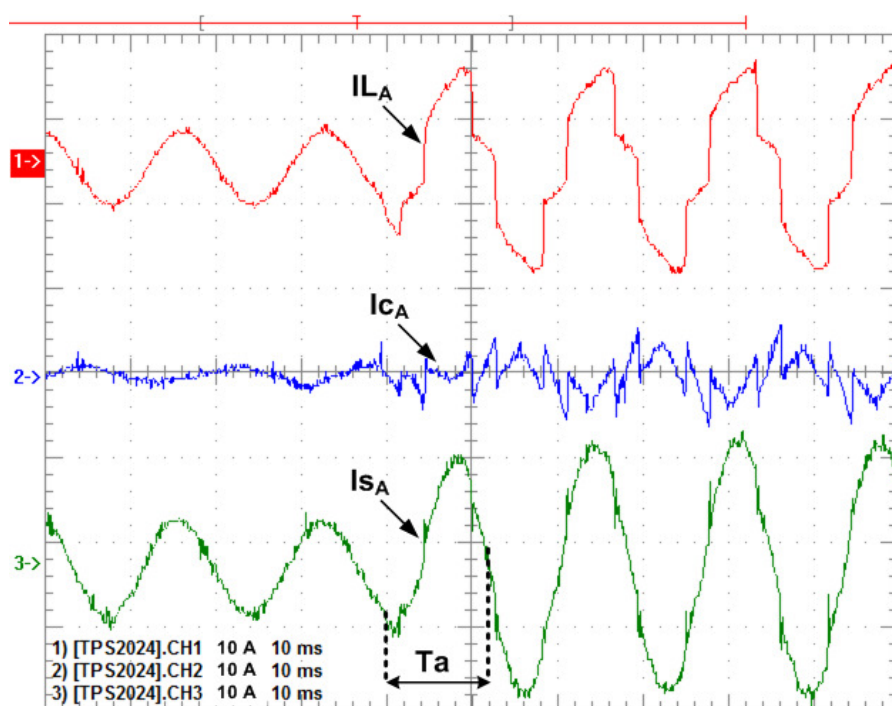
Figura 5.11: Transitório de uma carga linear para uma não-linear utilizando o algoritmo *LMS*.

A Figura 5.12 apresenta o comportamento do algoritmo diante de uma mudança no tipo da carga de não-linear para linear. Continuando o tempo de adaptação **Ta** inferior a um ciclo da freqüência fundamental.
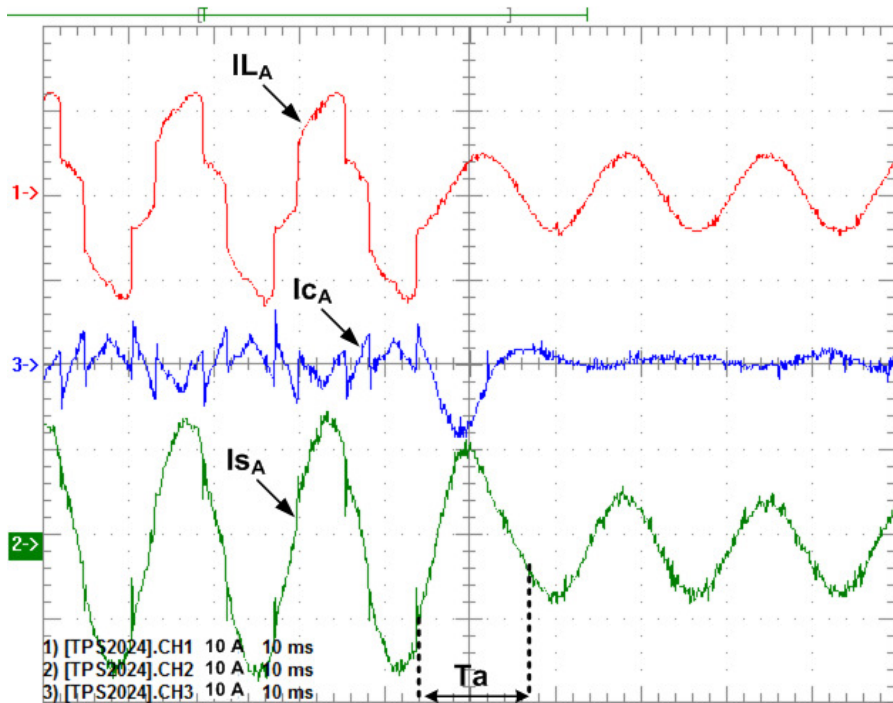
Figura 5.12: Transitório de uma carga não-linear para uma linear utilizando o algoritmo *LMS*.

5.2 Filtro Adaptativo Sintonizado *RLS*

Os resultados da implementação da extração de harmônicos utilizando o Filtro Adaptativo Sintonizado com o algoritmo *RLS* serão abordados nesta seção. Como mencionado anteriormente, foi necessário gerar dois sinais senoidais com deslocamento de fase de 90°, um em relação ao outro. Esta tarefa pode ser realizada de uma maneira simples com o uso da transformada de *Clarke* e posterior filtragem dos sinais ortogonais de saída, $I_{L\alpha}$ e $I_{L\beta}$, gerados pela transformada.

A corrente da carga, a corrente de compensação e a corrente da fonte, na fase A, são mostradas na Figura 5.13. Já na Figura 5.14 são apresentadas as correntes da fonte nas três fases com a compensação harmônica.

O espectro harmônico da corrente da fonte, com e sem o FAPP, é ilustrado pela Figura 5.15. Demonstrando o correto decréscimo do conteúdo harmônico da corrente da fonte. Os valores numéricos deste decréscimo podem ser encontrados na Tabela 5.2.
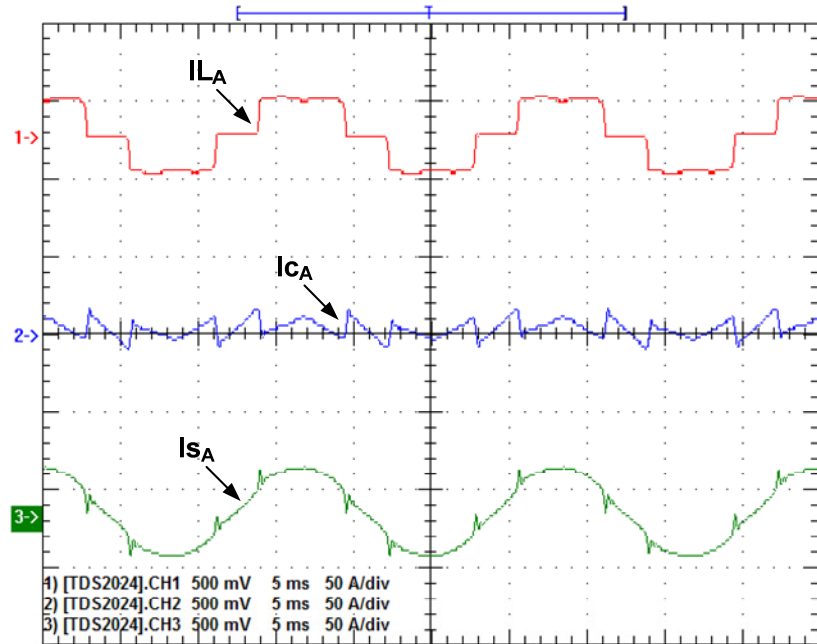
Figura 5.13: Corrente da carga, de compensação e da fonte, para I$_L$ com 19,2A *RMS*.
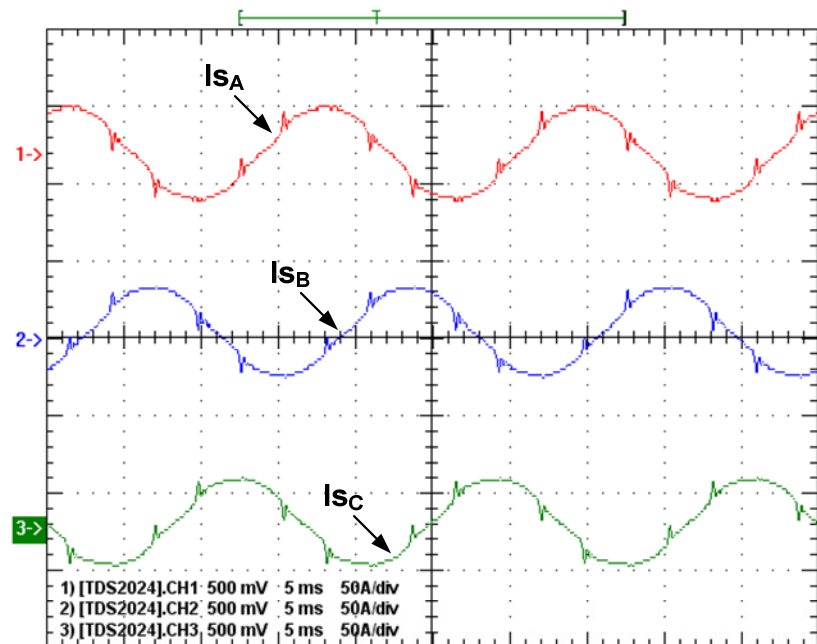

**Figura 5.14: Corrente da fonte nas fases as A, B e C, para I$_L$ com 19,2A *RMS*.**
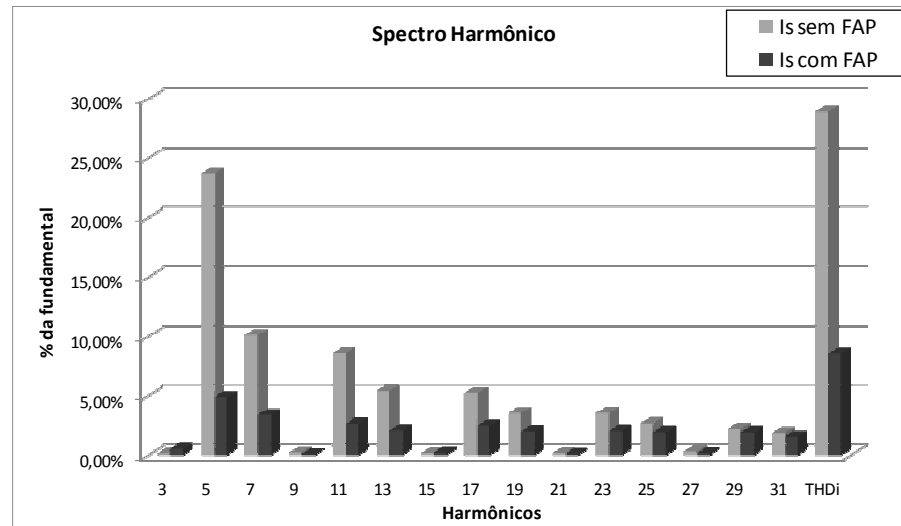
Figura 5.15: Espectro Harmônico da corrente da fonte para I$_L$ com 19,2A *RMS*.

Tabela 5.2: Corrente de cada componente harmônico, sem e com FAP, para I$_L$ com 19,2A *RMS*.

	I_s sem FAP		I_s com FAP	
	A *RMS*	**% da fundamental**	**A *RMS***	**% da fundamental**
3° Harmônico	0,02601	0,14%	0,10730	0,53%
5° Harmônico	4,53210	23,73%	0,98649	4,86%
7° Harmônico	1,92760	10,09%	0,68935	3,39%
9° Harmônico	0,04132	0,22%	0,01591	0,08%
11° Harmônico	1,64100	8,59%	0,53446	2,63%
13° Harmônico	1,02860	5,39%	0,42371	2,09%
15° Harmônico	0,03070	0,16%	0,03934	0,19%
17° Harmônico	0,99549	5,21%	0,50318	2,48%
19° Harmônico	0,67343	3,53%	0,41109	2,02%
21° Harmônico	0,03000	0,16%	0,01839	0,09%
23° Harmônico	0,67426	3,53%	0,41742	2,06%
25° Harmônico	0,50876	2,66%	0,39697	1,95%
27° Harmônico	0,06112	0,32%	0,03211	0,16%
29° Harmônico	0,42160	2,21%	0,39464	1,94%
31° Harmônico	0,35883	1,88%	0,31860	1,57%

Os valores na Tabela 5.2 mostram que a amplitude do 5° harmônico decresceu de 23,73% para 4,86% uma queda de 79,52%. A amplitude do 7° harmônico decresceu 66,40%, a do 11° harmônico decresceu 69,38%, a do 13° harmônico decresceu 61,22%, a do 17° harmônico decresceu 52,40%, a do 19° harmônico decresceu 42,78%, a do 23° harmônico decresceu 41,64% e a do 25° harmônico decresceu 26,69%.

O *THDi* foi alterado de 28,9% para 8,56%, um decréscimo de 70,38%.

A queda no valor de *THDi* após a inserção do Filtro Ativo de Potência Paralelo demonstra a correta ação do mesmo. Comprovando a exatidão da referência harmônica produzida pelo método de detecção de harmônicos utilizando um Filtro Adaptativo Sintonizado.

➢ **Transitório na Amplitude da Corrente da Carga de 6,5A para 12,8A**

Neste teste com transitório na amplitude da corrente da carga é observado o tempo de adaptação gasto para o Filtro Adaptativo Sintonizado com algoritmo *RLS*. Ao ser aplicado um transitório de aproximadamente 100%, o tempo de convergência obtido é inferior a um ciclo da freqüência fundamental. Resultado este, idêntico ao encontrado com o algoritmo de adaptação *LMS*.

A Figura 5.16 apresenta o resultado com uma variação de aproximadamente 100% na amplitude da corrente da carga, com a utilização da transformada de *Clarke* para gerar dois sinais ortogonais de entrada. Com isto, a corrente de compensação consegue acompanhar a alteração na corrente da carga com um tempo de adaptação **Ta** inferior a um ciclo da fundamental. Estando este resultado de acordo com o proposto inicialmente neste trabalho.
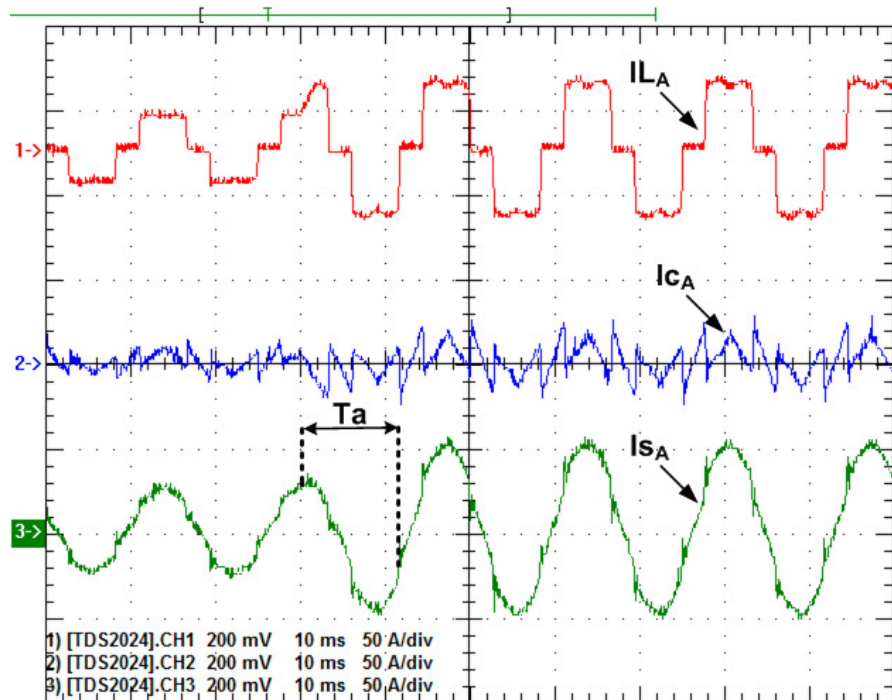
Figura 5.16: Variação de 100 % da amplitude da corrente da carga utilizando o algoritmo *RLS*.

➢ **Transitório na Amplitude e no Conteúdo Harmônico da Corrente da Carga.**

Como no caso do Filtro Adaptativo utilizando o algoritmo *LMS*, foi realizado um teste para comprovar o comportamento do algoritmo *RLS* quando ocorre uma alteração no conteúdo harmônico da corrente da carga.

A Figura 5.17 apresenta o comportamento do algoritmo diante de uma mudança no tipo da carga de linear para não-linear. Nesta alteração do conteúdo harmônico juntamente com o valor da amplitude da corrente da carga o tempo de adaptação **Ta** é inferior a um ciclo da freqüência fundamental.
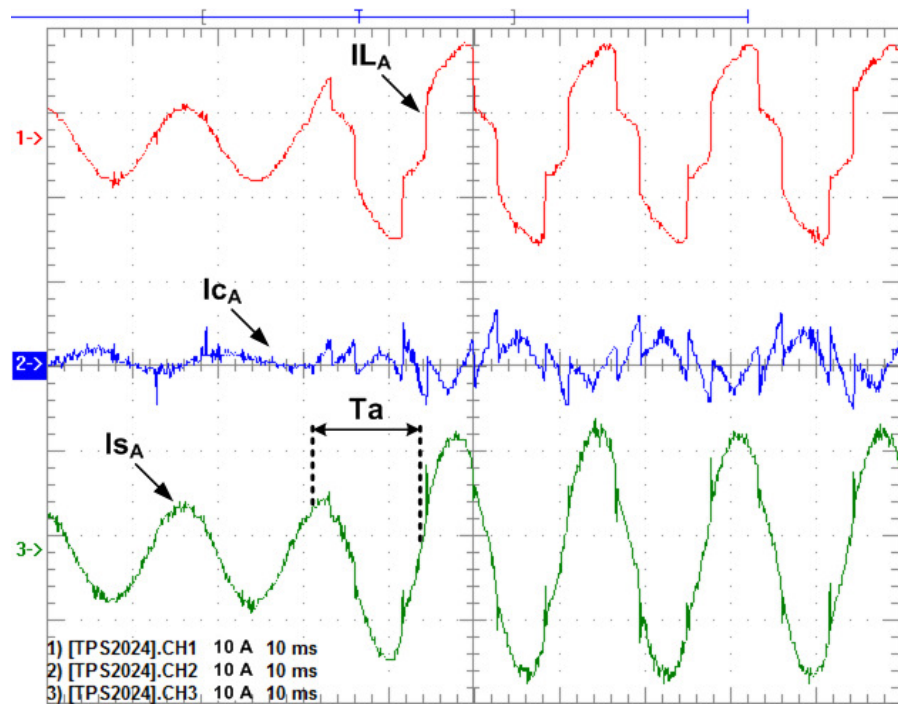
**Figura 5.17: Transitório de uma carga linear para uma não-linear utilizando o algoritmo *RLS*.**

A Figura 5.18 apresenta o comportamento do algoritmo diante de uma mudança no tipo da carga de não-linear para linear. Continuando o tempo de adaptação **Ta** inferior a um ciclo da freqüência fundamental.
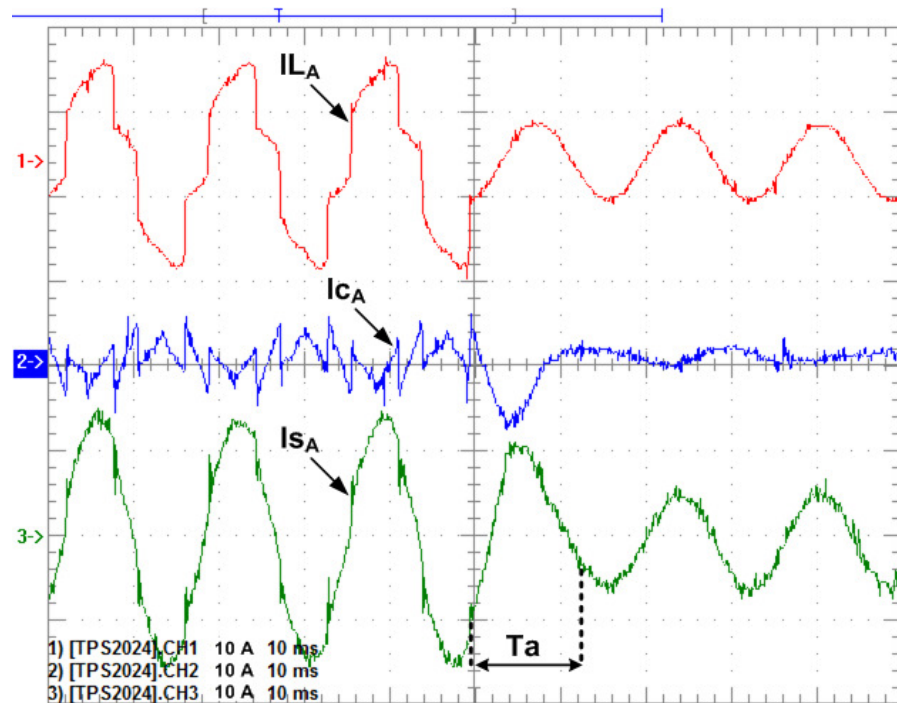

Figura 5.18: Transitório de uma carga não-linear para uma linear utilizando o algoritmo *RLS*.

5.3 Conclusões do Capítulo

Neste capítulo foram apresentados os resultados experimentais da compensação do conteúdo harmônico de uma carga não-linear através de um Filtro Ativo de Potência Paralelo. Sendo utilizado um Filtro Adaptativo Sintonizado com os algoritmos de adaptação *LMS* e *RLS*.

Os resultados apresentados correspondem a estrutura total do Filtro Ativo de Potência (tempo gasto na amostragem, processamento do algoritmo de controle, os circuitos de condicionamento de sinal e o tempo de resposta do inversor de freqüência). Com isto, o tempo de convergência foi de aproximadamente 14ms. Este tempo, superior ao encontrado na simulação, se deve ao fato de que na simulação somente o tempo de processamento do algoritmo foi levado em consideração.

Os testes experimentais comprovaram o correto desempenho da técnica de detecção de harmônicos com Filtros Adaptativos, aplicada na geração da corrente de referência harmônica em um Filtro Ativo de Potência Paralelo. Os resultados, tanto para o comportamento em regime permanente como no transitório da corrente da carga e do conteúdo harmônico, comprovaram a eficiência da técnica proposta neste trabalho.

Outro fato importante é a independência do algoritmo com relação ao sinal da carga. Pois, independente da característica deste sinal a saída do Filtro Adaptativo consegue reproduzir o sinal da componente fundamental presente na corrente da carga. Isto pode ser verificado pelas deduções do algoritmo apresentadas no Capítulo 3, em que as características do sinal desejado *d(n)* não são especificadas.

6 Conclusão

6.1 Conclusão Geral

Este trabalho apresentou a utilização da técnica de detecção de harmônicos, baseada na Filtragem Adaptativa, para extração do conteúdo harmônico, utilizado como sinal de referência em um Filtro Ativo de Potência Paralelo. Um Filtro Adaptativo Sintonizado foi usado na realização desta tarefa. Sendo os algoritmos *Least Mean Square* e *Recursive Least Square* utilizados na adaptação dos parâmetros.

Para o comportamento adequado de todo o sistema, é desejável ter uma velocidade de convergência e uma resposta em regime permanente apropriadas para um Filtro Ativo de Potência. Para isto, foi desenvolvida uma estratégia para detectar variações na amplitude da corrente da carga passando esta informação diretamente para os sinais ortogonais de entrada do Filtro Adaptativo Sintonizado. Para tanto, estes sinais ortogonais foram obtidos através da filtragem dos sinais de saída da Transformada de *Clarke,* aplicada à corrente da carga.

Os resultados das simulações, no *Matlab/Simulink,* e experimentais no *DSP* TMS320F2812 comprovaram a correta detecção do conteúdo harmônico, apresentando uma velocidade de convergência rápida o suficiente para este tipo de aplicação. O tempo gasto para a saída do Filtro Adaptativo se readaptar a componente fundamental da carga, após um transitório, foi inferior a um ciclo da fundamental. Resultado, este, mais veloz do que o encontrado na literatura, que é de 1 ciclo da fundamental.

Com os resultados experimentais foi possível verificar, realmente, as possibilidades da detecção de harmônicos com Filtragem Adaptativa, aplicada a um Filtro Ativo de Potência Paralelo, bem como, a efetividade do comportamento da estratégia desenvolvida para gerar os sinais ortogonais de entrada sem o uso de um *PLL*. Os valores para a Taxa de Distorção Harmônica Total da Corrente, obtidos com a compensação, foram promissores estando próximos ao nível recomendado pela norma IEEE 519.

Portanto, o método de detecção de harmônicos com Filtros Adaptativos, utilizando a nova estratégia, demonstrou ser uma proposta eficiente e promissora para ser utilizada nos algoritmos de controle de um Filtro Ativo de Potência.

6.2 Trabalhos Futuros

Para continuidade deste trabalho algumas propostas podem ser indicadas, visando um melhor desempenho da estratégia desenvolvida. Estas propostas são descritas a seguir:

➢ **Modificar a estratégia para a aplicação em um sistema desequilibrado.**

A estratégia abordada neste texto foi aplicada em um sistema equilibrado. Para que a mesma seja aplicada em um sistema desequilibrado algumas modificações devem ser feitas na obtenção dos sinais ortogonais de entrada. Pois, na atual estratégia estes sinais são gerados a partir da filtragem das duas saídas ortogonais da Transformada de *Clarke*. Sendo as correntes da carga das fases A, B e C as entradas da transformada.

Caso exista um desequilíbrio entre essas correntes os sinais ortogonais terão amplitudes diferentes, ocasionando um funcionamento incorreto da estratégia.

A solução, neste caso, é a obtenção dos dois sinais ortogonais de entrada por fase. Desta maneira os dois sinais ortogonais gerados pela corrente da fase A devem acompanhar a variação de amplitude apenas desta fase. Os sinais ortogonais da fase B devem acompanhar a variação de amplitude apenas da fase B e da mesma maneira deve ocorrer na fase C.

➢ **Testar o novo algoritmo para resposta em regime permanente.**

Como observado nos resultados das simulações com o algoritmo modificado, apresentados no Apêndice B, foi possível obter uma resposta em regime permanente mais precisa.

Desta maneira, é necessário a implementação deste algoritmo no Processador Digital de Sinal TMS320F2812 para os testes experimentais no Filtro Ativo de Potência Shunt. Verificando assim, a validade desta nova proposta.

➢ **Melhorar o valor da Taxa de Distorção Harmônica Total da Corrente.**

Apesar do correto decréscimo no valor do *THDi* da corrente da fonte este valor está um pouco acima do valor desejado. Este fato ocorre devido aos *notchs* encontrados

na corrente da fonte compensada, como pode ser observado nos resultados experimentais do Capítulo 5.

Uma análise realizada demonstrou que este efeito deteriorante é devido ao filtro *anti-aliansing* utilizado no circuito de condicionamento de sinais e a própria resposta do inversor de freqüência ao um degrau. A comprovação desta análise é apresentada no Apêndice C.

Com isto, é importante um trabalho mais detalhado sobre esses dois tópicos causadores do efeito na corrente da fonte. Buscando minimizar ou eliminar esses *notchs* na corrente compensada, alcançando assim um melhor *THDi*.

Referências Bibliográficas

[1]Sant'Ana, W. C., "Implementação de um Compensador Ativo Série para Sistemas de Distribuição". 188p. Dissertação de Mestrado, Universidade Federal de Itajubá, Itajubá, 2004.

[2]Da Silva, C. H., "Comportamento do Condicionador Ativo de Potência em Sistemas Desequilibrados E Distorcidos: um Sistema Combinado entre Filtros Ativos Série e Filtros Passivos Paralelos". 145p. Dissertação de Mestrado, Universidade Federal de Itajubá, Itajubá, 2005.

[3]L. Asiminoaei, F. Blaabjerg, S. Hansen, "Detection is Key", IEEE Industry Application Magazine, v. 13, pp. 22-33, 2007.

[4]A. M. Massoud, S. J. Finney, B. W. Williams, "Review of Harmonic Current Extraction Techniques for an Active Power Filter", IEEE/ICHQP, pp. 154-159, 2004.

[5]C. Donghua, X. Shaojun, "Review of the Control Strategies Applied to Active Power Filters", IEEE/DRPT, pp. 666-670, 2004.

[6]E. H. Watanabe, H. Akagi, M. Aredes, "Instantaneous p-q power Theory for compensating nonsinusoidal systems", IEEE/ISNCC, pp. 1-10, Lagow, 2008.

[7]S. Bhattacharya, D. Divan, "Synchronous frame based controller implementation for a hybrid series active filter system", IEEE/ IAS, v. 3, pp. 2531-2540, 1995.

[8]S. C. Douglas, "Introduction to Adaptive Filters". In: V. K. Madisetti, D. B. Williams, Digital Signal Processing Handbook. CRC Press LLC, 1999. p. 426- 444.

[9]ANALOG DEVICES. "Mixed-Signal and DSP Design Techniques". Walt Kester. 2000.

[10]B. Widrow, et al., "Adaptive Noise Cancelling: Principles and Applications", Proceedings of the IEEE, v. 63, n. 12, p. 1692, 1975.

[11]S. Välviita, S. J. Ovaska, "Delayless method to generate current reference for active filters", IEEE Transactions on Industrial Electronics, v. 45, n. 4, pp. 559–567, 1998.

[12]S. Bhattacharya, D. M.Divan, T. M.Frank, B. Banerje, "Active filter system implementation", IEEE Transaction Industry Applications, v. 4, no. 5, pp. 47-63, 1998.

[13]S. Lou, Z. Hou, "An adaptive detecting method for harmonic and reactive currents", IEEE Transactions on Industrial Electronics, v. 42, pp. 85-89, 1995.

[14] H. Karimi, M. Karimi-Ghatermani, M. R. Iravani e A. R. Bakhshai, "An adaptive filter for synchronous extraction of harmonics and distortions", IEEE Transactions on Power Delivery, v. 18, n. 2, 2003.

[15] R. H. Kwong, E. W. Johnston, "A variable step-size LMS algorithm", IEEE Trans. Signal Processing, 1992, 40(7), pp. 1633-1642.

[16] Mu Longhua, Jiangzi, "Application of adaptive filtering in harmonic analysis and detection", Transmission and Distribution Conference and Exhibition: Asia and Pacific, IEEE/PES, Dalian, 2005.

[17] H. Li, Z. Wu, F. Liu, "A Novel Variable Step Size Adaptive Harmonic Detecting Algorithm Applied to Active Power Filter", IEEE/ICIT, Mumbai, 2006.

[18] Y. Qu, W. Tan, Y. Dong, and Y. Yang, "Harmonic detection using fuzzy LMS algorithm for active power filter", IEEE/IPEC, Singapore, 2007.

[19] Pereira, R. R., "Aplicação de Filtros Adaptativos em Filtros Ativos de Potência". 190p. Dissertação de Mestrado, Universidade Federal de Itajubá, Itajubá, 2009.

[20] Pereira, R. R. ; Da Silva, C. H. ; Silva, L. E. B. ; Lambet-Torres, G. "Application of Adaptive Filters in Active Power Filters", IEEE/COBEP , Bonito , 2009.

[21] Pereira, R. R. ; Da Silva, C. H. ; Silva, L. E. B. ; Lambet-Torres, G. "A New Strategy to Step-Size Control of Adaptive Filters in the Harmonic Detection for Shunt Active Power Filter", IEEE/IAS, Houston, 2009.

[22] F. D. Freijedo, J. Doval-Gandoy, O. Lopez, P. Fernández-Comesaña and C. Martinez-Peñalver, "A signal-processing adaptive algorithm for selective current harmonic cancellation in active power filters," IEEE Transactions on Industrial Electronics, v. 56, n. 8, pp. 2829–2840, Aug. 2009.

[23] B. Singh, and J. Solanki, "An implementation of an adaptive control algorithm for a three-phase shunt active filter," IEEE Transactions on Industrial Electronics, v. 56, n. 8, pp. 2811–2820, Aug. 2009.

[24] M. Cirrincione, M. Pucci, G. Vitale, S. Scordato, and A. Miraoui, "Current harmonic compensation by a single-phase shunt active aower filter controlled by adaptive neural filtering," IEEE Transactions on Industrial Electronics, v. 56, n. 8, pp. 3128–3143, Aug. 2009.

[25] L. Asiminoaei, F. Blaabjerg, S. Hansen and P. Thogersen, "An improved adaptive detection method for power quality improvement," IEEE Transaction Industry Applications, v. 44, no. 2, pp. 525–533, 2008.

[26] S. Fukuda e S. Sugawa, "Adaptive signal processing based controlo f active Power filter", IEEE IAS 1996, San Diego, 1996.

[27] M. H. Byung, Y. B. Byung, S. J. Ovaska, "Reference signal generator for active power filters using improved adaptive predictive filter". IEEE Transactions on Industrial Electronics, v. 52, n. 2, 2005.

[28] C.H. da Silva, V.F.da Silva, L.E.Borges da Silva, G.L.Torres, R.R.Pereira, "DSP implementation of three-phase PLL using modified synchronous reference frame", IEEE/IECON, Taiwan, 2007.

Apêndice A – DSP TMS320F2812

A ferramenta principal deste trabalho é o Processador Digital de Sinais TMS320F2812 da *Texas Instruments*, pois neste processador o algoritmo será programado e executado. Então é importante realizar uma breve descrição das principais características deste *DSP*.

- Freqüência de *clock* (interna)150 MHz.
- Baixo consumo.
- CPU de 32 bits de alta performance.
- Memória RAM interna de 18 k *words* (1 *word* = 16 bits).
- Memória Flash EEPROM integrada de 128 k *words*.
- Interface para memória externa (até 1M *words*).
- Conversor Analógico-Digital de 12 bits, para até 16 entradas multiplexadas, com capacidade de 12,5 milhões de amostras por segundo.
- Suporta programação em C/C++/Assembly (*Code Composer Studio® IDE*).
- Módulo Gerenciador de Eventos.
- 16 saídas para modulação em largura de pulsos (PWM) ou comparação.
- 3 temporizadores de uso geral de 32 bits.
- Periféricos de Comunicação (SCI, SPI, McBSP, eCAN)

O TMS320F2812 pertence a família C2000 da *Texas Instruments*, que são processadores específicos para operações de controle industrial, conversão de potência, medidas e aplicação automotiva. Ele é eficiente tanto em operações matemáticas de processamento digital de sinais quanto em tarefas de controle de sistemas que tipicamente são realizadas por um microcontrolador. Não havendo a necessidade de um segundo processador, como ocorre em vários sistemas.

Este Processador Digital de Sinais possui um barramento de dados e um barramento de programa independentes, o que é conhecido como Arquitetura de *Harvard*. Devido sua habilidade de ler operandos não só da memória de dados, mas também, da memória de programas a *Texas Instruments* passou a denominar esta arquitetura como Arquitetura de *Harvard* Modificada.
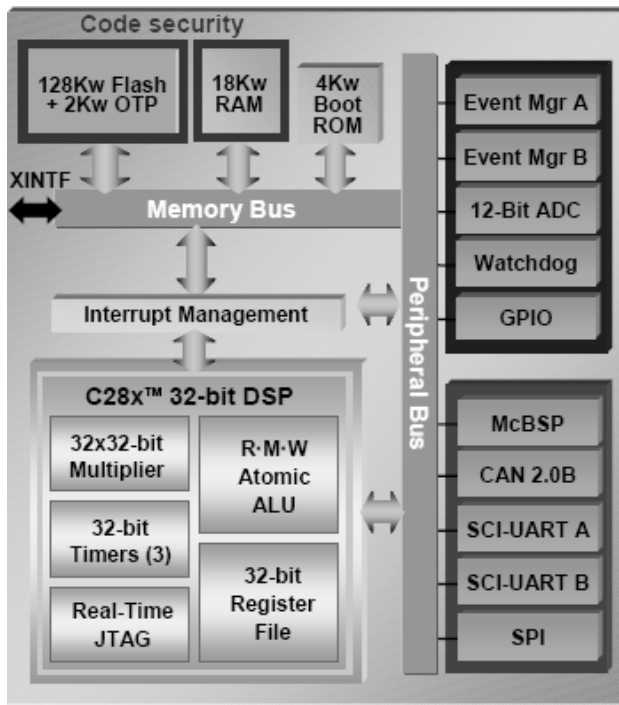
Figura A.1: Visão funcional do TMS320F2812.

A Figura A.1 apresenta a visão funcional deste DSP com seus periféricos, barramentos de comunicação internos e externos, memória interna e a CPU. Sendo justamente esta incorporação em um único chip de uma CPU, com recursos para processamento digital de sinais, juntamente com periféricos que tornam o TMS320F2812 tão eficiente em tarefas matemáticas e de controle.

A.1 O Espaço de Memória

O mapa da Figura A.2 apresenta o espaço de endereçamento do TMS320F2812, ou seja, apresenta as regiões de memória em que o processador pode ler e escrever. Isto não significa que nessas regiões exista, fisicamente, memória instalada. Apenas indica que o processador é capaz de reconhecer uma memória que seja instalada dentro dessa região.

O mapa da Figura A.2 pode ser dividido em duas regiões: Memória interna (on-chip) e memória externa (XINTF). A memória interna não pode ser expandida ou removida, enquanto que a memória externa pode ser expandida em até 1M (Mega) *words*.

Cada uma dessas duas regiões de memória pode ser dividida entre memória de dados e memória de programas. O TMS320F2812 utiliza 32 bits para o endereçamento de dados e 22 bits para o endereçamento de programas. Isto permite o endereçamento total de 4G (Giga) para dados e 4M para programas.

A memória de dados contém as variáveis e o *stack* (pilha). Enquanto que a memória de programa contém o código fonte e os registros de inicialização.
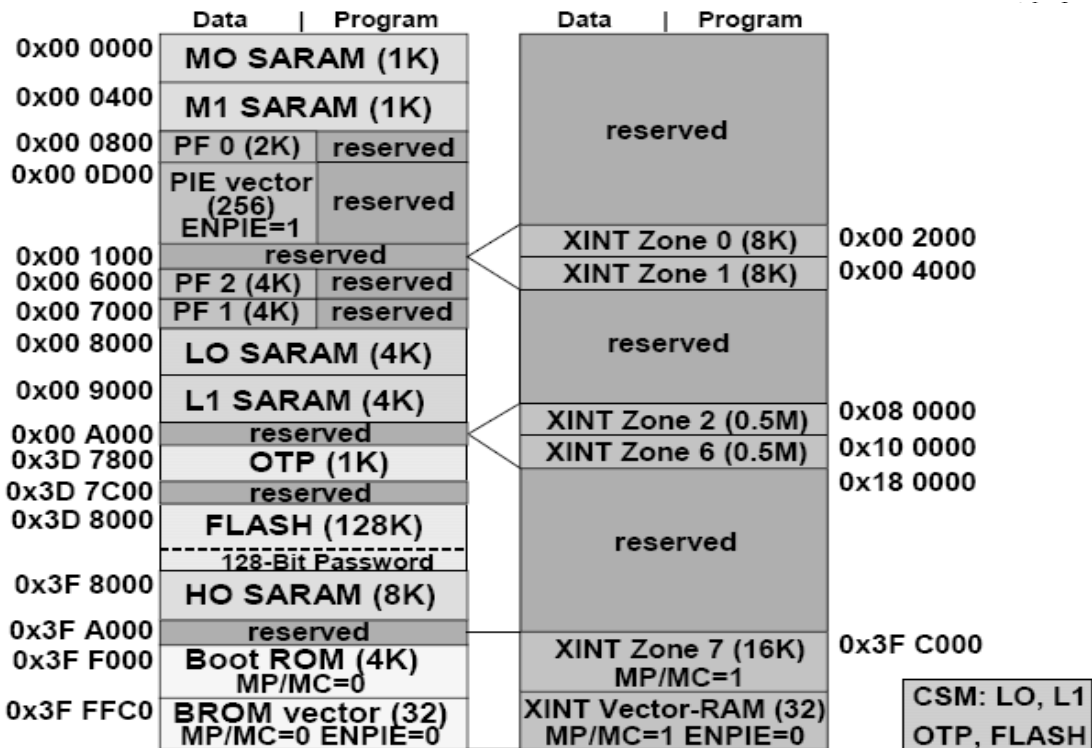
Figura A.2: Espaço de memória do TMS320F2812.

A memória interna do TMS320F2812 possui os seguintes blocos que podem ser utilizados pelos usuários para a alocação entre memória de dados e memória de programa:

- Bloco M0 – 1k *words* de 16 bits;
- Bloco M1 – 1k *words* de 16 bits;
- Bloco L0 – 4k *words* de 16 bits;
- Bloco L1 – 4k *words* de 16 bits;
- Bloco H0 – 8k *words* de 16 bits;
- Memória Flash – 128k *words* de 16 bits.

A memória Flash é dividida em 4 setores de 8k *words* e 6 setores de 16k *words*. Assim os programas desenvolvidos, após a fase de teste, podem ser gravados na mesma, já que ela não é uma memória volátil. Estes programas ainda podem ser protegidos por uma senha de 128 bits definida pelo usuário evitando engenharia reversa.

A.2 Conversor Analógico-Digital (*ADC*)

A função de um Conversor Analógico-Digital (*ADC*) é converter um sinal de tensão (cuja variação no tempo é proporcional à variação de uma determinada grandeza do mundo real, como temperatura, pressão, corrente ou mesmo tensão) em um número digital. Desta maneira podem-se realizar os cálculos necessários sobre este número com o auxílio de um computador digital.

O TMS320F2812 possui apenas um ADC de 12 bits de resolução que executa em torno de 12 milhões de conversões por segundo (12 MSPS) [7]. Porém ele possui 2 *sample/hold* (S/H) e cada S/H possui um multiplexador (MUX) de 8 canais, totalizando 16 canais de entrada. A faixa de tensão analógica de cada canal é 0 a 3V.

O ADC do TMS320F2812 tem capacidade para "auto-sequenciar" 16 aquisições. Isto significa que o ADC pode automaticamente continuar com a conversão do próximo canal depois que a atual terminar. Graças a esta funcionalidade não é necessário salvar o resultado a cada conversão. Basta ler todos os resultados ao fim da seqüência. Para cada resultado de conversão existe um registrador (ADCRESULTx). O *AutoSequencer* é uma máquina de estado que pode converter até 16 sinais. Cada estado do *AutoSequencer* escreve o resultado da conversão no seu respectivo ADCRESULTx.

O *Sequencer* pode operar como dois seqüenciadores independentes (*DualSequencerMode*) de 8 estados cada um ou como um único *sequencer* (*CascadedMode*) de 16 estados. Além destes dois modos (relativos ao *Sequencer*), o ADC também pode operar em mais dois modos (relativos aos S/H): *SimultaneousMode* e *SequentialMode*.

O *Sequencer* consiste, na verdade, em dois seqüenciadores independentes (SEQ1 e SEQ2) de 8 estados que podem ser cascateados para formar um único seqüenciador (SEQ) de 16 estados. O termo "estado" se refere ao número de conversões automáticas que podem ser realizadas com o *Sequencer*. As Figuras B.3 e B.4 apresentam, respectivamente, os diagramas em blocos para a operação do *Sequencer* como *CascadedMode* e *DualSequencerMode*.
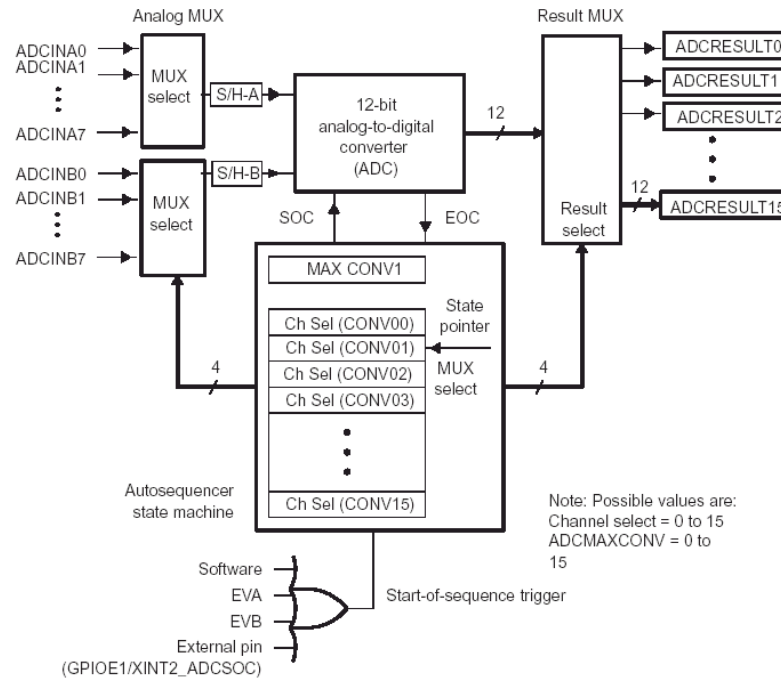
Figura A.3: Diagrama em blocos para o operação do *sequencer* como *CascadedMode*.
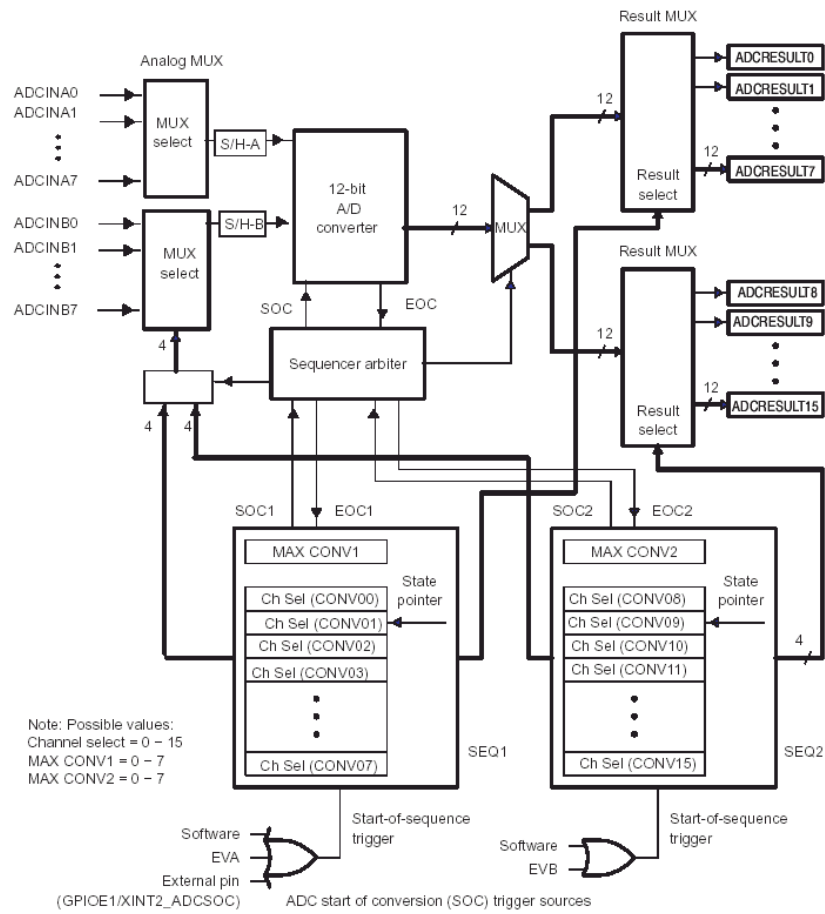
Figura A.4: Diagrama em blocos para o operação do *sequencer* como *DualSequencerMode*.

Em ambos os casos o ADC pode "autosequenciar" uma série de conversões. Isto significa que a cada vez que o ADC receber um *StartOfConversion* (SOC) ele pode realizar múltiplas conversões automaticamente. Para cada conversão, qualquer um dos 16 canais de entrada pode ser selecionado através do MUX. Após a conversão, o valor digital do canal selecionado é armazenado no respectivo ADCRESULTx. O primeiro resultado é armazenado em ADCRESULT0, o segundo em ADCRESULT1, e assim por diante. Também é possível amostrar o mesmo canal de entrada diversas vezes, permitindo ao usuário realizar um *over-sampling*, que aumenta a resolução do resultado frente ao método tradicional de conversão com uma única amostra.

A.3 Ambiente de Desenvolvimento

Para o desenvolvimento de programas neste DSP utiliza-se o ambiente integrado de desenvolvimento *Code Composer Studio®*. Os programas podem ser escritos utilizando as linguagens C, C++ ou Assembly. Permitindo um eficiente desenvolvimento em linguagem de alto nível.

Na Figura A.5, abaixo, podemos encontrar alguns dos importantes recursos disponibilizados pelo *Code Composer Studio®*. Como a visualização dos valores das variáveis em tempo real pela ferramenta *Watch Window* (canto inferior direito da Figura A.5) e a ferramenta *Graph* para visualização de gráficos (canto superior direito da Figura A.5).

Outro recurso integrado ao *Code Composer Studio®* e muito utilizado por todos os projetistas de sistemas é a ferramenta *On Chip Flash Programmer* para gravação dos programas na memória Flash.

Apêndice A
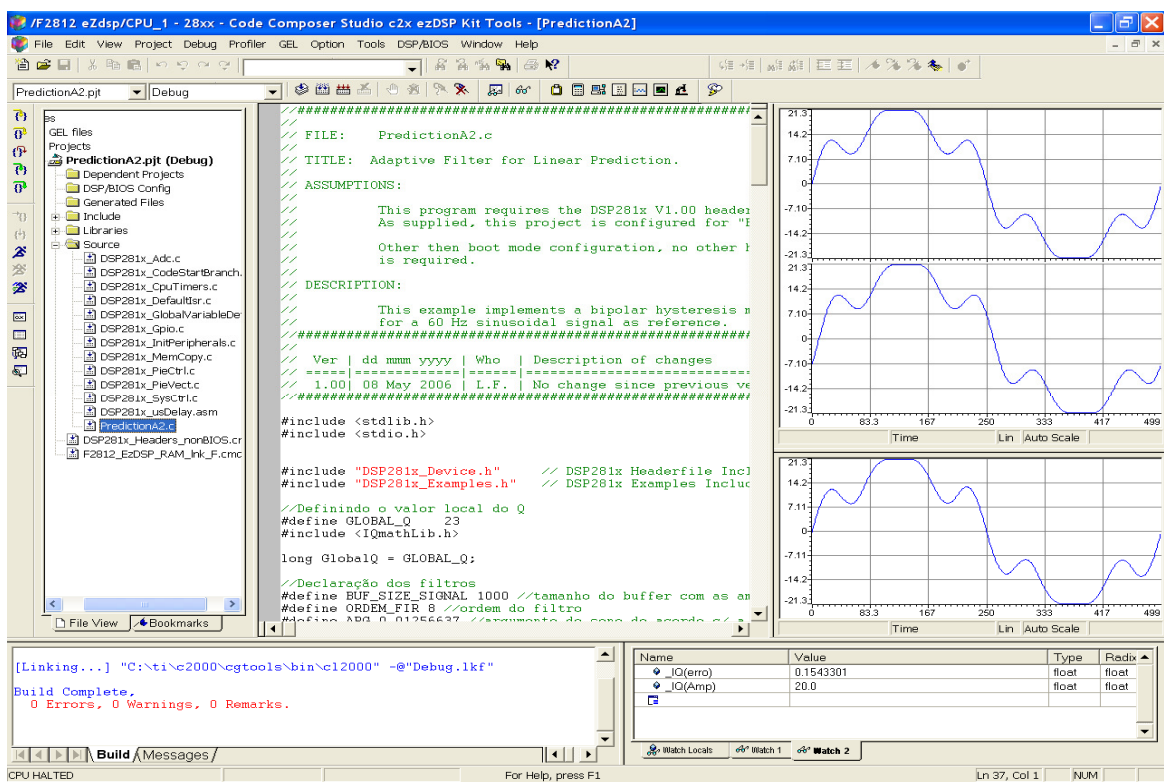
Figura A.5: Ambiente de desenvolvimento *Code Composer Studio®*.

O processo de desenvolvimento de um programa para o TMS320F2812 segue basicamente os passos normais do desenvolvimento de qualquer código em linguagem de alto nível para Processadores de Propósito Geral. Após concluir o código fonte o mesmo deve ser compilado e o projeto montado através do comando *Build*. Caso ocorra algum erro o *Code Composer Studio* disponibiliza também ferramentas para *Debug*. Já o arquivo final gerado com a extensão .*out* deve ser carregado na memória RAM através do comando *Load Program* ou armazenado na memória Flash com a ferramenta *On Chip Flash Programmer* para posterior execução.

Para facilitar o desenvolvimento de códigos a *Texas Instruments* fornece uma série de arquivos e bibliotecas que tornam a tarefa do programador mais concentrada nos problemas relevantes da aplicação em questão. Duas destas facilidades são apresentadas a seguir.

A.3.1 C/C++ Header Files and Peripheral Examples

O *C/C++ Header Files and Peripheral Examples* é disponibilizado pela *Texas Instruments* através do arquivo SPRC097. Trata-se de um *framework* para as aplicações

desenvolvidas para os *DSPs* da família C281x (família de dispositivos a qual pertence o TMS320F2812). Este *framework* já apresenta as estruturas todas programadas, sendo que o desenvolvedor necessita apenas inserir o código específico da aplicação.

Além disso, todos os periféricos e registradores do DSP estão mapeados, não sendo necessário o acesso através de suas posições de memória. Realizando assim uma abstração de *hardware*.

A vantagen de se utilizar o SPRC097 esta na facilidade de programação para os novos usuários e, principalmente, na padronização no desenvolvimento de aplicações.

A.3.2 IQMath

IQmath é uma biblioteca de funções utilizada para implementar algoritmos inicialmente concebidos em aritmética de ponto flutuante em processadores de ponto fixo (que é o caso do TMS320F2812). Esta biblioteca é disponibilizado pela *Texas Instruments®* através do arquivo SPRC087.

O TMS320F2812 é um processador de 32 bits, portanto os operandos aritméticos têm 32 bits. A biblioteca *IQmath* trabalha com números sinalizados, ou seja, o bit mais significativo (MSB) indica o sinal (positivo ou negativo) do número. Um número definido como _iq**n** possui **n** bits para representar a parte fracionária, (**31-n**) bits para representar a parte inteira e **1** bit para representar o sinal. Desta forma um número definido como _iq30 possui 30 bits para representar a parte fracionária e 1 bit para representar a parte inteira, além do bit de sinal.

As funções *IQmath* podem trabalhar com um formato **GLOBAL_Q**. Este formato **GLOBAL_Q** é, na verdade, apenas uma escolha arbitrária para um formato padrão.

As funções *IQmath* na forma _IQ**xxx**(), onde **xxx** é o nome da função, assumem que se está utilizando o formato padrão **GLOBAL_Q**. Já as funções na forma _IQ**N**xxx(), onde **xxx** é o nome da função e **N** é o formato do número, assumem que se está utilizando o formato _iq**N**.

Exemplificando: uma função _IQsin(*arg*) calcula o seno do argumento *arg* considerando que arg está no formato **GLOBAL_Q.** Já uma função _IQ21sin(*arg*) calcula o seno do argumento *arg* considerando que arg está no formato **_iq21**.

Apêndice B – Novo Algoritmo para Resposta em Regime Permanente

Como observado nos resultados das simulações o erro entre o sinal fundamental da corrente da carga e o gerado pelo Filtro Adaptativo Sintonizado não é perfeito. Permanecendo um pequeno resíduo no valor do erro mesmo em regime permanente.

Recentes simulações demonstraram ser possível minimizar o valor do erro a praticamente zero. Mas também, foi observado existir uma relação entre a velocidade de convergência e este erro entre o sinal fundamental da corrente da carga e o gerado pelo Filtro Adaptativo. A redução deste erro implica em uma velocidade de convergência um pouco mais lenta.

Com isto, foi desenvolvida uma solução satisfazendo tanto a velocidade de convergência do algoritmo quanto ao erro em regime permanente. Permitindo que estes dois critérios estejam adequados à aplicação proposta.

Modificação no Algoritmo *LMS*

Buscando uma resposta em regime permanente mais precisa, foi realizada uma modificação no algoritmo para geração do conteúdo harmônico. Devido à variação significativa apresentada pelos dois coeficientes do Filtro Adaptativo Sintonizado, verificou ser esta variação a causa principal do resíduo no valor do erro em regime permanente.

A solução desenvolvida utilizou dois filtros passa-baixa para filtrar o valor dos coeficientes do Filtro Adaptativo Sintonizado. O filtro usado foi um Butterworth de 3° ordem com freqüência de corte de 100Hz. Desde modo, o erro em regime permanente ficou sendo de aproximadamente 0,1% da amplitude da componente fundamental da corrente da carga. Anteriormente este erro era de aproximadamente 1%. Estes resultados são apresentados na Figura B.1.
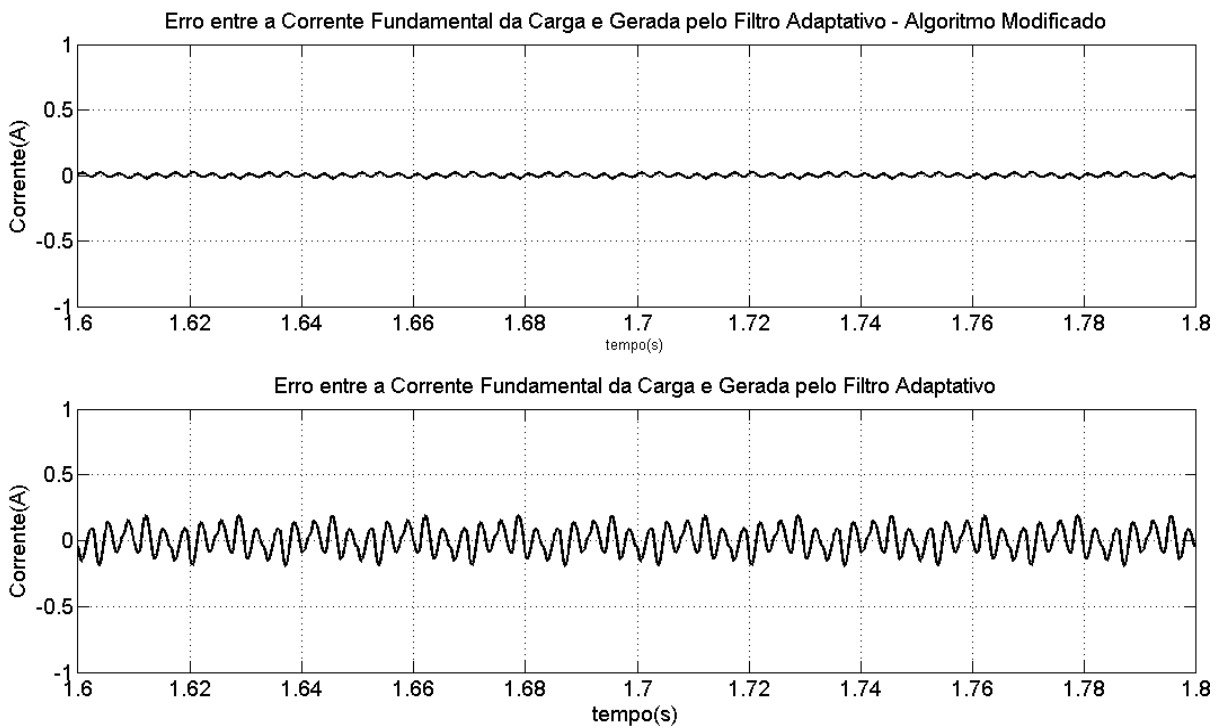
Figura B.1: Demonstração do erro entre a corrente fundamental da carga e a gerada pelo Filtro Adaptativo utilizando o algoritmo modificado e com o algoritmo convencional.

Nas próximas figuras serão apresentados os resultados das simulações obtidos com esta modificação usando o algoritmo *LMS*.

Na Figura B.2 foi aplicado à amplitude da corrente da carga um aumento de 100% de seu valor e em seguida um decréscimo de 25%. Uma comparação entre a corrente fundamental da carga e a corrente fundamental gerada pelo Filtro Adaptativo é apresentada na Figura B.3. Já a Figura B.4 demonstra o resultado da compensação com a corrente harmônica gerada.
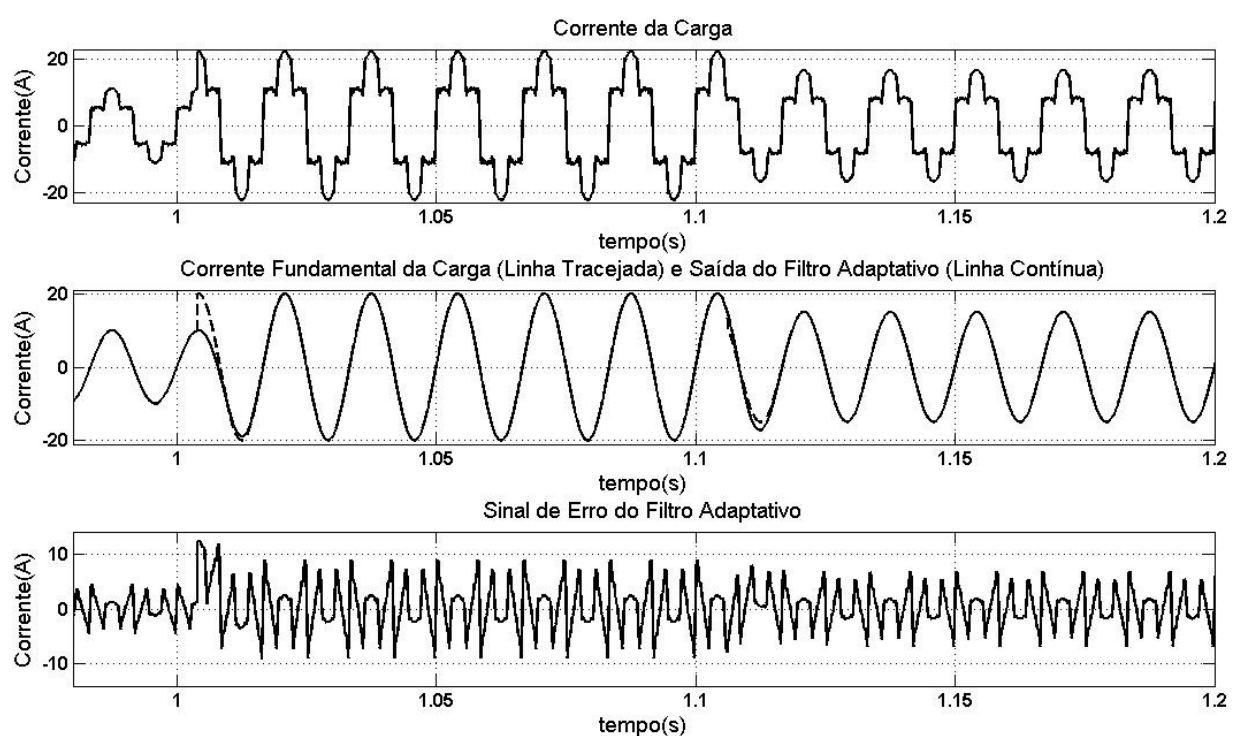
Figura B.2: Sinal desejado, sinal de saída e sinal de erro do Filtro Adaptativo Sintonizado com algoritmo *LMS* modificado com transitório.
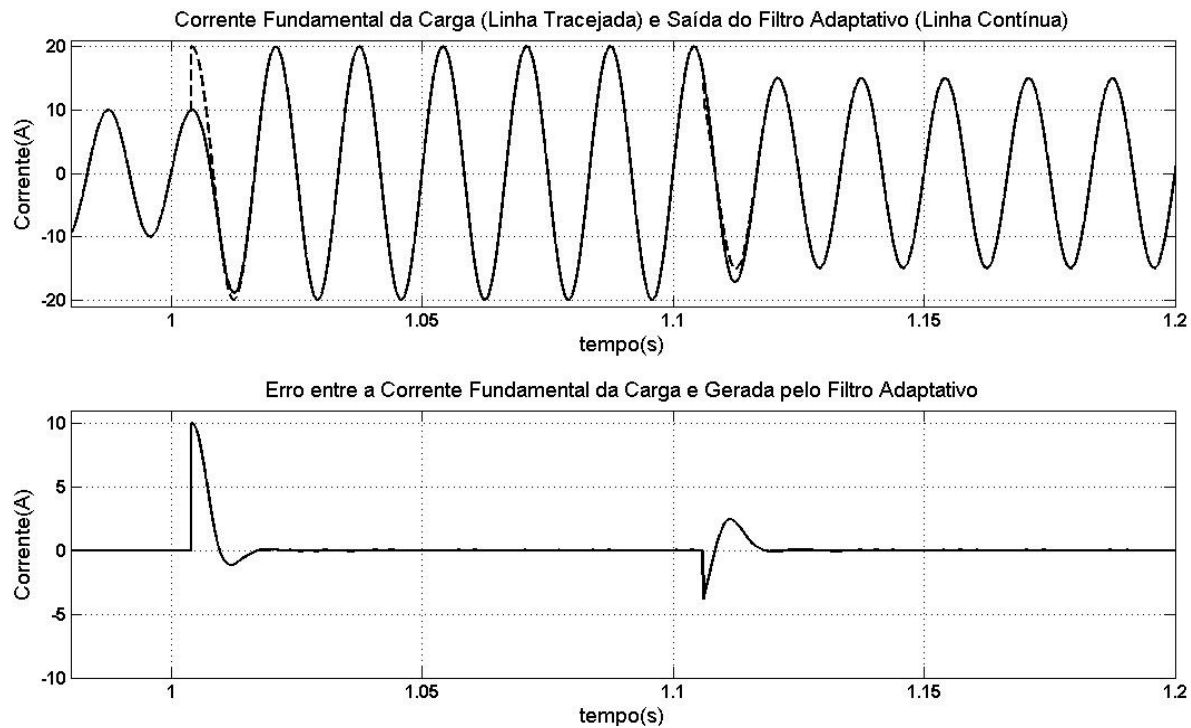
Figura B.3: Comparação entre a corrente fundamental da carga e a gerada pelo Filtro Adaptativo Sintonizado com algoritmo *LMS* modificado com transitório.
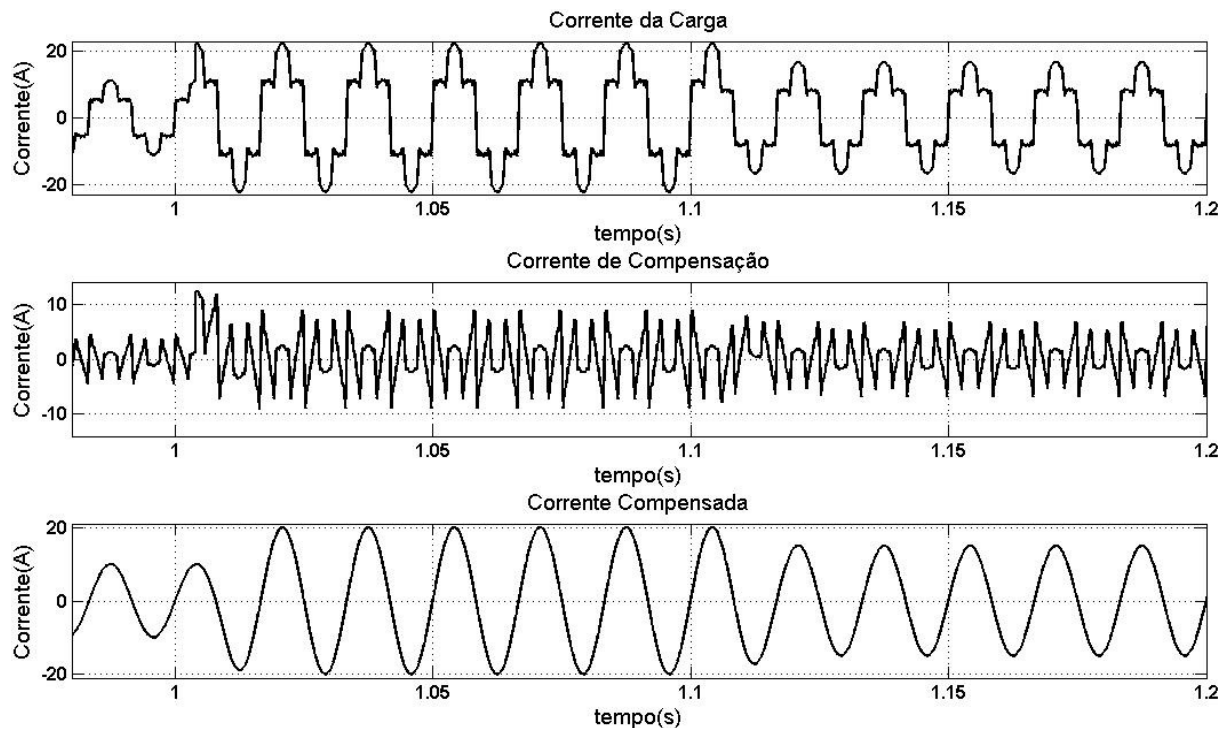
Figura B.4: Resultado da compensação com transitório utilizando o Filtro Adaptativo Sintonizado com algoritmo *LMS* modificado.

As Figuras B.5, B.6 e B.7 ilustram o comportamento do algoritmo quando ocorre um transitório de uma carga linear para uma carga não-linear. Ocorrendo juntamente com a variação do conteúdo harmônico um aumento de 100% na amplitude da componente fundamental da corrente da carga.
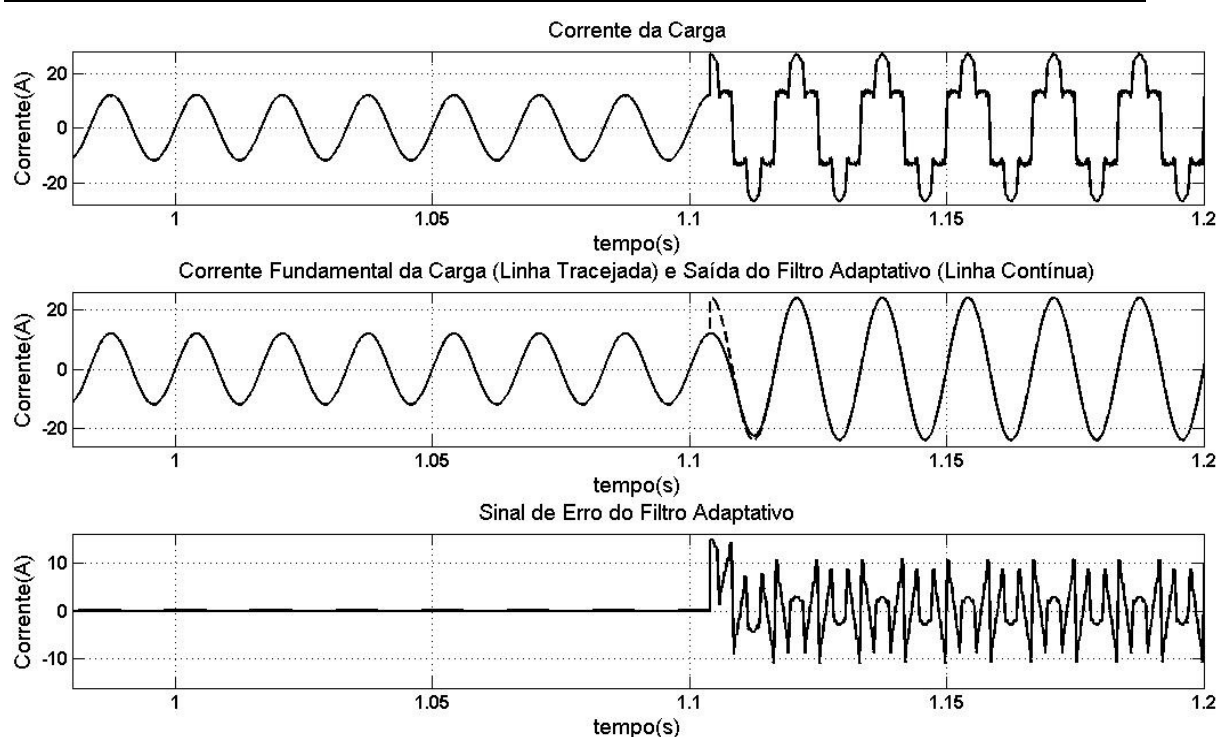
Figura B.5: Sinal desejado, sinal de saída e sinal de erro do Filtro Adaptativo Sintonizado com algoritmo *LMS* modificado e alteração da corrente da carga de linear para não-linear.
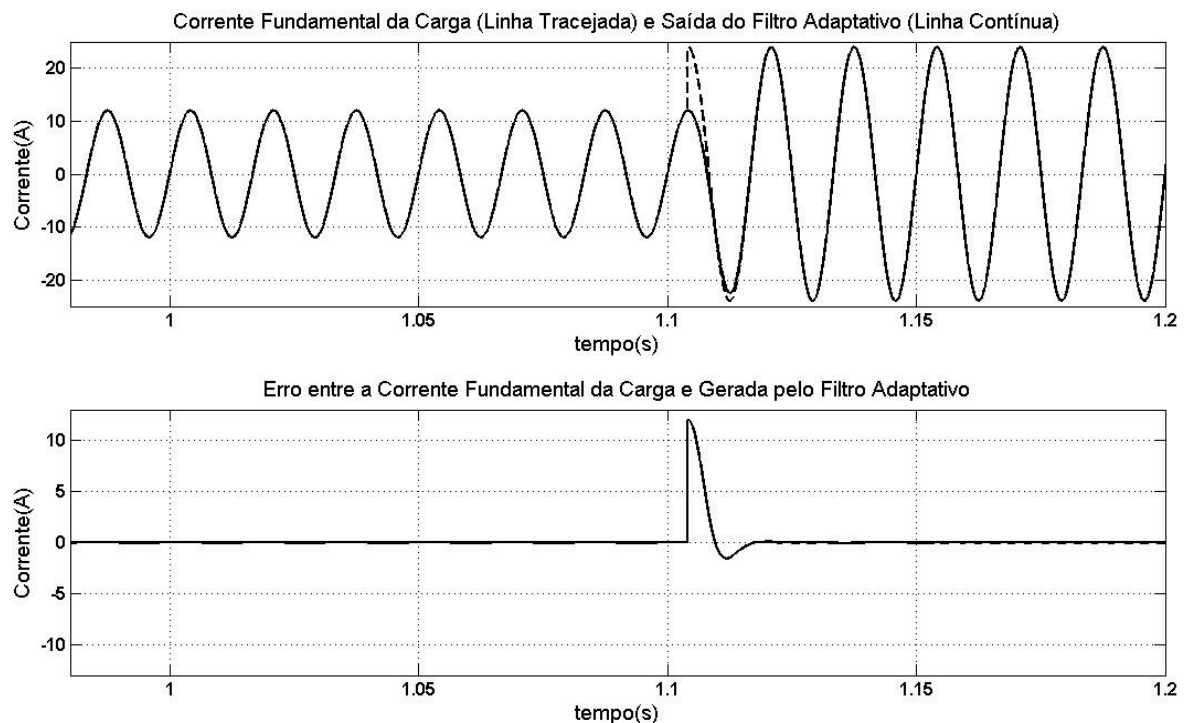
Figura B.6: Comparação entre a corrente fundamental da carga e a gerada pelo Filtro Adaptativo Sintonizado com algoritmo *LMS* modificado e alteração na corrente da carga de linear para não-linear.
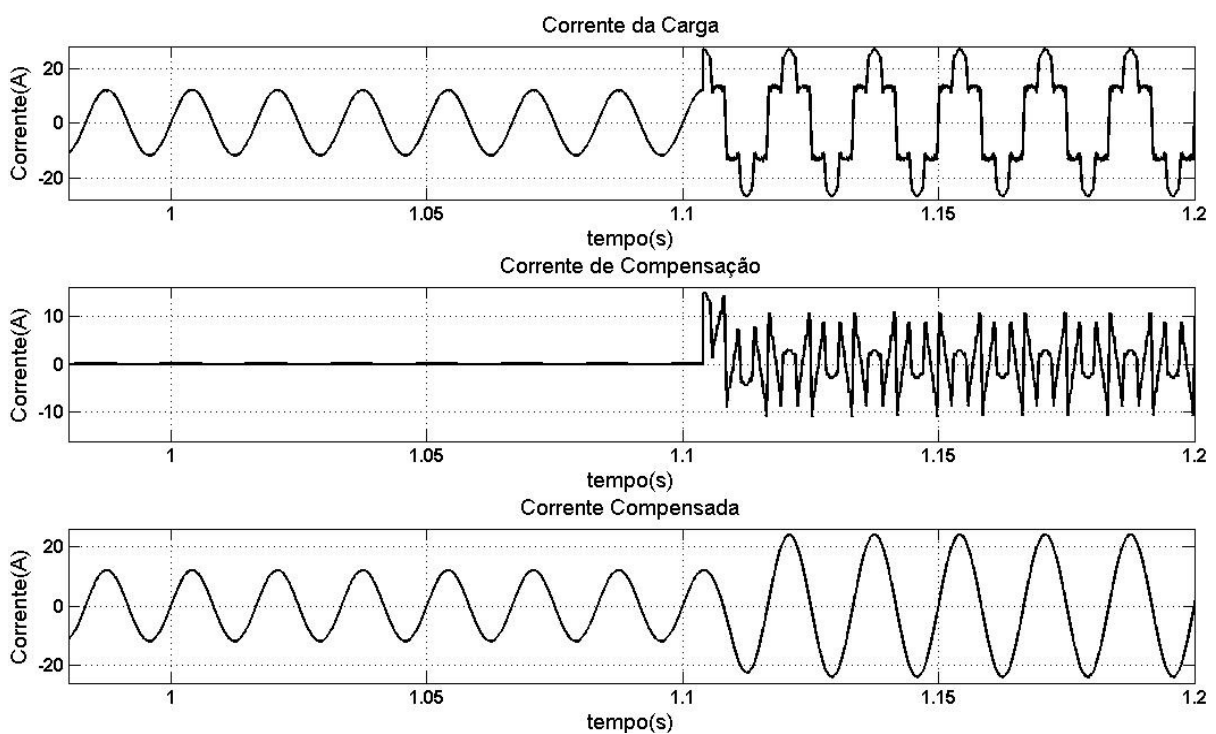
Figura B.7: Resultado da compensação com transitório utilizando o Filtro Adaptativo Sintonizado com algoritmo *LMS* modificado com alteração na corrente da carga de linear para não-linear.

O comportamento do algoritmo quando ocorre o transitório de uma carga não-linear para uma carga linear é ilustrado nas Figuras B.8, B.9 e B.10.
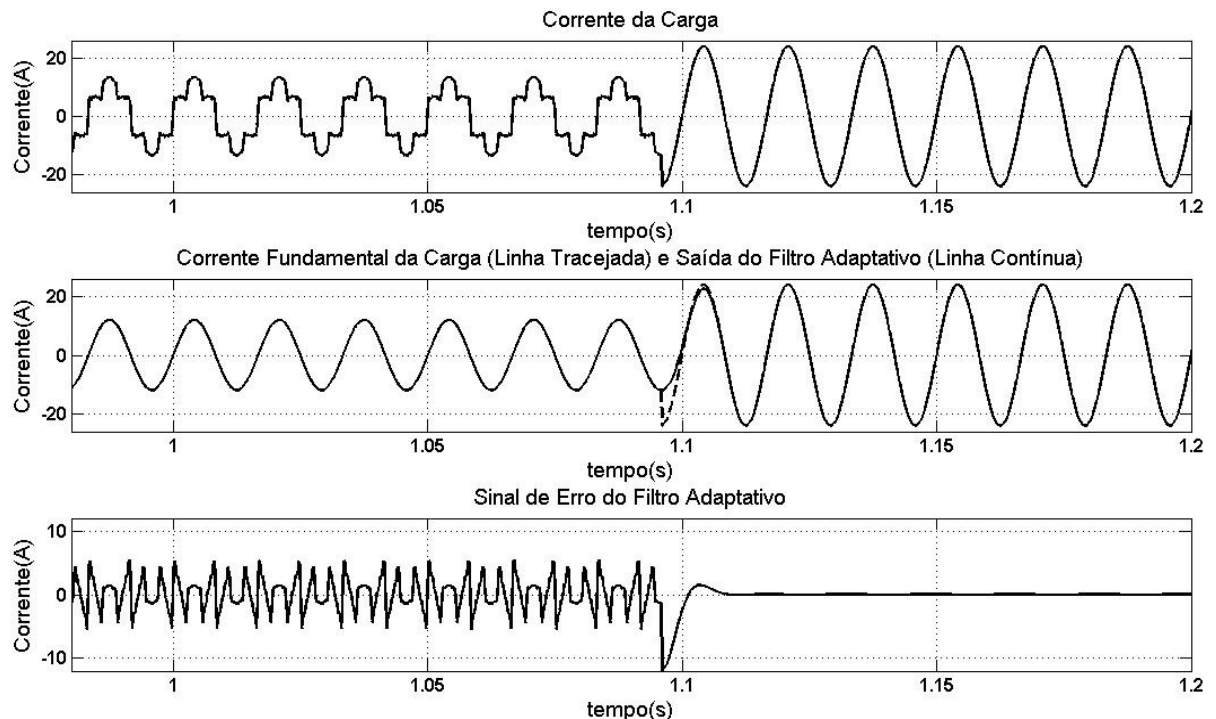
Figura B.8: Sinal desejado, sinal de saída e sinal de erro do Filtro Adaptativo Sintonizado com algoritmo *LMS* modificado e alteração da corrente da carga de não-linear para linear.
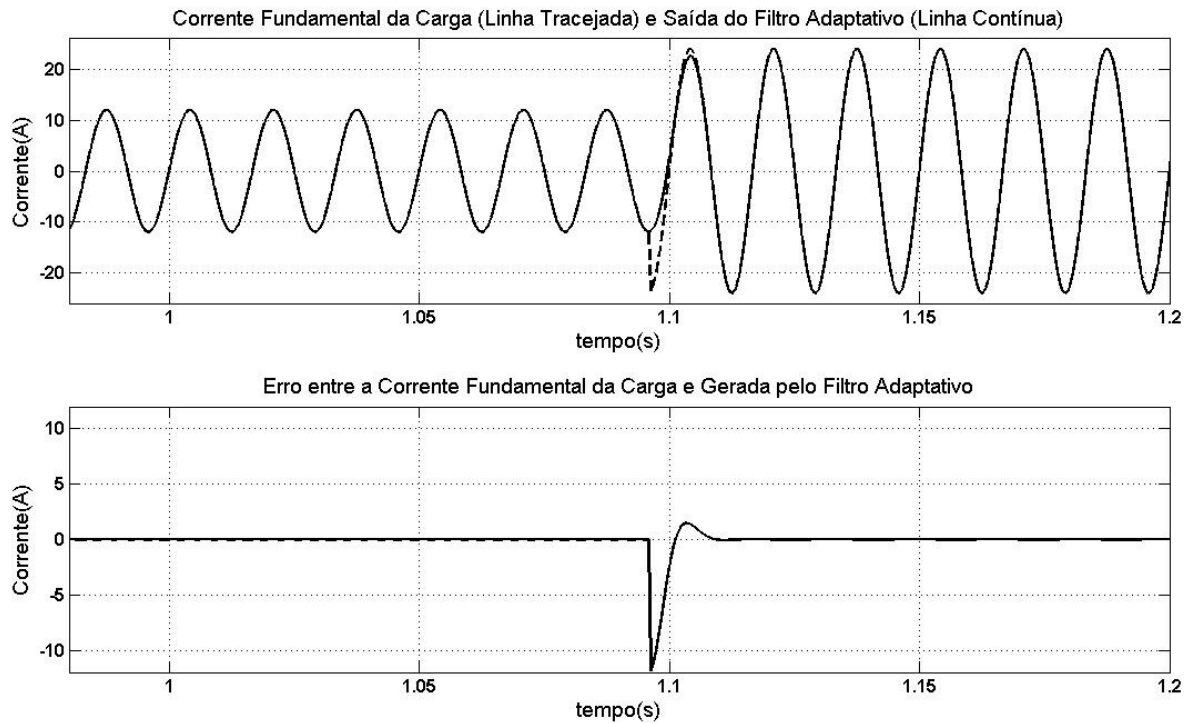
Figura B.9: **Comparação entre a corrente fundamental da carga e a gerada pelo Filtro Adaptativo Sintonizado com algoritmo *LMS* modificado e alteração na corrente da carga de não-linear para linear.**
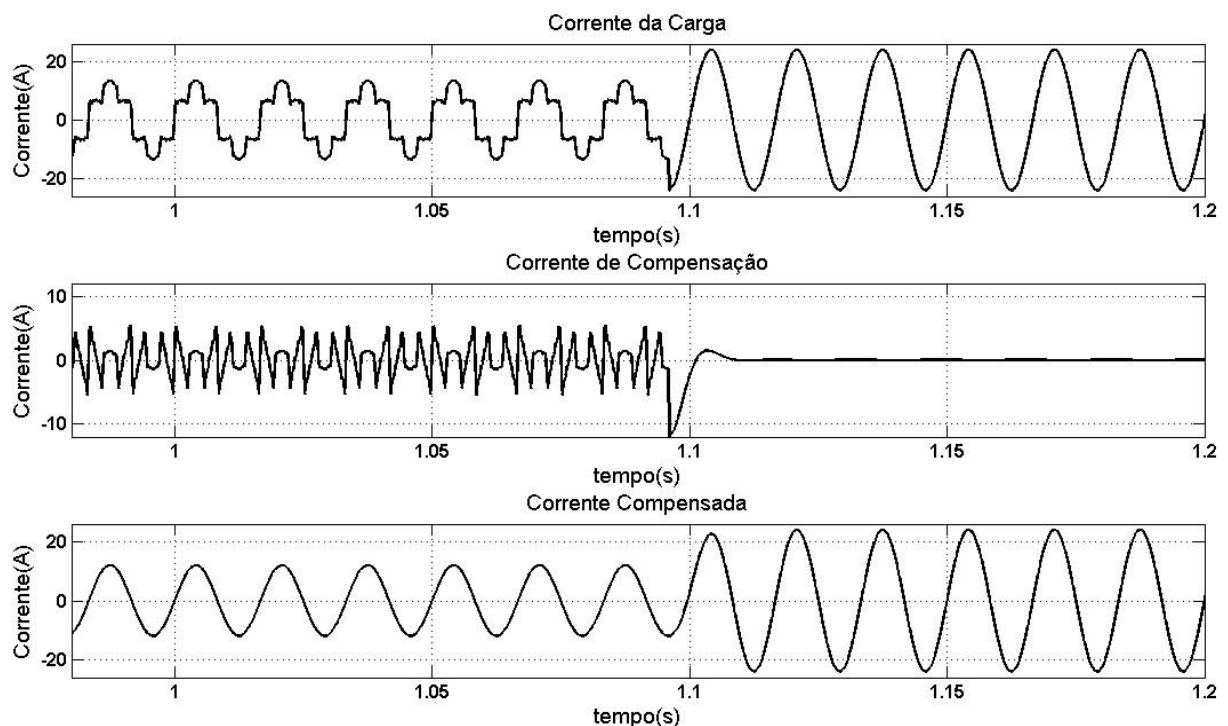
Figura B.10: **Resultado da compensação com transitório utilizando o Filtro Adaptativo Sintonizado com algoritmo *LMS* modificado com alteração na corrente da carga de não-linear para linear.**

As simulações realizadas com o Filtro Adaptativo Sintonizado demonstraram uma resposta em regime permanente mais precisa e uma adaptação dos coeficientes do Filtro Adaptativo inferior a um ciclo da fundamental.

A relação entre uma resposta em regime permanente mais precisa e a velocidade de convergência pode ser observada nas simulações apresentadas. Nestas simulações o tempo de convergência foi inferior a um ciclo da componente fundamental, tempo este superior ao demonstrado nas simulações anteriores na ordem de meio ciclo da componente fundamental. Mas sendo este um tempo adequado para aplicação em questão.

Com esta alteração no algoritmo o objetivo inicial de obter um erro em regime permanente mais preciso foi alcançado, ficando este erro em aproximadamente 0,1% da amplitude da componente fundamental da corrente da carga. Com isto, esta nova proposta para o algoritmo apresenta-se mais eficiente com relação tanto ao regime permanente quanto a velocidade de convergência.

Apêndice C – *Notchs* na Corrente da Fonte

Apesar do correto decréscimo no valor do *THDi* da corrente da fonte este valor está um pouco acima do valor desejado. O valor atual encontrado está em torno de 8%, sendo que o desejado para esta aplicação seria inferior a 5%. Este fato ocorre devido aos *notchs* encontrados na corrente da fonte compensada, como pode ser observado nos resultados experimentais do Capítulo 5 e na Figura C.1.
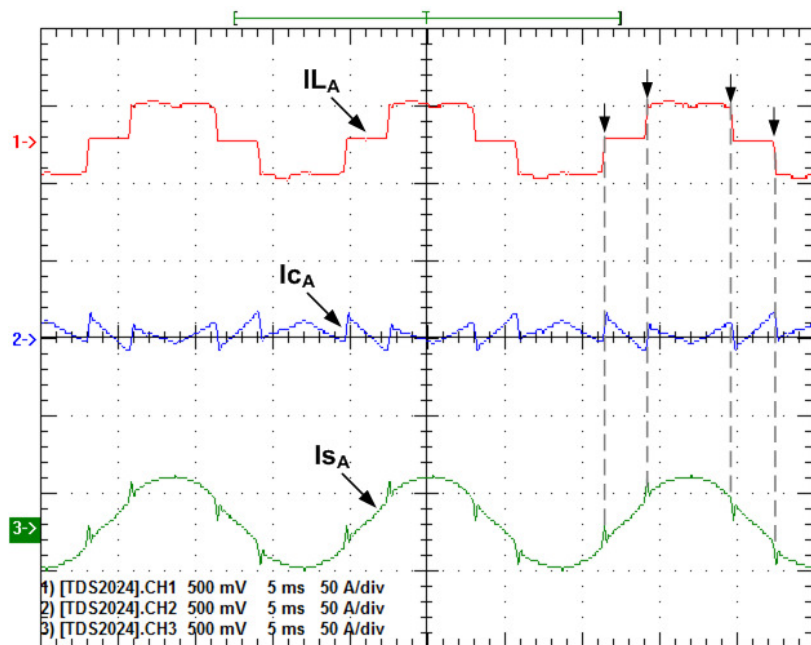
Figura C.1: Corrente da fonte compensada apresentando *notchs* acompanhando alterações em forma de degrau na corrente da carga.

Uma análise realizada demonstrou que este efeito deteriorante é devido a dois aspectos

- filtro *anti-aliansing* utilizado no circuito de condicionamento de sinais;
- resposta do inversor de freqüência a uma entrada em degrau.

O filtro *anti-aliasing* usado no circuito de condicionamento de sinais possui freqüência de corte de 20kHz. A resposta ao degrau desse filtro é apresentada nas Figuras C.2 e C.3. Estas figuras foram obtidas diretamente do circuito de condicionamento através do módulo de aquisição de dados NI USB-6215 da *National Instruments*.
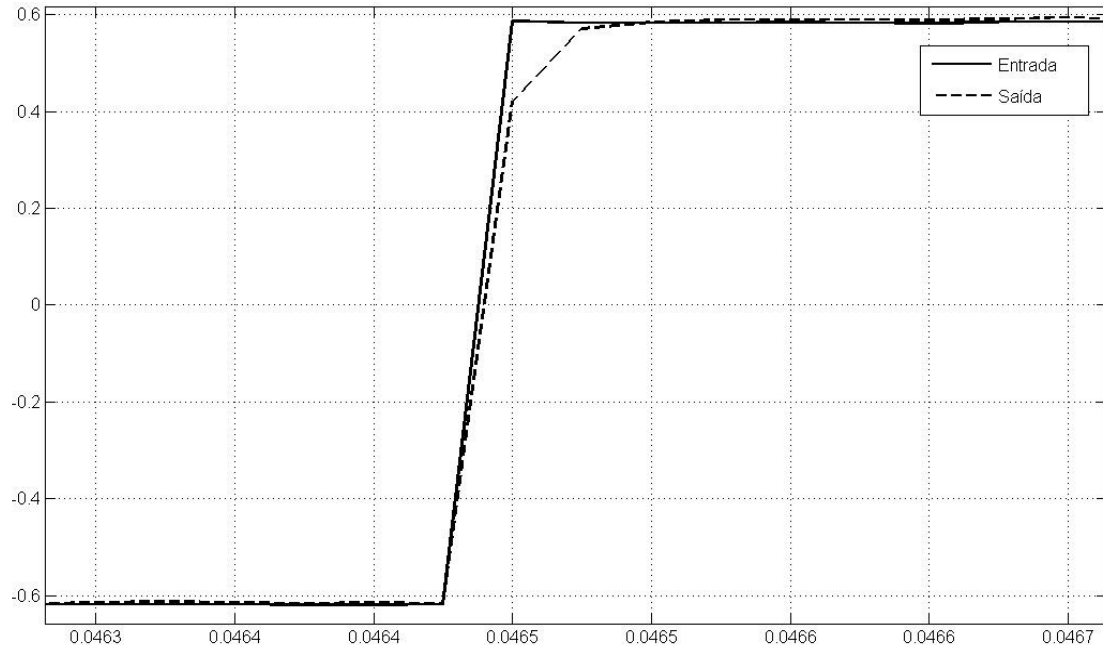
Figura C.2: Resposta ao degrau (subida) do filtro *anti-aliasing* usado no circuito de condicionamento.
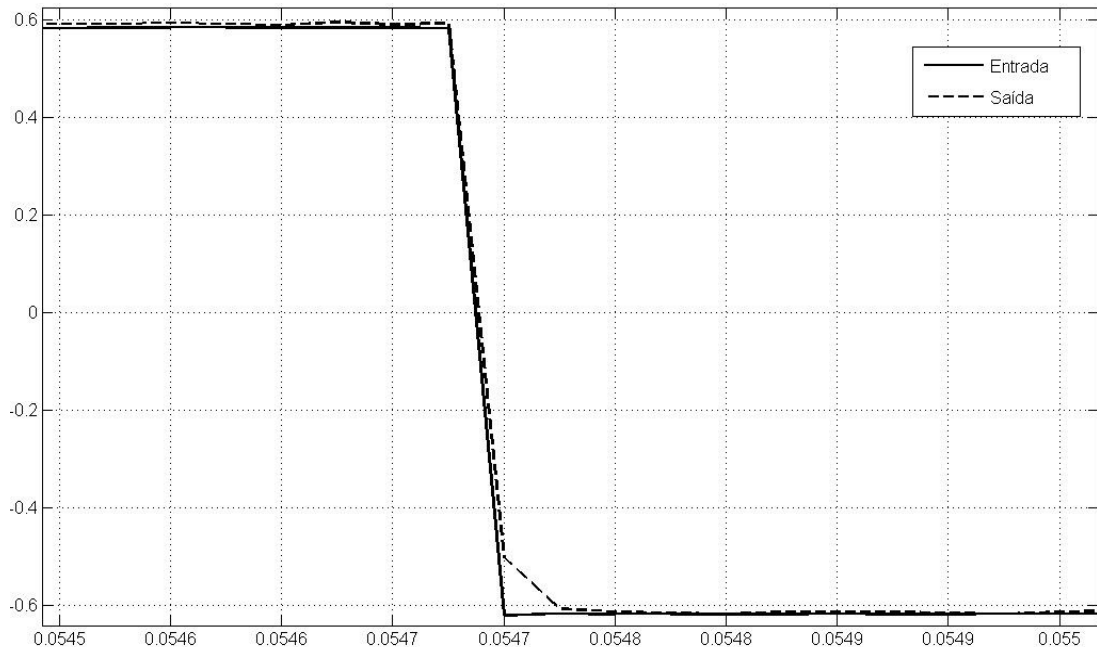
Figura C.3: Resposta ao degrau (descida) do filtro *anti-aliasing* usado no circuito de condicionamento.

O mesmo resultado pode ser encontrado através da simulação, o que é apresentado nas Figuras C.4 e C.5. Estas figuras demonstram a comparação entre a

entrada e a saída do filtro *anti-aliasing* para o sinal da corrente da carga típico. O gráfico infeiror das Figuras C.4 e C.5 demonstra a diferença entre o sinal de entrada e saída do filtro *anti-aliasing*.
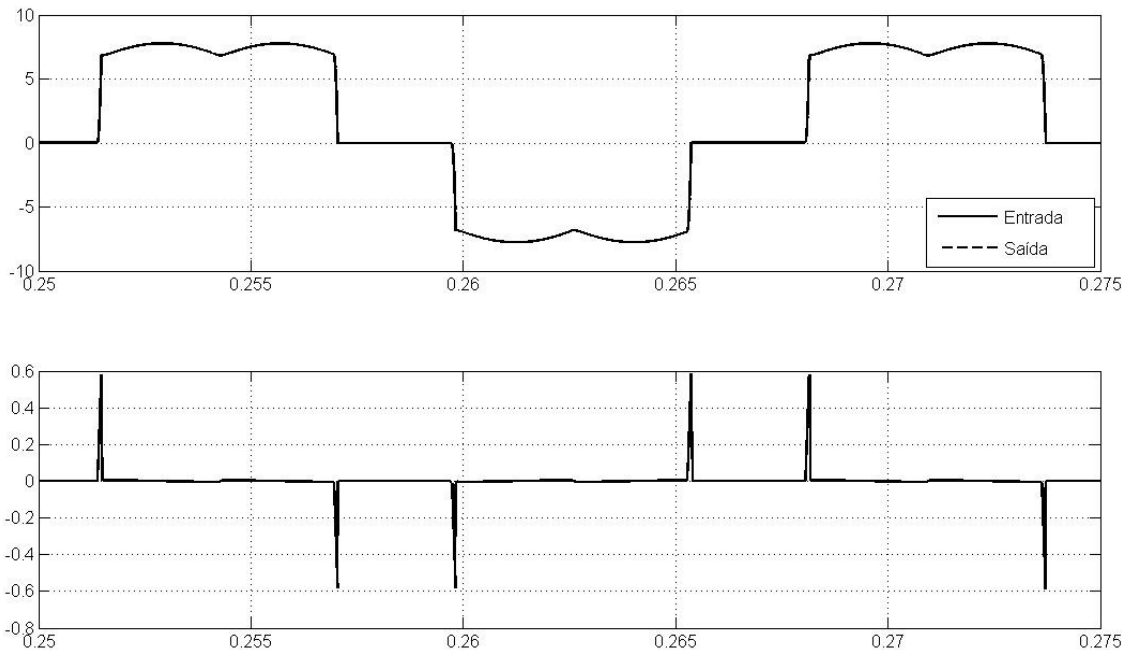
Figura C.4: Simulação usando o filtro *anti-aliasing* com a corrente da carga e comparação entre a entrada e a saída do filtro.
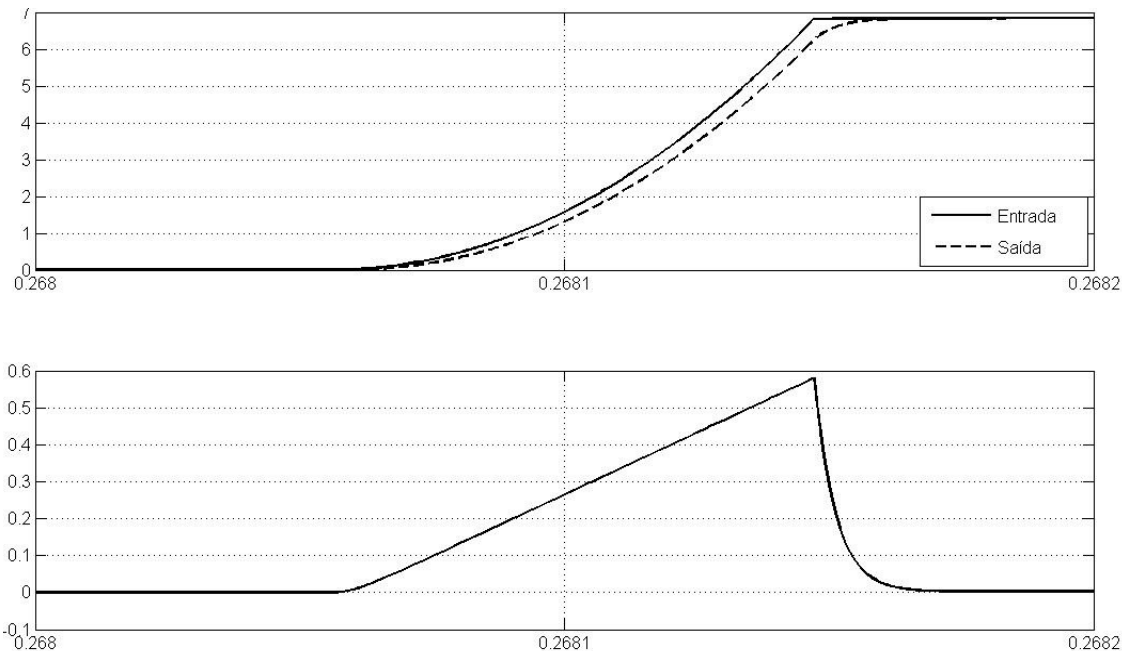
Figura C.5: Simulação usando o filtro *anti-aliasing* com a corrente da carga e comparação entre a entrada e a saída do filtro em detalhes.

Como observado nas figuras existe uma perda significativa no sinal de saída do filtro *anti-aliansing* em relação ao sinal de entrada. O sinal da corrente da carga utilizado no algoritmo de controle passa por esse filtro *anti-aliasing*, sofrendo também uma perda como demonstrado nas figuras anteriores. Desta maneira, comprometendo a ação do algoritmo na compensação do conteúdo harmônico. Pois, a corrente de compensação inserida no sistema pelo Filtro Ativo de Potência é gerada através do sinal da corrente da carga.

Outro ponto que contribui para o aparecimento desses *notchs* na corrente da fonte é a resposta do inversor de freqüência a uma entrada em degrau. Essa resposta deve ser rápida o suficiente para acompanhar (compensar) uma transição do tipo degrau na forma de onda da corrente da carga. Como a resposta do inversor a um degrau não é ideal, então existirá uma perda na compensação do conteúdo harmônico nestes pontos de transição do tipo degrau na forma de onda da corrente da carga. Contribuindo assim, para o aumento no valor do *THDi* da corrente da fonte compensada.

Com isto, é importante um trabalho mais detalhado sobre esses dois aspectos causadores do efeito na corrente da fonte. Buscando minimizar ou eliminar esses *notchs* na corrente compensada, alcançando assim um melhor *THDi*.

Apêndice D – Artigos Publicados

Os artigos publicados, durante o período deste trabalho, são apresentados a seguir.

ARTIGOS PUBLICADOS EM PERIÓDICO

1. DA SILVA, C. H. ; PEREIRA, R. R. ; SILVA, L. E. B. ; LAMBERT-TORRES, G. ; BOSE, B. K. ; AHN, S. U. . A Digital PLL Scheme for Three-Phase System Using Modified Synchronous Reference Frame. IEEE Transactions on Industrial Electronics, v. 57, no. 11, pp. 3814–3821, Nov. 2010.

2. PEREIRA, R. R.; DA SILVA, C. H.; SILVA, L. E. B.; LAMBERT-TORRES, G. ; BOSE, B. K. . Adaptive Hysteresis Current Control of a PWM Inverter at Constant Modulation Frequency Applied to Shunt Active Power Filters. In: Revista Eletrônica de Potência, v. 15, n. 4, p. 323-329, Set./Nov. 2010.

ARTIGOS ACEITOS PARA PUBLICAÇÃO EM PERIÓDICO

1. PEREIRA, R. R.; DA SILVA, C. H. ; SILVA, L. E. B.; LAMBERT-TORRES, G. . New Strategies for application of Adaptive Filters in Active Power Filters. In: IEEE Transactions on Industry Applications Society, 2011.

ARTIGOS PREMIADOS EM CONGRESSO:

1. PEREIRA, R. R. ; DA SILVA, C. H. ; SILVA, L. E. B. ; LAMBERT-TORRES, G. . A New Strategy to Step-Size Control of Adaptive Filters in the Harmonic Detection for Shunt Active Power Filter. In: IEEE Industry Applications Society 44th Annual Meeting, IEEE-IAS 2009, 2009, Houston - USA. Proceedings of the IEEE Industry Applications Society 44th Annual Meeting. Houston - USA : IEEE Press, 2009.

ARTIGOS PUBLICADOS EM ANAIS DE CONGRESSOS:

1. PEREIRA, R. R.; DA SILVA, C. H.; SILVA, L. E. B.; LAMBERT-TORRES, G.; PINTO, J. O. P. . Improving the Convergence Time of Adaptive Notch Filters to Harmonic Detection. In: 36th Annual Conference of the IEEE Industrial Electronics Society, IEEE- IECON 2010, 2010, Phoenix - USA. Proceedings of the 36th Annual Conference of the IEEE Industrial Electronics Society, 2010.

2. DA SILVA, C. H.; PEREIRA, R. R.; SILVA, L. E. B.; LAMBERT-TORRES, G.; GONZATTI, R. B. . A Hybrid Active Var Compensator (HAVarC). In: 14th IEEE International Conference on Harmonics and Quality of Power- ICHQP 2010, 2010, Bergamo - Italy. Proceedings of the 13th IEEE International Conference on Harmonics and Quality of Power, 2010.

3. DA SILVA, C. H.; PEREIRA, R. R.; SILVA, L. E. B.; LAMBERT-TORRES, G.; GONZATTI, R. B.. Charging and Regulating the DC Link Voltage of Hybrid Active Series Power Filters. In: 14th IEEE International Conference on Harmonics and Quality of Power- ICHQP 2010, 2010, Bergamo - Italy. Proceedings of the 14th IEEE International Conference on Harmonics and Quality of Power, 2010.

4. DA SILVA, C. H.; PEREIRA, R. R.; SILVA, L. E. B.; LAMBERT-TORRES, G.; PINTO, J. O. P.. Unified Hybrid Power Quality Conditioner (UHPQC). In: IEEE International Symposium on Industrial Electronics, 2010, Bari, Italy. Proceedings of the 20th IEEE International Symposium on Industrial Electronics, 2010.

5. PEREIRA, R. R.; DA SILVA, C. H.; SILVA, L. E. B.; LAMBERT-TORRES, G. . Application of Adaptive Filters in Active Power Filters. In: X Congresso Brasileiro de Eletrônica de Potência, COBEP 2009, Bonito - Brasil. Anais do X Congresso Brasileiro de Eletrônica de Potência, 2009.

6. PEREIRA, R. R.; DA SILVA, C. H.; SILVA, L. E. B.; LAMBERT-TORRES, G.. A New Strategy to Step-Size Control of Adaptive Filters in the Harmonic Detection for Shunt Active Power Filter. In: IEEE Industry Applications Society 44th Annual Meeting, IEEE-IAS 2009, 2009, Houston - USA. Proceedings of the IEEE Industry Applications Society 44th Annual Meeting. Houston - USA : IEEE Press, 2009.

7. DA SILVA, C. H.; PEREIRA, R. R.; SILVA, L. E. B.; LAMBERT-TORRES, G.. Modified Synchronous Reference Frame Strategy for Selective-Tuned Single Phase Hybrid Active Power Filter. In: IEEE Industry Applications Society 44th Annual Meeting, IEEE-IAS 2009, 2009, Houston - USA. Proceedings of the IEEE Industry Applications Society 44th Annual Meeting. Houston - USA : IEEE Press, 2009.

8. Giscard F. C. Veloso; SILVA, L. E. B.; I. Noronha; LAMBERT-TORRES, G.; PEREIRA, R. R.; J. HADDAD. Detection of partial discharge in power transformers using Rogowski coil and multiresolution analysis. In: Congresso Brasileiro de Eletrônica de Potência - X COBEP, 2009, Bonito, MS. Anais do X Congresso Brasileiro de Eletrônica de Potência, 2009.

A Digital PLL Scheme for Three-Phase System Using Modified Synchronous Reference Frame

Carlos Henrique da Silva, Rondineli Rodrigues Pereira, Luiz Eduardo Borges da Silva, *Member, IEEE*, Germano Lambert-Torres, *Member, IEEE*, Bimal K. Bose, *Life Fellow, IEEE*, and Se Un Ahn

Abstract—This paper proposes a novel phase-locked loop (PLL) control strategy to synthesize unit vector using the modified synchronous reference frame (MSRF) instead of the traditional synchronous reference frame. The unit vector is used for vector rotation or inverse rotation in vector-controlled three-phase grid-connected converting equipment. The developed MSRF-PLL is fast in transient response compared to standard PLL technique. The performance is robust against disturbances on the grid, voltage wave with harmonic distortion, and noise. The proposed algorithm has been analyzed in detail and was fully implemented digitally using digital signal processor TMS320F2812. The experimental evaluation of the MSRF-PLL in a shunt active power filter confirms its fast dynamic response, noise immunity, and applicability.

Index Terms—Active filter, digital signal processor (DSP), phase-locked loop (PLL), synchronous reference frame (SRF).

I. INTRODUCTION

CONVERTING equipment, such as pulsewidth modulation (PWM) active rectifier, static VAR compensator, UPS system, active harmonic filter (AHF), etc., operating on utility grid, often require vector control to enhance performance. The vector control requires the unit vector signal which performs vector rotation (VR) or inverse rotation (VR-1) in the vector controller. The common method of unit vector generation is based on a synchronous reference frame (SRF) phasor diagram [1], as shown in Fig. 1. The utility phase voltages (v_{sa}, v_{sb}, v_{sc}) are converted to v_{ds}^s, v_{qs}^s (stationary $a - b - c$ frame to $d^s - q^s$ frame conversion), which are then converted to V_d and V_q in a synchronously rotating reference frame $(d^e - q^e)$, as shown in the Fig. 1.

Fig. 1. SRF phasor diagram for vector transformation.

The following equations can be written from the phasor diagram:

$$v_{qs}^s = v_{sa} = \hat{V}_s \sin(\omega_e t + \phi_1) \tag{1}$$
$$v_{ds}^s = \hat{V}_s \cos(\omega_e t + \phi_1) \tag{2}$$
$$V_d = \hat{V}_s \cos \phi_1 \tag{3}$$
$$V_q = \hat{V}_s \sin \phi_1 \tag{4}$$

where $\hat{V}_s = \sqrt{v_{ds}^{s2} + v_{qs}^{s2}} = \sqrt{V_d^2 + V_q^2}$ is the voltage vector magnitude that corresponds to the peak value of phase voltage, and ϕ_1 is the phase angle shown. If $\hat{V}_s$ is aligned to d^e-axis, i.e., $\phi_1 = 0$, then the unit vector $(\sin \omega_e t, \cos \omega_e t)$ in Cartesian form can be derived by the expressions

$$\sin \omega_e t = \frac{v_{qs}^s}{\hat{V}_s} \tag{5}$$
$$\cos \omega_e t = \frac{v_{ds}^s}{\hat{V}_s}. \tag{6}$$

Note that v_{qs}^s and v_{sa} are in phase alignment, and the unit vector components are cophasal to v_{qs}^s and v_{ds}^s, respectively. The SRF method of unit vector generation works well and is widely accepted, except that it is vulnerable to grid disturbance as well as harmonic distortion and noise in the grid voltage wave.

Phase-locked loop (PLL) schemes were known for a long time [1] for generation of control signals of phase-controlled

thyristor converters operating on utility system with distorted line voltage waves. Kaura and Blasko [2] proposed a PLL scheme that generates unit vector from three-phase utility voltage waves. The SRF-based PLL (SRF-PLL) uses standard proportional-integral (PI) control in the loop. The scheme works well for distorted utility conditions, such as harmonic distortion, line notching, voltage unbalance, frequency variation, line dip/loss, etc. However, the transient response is somewhat sluggish, and the PLL output is not free from pollution. A similar PLL structure was proposed in [3], [4], based on instantaneous power theory, which had similar limitations. A number of other SRF-PLL algorithms have been proposed in [5] and [6]. These algorithms have the usual slow dynamic response due to PI-based control, in addition to the problem of wrong phase lock under dc offset, harmonic distortion, and voltage unbalance.

The PLL algorithm introduced in this paper is designated as modified SRF-PLL (MSRF-PLL) because it uses only one phase voltage (i.e., v_{sa}) wave instead of three phase voltage waves used in the SRF-based algorithms. In addition, the PI control in the PLL control loop is eliminated. The concept of MSRF-PLL is not new. It was first developed and used in active series harmonic filters [7] to suppress the zero sequence harmonic current in a three-phase four-wire unbalanced system. Later, the scheme was used in a similar three-phase system, where the MSRF-PLL-based series active filter, inserted in the neutral wire, controls the zero sequence harmonic currents [8].

In terms of dynamics response, computational burden, and phase-angle error, a brief comparison between the proposed PLL and three selected single-phase PLL algorithms, cited in [9], is provided.

The first PLL algorithm is based on fictitious electrical power, power-based PLL (pPLL) [3], a single-phase version [9].

The pPLL has a PI controller, which is needed to meet closed-loop performance specifications where parameters design based on the frequency response method uses a trial-and-error approach. Additionally, the pPLL has a low-pass filter to extract the mean power. In addition, a feedforward term, that defines the central frequency around which the PLL will lock to, has to be provided.

In the MSRF-PLL, the cutoff frequency of the IIR filter and its order are the only design parameters needed, where the cutoff frequency, which must be lower than the lowest frequency component present in the signal, i.e., 120 Hz.

The second algorithm is based on the inverse Park transformation (parkPLL) [5], [6], which is a single-phase version of the three-phase SRF PLL [2], tries to emulate a balanced three-phase system with one input voltage signal, and then mimic the three-phase PLL structure.

The MSRF-PLL is not a single-phase version of the SRF PLL [2] as the structure presented in [5] and [6]. The MSRF-PLL uses its own structure [10], based on the concept of a single phase SRF, which was derived from Coulon oscillator [11]. Here, no compensator gains have to be defined in order to meet dynamic and disturbance rejection specifications, as needed in parkPLL and pPLL.
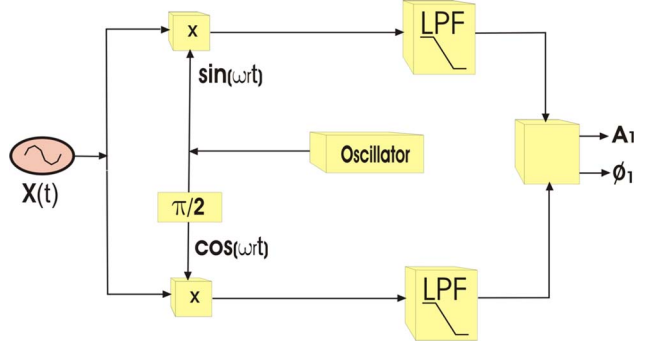
Fig. 2.   Block diagram of Coulon oscillator.

The third algorithm, based on an adaptive phase detection scheme, was originally called enhanced PLL (EPLL) [12], [13]. Basically, it reconstructs in real time the fundamental component of the input signal, by estimating its amplitude, phase, and frequency through the steepest descent algorithm. This algorithm has to face a tradeoff between speed of response and rejection of harmonic components, as in the parkPLL [9].

In the proposed MSRF-PLL, the speed response and rejection of harmonics are independent.

II. DESCRIPTION OF COULON OSCILLATOR

The new algorithm is based on the principle of Coulon oscillator [11]. Therefore, the theory of Coulon oscillator will be discussed first.

Fig. 2 shows the block diagram of Coulon oscillator, where the input signal $x(t)$ is harmonic rich, and is given by

$$x(t) = \sum_{i=1}^{N} A_i \sin(\omega_i t + \phi_i) \qquad (7)$$

where N is the harmonic order, A_i is the harmonic amplitude, and φ_i is the phase angle. It is possible to define the coupled oscillator frequency $f_r = \omega_r/2\pi$, which generates the $\sin(\omega_r t)$ and $\cos(\omega_r t)$ signals, as shown in the figure. Therefore, after multiplication (or modulation), the signals $x_1(t)$ and $x_2(t)$ are given, respectively, by

$$x_1(t) = \sum_{i=1}^{N} A_i \sin(\omega_i t + \phi_i) \cdot \sin(\omega_r t) \qquad (8)$$

$$x_2(t) = \sum_{i=1}^{N} A_i \sin(\omega_i t + \phi_i) \cdot \cos(\omega_r t). \qquad (9)$$

Equations (8) and (9) can be written in the form

$$x_1(t) = \sum_{i=1}^{N} \frac{A_i}{2} \{ \cos[(\omega_i - \omega_r)t + \phi_i] \\ - \cos[(\omega_i + \omega_r)t + \phi_i] \} \qquad (10)$$

$$x_2(t) = \sum_{i=1}^{N} \frac{A_i}{2} \{ \sin[(\omega_i - \omega_r)t + \phi_i] \\ + \sin[(\omega_i + \omega_r)t + \phi_i] \}. \qquad (11)$$

Defining the fundamental frequency $f_1 = \omega_1/2\pi$, and correspondingly, $\omega_i = i\omega_1$ and $\omega_r = r\omega_1$ (i and r are harmonic

orders), (10) and (11) can be written as

$$x_1(t) = \sum_{i=1}^{N} \frac{A_i}{2} \{\cos[(i-r)\omega_1 t + \phi_i]$$
$$- \cos[(i+r)\omega_1 t + \phi_i]\} \qquad (12)$$

$$x_2(t) = \sum_{i=1}^{N} \frac{A_i}{2} \{\sin[(i-r)\omega_1 t + \phi_i]$$
$$+ \sin[(i+r)\omega_1 t + \phi_i]\}. \qquad (13)$$

In order to extract the fundamental component of $x(t)$, the oscillator frequency ω_r should be tuned to be the same frequency as ω_1, i.e., $r = i = 1$. Therefore

$$x_1(t) = \frac{A_1}{2}\cos(\phi_1) - \frac{A_1}{2}\cos(2\omega_1 t + phi_1)$$
$$+ \sum_{i=2}^{N} \frac{A_i}{2} \{\cos[(i-1)\omega_1 t + \phi_i]$$
$$+ \cos[(i+1)\omega_1 t + \phi_i]\} \qquad (14)$$

$$x_2(t) = \frac{A_1}{2}\sin(\phi_1) - \frac{A_1}{2}\sin(2\omega_1 t + \phi_1)$$
$$+ \sum_{i=2}^{N} \frac{A_i}{2} \{\sin[(i-1)\omega_1 t + \phi_i]$$
$$+ \sin[(i+1)\omega_1 t + \phi_i]\}. \qquad (15)$$

The first term of (14) and (15) is a dc component related with the fundamental magnitude A_1 and phase angle ϕ_1, the second term is the second harmonic, and the remaining terms are higher frequency components. A low-pass filter, filters out the dc component of each signal which is given as

$$V_d' = \frac{A_1}{2}\cos\phi_1 \qquad (16)$$

$$V_q' = \frac{A_1}{2}\sin\phi_1. \qquad (17)$$

Therefore, the output of the Coulon oscillator can be derived

$$A_1 = \sqrt{(2V_d')^2 + (2V_q')^2} \qquad (18)$$

$$\phi_1 = \tan^{-1}(V_q'/V_d'). \qquad (19)$$

If the phase of the oscillator coincides with the phase of the fundamental component of input signal $x(t)$, i.e., $\phi_1 = 0$, then $V_d' = 0.5A_1$ and $V_q' = 0$. It can be shown that the Coulon oscillator cannot only filter out the fundamental component of input signal, but any other harmonic component can be filtered out by appropriately tuning the coupled oscillator.

An adaptation of the circuit has been used in an AHF to suppress neutral harmonic current in three-phase four-wire system [7], [8].

III. MSRF-PLL CONTROL STRATEGY

Fig. 3 shows the block diagram of the proposed MSRF-PLL structure, where v_{sa} = phase-a utility voltage at 60 Hz, that can
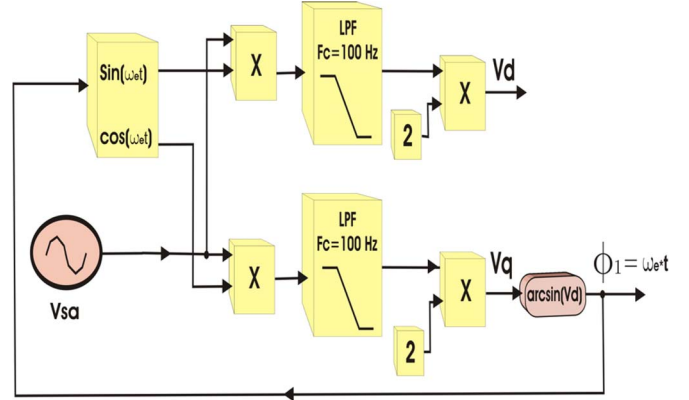
Fig. 3. MSRF-PLL block diagram.
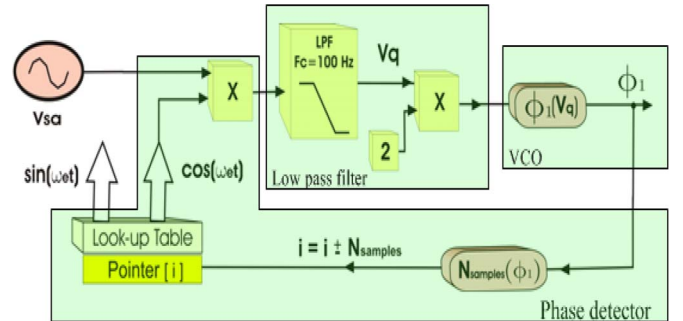
Fig. 4. Close loop control block diagram of actual MSRF-PLL.

be distorted with harmonics and A_1 = fundamental peak value. In the figure

$$V_d = 2V_d' = A_1 \cos\phi_1 \qquad (20)$$

$$V_q = 2V_q' = A_1 \sin\phi_1 \qquad (21)$$

where $\phi_1 = \arcsin(V_q)$ and $A_1 = 1.0$.

The phase angle ϕ_1 at the output can be fed back to the oscillator to lock its frequency and phase, so that ϕ_1 approaches zero. At this condition, $\sin\omega_e t$ and $\cos\omega_e t$ can be defined as unit vectors generated from utility phase voltage v_{sa}. The unit vector can be used for VR and VR-1 (VR^{-1}) in a three-phase vector control system similar to that shown in Fig. 1. This scheme is designated as MSRF-PLL. The advantage of the MSRF-PLL in comparison with the SRF-based scheme is that it is derived from only one phase voltage, and the unit vector output is not affected by harmonic distortion, unbalance, or sag/swell of the utility voltage waves.

The close loop control diagram of the MSRF-PLL is shown in Fig. 4. The output V_d is ignored, and $\phi_1 \cong V_q$ if ϕ_1 is small.

To reach the phase lock, the control loop, just shifts the pointer (i), of sin–cos lookup table, by a number of samples (N) proportional to the phase angle ϕ_1, as shown in Fig. 6. In stable conditions, $\phi_1 = 0$ and the phase of $\sin(\omega_e t)$ is locked with that of the v_{sa} fundamental component.

Any drift in the phase angle will be corrected by the PLL loop. For any transient phase deviation, the dynamic response of the MSRF-PLL depends only on the response of the low-pass filter that is used to filter out harmonic ripple from V_q. In this project, a fourth-order elliptic filter with 100-Hz cutoff
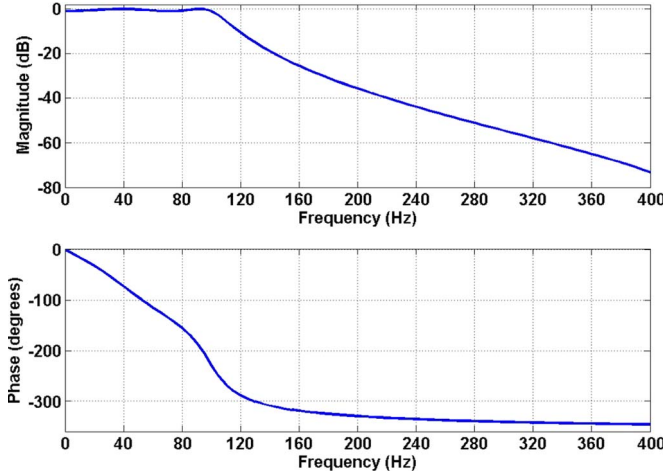
Fig. 5. Fourth-order elliptic filter Bode diagram.

TABLE I
SALIENT FEATURES OF TI-TMS320F2812 DSP

• 32-BIT FIXED-POINT
• 150 MHz FREQUENCY
• STATIC CMOS WITH HARVARD ARCHITECTURE
• COMPUTATION RATE: 150 MIPS (6.67 ns CYCLE TIME)
• 18K WORDS RAM AND 128K WORDS FLASH MEMORY
• 12-BIT, 16-CHANNEL A/D CONVERTER – 80 ns CONVERSION TIME
• 16 PWM CHANNELS WITH TWO EVENT MANAGERS
• THREE 32-BIT TIMERS
• 32X32-BIT MULTIPLIER
• FOUR POWER-DOWN MODES
• C AND ASSEMBLY LANGUAGE SUPPORT

frequency is used, which represents the bandwidth of the MSRF-PLL.

The unit vector, generated by the lookup table, is a pure sinusoidal free of distortion.

Equation (22) describes the difference equation of the elliptic filter

$$
\begin{aligned}
Y(n) = {} & bo\left[X(n)\right] + b1\left[X(n-1)\right] + b2\left[X(n-2)\right] \\
& + b3\left[X(n3)\right] + b4\left[X(n-4)\right] \\
& - \{a1\left[Y(n-1)\right] + a2\left[Y(n-2)\right] \\
& \quad + a3\left[Y(n-3)\right] + a4\left[Y(n-4)\right]\}
\end{aligned}
\tag{22}
$$

where an and bn are the filter coefficients, shown at the bottom of the page.

Fig. 5 shows the Bode diagram of the implemented IIR filter. The program Matlab/FDATools has been used to design the filter.

IV. DSP IMPLEMENTATION OF MSRF-PLL

The MSRF-PLL, shown in Fig. 4, was implemented digitally by a Texas Instruments digital signal processor (DSP)-type TMS320F2812 [14]. The 32-b fixed-point DSP has a computation speed of 150MIPS (6.7-ns instruction cycle time), and the embedded A/D converter has 16 channels with 12-b resolution and 80-ns conversion time. All the control codes were written in C language, which are then compiled into object code. Its features are summarized in Table I.
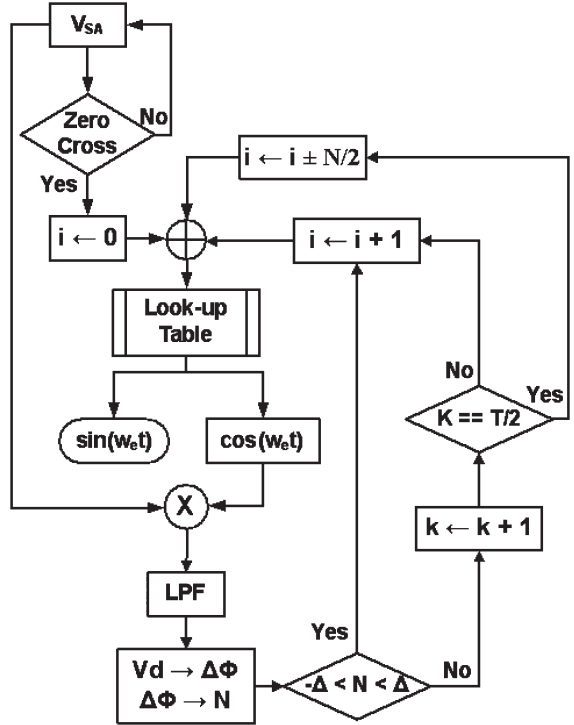
Fig. 6. DSP implementation flowchart of MSRF-PLL.

The flowchart for MSRF-PLL implementation is shown in Fig. 6. The sampling frequency is set to 40 kHz giving 668 samples per period (T) of fundamental frequency of 60 Hz.

$b0 = 0.00010192857257854628$

$b1 = -0.00039392157592801051$

$b2 = 0.00058422662879269519$

$b3 = -0.00039392157592801056$

$b4 = 0.00010192857257854628$

$a1 = -3.9691904476429422$

$a2 = 5.9090193350032472$

$a3 = -3.9104440317963309$

$a4 = 0.97061541441845633$
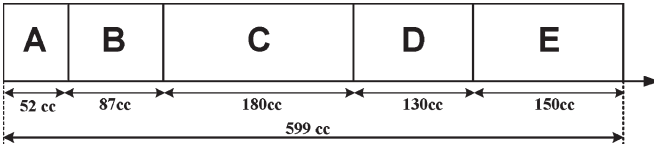
Fig. 7.   MSRF-PLL task time diagram.
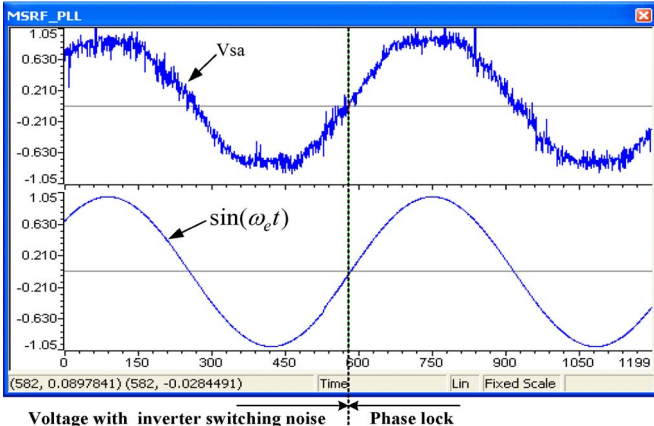
Fig. 8.   Noise filtering performance of MSRF-PLL.
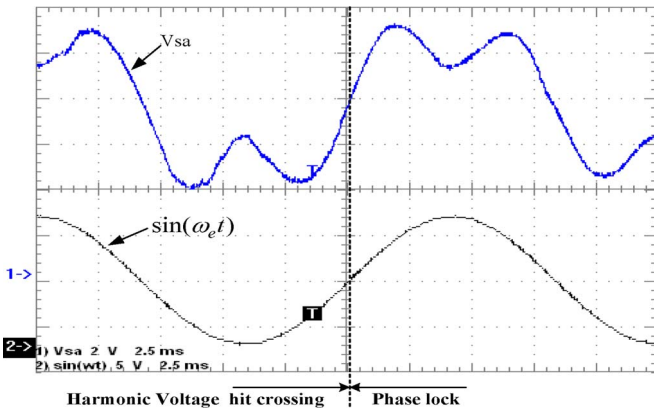
Fig. 9.   MSRF-PLL performance for distorted grid voltage wave.

Fig. 10.   MSRF-PLL response for grid voltage sag of 50%.
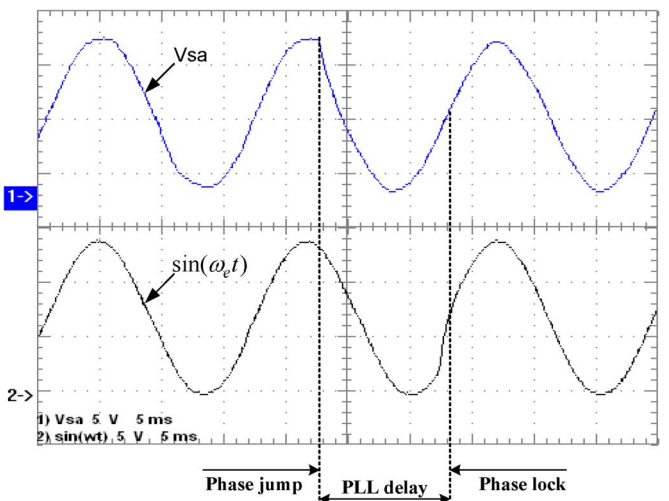
Fig.11.   MSRF-PLL response for 30° phase jump of grid voltage wave.
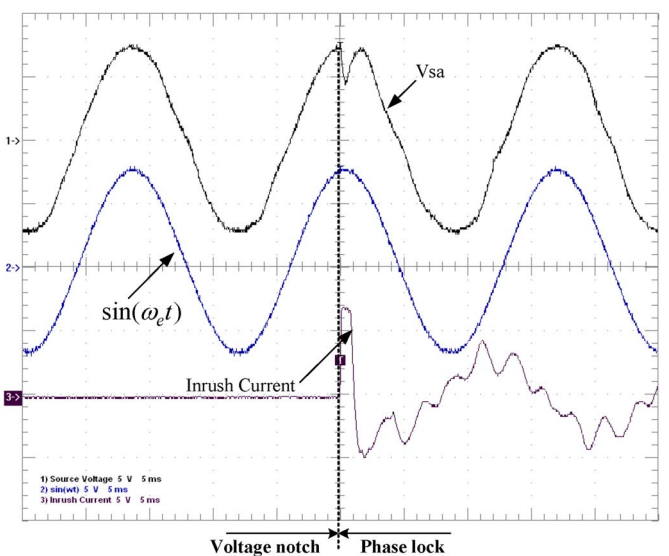
Fig. 12.   MSRF-PLL response for capacitor bank inrush current.

This corresponds to the sampling time of 25 μs and an angle resolution of 0.53°.

Initially, the DSP waits and searches for the first zero crossing of the v_{sa} wave, to speed up the first phase lock, by minimizing the starting phase error, as indicated. Then, it updates the PLL pointer to zero location and enters the MSRF-PLL control loop. The algorithm calculates the phase angle error ϕ_1 during every sample time (25 μs) and determines the proportional value of count N. The maximum value of Δ allowed for normal operation is 4, which corresponds to an angular deviation of 2.12° in leading or lagging. This hysteresis-band is provided to compensate the supply voltage fluctuation and the 15% drift in frequency, operating on 100% of frequency output accuracy. The computation of the algorithm takes approximately 4.0 μs or 599 clock cycles (1 cc = 6.67 ns).

The PLL instruction cycles is shown in the MSRF-PLL Task Time Diagram, Fig. 7, expressed in clock cycles, where

A   PLL Input signal (v_{sa}) acquisition time = 0.35 μs or 52 cc;
B   phase comparator time execution = 0.58 μs or 87 cc;

TABLE II
PLL COMPARISON SUMMARY

	pPLL	*parkPLL*	*EPLL*	*MSRF_PLL*
+40° phase angle jump				
Settling time	7 cycles	3 cycles	2.5 cycles	0.75 cycle
Overshoot	23°	14°	15°	0°
30% Voltage Sag				
Settling time	5 cycles	2 cycles	2.5 cycles	0 cycle
Peak error	2°	4°	3°	0°
Harmonic Distortion				
Peak-to-Peak error	$\approx 0°$	3°	5°	0°
Execution Time	2.58μs	3.8μs	3.04μs	4μs
Input Signal	generated	generated	generated	acquired
Sampling frequency	30720 Hz	30720 Hz	30720 Hz	40080 Hz
Writing Language	assembly	assembly	assembly	C
Data type	fixed point	fixed point	fixed point	Emulated float point
Noise immunity	unknown	unknown	unknown	High immunity
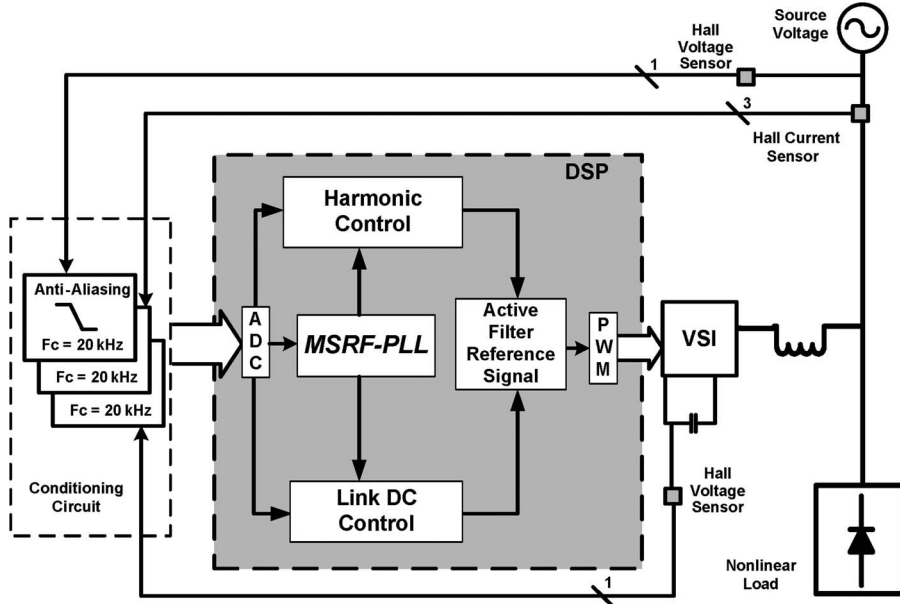
Fig. 13. Shunt active power filter block diagram.

C   low pass filter execution time $= 1.2\ \mu s$ or 180 cc;
D   VCO block execution time $= 0.87\ \mu s$ or 130 cc;
E   PLL Output signal (PWM) execution time $=\ 1\ \mu s$ or 150 cc.

V. EXPERIMENTAL PERFORMANCE

The Fig. 8 shows the noise filtering property of the MSRF-PLL while the fundamental components of v_{sa} with a 14-dB SNR, and $\sin(\omega_e t)$ remain aligned. Fig. 9 shows the MSRF-PLL performance when the grid voltage is distorted with low-frequency harmonics. Fig. 10 shows the response when the v_{sa} wave is sagged by 50%. The sin wave does not show any deviation by sagging. Fig. 11 shows the response when v_{sa} wave jumps in phase (leading) by 30°. Finally, Fig. 12 shows the response to a severe line voltage notch due capacitor bank inrush current.

Three selected single-phase PLL algorithms cited in [9] are compared with the proposed MSRF-PLL, and the related performance indexes are summarized in Table II.
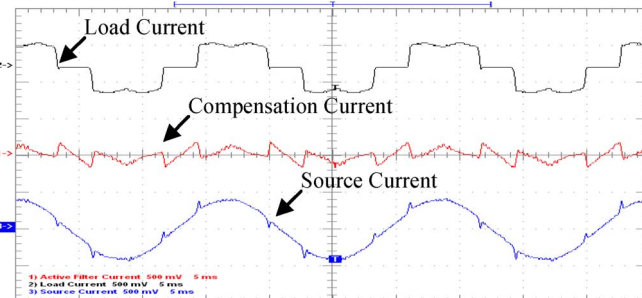
Fig. 14. SAPF-based MSRF-PLL: Phase A system currents.
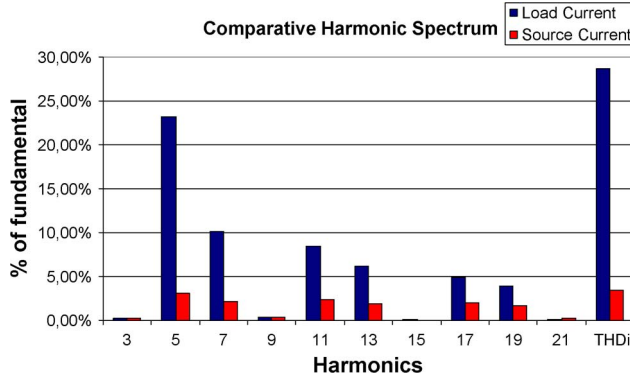
Fig. 15. Comparative source harmonic current Spectrum to 30 A.

The convergence time important in PLL algorithms are also pointed out to two different situations, critical issues on PLL handling.

VI. APPLICATION PERFORMANCE

The environment test chosen to evaluate the MSRF-PLL behavior is a shunt active power filter, shown in Fig. 13, where the objective is to evaluate the performance of a three-phase shunt active filter based on SRF controller using the MSRF-PLL [15].

Taking into account that the dynamic response, the stability on load variation and the accuracy of the harmonic current compensation are extremely dependent on the PLL response, the following results highlight the MSRF-PLL contribution to the shunt active power filter (SAPF) performance.

Fig. 14 shows the current harmonic mitigation to a demanding source current of 30 Arms, related to phase A. The THDi changes from 29% (before) to 3.4% after compensation, shown in Fig. 15.

Fig. 16 shows the behavior of the SAPF to a heavy load current variation, 100%, rising from 12 to 24 A (rms).

VII. CONCLUSION

An MSRF-based PLL was described. The strategy is simple, fast in transient response compared to standard PLL technique, and the performance is robust against grid disturbances, voltage harmonic distortion, and noise. The proposed technique synthesizes the unit vector signals, without distortions, in applications where VR or inverse VR are required. The strategy was analyzed in detail and its validity was verified applying the scheme
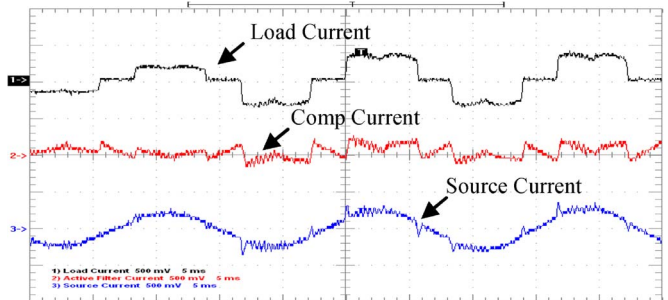
Fig. 16. SAPF-based MSRF-PLL: 100% load variation.

in a shunt active power filter. The algorithm was implemented digitally with DSP TI-TMS320F2812, and tested extensively in laboratory.

The performances of the proposed MSRF-PLL were found to be excellent in steady state and transient conditions. The comparison with others PLL schemes has demonstrated the effectiveness and high performance of the methodology.

REFERENCES

[1] B. K. Bose, *Modern Power Electronics and AC Drives*. Upper Saddle River, NJ: Prentice-Hall, 2001.
[2] V. Kaura and V. Blasko, "Operation of a phase locked loop system under distorted utility conditions," *IEEE Trans. Ind. Appl.*, vol. 33, no. 1, pp. 58–63, Jan./Feb. 1997.
[3] L. G. B. Rolim, D. R. da Costa, and M. Aredes, "Analysis and software implementation of a robust synchronizing PLL circuit based on the pq theory," *IEEE Trans. Ind. Electron.*, vol. 53, no. 6, pp. 1919–1926, Dec. 2006.
[4] S. A. O. Silva and E. A. A. Coelho, "Analysis and design of a three-phase PLL structure for utility connected systems under distorted conditions," in *Proc. 6th Int. Conf. Ind. Appl. IEEE/INDUSCON*, 2004, pp. 218–223.
[5] S. M. Silva, B. M. Lopes, B. J. C. Filho, R. P. Campana, and W. C. Boaventura, "Performance evaluation of PLL algorithms for single-phase grid-connected systems," in *Conf. Rec. IEEE IAS Annu. Meeting*, 2004, pp. 2259–2263.
[6] L. N. Arruda, S. M. Silva, and B. J. C. Filho, "PLL structures for utility connected systems," in *Conf. Rec. IEEE IAS Annu. Meeting*, 2001, pp. 2655–2660.
[7] C. H. Silva, V. F. Silva, and L. E. Borges da Silva, "Synchronous frame based controller improvement for active series filters under unbalanced conditions in three-phase four-wire systems," in *Proc. 7th Int. Conf. Ind. Appl. IEEE/INDUSCON*, 2006, pp. 156–160.
[8] C. H. Silva, V. F. Silva, L. E. Borges da Silva, and G. Lambert-Torres, "Optimizing the series active filters under unbalanced conditions acting in the neutral current," in *Proc. Int. Conf. IEEE/ISIE*, 2007, pp. 943–948.
[9] R. M. Santos Filho, P. F. Seixas, P. C. Cortizo, L. A. B. Torres, and A. F. Souza, "Comparison of three single-phase PLL algorithms for UPS applications," *IEEE Trans. Ind. Electron.*, vol. 55, no. 8, pp. 2923–2932, Aug. 2008.
[10] C. H. da Silva, R. R. Pereira, L. E. Borges da Silva, G. Lambert-Torres, and V. F. da Silva, "DSP implementation of three-phase PLL using modified synchronous reference frame," in *Proc. 33rd IEEE/IECON*, 2007, pp. 1697–1701.
[11] S. Tnani, M. Mazaudier, A. Berthon, and S. Diop, "Comparison between different real-time harmonic analysis methods for control of electrical machines," in *Proc. PEVD*, 1994, pp. 4946–4951.
[12] M. Karimi-Ghartemani and M. R. Iravani, "A method for synchronization of power electronic converters in polluted and variable-frequency environments," *IEEE Trans. Power Syst.*, vol. 19, no. 3, pp. 1263–1270, Aug. 2004.
[13] M. Karimi-Ghartemani and M. R. Iravani, "A new phase-locked loop (PLL) system," in *Proc. IEEE MWSCAS*, 2001, pp. 421–424.
[14] *Texas Instruments DSP Platforms*, Nov. 2004. [Online]. Available: http://focus.ti.com/docs/prod/folders/print/tms320c2812.html
[15] C. H. da Silva, R. R. Pereira, L. E. Borges da Silva, G. Lambert-Torres, and B. K. Bose, "Improving the dynamic response of shunt active power filter using modified synchronous reference frame PLL," in *Proc. 34th IEEE/IECON*, 2008, pp. 790–795.

Carlos Henrique da Silva was born in João Monlevade, Brazil, in 1977. He received the B.Sc. degree in electrical engineering from the Federal University of Sao Joao Del Rei, São Joao del Rei, MG, Brazil, in 2003 and the M.Sc. degree in electrical engineering from Itajubá Federal University, Itajubá, MG, Brazil, in 2005, where he is currently working toward the D.Sc degree.

His research interests include active power filters, digital signal processing, and control systems.

Rondineli Rodrigues Pereira received the B.Sc. degree in computation engineering and the M.Sc. degree in electrical engineering from Itajubá Federal University, Itajubá, MG, Brazil, in 2007 and 2009, respectively, where he is currently working toward the Ph.D. degree.

His research interests include digital signal processing, adaptive filters, control algorithms for active power filters, harmonics, and power quality.

Luiz Eduardo Borges da Silva (M'88) received the B.S. and M.Sc. degrees in electrical engineering from Itajubá Federal University (UNIFEI), Itajubá, MG, Brazil, in 1977 and 1982, respectively, and the Ph.D. degree from École Polytechnique de Montréal, Montréal, QC, Canada, in 1988.

He was a Visiting Professor with the University of Tennessee, Knoxville, in 1998. He is currently a Professor of the Electronic Engineering Department, UNIFEI. His research focuses on power electronics, electronic power systems, power converters, and applications of adaptive and intelligent control in industrial problems. He is the Head of Power Electronics at UNIFEI. He has directed many projects in the field of industrial electronics, and coauthored over 200 technical papers. He has supervised more than 30 master and doctoral thesis.

Germano Lambert-Torres (M'90) received the Ph.D. degree in electrical engineering from École Polytechnique de Montréal, Montréal, QC, Canada, in 1990, the B.S. and M.Sc. degrees in electrical engineering from Itajubá Federal University (UNIFEI), Itajubá, MG, Brazil, the B.S. degree in economics from Faculty of Economic Sciences at South of Minas, and the B.S. degree in mathematics from Itajubá Faculty of Sciences and Letters.

From 1995 to 1996, he was a Visiting Professor with the University of Waterloo, Waterloo, ON, Canada. From 2000 to 2004, he was served as Pro-Rector of Research and Graduate Studies, UNIFEI. He is currently a Professor and Dean of the Electrical Engineering Department, UNIFEI. He serves on a number of committees related to intelligent systems, in IEEE and CIGRE. He also serves as a Consultant for many power industries in Brazil and South America. He is a member of Intelligent System Applications to Power Systems (ISAP) international board. He has been teaching many tutorials by IEEE in U.S., Europe and Asia. He served as General Chair for ISAP in 1999 and 2009, as well Vice-General Chair for ISAP 2001, LACTEC (Congress on Logic Applied to Technology) in 2003 and 2007. He has more than 70 master and doctoral thesis complete supervisions, and more than 400 journal and conference technical papers published. He is also author/editor and coauthor of nine books and more than 30 book chapters in intelligent systems and nonclassical logics.

Prof. Lambert-Torres is a recipient of some awards, including "Technical Committee Working Group Recognition Award on New Technologies and Practical Applications," from the IEEE-PES (2006), "Outstanding Leadership as Member of the ISAP Board of Directors," from the International Council of ISAP (2007), and "Technical Committee Working Group Recognition Award on Multi-Agent Systems," from the IEEE-PES (2008).

Bimal K. Bose (S'59–M'60–SM'78–F'89–LF'96) received the B.E. degree from Bengal Engineering College (currently Bengal Engineering and Science University), Calcutta, India, in 1956, the M.S. degree from the University of Wisconsin, Madison, in 1960, and the Ph.D. degree from Calcutta University, Calcutta, in 1966.

Since 1987, has held the Condra Chair of Excellence (Endowed Chair) in power electronics with The University of Tennessee, Knoxville, where he is responsible for the teaching and research program in power electronics and motor drives. Concurrently, he served as the Distinguished Scientist (1989–2000) and Chief Scientist (1987–1989) of Electric Power Research Institute, Power Electronics Applications Center, Knoxville. Prior to this, he was a Research Engineer with the General Electric (GE) Corporate Research and Development Center (currently GE Global Research Center), Schenectady, NY, for 11 years (1976–1987), an Associate Professor of electrical engineering with Rensselaer Polytechnic Institute, Troy, NY, for five years (1971–1976), and a Faculty Member with Bengal Engineering and Science University for 11 years (1960–1971). He has specialized in power electronics and motor drives, specially including power converters, pulsewidth modulation techniques, microcomputer/DSP control, electric/hybrid vehicle drives, renewable energy systems, and artificial intelligence (expert system, fuzzy logic, and neural network) applications in power electronics and motor drives. He has been a Power Electronics Consultant in a large number of industries. He is the holder of an Honorary Professorship with Shanghai University (1991), China University of Mining and Technology (1995), X'ian Mining University (1998) (also an Honorary Director of the Electrical Engineering Institute), and Huazhong University of Science and Technology (2002). He has authored more than 200 papers and is the holder of 21 U.S. patents. He has authored/edited seven books in power electronics: *Power Electronics and Motor Drives—Advances and Trends* (New York: Academic, 2006), *Modern Power Electronics and AC Drives* (Englewood Cliffs, NJ: Prentice-Hall, 2002), *Power Electronics and AC Drives* (Englewood Cliffs, NJ: Prentice-Hall, 1986), *Power Electronics and Variable Frequency Drives* (New York: Wiley, 1997), *Modern Power Electronics* (Piscataway, NJ: IEEE Press, 1992), *Microcomputer Control of Power Electronics and Drives* (Piscataway, NJ: IEEE Press, 1997), and *Adjustable Speed AC Drive Systems* (Piscataway, NJ: IEEE Press, 1981). He has given tutorials, keynote addresses, and invited seminars extensively throughout the world, particularly in IEEE-sponsored programs and conferences.

Dr. Bose is a recipient of a number of awards and honors that include IEEE Power Electronics Society Newell Award (2005), IEEE Millennium Medal (2000), IEEE Meritorious Achievement Award in Continuing Education (1997), IEEE Lamme Gold Medal (1996), IEEE Industrial Electronics Society (IES) Eugene Mittelmann Award for lifetime achievement in power electronics and motor drives (1994), IEEE Region 3 Outstanding Engineer Award (1994), IEEE Industry Applications Society (IAS) Outstanding Achievement Award (1993), Calcutta University Mouat Gold (1970), GE Silver Patent Medal (1986), GE Publication Award (1985), and the Distinguished Alumnus Award (2006) from Bengal Engineering and Science University. He has served the IEEE in various capacities, including Chair of the IEEE IES Power Electronics Council, Associate Editor of IEEE TRANSACTIONS ON INDUSTRIAL ELECTRONICS, IEEE-IECON Power Electronics Chair, Chair of the IEEE IAS Industrial Power Converter Committee, IAS member of the Neural Network Council, Vice-Chair of the IEEE Medals Council, member of IEEE Energy Policy Committee, member of the IEEE Fellow Committee, member of Lamme Medal Committee, and a Distinguished Lecturer of both the IAS and IES, and is currently the Vice-Chair of the IAS Distinguished Lecturer Program. He has been a member of the editorial board of Proceedings of the IEEE since 1995 and *Journal of Intelligent and Fuzzy Systems* since 2001. He was the guest editor of the Proceedings of the IEEE "Special Issue on Power Electronics and Motion Control" (August 1994).

Se Un Ahn was born in Incheon, Korea, in 1957. He received the B.Sc. degree from Mackenzie Engineering School, São Paulo, Brazil, in 1981 and the M.Sc. and Ph.D. degrees in the electrical engineering from the University of São Paulo, São Carlos-SP, Brazil, in 1993 and 1997, respectively.

Currently, he is working for Postdoctoral Research in power quality. Since 1986, he has been with CPFL Piratininga Power and Light, (former Eletropaulo and Bandeirante, all Electrical Utility Company) as a Distribution System Researching Engineer. His professional activities include the following: load curve, transformers, power cables, power quality troubleshooting, and the use of artificial neural network at distribution system applications.

ADAPTIVE HYSTERESIS CURRENT CONTROL OF A PWM INVERTER AT CONSTANT MODULATION FREQUENCY APPLIED TO SHUNT ACTIVE POWER FILTERS

R.R. Pereira   C.H. da Silva   L.E. Borges da Silva   G. Lambert-Torres

Federal University of Itajubá - UNIFEI

Itajubá, Brazil

e-mail: rondi@unifei.edu.br; carloschedas@unifei.edu.br; leborges@unifei.edu.br; germano@unifei.edu.br

B. K. Bose

University of Tennessee

Knoxville, USA

e-mail: bbose@utk.edu

Abstract— **This paper proposes a novel adaptive hysteresis current control strategy of a voltage-fed PWM inverter, where the switching frequency always remains constant and the harmonic ripple is minimum, irrespective of dc link voltage fluctuation and load parameter variation. The developed algorithm works well for single-phase as well as multi-phase inverters, although single-phase inverter operation, particularly in active harmonic filter mode, is emphasized in this paper. The algorithm uses fuzzy logic-based current error compensation, and it is simple to implement and does not involve any hysteresis-band calculation. The control strategy has been implemented digitally with a high-speed digital signal processor (TI-TMS320F2812). The proposed scheme has been thoroughly evaluated in laboratory by simulation as well as in experimental studies on a single-phase inverter, and its performance was found to be excellent.**

Keywords **- Adaptive hysteresis, current control, PWM, constant modulation frequency, fuzzy control, active harmonic filter, digital signal processor (DSP).**

I. INTRODUCTION

The hysteresis-band current control PWM technique has been widely used for voltage-fed inverters primarily because of its simplicity of implementation. In addition, it is characterized by the advantages of fast response, inherent peak current limiting capability, and practical insensitivity to dc link voltage and load parameter variation. However, the main drawback of this method is the variation of modulation frequency that causes excessive harmonic ripple in the current wave. A number of hysteresis current control techniques are described in the literature [1]-[15]. Some of them are simple hysteresis current controls, while others are sophisticated adaptive strategies [1][2] to optimize the ripple by maintaining the modulation frequency constant. In the adaptive hysteresis-band current control strategy described by Bose [1] for machine [1]drive system, the band calculation is based on reference current derivative, dc link voltage, and load parameters, which are quite complex to implement in real time, particularly at high switching frequency. The scheme is again difficult to implement for applications such as active power filter and static VAR compensator, where the ac load parameters cannot be easily determined. Malesani's [2] adaptive hysteresis-band technique is more powerful, but

it needs information of load current derivatives, dc link voltage, and load parameters to predict the band width for minimization of current error, while maintaining the modulation frequency constant. The technique is more difficult to implement because load current is generally polluted with noise. Both schemes are normally implemented digitally with a high-speed digital signal processor (DSP).

The approach described in this paper uses the adaptive idea proposed by Malesani, but does not use any hysteresis band directly. The main idea here is to look into the current errors between the reference current and the actual current peak in two consecutive half cycles and control the errors to be as symmetrical as possible about the reference current [16]. Indirectly, it tends to control the upper hysteresis-band to be equal to that of the lower band. The strategy is much simpler to implement digitally because it avoids the calculation of current derivatives and the tracking of the load and source parameters. The technique guarantees fast response and clock-synchronized constant switching frequency.

II. DESCRIPTION OF ALGORITHM

The adaptive hysteresis current control algorithm proposed in the paper will be developed and validated first for a single-phase H-bridge inverter with *R-L* load, as shown in Figure 1. However, the algorithm is also valid for a three-phase inverter with connected or isolated neutral load of arbitrary load parameters (including counter-electromotive force (counter EMF)). The inverter operates in the usual bipolar mode, i.e., when the device pair 1-3 is switched on, the load current increases with positive slope, whereas the current decreases with negative slope as the pair 2-4 is turned on. It is assumed that the load is highly inductive so that the load current variation is nearly linear with constant dc voltage V_d.

Figure 2 explains the algorithm with the help of waveforms. The "clock" wave on the top with time period T and symmetrical half period $T/2$ determines the switching frequency of the inverter. In this project, the switching frequency is maintained constant at 20 kHz, i.e., $T = 50$ μs. The three vertical dashed lines in every half-cycle, as indicated in the figure, are at 5 μs intervals. The time $t_k = t_0,$ $t_1,$ $t_2,$ etc., as shown at the bottom at half-cycle interval, but lagging by 20 μs from the clock edge, is the reference time

for synchronizing the switching action of the inverter devices. At the middle of the figure, the inverter reference current (i_{ref}) is shown as the horizontal line, and the zigzag triangular wave is the actual inverter current (i_{actual}) wave, the mean value of which is trying to follow the i_{ref} wave. The current error parameters $\varepsilon(t_0)$, $\varepsilon(t_1)$, $\varepsilon(t_2)$, etc., as shown, are the differences between the peak of actual current wave and the i_{ref} wave at the corresponding reference times shown in the figure, i.e.,

$$\varepsilon(t_k) = i_{ref}(t_k) - i_{actual}(t_k) \qquad (1)$$
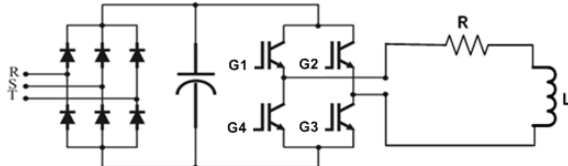
Fig. 1. Block diagram of converter system.
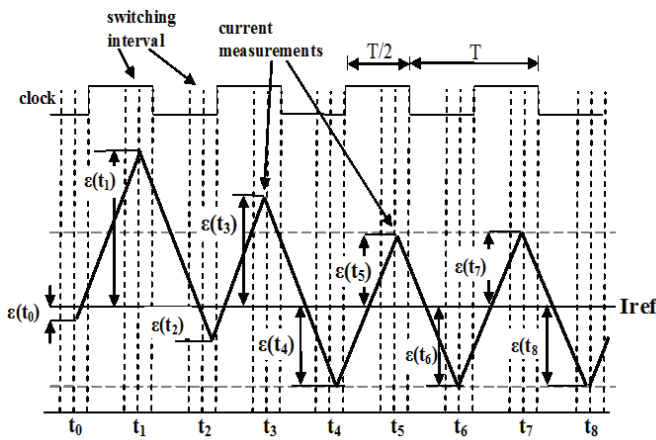
Fig. 2. Waveforms explaining the adaptive hysteresis current control strategy.

The initial part of the actual current wave is shown as unsymmetrical about the reference current wave (i.e., $|\varepsilon(t_1)| > |\varepsilon(t_2)|$), indicating that it is in transient condition, whereas in the latter part it is symmetrical (i.e., $|\varepsilon(t_6)| = |\varepsilon(t_7)| = |\varepsilon(t_8)|$), indicating the steady state condition. The algorithm tends to identify the asymmetry of the current error and controls the switching action of the devices, delaying or advancing with respect to the reference time t_k so that it tends to be symmetrical in the steady state. Of course, in the switching control strategy, the variation of i_{ref}, if any, should also be taken into consideration.

Assume that initially at $t_k = t_0$, the current error $\varepsilon(t_0)$ is negative as shown. Switching of the inverter devices 1-3 at t_0 will increase the current linearly. Then, when the devices 2-4 are switched at t_1, the current will start to fall and the peak positive current error is $\varepsilon(t_1)$, as indicated in the Figure 2. There may be three possible scenarios:

Case 1: $|\varepsilon(t_1)| = |\varepsilon(t_0)|$
Case 2: $|\varepsilon(t_1)| > |\varepsilon(t_0)|$
Case 3: $|\varepsilon(t_1)| < |\varepsilon(t_0)|$

Case 1 indicates the steady state condition with symmetrical current errors, and therefore, the next switching action has to occur at the instant t_2, where $t_2 = t_1 + T/2$. This means that the duty cycle is 50%, as shown in the latter part of the current wave. Note that 50% duty cycle means that the average output voltage is zero. This is true for the ideal inductive load. However, with counter EMF and/or resistive parameter loads, the duty cycle will deviate from 50% and the slope of the rising current and falling current will be unsymmetrical. For Case 2, which is the actual case in Figure 2, the switching of the device pair 1-3 has to be delayed beyond the instant t_2 by Δt_2 for compensation of the current error asymmetry. For Case 3, on the other hand, the switching action has to be advanced by Δt_2 for compensation. The total compensation time at t_k, is given by the expression

$$\Delta t_k = \Delta t_{k-1} + \alpha \qquad (2)$$

where Δt_{k-1} = value of cumulative compensation time at time t_{k-1} and α = estimated compensation time at the reference time t_k. The value of α depends on the difference between the past two values of current errors $\delta(k)$, where

$$\delta(k) = |\varepsilon(k-1)| - |\varepsilon(k-2)| \qquad (3)$$

The compensation proceeds in sequence at every half cycle until the steady state condition is reached. If there is any variation in the reference current, i.e.,

$$\Delta i_{ref}(k) = i_{ref}(k) - i_{ref}(k-1) \qquad (4)$$

It should also be taken into consideration for compensation. Therefore, α can be expressed as

$$\alpha = f(\delta, \Delta i_{ref}) \qquad (5)$$

where the term k has been dropped for simplicity.

A. Fuzzy Control of Compensation Time α

The optimum value of α is given by the nonlinear relation with δ and Δi_{ref} in (5), and can be estimated by using fuzzy logic. Fuzzy computation in real time is not a problem in high-frequency inverters considering the high speed of the DSP used in the controller. The fuzzy input variables (δ and Δi_{ref}) and the output variable α are bipolar, and can be described by triangular membership functions (MF) within a universe of discourse for a practical inverter. Figure 3 shows the membership functions of α, where each of the seven fuzzy sets, i.e., negative large (*nl*), negative medium (*nm*), negative small (*ns*), zero (*zr*), positive small (*ps*), positive medium (*pm*), and positive large (*pl*), are described by an asymmetrical triangle. The universe of discourse of α is limited to ±10 μs, as shown in the Figure 3. The variables δ and Δi_{ref} are described by five triangular membership functions (not shown) with overlap of 50%, and the MFs are identical for both the variables. The rule matrix for the estimation relating the fuzzy variables is given in Figure 4. A typical rule for estimation using Mamdani type implication can be read from Figure 4 as

IF δ is NS AND Δi_{ref} is ZR THEN α is NS.
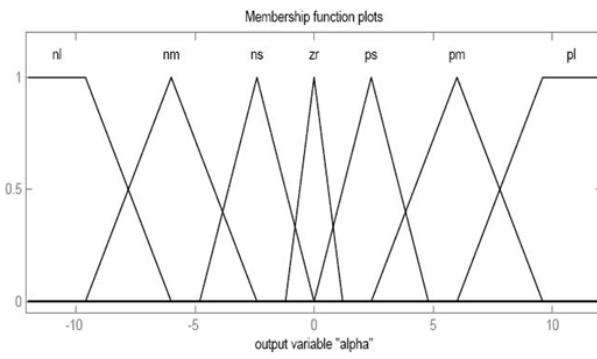
Fig. 3. Membership functions of fuzzy variable α.

Fig. 4. Rule table for fuzzy variable α relating with i_{ref} and δ.

All the variables are normalized for convenience of implementation. Figure 4 indicates that a $+\delta$ of higher magnitude will force higher $+\alpha$, and vice versa for $-\delta$ value. On the other hand, $+\Delta i_{ref}$ of higher magnitude will make higher $-\alpha$, and vice versa for $-\Delta i_{ref}$ value. The input variables are fuzzified, the control rules are evaluated, and the corresponding outputs are aggregated to compose the fuzzy output of α. Then, α is defuzzified using the simplified version of the Centroid (Center of Gravity) [17] method. The MATLAB-based Fuzzy Logic Toolbox [18] was used to develop the fuzzy control algorithm. All the membership functions and the rule table are iterated several times so that the performance of the fuzzy controller is the best reached.

III. DSP IMPLEMENTATION METHODOLOGY

The proposed PWM algorithm was fully implemented digitally with a high speed Texas Instruments DSP type TMS320F2812, the features of which are summarized in Table 1.

The 32-bit fixed-point DSP has a computation speed of 150 MIPS (6.7 ns instruction cycle time), and the embedded A/D converter has 16 channels with 12-bit resolution and 80 ns conversion time. Besides, there are three 32-bit dedicated timers and one 32-bit X 32-bit hardware multiplier to enhance the computation speed.

Figure 5 shows the flowchart for implementation of the proposed PWM algorithm. The flowchart, including the fuzzy controller, is executed every half cycle ($0.5T$) of inverter operation, as explained in the task timing diagram of Figure 6. The half cycle interrupt (INT) is generated by a hardware timer in the DSP. At the point named INT the system loads the timer with the calculated value of the IGBT´s switching time t_d. After that, the computations for the inverter are first done during the time interval A and it takes typically 10 µs to complete. The inverter IGBT´s switching occurs at the instant F. This time lies within the permitted compensation zone B. The instant of IGBT´s commutations is defined by $\pm\Delta t_k$ which is synchronized about the reference time t_k, as shown in the figure as the center of the compensation interval B. The actual advance time ($-\Delta t_k$) or delay ($+\Delta t_k$) is calculated during the interval C in the previous half cycle and implemented with a downcounter with delay time t_d. The flowchart with the fuzzy control (shown in Figure 5) is executed in time C (3 µs) just after the switching command is placed to the IGBT´s.

TABLE I
Salient Features of TI- TMS320F2812 DSP

32-Bit Fixed-Point
150 MHz Frequency
Static Cmos With Harvard Architecture
Computation Rate: 150 MIPS (6.67 ns Cycle Time)
18k Words Ram And 128k Words Flash Memory
12-Bit, 16-Channel A/D Converter – 80 ns Conversion Time
16 PWM Channels With Two Event Managers
Three 32-Bit Timers
32x32-Bit Multiplier
Four Power-Down Modes
C And Assembly Language Support

When the downcounter clears, the interrupt signal first measures the current with A/D converter at point E (80 ns) before switching the inverter devices at F (indicating an advanced compensation time $-\Delta t_k$ about the point t_k in the figure). The measurement of current before switching the devices is important because of the noise introduced by the switching.

After the measurement of the current, $\varepsilon(k) = i_{ref}(k) - i_{actual}(k)$ is estimated based on the measured value of $i_{actual}(k)$. The device pair 1-3 is switched on for the positive value of $\varepsilon(k)$, or else, the 2-4 pair is switched on for the negative value of $\varepsilon(k)$, as indicated in the figure. If these criteria are not satisfied, the switching action of device pair is maintained (for transient situation of i_{ref}).

At the flowchart in Figure 5, the adaptive scale factor $\varepsilon_s(k)$ is calculated for the variable δ and then used to compute $\delta(k)$ pu by the expression

$$\delta(k)pu = \frac{\delta(k)}{\varepsilon_s(k)} = \frac{[|\varepsilon(k-1)| - |\varepsilon(k-2)|]}{\varepsilon_s(k)} \qquad (6)$$

where $\varepsilon_s(k) = |\varepsilon(k-1)| + |\varepsilon(k-2)|$ is given by the sum of the previous consecutive positive and negative current errors. The adaptive scale factor essentially gives slope-sensitive correction of $\delta(k)$ pu, which means the $\delta(k)$ pu parameter decreases with higher current slope, and vice versa. Both $\delta(k)$ pu and Δi_{ref} are the variables of the fuzzy controller that estimates the value of α as shown. The variables Δi_{ref} and α are also normalized with fixed scale factor, but are not indicated in Figure 5 for simplicity. Next, the compensation time α is subtracted or added, respectively, from $\Delta t(k-1)$ to calculate the delay time $\Delta t(k)$, as shown in the figure.

The resulting time delay $\Delta t(k)$ is used for computation of downcounting time t_d for the next half cycle.
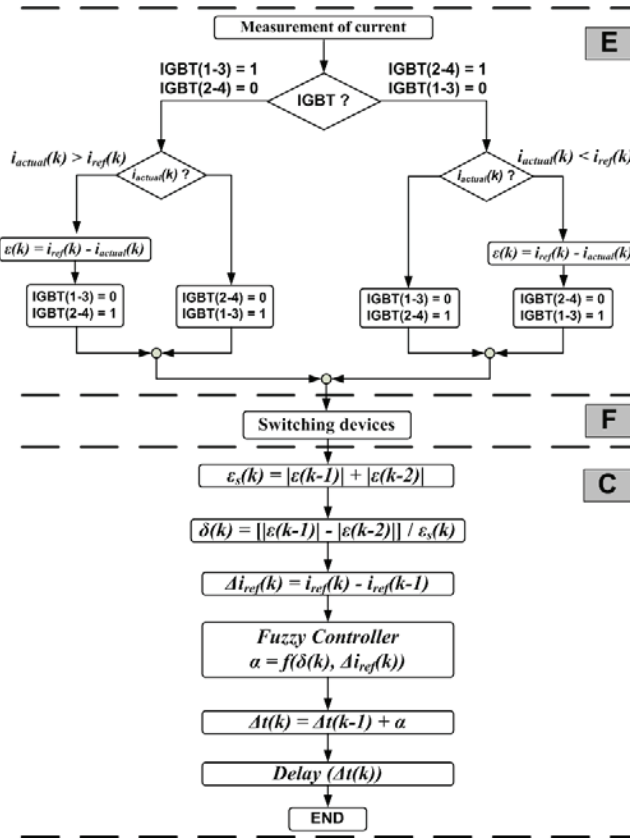
Fig. 5. Flowchart implementation for PWM algorithm.
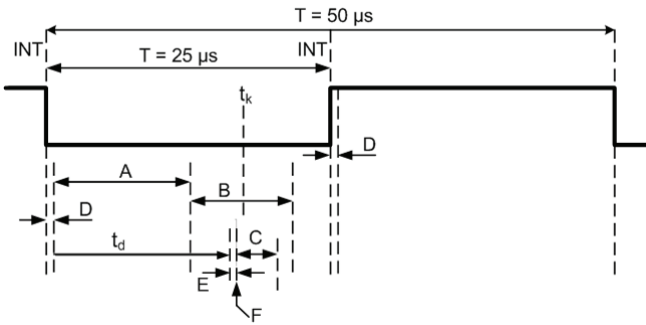
A - Time used for other calculations
B - Zone for variation of Δt_k (10 µs)
C - Fuzzy Computation + Downcounter value
   calculation (around 3 µs)
D - Time to load the Downcounter and start it with time t_d
   (calculated during previous C time)
E - Measurement of current + Switching strategy (1 µs)
F - Switching of devices

Fig. 6. Timing diagram of the tasks.

IV. SIMULATION STUDY

Once the compensation algorithm and the fuzzy controller were developed in detail, a simulation study of the converter system was conducted to validate the proposed control strategy. The MATLAB/Simulink program was used for the simulation study. The fuzzy control program developed by the MATLAB/Fuzzy Logic Toolbox was embedded in the Simulink program. The converter circuit, shown in Figure 1, was simulated with 120 V, 60 Hz single-phase ac supply and

large filter capacitor so that dc voltage V_d was reasonably smooth. The inverter frequency was fixed at 20 kHz with nominal passive load of $L = 5.0$ mH and $R = 1.0$ Ω. Figure 7 shows the response for a trapezoidal reference current wave varying within ±15 A. The device switching command wave is also included in the figure. Note that the command current slopes are gentle enough so that the PWM actual current wave can follow it. The response with load inductance variation from 5.0 mH to 2.5 mH is shown in the negative half cycle.

Evidently, the current error is larger when the inductance is lower. The constant switching frequency and equal current error are evident during the entire cycle. Figure 8 gives the expanded view of Figure 7 near zero crossing of the current wave highlighting the inductance variation effect. The algorithm tries to control the positive and negative current errors to be equal before and after the inductance variation. The duty cycle of the inverter remains nearly 50% because average load voltage is small. Figure 9 shows the transient response when the reference current changes abruptly from +10 A to –10 A. At initial and final steady states, the slopes of the rising and falling currents are equal and the duty cycle is 50% as shown. At transition of the reference current, the slope is too high for the actual current to follow, and therefore, the device pair 2-4 remains on until the natural falling current reaches the reference value.
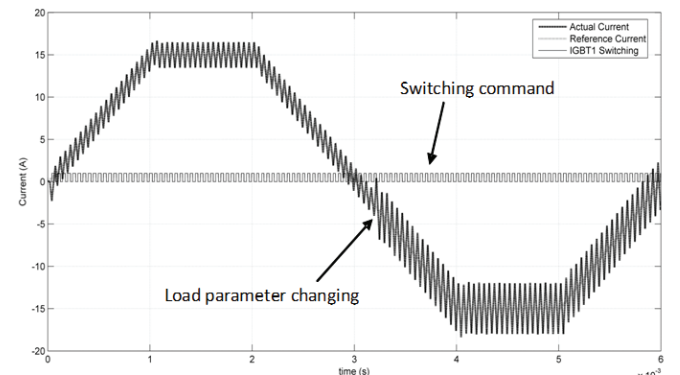
Fig. 7. Trapezoidal current wave synthesis showing load inductance variation (L=5mH to 2.5mH) effect.
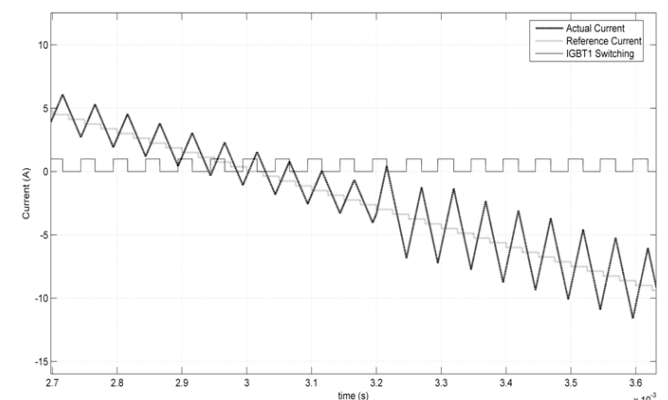
Fig. 8. Load inductance variation effect on current wave in Figure 7 (shown in detail).
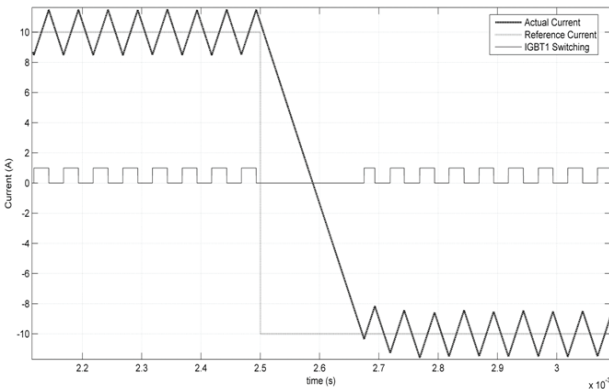
Fig. 9. Transient response of current wave (for +10A to -10A).

V. EXPERIMENTAL STUDY

Once the validation of the algorithm was completed by simulation study, a set-up was organized in the laboratory for experimental study. A single-phase H-bridge converter system with variable L and R load, as shown in Figure 1, was available for the study. A Spectral Digital Board based on the DSP type TMS320F2812 was available for the control system. The timing diagram in Figure 6 discusses all the tasks computed and their execution times by the DSP. All the control programs were written in C language, but a few time-critical code segments were used in assembly language that were translated from the C code through Code Composer. All the tasks were repeated every 25 µs, as shown in Figure 6, while maintaining the inverter frequency constant at 20 kHz. The fuzzy controller for real-time implementation in the DSP was somewhat simplified from the corresponding simulation program to economize execution time.

Figure 10 shows the typical inverter current and the device switching waves in steady state for constant reference current. The small difference between the upper and lower error, and the corresponding asymmetry in the switching wave were caused by the error in the current measurement due to large noise. The large current spike at the instant of switching of every half cycle was due to recovery current through the feedback diode of the snubberless inverter. Figure 11 shows the transient response for abrupt change of reference current from +8 A to –8 A, and the corresponding switching wave. It well corresponds with the simulation wave in Figure 9. During the free fall of the current wave, as usual, the devices 2 and 4 remain on. Figure 12 shows the steady state waves with constant reference current, but with load inductance varying from 6.3 mH to 2.5 mH (resistance is the same). The resulting alteration of current slope and error amplitude is evident. After experimental validation of the inverter with R-L load, it was decided to test the inverter operation as an active harmonic filter, where the passive R-L load was removed and the output was tied to a single-phase 60 Hz ac line. In this mode, the inverter command current wave was composed of a 5th harmonic (300 Hz) current wave at 8 A superimposed with 7th harmonic (420 Hz) current at 5.7 A. The inverter was then tested for harmonic follow-up operation. Figure 13 shows the excellent performance in the harmonic follow-up operation.
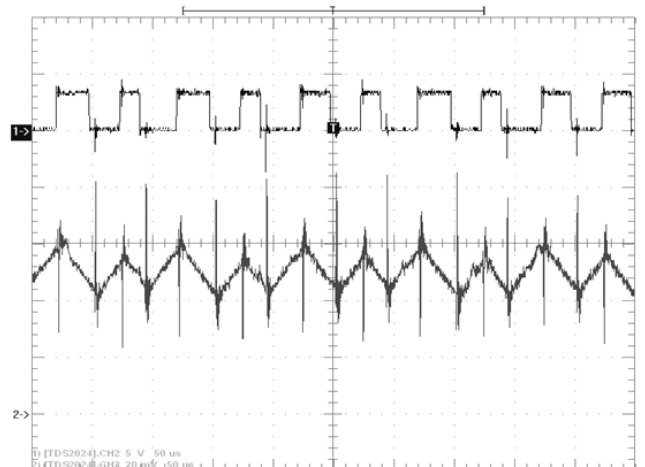
Fig. 10. Experimental steady state switching (top) and current waves (bottom).
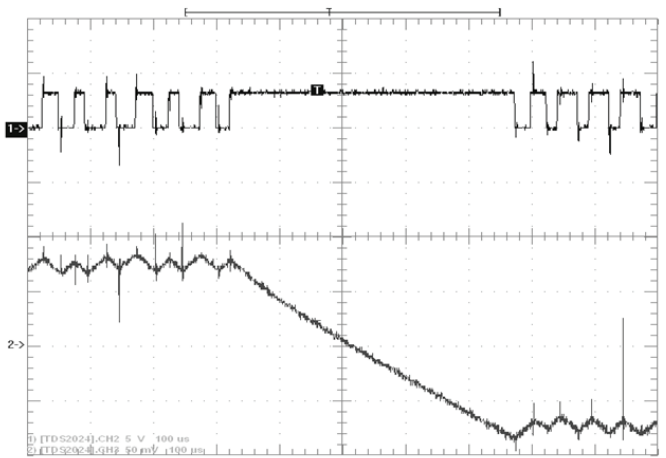
Fig. 11. Experimental transient response for current (from +8 A to -8 A) -L=6.3mH .
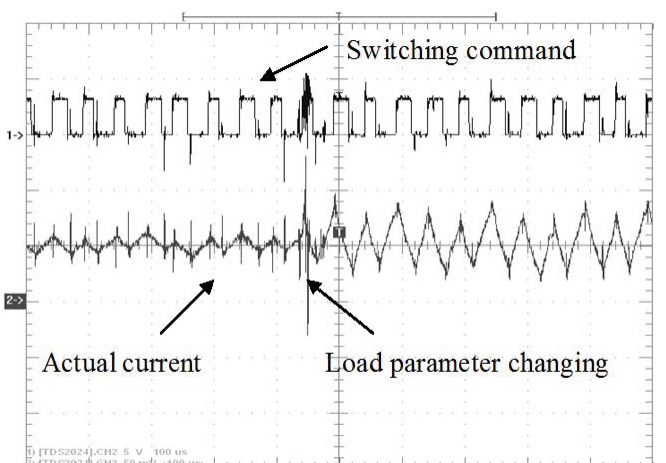
Fig. 12. Experimental switching and current waves for load inductance variation (L=6.3mH to 2.5mH).
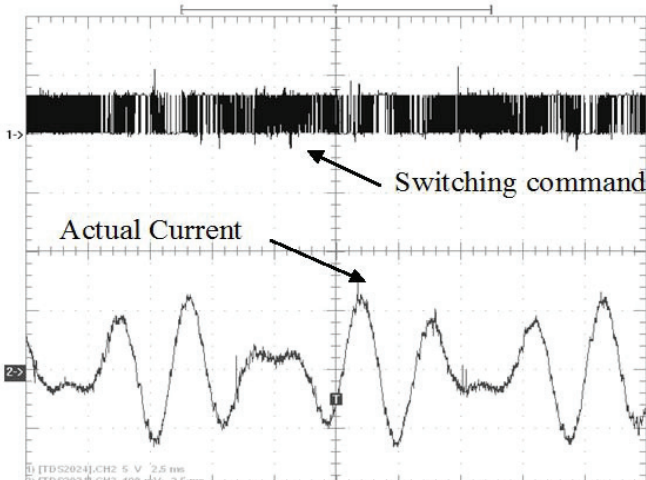
Fig. 13. Experimental current harmonic (5th and 7th) follow-up for active filter operation.

VI.   CONCLUSION

The project successfully demonstrates a new hysteresis current control PWM strategy of a voltage-fed inverter that is fast and adaptive in nature. The harmonic ripple is minimum because the positive current error is controlled to be equal with the negative current error, while operating the inverter at constant frequency. The algorithm is simple to implement and does not need any information about the load and source parameters.

The algorithm has been demonstrated on a single-phase inverter for normal operation with passive *R-L* load as well as active harmonic filter mode of operation. However, it is also valid for a three-phase inverter with arbitrary load and active filter operation. The algorithm uses fuzzy logic for current error compensation. The whole algorithm has been implemented digitally with the high speed DSP type TMS320F2812. The complete inverter with the algorithm was studied extensively by simulation and laboratory experimentation, and performance was found to be excellent.

REFERENCES

[1] B.K. Bose, "An adaptive hysteresis-band current control technique of a voltage-fed PWM inverter for machine drive system", IEEE Trans. Ind. Electron., vol.37, no. 5, pp. 402-408, October 1990.

[2] L. Malesani, L. Rossetto, P. Tomasin, and A. Zuccato, "Digital adaptive hysteresis control with clocked commutation and wide operating range", IEEE Trans. Ind. Appl., vol.32, no. 2, pp.316-325, March/April, 1996.

[3] L.Malesani and P. Tenti, "A novel hysteresis control method for current controlled PWM inverters with constant modulation frequency", IEEE/IAS'87 Annu. Meet. Conf. Rec. Oct. 1987, pp. 851-855.

[4] L. Fangrui, A.I. Maswood, "A Novel Variable Hysteresis Band Current Control of Three-Phase Three-Level Unity PF Rectifier With Constant Switching Frequency", IEEE Trans. Power Electron., vol. 21, no. 6, pp. 1727-1734, November 2006.

[5] S. R. Bowes and D. Holliday, "Optimal Regular-Sampled PWM Inverter Control Techniques", IEEE Trans. Ind. Electron., vol.54, no. 3, pp. 1547-1559, June 2007.

[6] Z. Yao, L. Xiao, and Y. Yan, "Dual-Buck Full-Bridge Inverter With Hysteresis Current Control", IEEE Trans. Ind. Electron., vol.56, no. 8, pp. 3153-3160, August 2009.

[7] M.A.M. Radzi, N.A. Rahim, "Neural Network and Bandless Hysteresis Approach to Control Switched Capacitor Active Power Filter for Reduction of Harmonics", IEEE Trans. Ind. Electron., vol.56, no. 5, pp. 1477-1484, May 2009.

[8] L. Malesani and P. Tomasin, "PWM current control techniques for voltage source inverters-a survey", in IEEE IECON'93 Conf. Rec., Hawaii, Nov. 1993, pp. 670-675.

[9] A. Nabae, S. Ogasawara, and H. Akagi, "A novel control scheme of current-controlled PWM inverters,'' IEEE Trans. Ind. Appl., vol IA-2, no. 4, 1986, pp 697-701.

[10] D. Wuest and F. Jenni, "Space vector based current control schemes for voltage source inverters," in IEEE PESC'93 Conf. Rec., Seattle, 1993, pp 986-992.

[12] S. Buso, S. Fasolo, L. Malesani, and P. Mattavelli, "A dead-beat adaptive hysteresis current control", IEEE Trans. Ind. Appl., vol. 36, no. 4,   pp. 1174-1180, July/August. 2000.

[13] M. P. Kazmierkowski and M. A. Dzieniakowski, "Review of current regulation techniques for three-phase PWM inverters," in IEEE IECON'94 Conf. Rec., 1994, pp. 567–575.

[14] J. W. Dixon, S. Tepper, and L. Moran, "Analysis and evaluation of different modulation techniques for active power filters," in IEEE APEC'94 Conf. Rec., Orlando, FL, Feb. , 1994, pp. 894–900.

[15] R. B. Sepe, Jr., "A unified approach to hysteretic and ramp-comparison current controllers," in IEEE/IAS'93 Annu. Meeting Conf. Rec., Toronto, Ont., Canada, Oct. 2–8, 1993, pp. 724–731.

[16] Q. Yao and D. G. Holmes, "A simple, novel method for variable hysteresis-band current control of a three phase inverter with constant switching frequency," in IEEE IAS'93 Annu. Meeting Conf. Rec., Toronto, Canada, Oct. 1993, pp. 1122–1129.

[17] R. R. Pereira, et al., "A Simple Full Digital Adaptive Current Hysteresis Control with Constant Modulation Frequency for Active Power Filters", in IEEE/IAS'07 Annu. Meeting Conf. Rec., New Orleans, EUA, Sept. 23–27, 2007, pp. 1644–1648.

[18] B. K. Bose, Modern Power Electronics and AC Drives, Prentice Hall, 2001.

[19] B. K. Bose, Power Electronics and Motor Drives – Advances and Trends, Academic Press, 2006.

BIOGRAPHIES

Rondineli Rodrigues Pereira graduated in computation engineering in 2007 and received M.Sc. degree in electrical engineering in 2009, from Itajubá Federal University, Brazil, where he is currently working toward the D.Sc degree. His research interests include digital signal

processing, adaptive filters, control algorithms for active power filters, harmonics and power quality.

Carlos Henrique da Silva received the B.Sc in electrical engineering from the Federal University of Sao Joao Del Rei in 2003, the M.Sc. and D.Sc degree in electrical engineering from the Federal University of Itajubá in 2005 and 2009 respectevely. Currently he is a Professor of the Electrical Engineering Department at Itajuba Federal University (UNIFEI), Brazil. His research interests include active power filters, digital signal processing and control systems.

Luiz Eduardo Borges da Silva (M'88) received his B.S. and a M.Sc. degrees in Electrical Engineering from Itajuba Federal University, in 1977 and 1982, respectively, and his Ph.D. degree from École Polytechnique de Montréal, Canada, in 1988. Currently, he is a Professor of the Electronic Engineering Department at Itajuba Federal University (UNIFEI), Brazil. He was a Visiting Professor at University of Tennessee at Knoxville, in 1998. His research focuses on power electronics, electronic power systems, power converters and applications of adaptive and intelligent control in industrial problems.

Germano Lambert-Torres (M'90) received the Ph.D. degree in Electrical Engineering from École Polytechnique de Montréal, Canada, in 1990. He received a B.S. and a M.Sc. degrees in Electrical Engineering from Itajuba Federal University, B.S. in Economics from Faculty of Economic Sciences at South of Minas, and a B.S. in Mathematics from Itajuba Faculty of Sciences and Letters.

He is currently a Professor and Dean of the Electrical Engineering Department at Itajuba Federal University (UNIFEI), Brazil. From 1995 to 1996 he was a Visiting Professor at University of Waterloo, Canada. From 2000 to 2004, he was served as Pro-Rector of Research and Graduate Studies at UNIFEI. He serves on a number of committees related to intelligent systems, in IEEE and CIGRE.

Bimal K. Bose (S'59-M'60-SM'78-F'89-LF'96) has held the Condra Chair of Excellence (endowed chair) in power electronics at the University of Tennessee, Knoxville, since 1987, where he was responsible for the teaching and research program in power electronics and motor drives. Concurrently, he served as the distinguished scientist (1989–2000) and chief scientist (1987–1989) of EPRI – Power Electronics Applications Center, Knoxville, Tennessee. Prior to this, he was an associate professor of electrical engineering, Rensselaer Polytechnic Institute, Troy, New York (1971–1976).

He is a Life Fellow of the IEEE. He is a specialist in power electronics and motor drives, including power converters, PWM techniques, micro-computer/DSP control, electric/hybrid vehicle drives, renewable energy systems, and AI applications in power electronics and motor drives.

De: Luiz Eduardo Borges da Silva (leborges@unifei.edu.br)
Para: rondinelipereira@yahoo.com.br;
Data: Sexta-feira, 19 de Novembro de 2010 14:52:58
Cc:
Assunto: Fw: Decision on Manuscript ID 2009-IACC-469.R1 (T-IA)

----- Original Message ----- From: <muddin@lakeheadu.ca>
To: <leborges@unifei.edu.br>
Cc: <c.speck@ieee.org>; <muddin@lakeheadu.ca>
Sent: Friday, November 19, 2010 1:28 PM
Subject: Decision on Manuscript ID 2009-IACC-469.R1 (T-IA)

19-Nov-2010

Dear Dr. da Silva:

We are pleased to advise that your paper, "NEW STRATEGIES FOR APPLICATION OF ADAPTIVE
FILTERS IN ACTIVE POWER FILTERS", 2009-IACC-469.R1, has been accepted for publication in the
IEEE Transactions on Industry Applications.

PLEASE READ AND FOLLOW THE MANUSCRIPT SUBMISSION PROCEDURES BELOW

You must now submit a package of material for use in preparing your paper for publication. Please return
to your Author Center in ScholarOne Manuscripts (http://mc.manuscriptcentral.com/ieee-ias)
and click on the "Awaiting Final Files". Look for this manuscript in the listing that will appear at the
bottom of the page.

You should have already executed an IEEE Copyright Transfer on this manuscript. However, if not, you
will see a "Copyright Transfer" link in the status column next to this paper - please click that link and
complete the transfer formalities. Your paper will not be published if you have not executed an IEEE
Copyright Transfer.

You must submit the following materials:

1. a final text file for the manuscript. Your paper has been accepted for publication in the version seen
by the reviewers, so you may not make substantive technical changes. However, you are free to make
editorial enhancements to your paper. Comments from the reviewers have been appended to this letter
for your consideration. Acceptable text file formats include those created directly by Microsoft Word,
WordPerfect, and LaTex. PDF files, files in the postscript format, or files prepared with commercial page
layout software such as PageMaker or QuarkExpress are NOT ACCEPTABLE.

2. original high-resolution graphics files for each of the figures in the manuscript. Acceptable file formats
include jpg, gif, tif, bmp, ppt, and vsd. PDF files, and files in the postscript format are NOT
ACCEPTABLE. Resolution should be 300 dpi or better. You may embed figures in the text file identified
above, but please understand that the publication process requires that you provide a separate, original
graphic file for each figure.

By the way, the hardcopy version of Transactions normally publishes grayscale figures. It is possible for
the figures in your paper to be published in color in the hardcopy version of Transactions if you are
prepared to accept financial responsibility for the incremental cost of color reproduction. If you are
interested in this option, please contact the Transactions EiC for further details.

If you provide color graphic files, the graphics in the version of Transactions that is archived in IEEE Xplore will be in color. However, if you do not opt for color reproduction in the hardcopy version of Transactions, your color graphics will be printed in grayscale. Please take this into account as you plan your graphics.

3. a reference copy of the final manuscript, with all figures and tables embedded and captioned. The reference copy will be used only to resolve questions as to the authors' intent and may be a PDF file

4. a short biography for yourself and each of your coauthors. Biographies should not exceed 200 words in length. Biographies should identify those authors who are IEEE members and show their grade of membership. Biographies should be submitted as text files in one of the formats listed above.

5. an individual high-resolution digital photograph of yourself and each of your coauthors. Photo files should be in the jpg, gif, tif or bmp format. Please use the name of the individual as the name of the file so that photos can be associated with the correct biography.

Please submit all final files through the "Awaiting Final Files" queue in your author center on ScholarOne Manuscripts. Files must have unique names and should be uploaded in a single session. There is a 100MB limit on the total of all files associated with a manuscript. Note that you must upload a complete set of final files even though there have been no changes in the files that you submitted for peer review.

You may upload and save final files in multiple log-in sessions. However, after clicking the "submit" button, you will be unable to return to the "Awaiting Final Files" area of S1M, so please make sure your final package is correct and complete before clicking "submit".

Please submit your final files as soon as possible, and no later than 45 days from today's date. Papers will be queued for publication on a first-in, first-out basis. Your paper cannot go into the publication queue until you have complete the final file submission. The time from submission to publication depends on the number of manuscripts in the queue and the number of papers published in each of the bi-monthly issues of Transactions; this time will not be less than three months, and could be longer. The paper will be posted on IEEE Xplore® as "Accepted for Future Publication" 3-4 weeks after it has been reviewed and accepted by the Transactions EiC.

The Editor-in-Chief of IEEE Transactions on Industry Applications is:
Dr. Carlton E. Speck
5 Woodside Park Blvd
Pleasant Ridge, MI 48069, USA
e-mail: cspeck@ieee.org

The Staff Editor of IEEE Transactions on Industry Applications is:
Mr. Keith Edick
IEEE Publications
445 Hoes Lane
Piscataway, NJ 08854, USA
e-mail: k.edick@ieee.org

You will receive a page proof of the final layout of your paper about six weeks prior to publication of the issue of IEEE Transactions on Industry Applications that will contain your paper. The process of preparing a manuscript for publication can, on occasion, change, delete, or modify characters and equations. It will be your responsibility to check that proof carefully and return any comments to our Staff Editor within five days of receiving the proof. Please note when checking your proof:

• Text and biographies will be edited to IEEE style.
• You should check all mathematics and equations very carefully because this material may not be

properly converted.
• Check all figures and tables and verify that they are numbered correctly.
• Biographies and photos, if included, should be verified.

If your corrected proof is not returned in the allotted time frame, your paper will be deferred to a future issue.

This manuscript was originally submitted for review on 24-Mar-2010.

Mohammad Uddin
Associate Editor and Papers Review Chair
Industrial Automation and Control Committee

[D17ff]

Comments to the author.

Associate Editor
Comments to the Author:
(There are no comments. Please check to see if comments were included as a file attachment with this e-mail or as an attachment in your Author Center.)

These are the Reviewer's comments to the author.

NEW STRATEGIES FOR APPLICATION OF ADAPTIVE FILTERS IN ACTIVE POWER FILTERS

R.R. Pereira   C.H. da Silva
L.E. Borges da Silva   G. Lambert-Torres
Federal University of Itajuba - UNIFEI
Itajuba, Brazil
rondi@unifei.edu.br, carloschedas@unifei.edu.br,
leborges@unifei.edu.br, germano@unifei.edu.br

J. O. P. Pinto
Federal University of Mato Grosso do Sul
Campo Grande, Brazil
jpinto@nin.ufms.br

Abstract – **This paper describes new strategies to improve the transient response time of harmonic detection using adaptive filters applied to shunt active power filters (SAPF). Two cases are presented and discussed, both using an adaptive notch filter, but one uses the least mean square (LMS) algorithm to adjust the coefficients and the other uses the recursive least square (RLS) algorithm. The synchronization of the adaptive notch filter orthogonal input signals, which are generated by the Clarke transformation of the load currents, is achieved automatically without the need of a phased locked loop (PLL). This procedure significantly reduces the real time computation burden. Simulations using Matlab/Simulink are presented to clarify the algorithm and practical implementation is performed using the DSP Texas Instruments TMS320F2812. The experimental results are presented and discussed.**

Keywords – **Adaptive filters, active power filter, least mean square, recursive least square, adaptive notch filter, harmonic compensation.**

I. INTRODUCTION

The compensation for harmonic currents, generated by power electronic equipments, has become important because of its growing use in industrial applications. Mitigation solutions have been proposed using passive filters, active power filters, and hybrid active power filters. In this context, many new techniques are being developed in order to improve the effectiveness of active power filters (APF) in harmonic mitigation. This work copes specifically with the strategy of extract the harmonic content of the load current necessary to control the active power filter action.

The performance of active power filters basically depends on the extraction method used to generate the reference signal, the control method used to generate the harmonic compensation and the dynamic characteristic of the entire filter [1].

In a power system, the current can be described as

$$i(t) = \sum_{n=1}^{N} A_n \sin(n\omega t + \theta_n) \qquad (1)$$

The fundamental current is denoted by $i_1(t)$ and the harmonic current as

$$i_h(t) = \sum_{n=2}^{N} A_n \sin(n\omega t + \theta_n) \qquad (2)$$

The harmonics can be obtained by just eliminating the fundamental components. The problem is how to extract the sinusoidal waveform, separating the harmonic components.

In fact, synchronous reference frame [2], [3] and instantaneous power theory [4] are two very known methods of harmonic extraction, frequently used in active power filter control [5].

Instantaneous active-reactive power theory calculates the active and reactive powers through three-phase to two-phase transformation and not work correctly under a distorted voltage condition [4]. The synchronous reference frame theory is based on the filtering of dc components of currents by a low-pass filter in synchronously rotating frame [6]. Both techniques are very dependent on the low-pass filters used in the algorithm which interferes with the dynamic response.

In recent years, the use of adaptive filters [7] has shown a powerful technique to perform the extraction of the sinusoidal waveform, separating the harmonic components [8]-[13]. Recent literature has shown important effort to improve the transient response time of adaptive filters under variation of the signal polluted by harmonics. The response time presented in the literature is around one to two cycles of the fundamental signal (60Hz) [8]-[16]. The strategy described in this work improves the transient time and diminish the computer burden of the algorithm. The achieved response time, as shown in the practical results, reaches the mark below one cycle for a 100% of load current variations.

Compared to the adaptive methods presented in the literature, the method doesn´t use a PLL to generate the orthogonal input signals. The algorithm uses Clarke transformation of the load current to generate the necessary orthogonal signals. This strategy guarantees the orthogonal input signals follow straight the variations of the load current producing, as consequence, a significative improvement in convergence time of the adaptive algorithm. It does not matter the adaptive algorithm used, LMS or RLS, the total transient response drops below one cycle of the fundamental frequency (60Hz). The simulations and practical results demonstrate the effectiveness of the strategy.

The Section II describes the entire structure of the proposed algorithm and details the simplifications used in the adaptive algorithms (LMS and RLS). The Section III presents the simulation results and Section IV the experimental results. Conclusions are given in Section V.

II. HARMONIC DETECTION WITH ADAPTIVE FILTERS

The adaptive noise canceling technique based on the Wiener theory has been widely used in many signal processing applications [7]. It can maintain the system in the best operating state by continuously self-adjusting its parameters. The Fig. 1 illustrates the basic principle of adaptive harmonic detecting method, based on the adaptive noise canceling theory.
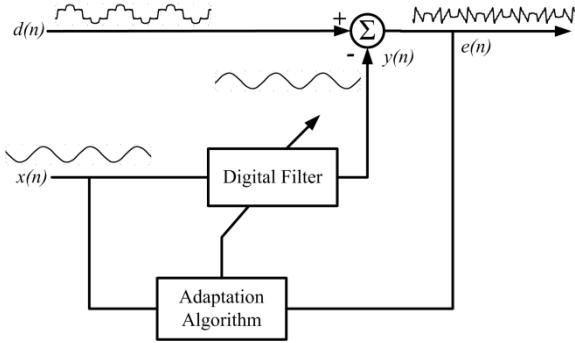

Fig. 1. The principle of adaptive harmonic detecting method.

In this basic structure of adaptive filter applied to current harmonic detection, $d(n)$ represents the load current $i_L(t)$ the current blurred with harmonics and $x(n)$ represents the sinusoidal waveform $v_{sin}(t)$ in phase with the source voltage, generated by a PLL [8]-[16]. The reference input signal $x(n)$ is processed by the adaptive filter producing the output signal $y(n)$ that tracks the variation in the fundamental signal of the load current. The objective of adaptive filter is approximate $y(n)$, both in amplitude and phase, to the fundamental signal $i_1(n)$ of load current. So, the desired harmonics content $i_h(n)$ can be directly obtained from the error signal $e(n)$ given by subtracting $y(n)$ from $d(n)$. The coefficients of the adaptive filter are adjusted using an adaptation algorithm.

In this work an adaptive notch filter [7] were tested. The adaptive notch filter is shown in Fig. 2. This structure uses two orthogonal signals as input, one for the input $x(n)$ and other 90° phase shifted. In this way only two coefficients are needed to be adapted. The adaptation procedure is the same as that used in the general structure of adaptive filters, and the output signal $y(n)$ tracks the variation of the fundamental signal of load current.
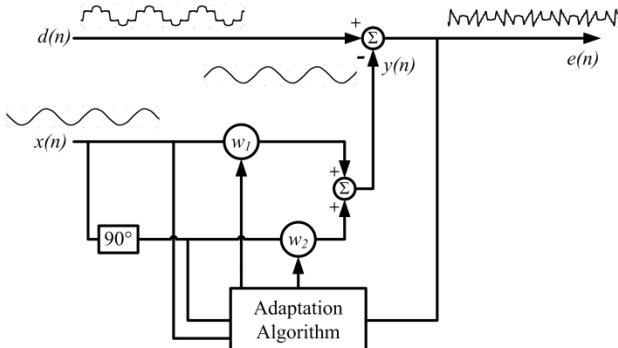

Fig. 2. Adaptive notch filter principle.

Two algorithms, the least mean square (LMS) and the recursive least square (RLS), are widely used as adaptation algorithms for adaptive filters [17],[18].

The recursion formula of LMS algorithm is given by the equations:

$$e(n) = d(n) - y(n) = d(n) - X^T(n)W(n) \tag{3}$$

$$W(n + 1) = W(n) + \mu e(n)X(n) \tag{4}$$

Where:
$X(n)$ - input vector.
$W(n)$ - coefficient vector.
μ - step-size.

The parameter μ controls the rate of convergence of the algorithm to the optimum solution. In this work the value of μ used is 0.0000015.

The recursion formula of LMS algorithm applied for adaptive notch filters is given by the equations:

$$w_1(n + 1) = w_1(n) + \mu e(n)x(n) \tag{5}$$

$$w_2(n + 1) = w_2(n) + \mu e(n)x_{90°}(n) \tag{6}$$

Where:
$x_{90°}(n)$ is $x(n)$ 90° phase shifted.

The formula of RLS algorithm applied for adaptive notch filters, divided in five steps, is given below.

Step 01 (initialization):

$$P_{\lambda 1}(0) = 0.1$$
$$P_{\lambda 2}(0) = 0.1$$
$$w_1(0) = 0$$
$$w_2(0) = 0$$
$$\lambda = 0.99995 \text{ (practical tested value)}$$

Step 02 (gain calculation):

$$k_1(n) = \frac{P_{\lambda 1}(n-1)x(n)}{\lambda + x^2(n)P_{\lambda 1}(n-1)} \tag{7}$$

$$k_2(n) = \frac{P_{\lambda 2}(n-1)x_{90°}(n)}{\lambda + x_{90°}^2(n)P_{\lambda 2}(n-1)} \tag{8}$$

Step 03 (output and error calculation):

$$y(n) = w_1(n-1)x(n) + w_2(n-1)x_{90°}(n) \tag{9}$$

$$e(n) = d(n) - y(n) \tag{10}$$

Step 04 (coefficients adaptation):

$$w_1(n) = w_1(n-1) + k_1(n)e(n) \tag{11}$$

$$w_2(n) = w_2(n-1) + k_2(n)e(n) \tag{12}$$

Step 05 (inverted autocorrelation coefficients):

$$P_{\lambda1}(n) = \lambda^{-1}P_{\lambda1}(n-1) - \lambda^{-1}k_1(n)x(n)P_{\lambda1}(n-1) \quad (13)$$

$$P_{\lambda2}(n) = \lambda^{-1}P_{\lambda2}(n-1) - \lambda^{-1}k_2(n)x_{90°}(n)P_{\lambda2}(n-1) \quad (14)$$

As demonstrated by the equations, in the case of the adaptive notch filter, the gain vector $k(n)$ is transformed in to gains $k_1(n)$ and $k_2(n)$, calculated in Step 02. The inverse of autocorrelation matrix $P(n)$ is transformed in two scalar values $P_{\lambda1}(n)$ and $P_{\lambda2}(n)$, calculated in Step 05. This made the algorithm implementation more simple in terms of computational complexity.

The parameter λ is the forgetting factor that is a positive constant close to, but smaller than one. The choice of $\lambda < 1$ results in a scheme that puts more emphasis on the recent samples of the observed values and tends to forget the past.

In literature the adaptive notch filters are normally implemented using a PLL to generate the orthogonal input signals [8]-[16].

In this work a new strategy for generate the orthogonal input signals is presented. These two signals are generated with Clarke transformation of the load current:

$$\begin{bmatrix} I_{L0} \\ I_{L\alpha} \\ I_{L\beta} \end{bmatrix} = \sqrt{\frac{2}{3}} \cdot \begin{bmatrix} 1/\sqrt{2} & 1/\sqrt{2} & 1/\sqrt{2} \\ 1 & -1/2 & -1/2 \\ 0 & \sqrt{3}/2 & -\sqrt{3}/2 \end{bmatrix} \cdot \begin{bmatrix} I_{LA} \\ I_{LB} \\ I_{LC} \end{bmatrix} \quad (15)$$

Then the two orthogonal signals, $I_{L\alpha}$ and $I_{L\beta}$, are filtered by a third order Butterworth with a 100Hz cutoff frequency. The low-pass filter frequency response is presented in Fig. 3.

And two sinusoidal input signals, $x(n)$ and $x_{90°}(n)$, with 60Hz frequency are obtained without a PLL, as shown in Fig. 4.
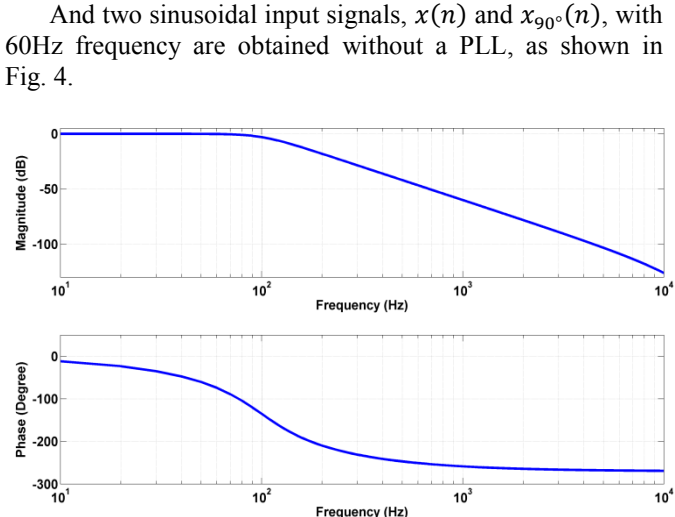

Fig. 3. Butterworth low-pass filter frequency response.

This strategy guarantees the orthogonal input signals follow straight the variations of the load current. The simulations and real time implementation results demonstrated the convergence speed less than one cycle for the adaptive notch filter with both adaptation algorithm, against a minimum of one to two cycles reported in the literature [8]-[16].
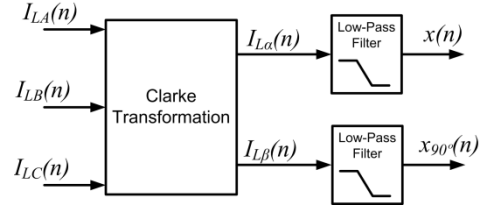

Fig. 4. Orthogonal signals generation.

III. SIMULATION RESULTS

The simulation results are shown in Figs. 5, 6, 7 and 8. The transient behavior of the adaptive notch filter, with LMS adaptation algorithm, is presented in Figs. 5 and 6 for a 100% load current variation. The Fig. 5 shows the load current, signal $d(n)$ in the plot (a), the fundamental of the load current (dashed line) and the adaptive notch filter output $y(n)$ (solid line) in the plot (b) and the harmonic current content $e(n)$ in the plot (c). The Fig. 6 shows the load current fundamental signal and the output of the adaptive notch filter in the plot (a) and the error between them in the plot (b).
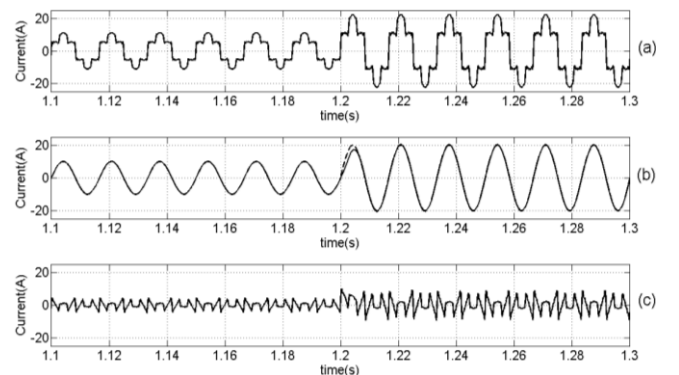
Fig. 5. Simulation results of adaptive notch filter with LMS algorithm. (a) Load current with 100% increase. (b) Fundamental load current (dashed line) and adaptive filter output (solid line). (c) Adaptive filter error signal or generated harmonic reference.
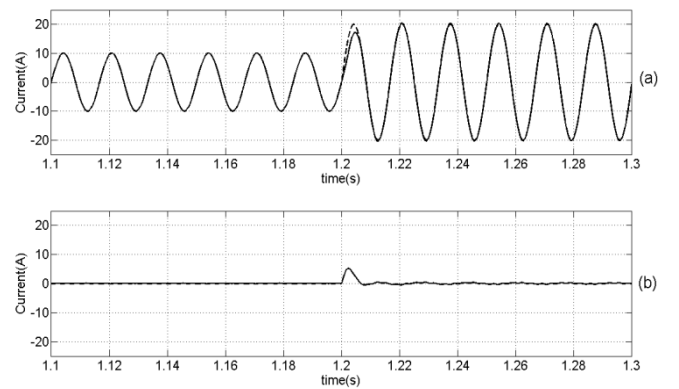
Fig. 6. (a) Load current fundamental signal (dashed line) and output of the adaptive notch filter with LMS algorithm (solid line). (b) Error between then with load current transient.

The transient behavior of the adaptive notch filter with RLS algorithm, for a 100% load current variation, is

presented in Figs. 7 and 8. The Fig. 7 shows the following signals: the load current $d(n)$ in the plot (a), the fundamental of the load current (dashed line) and the adaptive notch filter output $y(n)$ (solid line) in the plot (b) and the harmonic current content $e(n)$ in the plot (c). The Fig. 8 shows the load current fundamental signal and the output of the adaptive notch filter in the plot (a) and the error between them in the plot (b).
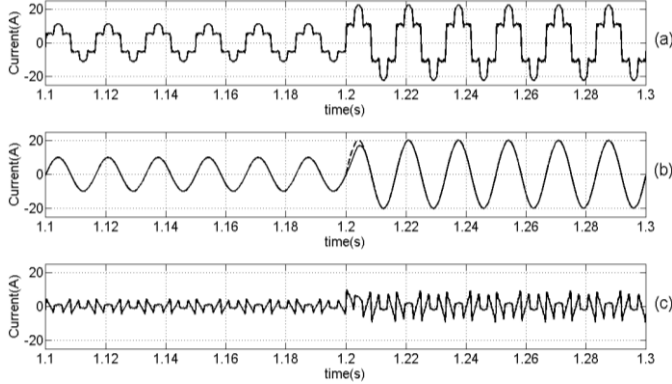

Fig. 7. Simulation results of adaptive notch filter with RLS algorithm. (a) Load current with 100% increase. (b) Fundamental load current (dashed line) and adaptive filter output (solid line). (c) Adaptive filter error signal or generated harmonic reference.
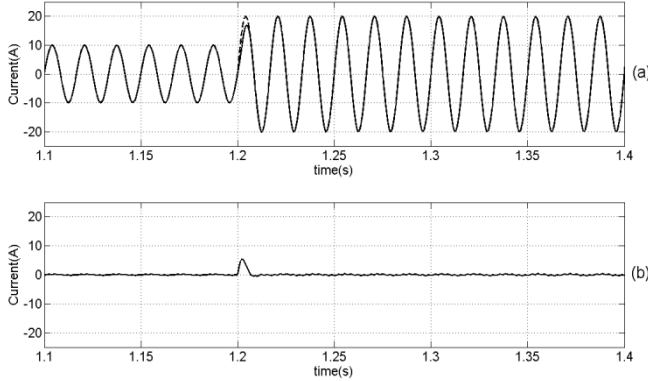

Fig. 8. (a) Load current fundamental signal (dashed line) and output of the adaptive notch filter with RLS algorithm (solid line). (b) Error between then with load current transient.

The simulations demonstrate that the adaptive notch filter with LMS or RLS algorithm produces a transient response smaller one cycle of fundamental frequency. It is faster than the results presented in the literature [8]-[16].

IV. EXPERIMENTAL RESULTS

The practical results are obtained using a shunt active power filter (SAPF) composed of three single-phase full H-bridges voltage source inverter (VSI) type, rated 35kVA, working in 40kHz switching frequency. The DC link voltage is adjusted to 500V. The smooth inductor used to connect the SAPF to power system is rated 5mH. The harmonic current injection is controlled by a VSI PWM. The power system voltage is 220V line to line. The load is a rated 100kVA, 6 pulse rectifier, CSI type. The shunt active power filter

diagram is shown in Fig. 9. Three Hall current sensors measure the three-phase source current representing the signal $d(n)$ in the block diagram of Fig. 2. The entire control algorithm was implemented in a Texas DSP TMS320F2812.

The Fig. 10 presents the load current (IL_A) of 19A, the compensation current (Ic_A) and the source current (Is_A) of phase A after compensation, using the adaptive notch filter strategy, with LMS algorithm, to extract the harmonic content. In Fig. 11, the harmonic spectrum of source current before and after compensation is shown; the current Total Harmonic Distortion (THDi) of Is_A is reduced from 28.9% to 4.63%.
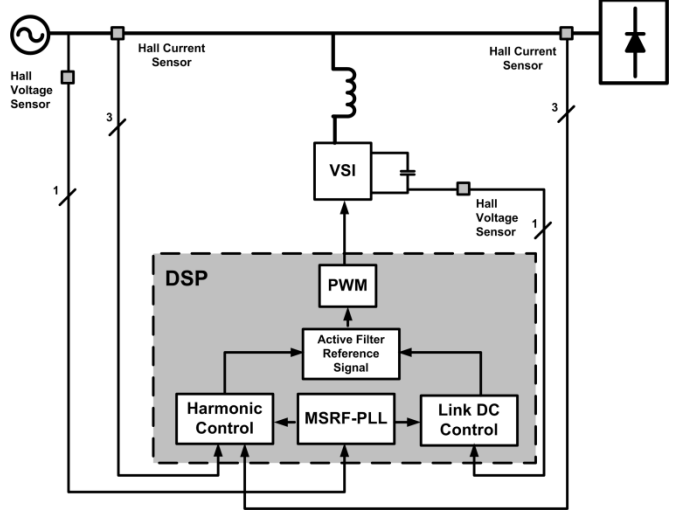
Fig. 9. Shunt Active Power Filter Block Diagram.
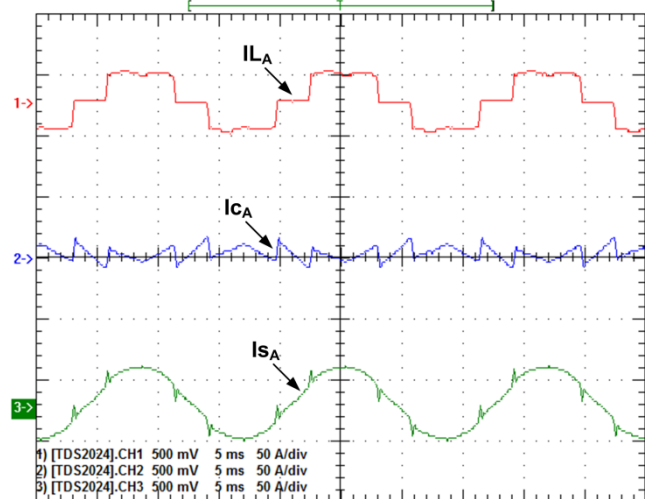
Fig. 10. Experimental results of adaptive notch filter LMS algorithm with a load current of 19A.

The Fig. 12 shows the adaptive notch filter transient behavior for a 100% load current variation. The result illustrates the convergence time Tc less than one cycle. This result confirms the one obtained by simulations.

The Fig. 13 presents IL_A, Ic_A and Is_A after compensation using an adaptive notch filter, with RLS algorithm, for a load current of 19A. The Fig. 14 shows the harmonic spectrum of source current; the THDi of Is_A is reduced from 28.9% to 4.32%.

Fig. 11. Source current harmonic spectrum of the adaptive notch filter LMS algorithm.
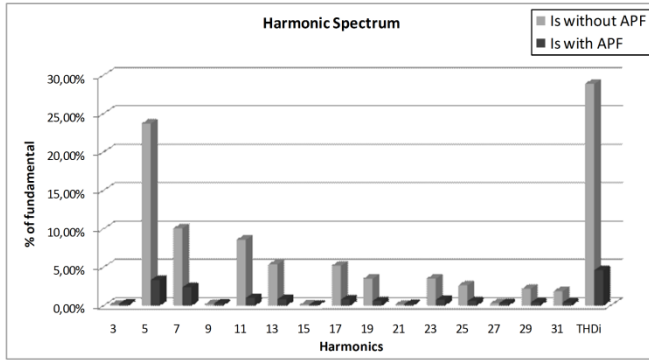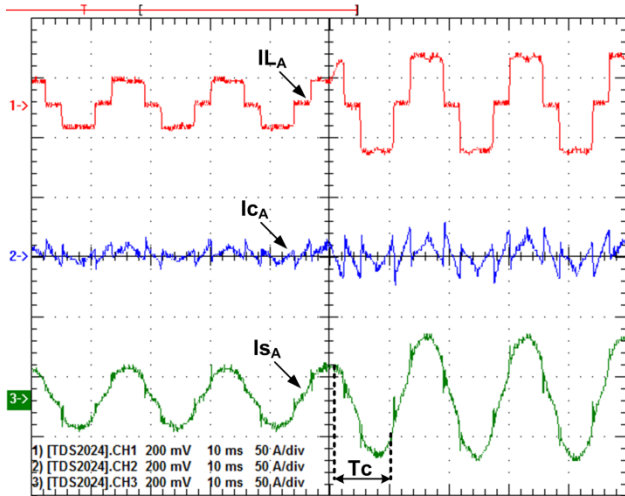
Fig. 14. Source current harmonic spectrum of the adaptive notch filter RLS algorithm.

Fig. 12. Experimental results: 100% load current increase with adaptive notch filter LMS algorithm.

Fig. 15. Experimental results: 100% load current increase with adaptive notch filter RLS algorithm.

Fig. 15 shows the adaptive notch filter, with RLS algorithm, transient behavior for a 100% load current variation. The result shows the convergence time Tc less than one cycle. This result also confirms that obtained by simulations and is an important improvement over the results of the adaptive notch filter presented in the literature.


Fig. 13. Experimental results of adaptive notch filter RLS algorithm with a load current of 19A.
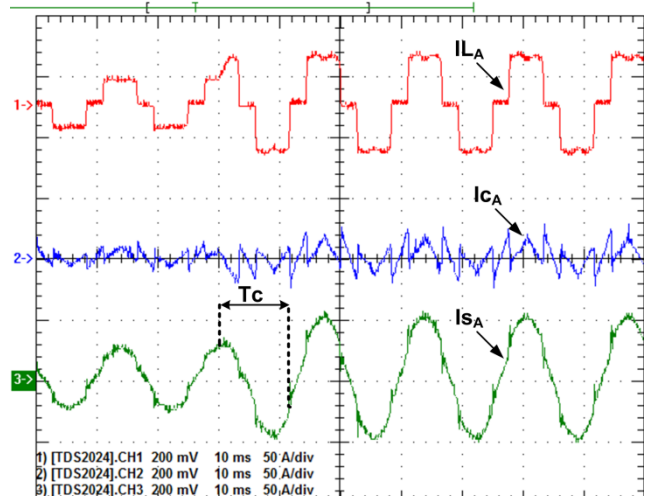
V. CONCLUSION

In real time applications, as active power filters, the calculation time and the transient response time are critical matters to be taken into consideration during the design process. The improvement in these characteristics comparing to those proposed in the literature is a main contribution of this work. The experimental results show a very close correspondence with that investigating by simulations.

The implementation of adaptive notch filter was found to be the best choice with respect to calculation time because it has just two coefficients to be adjusted. The use of the Clarke transformation directly in the load current generating the two orthogonal inputs signals for the notch filter has shown a important issue to speed up the convergence time of the adaptive algorithm.

The results using both adaptive algorithms, LMS and RLS, has shown faster transient response than that reported in the literature. The simulations and the experimental results showed that the convergence time was less than one cycle of the fundamental. This result is faster than the minimum of one cycle reported in the literature.

Another advantage of the proposed strategy is the absence of a PLL to generate the input of the adaptive filters which diminish the computation burden very crucial in real time implementations.

REFERENCES

[1] S. Bhattacharya, D. M.Divan, T. M.Frank, B. Banerje – "Active filter system implementation", *IEEE Ind. Appl. Mag.*, vol. 4, no. 5, pp 47-63, Set/Oct 1998.

[2] D. M. Divan, S. Bhattacharya, and B. Banerjee, "Synchronous frame harmonic isolator using active series filter," in *Proc. Eur. Power Electron. Conf.*, 1991, pp. 3030–3035.

[3] C.H. da Silva, V.F.da Silva, L.E.Borges da Silva, G.L.Torres, R.R.Pereira, "DSP implementation of three-phase PLL using modified synchronous reference frame", IEEE IECON07, Taiwan, 2007.

[4] H. Akagi, E. H. Watanabe, and M. Aredes, *Instantaneous Power Theory and Applications to Power Conditioning*. Hoboken, NJ: Wiley, 2007.

[5] L. Asiminoaei, F. Blaabjerg, and S. Hansen, "Detection is key - Harmonic detection methods for active power filter applications," *IEEE Ind.Appl. Mag.*, vol. 13, no. 4, pp. 22–33, Jul/Aug 2007.

[6] L. Asiminoaei, F. Blaabjerg, S. Hansen and P. Thogersen, "Adaptive compensation of reactive power with shunt active power filters," *IEEE Trans. Ind. Appl.*, vol. 44, no. 3, pp. 867–877, May/Jun 2008.

[7] B. Widrow, et al. – "Adaptive noise cancelling: principles and applications", Proceedings of the IEEE, v. 63, n. 12, p. 1692, 1975.

[8] L. Asiminoaei, F. Blaabjerg, S. Hansen and P. Thogersen, "An improved adaptive detection method for power quality improvement," *IEEE Trans. Ind. Appl.*, vol. 44, no. 2, pp. 525–533, Mar/Apr 2008.

[9] F. D. Freijedo, J. Doval-Gandoy, O. Lopez, P. Fernández-Comesaña and C. Martinez-Peñalver, "A signal-processing adaptive algorithm for selective current harmonic cancellation in active power filters," *IEEE Trans. Ind. Electron.*, v. 56, n. 8, pp. 2829–2840, Aug. 2009.

[10] B.Singh, and J. Solanki, "An implementation of an adaptive control algorithm for a three-phase shunt active filter," *IEEE Trans. Ind. Electron.*, v. 56, n. 8, pp. 2811–2820, Aug. 2009.

[11] M. Cirrincione, M. Pucci, G. Vitale, S. Scordato, and A. Miraoui, "Current harmonic compensation by a single-phase shunt active aower filter controlled by adaptive neural filtering," *IEEE Trans. Ind. Electron.*, v. 56, n. 8, pp. 3128–3143, Aug. 2009.

[12] S. Välviita, S. J. Ovaska – "Delayless method to generate current reference for active filters," *IEEE Trans. Ind. Electron.*, v. 45, n. 4, pp. 559–567, Aug. 1998.

[13] M. H. Byung, Y. B. Byung, S. J. Ovaska – "Reference signal generator for active power filters using improved adaptive predictive filter," *IEEE Trans. Ind. Electron.*, v. 52, n. 2, pp. 576–584, Apr. 2005.

[14] Mu Longhua, Jiangzi – "Application of adaptive filtering in harmonic analysis and detection", Transmission and Distribution Conference and Exhibition: Asia and Pacific, 2005 IEEE/PES, Dalian, 2005.

[15] Y. Qu, W. Tan, Y. Dong, and Y. Yang – "Harmonic detection using fuzzy LMS algorithm for active power filter", IEEE IPEC 2007, Singapore, 2007.

[16] H. Li, Z. Wu, F. Liu – "A novel variable step-size adaptive harmonic detecting algorithm applied to active power filter", IEEE ICIT 2006, Mumbai, 2006.

[17] R. R. Pereira, C.H. da Silva, L.E.Borges da Silva, G.L.Torres, "A new strategy to step-size control of adaptive filters in the harmonic detection for shunt active power filter", IEEE IAS09, Houston, 2009.

[18] B. Farhang-Boroujeny, "Adaptive Filters: Theory and Applications". Chichester: John Wiley and Sons, 1998, ch. 12.

A NEW STRATEGY TO STEP-SIZE CONTROL OF ADAPTIVE FILTERS IN THE HARMONIC DETECTION FOR SHUNT ACTIVE POWER FILTER

Rondineli Rodrigues Pereira, Carlos Henrique da Silva, Giscard Francimeire Cintra Veloso, Luiz Eduardo Borges da Silva, Germando Lambert Torres

Federal University of Itajubá - UNIFEI

Itajubá, Brazil

rondi@unifei.edu.br, carloschedas@unifei.edu.br, leborges@unifei.edu.br, germano@unifei.edu.br

Abstract – **This paper presents a new strategy to improve the applicability of adaptive filters for harmonic detection in shunt active power filters (SAPF). The final objective of the strategy is improving the speed of convergence of the adaptive filter and reduces the steady-state error. Two cases are presented and discussed, one with a Finite Impulse Response (FIR) adaptive filter with 32 coefficients and another with an adaptive notch filter. The Least Mean Square (LMS) algorithm was used to adjust the coefficients in the both cases. Simulations using Matlab are presented to clarify the algorithm. Also practical implementation is performed using the DSP Texas Instruments TMS320F2812 and the results depicted. Important aspects concerning the calculation time of the adaptive filter, convergence speed during changes in the load and the steady-state error, are presented.**

Keywords – **Adaptive filters, active power filter, adaptive FIR filter, adaptive notch filter, harmonic compensation.**

I. INTRODUCTION

The compensation for harmonic currents, generated by power electronic equipments, has become important as its growing use in the industrial applications. In this context, more and more, new techniques are developed in order to improve the effectiveness of active power filters (APF) in harmonic mitigation. The performance of active power filters basically depend on the extraction method used to generate the current reference signal, the control method used to generate the compensation harmonic current and the dynamic characteristic of the entire filter [1].

In power system, the current can be described as $i(t) = \sum_{n=1}^{N} A_n \sin(n\omega t + \theta_n)$. The fundamental current is denoted by $i_1(t)$. The harmonics can be obtained just eliminating the fundamental components. The problem arisen is how to extract the sinusoidal waveform, separating the harmonic components.

Actually the synchronous reference frame and the instantaneous power theory are the two methods of harmonic extraction more used in active power filters control. In recent years the use of Adaptive Filters has shown a powerful technique to perform this job.

II. ADAPTIVE FILTERS FOR HARMONIC DETECTION

The adaptive noise canceling technique based on the Wiener theory has been widely used in many signal processing applications [2]. It can maintain the system in the best operating state by continuously self-adjusting its parameters. According to the adaptive noise canceling theory, the principle of adaptive harmonic detecting method is that illustrated in Fig 1.


Fig. 1. The principle of adaptive detecting of harmonics.

In this basic structure of adaptive filter (Fig. 1) applied to current harmonic detection, $d(n)$ represents the current $i(t)$ blurred with harmonics and $x(n)$ represents the sinusoidal waveform $v_{sin}(t)$ in phase with the source voltage. The reference input signal $x(n)$ is processed by adaptive filter producing the output signal $y(n)$ that tracks the variation of fundamental signal of the load current. The objective of adaptive filter is approximates $y(n)$, in both amplitude and phase, to the fundamental signal $i_1(n)$. So, the desired harmonics content $i_h(n)$ can be directly obtained from the error signal $e(n)$ given by the subtracting of $y(n)$ from $d(n)$. The coefficients of the adaptive filter are adjusted using the Least Mean Square (LMS) algorithm. The recursion formula of LMS algorithm is given by the equations:

$$e(n) = d(n) - y(n) = d(n) - \mathbf{X}^T(n)\mathbf{W}(n) \qquad (1)$$

$$\mathbf{W}(n+1) = \mathbf{W}(n) + \mu e(n)\mathbf{X}(n) \qquad (2)$$

Where:

$\mathbf{X}(n)$ - input vector.
$\mathbf{W}(n)$ - coefficient vector.
μ - step-size.

The parameter μ controls the rate of convergence of the algorithm to the optimum solution.

In this work a Finite Impulse Response (FIR) adaptive filter [2-4] with 32 coefficients and an adaptive notch filter [2][5-7] were tested. The adaptive FIR filter structure uses the general structure of adaptive filter shown in Fig.1. The adaptive notch filter is shown in Fig. 2. This structure (Fig. 2) uses two orthogonal signals as input, one for the input $x(n)$ and other 90° phase shifted. In this way only two coefficients are needed to be adapted. The adaptation procedure is the same as used in the general structure of adaptive filters.


Fig. 2. Adaptive notch filter principle.

To overcome the problems with the speed of convergence, several approaches based on a variable step-size method were proposed in recent years [5-8]. The approach proposed in this work also plays with the step-size to speed-up the adaptation algorithm. But, instead of looking to the error signal, which is polluted with noise complicating the adaptation algorithm behavior, it looks directly to the load current value searching for significative transients. Once the transient in the load current is detected the algorithm starts the step-size adjustments. That shows up to improve the adaptation algorithm behavior. In the simulations the convergence speed reaches the maximum of 1.5 cycles for both cases, the adaptive FIR filter and the adaptive notch filter, against the minimum of 2 cycles reported in the literature [4][6-7]. The amplitude of the load current is determined with a simple algorithm described in [9], based Coulon oscillator principle. This algorithm is illustrated in Fig. 3.
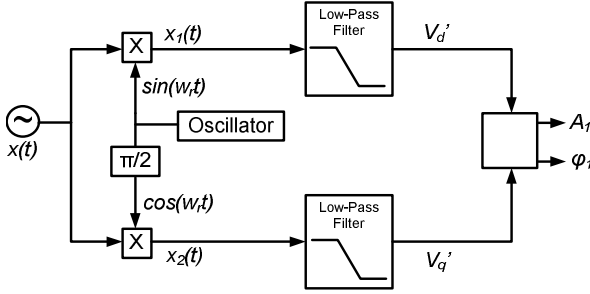

Fig. 3. Coulon oscillator principle.

The oscillator frequency w_r is defined in 60Hz and the load current is used as the signal $x(t)$. In this way, the amplitude of the load current fundamental component can be detected with the algorithm.

With a low-pass filter the components V_d' and V_q' can be extracted as shown in (3) and (4):

$$V_d' = \frac{A_1}{2}\cos(\varphi_1) \tag{3}$$

$$V_q' = \frac{A_1}{2}\sin(\varphi_1) \tag{4}$$

And the amplitude of the load current fundamental component is calculated as demonstrated in (5):

$$A_1 = \sqrt{(2V_d')^2 + \left(2V_q'\right)^2} \tag{5}$$

When any significant changes happen in the load current value, it is detected and the step-size is immediately increased to a certain value and then decreased slowly two times until it reaches the initial value. This procedure guaranties a fast transient response to adaptive filter action.

III. SIMULATION RESULTS

The simulation results are shown in Figs. 4, 5, 6 and 7. The transient behavior of the adaptive FIR filter strategy, for a 100% load current variation, is presented in Fig. 4 and Fig. 5. The Fig. 4 shows the signals: the load current $d(n)$ in the first graphic, the fundamental of the load current (in blue) and the adaptive FIR filter output $y(n)$ (in red) in the second graphic and the harmonic current reference $e(n)$ in the third graphic. The Fig. 5 shows the desired harmonic reference and the harmonic reference generated by the adaptive FIR filter in the first graphic and the error between them in the second graphic.
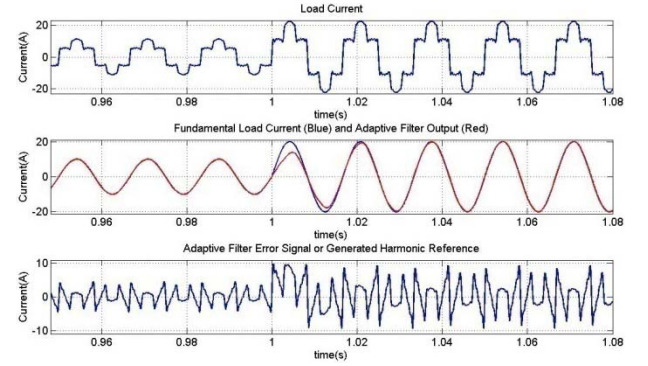

Fig. 4. Simulations results: 100% load current increase with adaptive FIR filter.
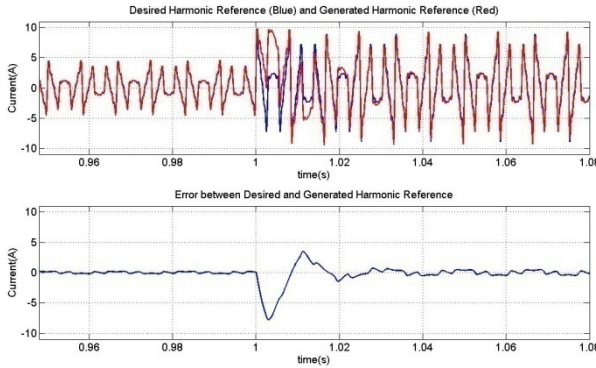
Fig. 5. Error between desired harmonic reference and generated harmonic reference by adaptive FIR filter with load current transient.

The transient behavior of the adaptive notch filter strategy, for a 100% load current variation, is presented in Fig. 6 and Fig. 7. The Fig. 6 shows the signals: the load current $d(n)$ in the first graphic, the fundamental of the load current (in blue) and the adaptive notch filter output $y(n)$ (in red) in the second graphic and the harmonic current reference $e(n)$ in the third graphic. The Fig. 7 shows the desired harmonic reference and the harmonic reference generated by the adaptive notch filter in the first graphic and the error between them in the second graphic.
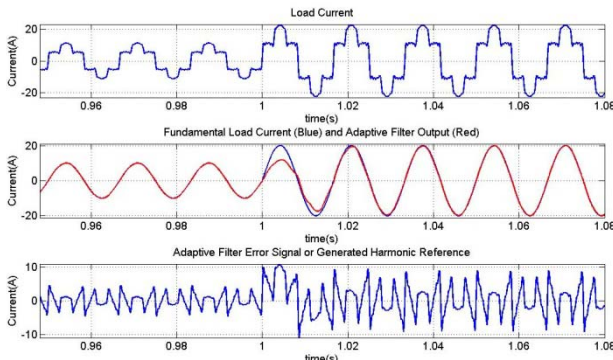

Fig. 6. Simulations results: 100% load current increase with adaptive notch filter.
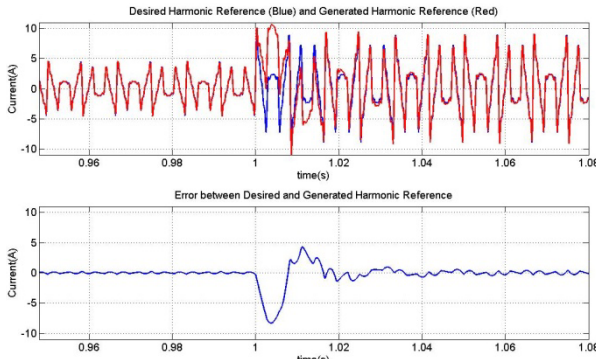

Fig. 7. Error between desired harmonic reference and generated harmonic reference by adaptive notch filter with load current transient.

The simulations demonstrate that there is a slightly difference between the steady-state error for the two strategies. The adaptive FIR filter presents an error a little bit bigger than for adaptive notch filter. The proposed algorithm for the step-size adjusts produces the same speed of convergence in both cases.

IV. EXPERIMENTAL RESULTS

The practical results are obtained from a shunt active power filters (SAPF) composed by three single-phase full H-bridges voltage source (VSI) type, rated 35kVA, working in 40kHz switching frequency. The DC link voltage is adjusted in 500V. The smooth inductor used to connect the SAPF to power system is rated 5mH. The harmonic current injection is controlled by a VSI PWM. The power system voltage is 220V line to line. The load is a rated 100kVA, 6 pulse rectifier, CSI type. The shunt active power filter diagram is shown in the Fig. 8. The control algorithm was implemented in a Texas DSP TMS320F2812. The Fig. 9 presents the load current (IL_A) of 27A, the compensation current (Ic_A) and the source current (Is_A) of phase A after compensation using an adaptive FIR filter strategy to extract the harmonic content. In Fig. 10 the harmonic spectrum of source current before and after compensation is shown, the current Total Harmonic Distortion (THDi) of Is_A is reduced from 28,9% to 7,56%.
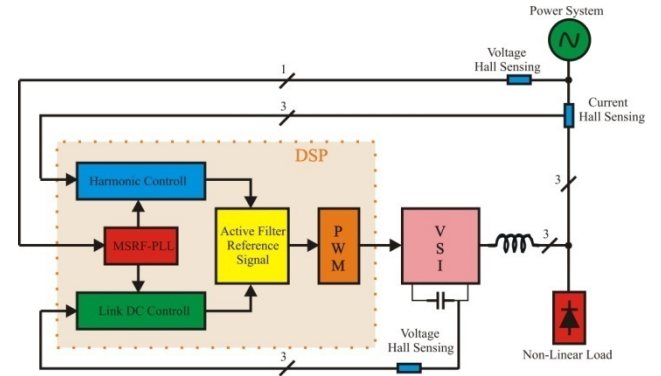

Fig. 8. Shunt Active Power Filter Block Diagram.
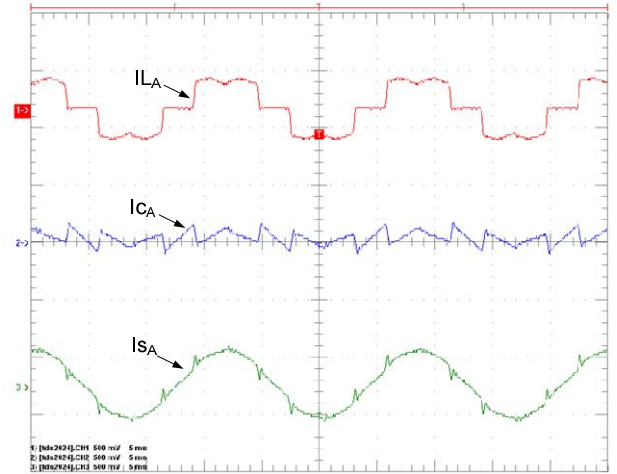
Fig. 9. Experimental results of adaptive FIR filter with a load current of 27A.
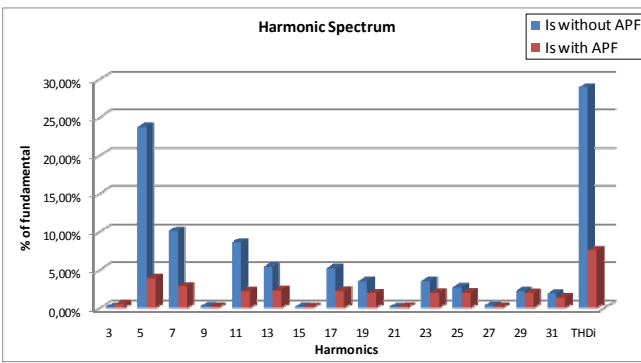
Fig. 10. Source current harmonic spectrum of the adaptive FIR filter.

The Fig. 11 presents IL_A, Ic_A and Is_A after compensation using an adaptive notch filter for a load current of 27A. The Fig. 12 shows the harmonic spectrum of source current, the THDi of Is_A is reduced from 28,9% to 8,29%.
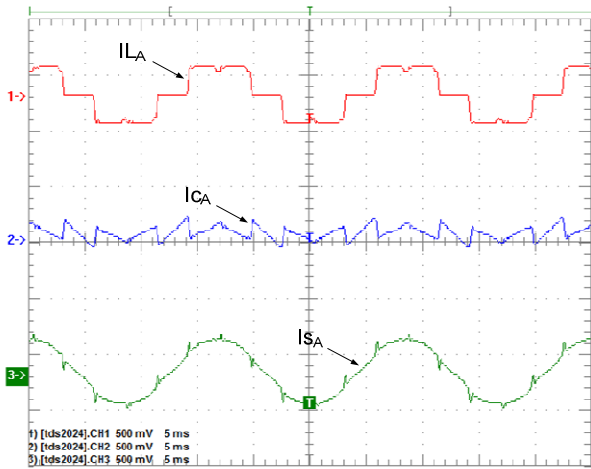

Fig. 11. Experimental results of adaptive notch filter with a load current of 27A.
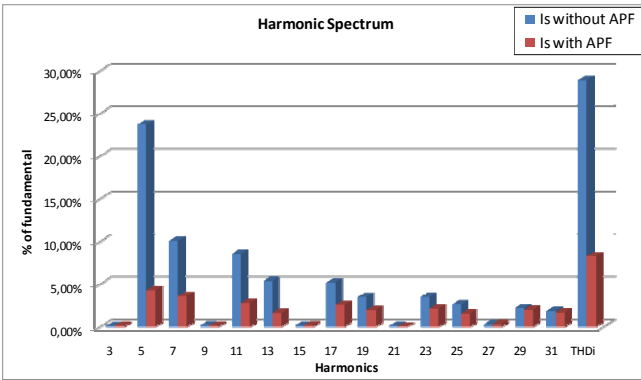
Fig. 12. Source current harmonic spectrum of the adaptive notch filter.

The Fig. 13 shows the adaptive notch filter transient behavior for a 100% load current variation. The result illustrates the convergence time Tc of 1.5 cycles. This result confirms that obtained by simulations.

The reduction of THDi in the two types of adaptive filter implemented is very similar. But the calculation time of the adaptive FIR filter and adaptive notch filter are completely different. The adaptive notch filter has just two coefficients to be adjusted, so its calculation time is significantly smaller than adaptive FIR filter that uses 32 coefficients for the same task.

Fig. 13. Experimental results: 100% load current increase with adaptive notch filter.

V. CONCLUSION

In real time applications, as active power filters, the calculation time, the speed of convergence and steady-state error are critical matters to be taken in consideration during the design process. The proposed step-size adjustments algorithm, for the two types of adaptive filters, demonstrates good results concerning speed of convergence and steady-state error.

The results of the new strategy were faster than the results reported in the literature. The simulations and experimental results showed that the convergence time last 1.5 cycles of the fundamental, against the minimum of 2 cycles reported in the literature.

The adaptive notch filter algorithm has shown to be more interesting in terms of computational burden and steady-state error.

ACKNOWLEDGEMENT

REFERENCES

[1] S. Bhattacharya, D. M.Divan, T. M.Frank, B. Banerje – "Active filter system implementation", IEEE Trans. Ind. Appl. Set/Oct 1998, pp 47-63.

[2] B. Widrow, et al. – "Adaptive noise cancelling: principles and applications", Proceedings of the IEEE, v. 63, n. 12, p. 1692, 1975.

[3] S. Välviita, S. J. Ovaska – "Delayless method to generate current reference for active filters". IEEE Transactions on Industrial Electronics, v. 45, n. 4, 1998.

[4] M. H. Byung, Y. B. Byung, S. J. Ovaska – "Reference signal generator for active power filters using improved adaptive predictive filter". IEEE Transactions on Industrial Electronics, v. 52, n. 2, 2005.

[5] Mu Longhua, Jiangzi – "Application of adaptive filtering in harmonic analysis and detection", Transmission and Distribution Conference and Exhibition: Asia and Pacific, 2005 IEEE/PES, Dalian, 2005.

[6] Y. Qu, W. Tan, Y. Dong, and Y. Yang – "Harmonic detection using fuzzy LMS algorithm for active power filter", IEEE IPEC 2007, Singapore, 2007.

[7] H. Li, Z. Wu, F. Liu – "A Novel Variable Step Size Adaptive Harmonic Detecting Algorithm Applied to Active Power Filter", IEEE ICIT 2006, Mumbai, 2006.

[8] R. H. Kwong, E. W. Johnston – "A variable step-size LMS algorithm", IEEE Trans. Signal Processing, 1992, 40(7), pp. 1633-1642.

[9] C.H. da Silva, V.F.da Silva, L.E. Borges da Silva, G.L.Torres, R.R.Pereira, "DSP implementation of three-phase PLL using modified synchronous reference frame", IEEE IECON07, Taiwan, 2007.

Improving the Convergence Time of Adaptive Notch Filters to Harmonic Detection

R. R. Pereira[1], C. H. da Silva[1], L. E. Borges da Silva[1], G. Lambert-Torres[1], J. O. P. Pinto[2]

1 Federal University of Itajuba – UNIFEI
Itajuba, Brazil
2 Federal University of Mato Grosso do Sul
Campo Grande, Brazil

rondi@unifei.edu.br, carloschedas@unifei.edu.br, leborges@unifei.edu.br, germano@unifei.edu.br, jpinto@nin.ufms.br

Abstract – **This paper presents the application of adaptive notch filters for harmonic detection in shunt active power filters (SAPF). The orthogonal input signals to the adaptive notch filter are generated using the Clarke transformation of the load currents in such way that the Phased Looked Loop (PLL) is not necessary any more. The least mean square (LMS) and recursive least square (RLS) algorithms were used to adjust the coefficients of the adaptive notch filter. The final objective of the described strategy is to improve the speed of convergence of the adaptive notch filter, reducing the steady-state error and the transient response. All these features are very important to real time applications in active power filters. Simulations using Matlab/Simulink are presented to clarify the algorithm. Also, the implementation of the technique in a shunt active power filter is performed using the DSP Texas Instruments TMS320F2812, and the experimental results depicted.**

I. INTRODUCTION

Nonlinear loads such as single-phase and three-phase rectifiers, thyristor converters and a number of low-power electronics appliances generate considerable disturbance in the ac mains. The compensation for harmonic currents, generated by power electronic equipments, has become important because of its growing use in industrial applications.

The choice of active power filters (APF) arises to improve the filtering efficiency and solve the issues of passive filters. In this context, many new techniques have being developed in order to improve the effectiveness of active power filters in harmonic mitigation [1], [2].

In a power system, the current can be described as

$$i(t) = \sum_{n=1}^{N} A_n \sin(n\omega t + \theta_n) \qquad (1)$$

The fundamental current is denoted by $i_1(t)$ and the harmonic current as

$$i_h(t) = \sum_{n=2}^{N} A_n \sin(n\omega t + \theta_n) \qquad (2)$$

The harmonics can be obtained by just eliminating the fundamental components. The problem is how to extract the sinusoidal waveform, separating the harmonic components.

In fact, synchronous reference frame and instantaneous power theory are the two methods of harmonic extraction frequently used in active power filter control [2], [3]. In recent years, the use of adaptive filters has shown a powerful technique to perform this job.

This paper describes the real time application of an adaptive notch filter, to harmonic detection, using both the least mean square (LMS) and recursive least square (RLS) as adaptation algorithm. In these two cases the convergence time of the adaptation algorithm has shown better results than reported in the literature [4]-[12], as it is demonstrated by the simulation and experimental results.

In Section II, an adaptive notch filter with the LMS algorithm is presented. In Section III, presents an adaptive notch filter with the RLS algorithm. In these two cases the orthogonal reference signals are generated without a PLL. In Section IV and V, simulation and the experimental results are shown, respectively. Conclusions are given in Section VI.

II. HARMONIC DETECTION WITH ADAPTIVE NOTCH FILTER USING LMS ALGORITHM

The adaptive noise canceling technique based on the Wiener theory has been widely used in many signal processing applications [13]. It can maintain the system in the best operating state by continuously self-adjusting its parameters. Based on the adaptive noise canceling theory, the principle of adaptive harmonic detecting method [7], [9] is illustrated in Fig 1.
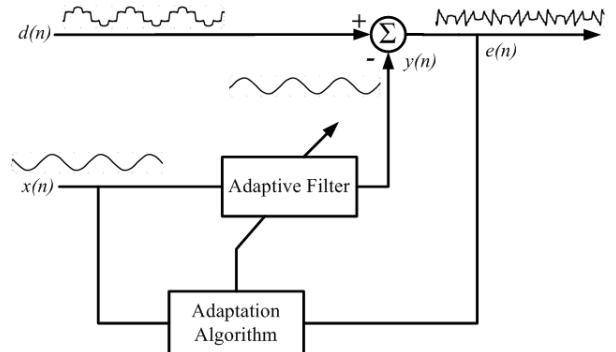

Fig. 1. The principle of adaptive detecting of harmonics.

In this basic structure of adaptive filter applied to current harmonic detection, $d(n)$ represents the load current $i_L(t)$ blurred with harmonics and $x(n)$ represents the sinusoidal waveform with a fundamental frequency of 60Hz. The

reference input signal $x(n)$ is processed by the adaptive filter producing the output signal $y(n)$ that tracks the variation in the fundamental signal of the load current. The objective of adaptive filter is approximate $y(n)$, both in amplitude and phase, to the fundamental signal $i_1(n)$. So, the desired harmonics content $i_h(n)$ can be directly obtained from the error signal $e(n)$ given by subtracting $y(n)$ from $d(n)$. The coefficients of the adaptive filter are adjusted using the least mean square (LMS) or recursive least square (RLS) adaptation algorithms.

The recursion formula of LMS algorithm is given by the equations:

$$e(n) = d(n) - y(n) = d(n) - \sum_{k=0}^{p} w(k)x(n-k) \qquad (3)$$

$$e(n) = d(n) - X^T(n)W(n) \qquad (4)$$

$$W(n+1) = W(n) + \mu e(n)X(n) \qquad (5)$$

Where:
$X(n)$ - input vector.
$W(n)$ - coefficient vector.
μ - step-size value.
p - number of coefficients of the adaptive filter.

The parameter μ controls the rate of convergence of the algorithm to the optimum solution.

In this work an adaptive notch filter [10]-[12] were tested. The adaptive notch filter is shown in Fig. 2. This structure uses two orthogonal signals as input, one for the input $x(n)$ and other 90° phase shifted. In this way only two coefficients are needed to be adapted. The adaptation procedure is the same as that used in the general structure of adaptive filters, and the output signal $y(n)$ tracks the variation of the fundamental signal of load current. The recursion formula of LMS algorithm applied for adaptive notch filters is given by the equations:

$$w_1(n+1) = w_1(n) + \mu(n)e(n)x(n) \qquad (6)$$

$$w_2(n+1) = w_2(n) + \mu(n)e(n)x_{90°}(n) \qquad (7)$$

Where:
$x_{90°}(n)$ - is $x(n)$ 90° phase shifted.
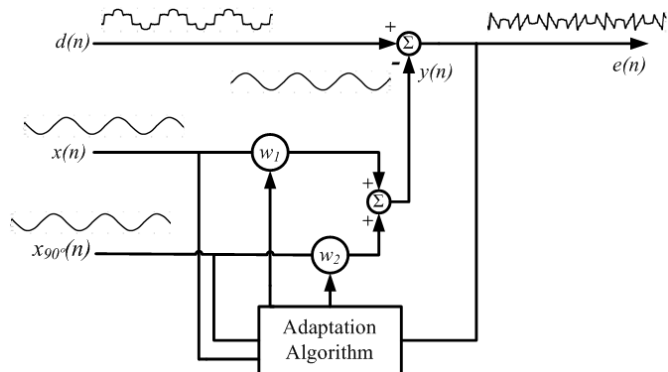
Fig. 2. Adaptive notch filter principle.

To overcome the problems regarding speed of convergence, several approaches based on a variable step-size method have been proposed in recent years [9]-[15]. In the strategy proposed here the step-size used in LMS algorithm is kept fixed.

The two orthogonal input signals are generated with Clarke transformation of the load current:

$$\begin{bmatrix} I_{L0} \\ I_{L\alpha} \\ I_{L\beta} \end{bmatrix} = \sqrt{\frac{2}{3}} \cdot \begin{bmatrix} 1/\sqrt{2} & 1/\sqrt{2} & 1/\sqrt{2} \\ 1 & -1/2 & -1/2 \\ 0 & \sqrt{3}/2 & -\sqrt{3}/2 \end{bmatrix} \cdot \begin{bmatrix} I_{La} \\ I_{Lb} \\ I_{Lc} \end{bmatrix} \qquad (8)$$

The two orthogonal signals, $I_{L\alpha}$ and $I_{L\beta}$, are filtered by a third order Butterworth with 100Hz cutoff frequency. And two sinusoidal input signals, $x(n)$ and $x_{90°}(n)$, in 60Hz are obtained without a PLL. Fig. 3 presents the block diagram of orthogonal signal generation.
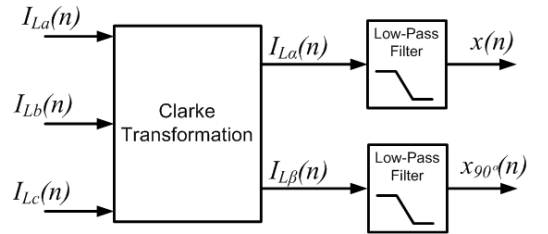
Fig. 3. Orthogonal signal generation.

The results of simulation and implementation show a convergence speed less than half cycle (~8ms) for the adaptive notch filter with LMS adaptation algorithm.

III. HARMONIC DETECTION WITH ADAPTIVE NOTCH FILTER USING RLS ALGORITHM

As second case studied in this work, the standard RLS algorithm [16] was applied for adaptive notch filter to adjust the two coefficients.

The formula of RLS algorithm applied for adaptive notch filters is given by the equations:

$$k_1(n) = \frac{\psi_{\lambda 1}^{-1}(n-1)x(n)}{\lambda + x^2(n)\psi_{\lambda 1}^{-1}(n-1)} \qquad (9)$$

$$k_2(n) = \frac{\psi_{\lambda 2}^{-1}(n-1)x_{90°}(n)}{\lambda + x_{90°}^2(n)\psi_{\lambda 2}^{-1}(n-1)} \qquad (10)$$

$$y(n) = w_1(n-1)x(n) + w_2(n-1)x_{90°}(n) \qquad (11)$$

$$e(n) = d(n) - y(n) \qquad (12)$$

$$w_1(n) = w_1(n-1) + k_1(n)e(n) \qquad (13)$$

$$w_2(n) = w_2(n-1) + k_2(n)e(n) \qquad (14)$$

$$\psi_{\lambda 1}^{-1}(n) = \lambda^{-1}\psi_{\lambda 1}^{-1}(n-1) - \lambda^{-1}k_1(n)x(n)\psi_{\lambda 1}^{-1}(n-1) \qquad (15)$$

$$\psi_{\lambda 2}^{-1}(n) = \lambda^{-1}\psi_{\lambda 2}^{-1}(n-1) - \lambda^{-1}k_2(n)x_{90°}(n)\psi_{\lambda 2}^{-1}(n-1) \qquad (16)$$

The gain vector $k(n)$ is transformed in two gains $k_1(n)$ and $k_2(n)$. The matrix $\psi_\lambda^{-1}(n)$ is transformed in two scalar values $\psi_{\lambda 1}^{-1}(n)$ and $\psi_{\lambda 2}^{-1}(n)$. Then, the entire algorithm is implemented more easily, simple and fast.

The parameter λ is the forgetting factor, positive constant close to one, but a little bit smaller. The choice of $\lambda < 1$ results in a scheme that puts more emphasis on the recent samples of the observed values and tends to forget the past.

As the same as the case of LMS algorithm, the simulations and experimental results demonstrated the convergence speed less than half cycle for the adaptive notch filter with RLS adaptation algorithm.

IV. SIMULATION RESULTS

The simulation results are shown in the next figures. The transient behavior of the adaptive notch filter with LMS algorithm, for a 100% load current variation, is presented in Figs. 4 and 5. Fig. 4(a) shows the load current $d(n)$. The fundamental of the load current (dashed line) and the adaptive notch filter output $y(n)$ (solid line) is shown in Fig.4 (b). Fig. 4(c) shows the harmonic current reference $e(n)$. Fig. 5(a) shows the desired harmonic reference (dashed line) and the harmonic reference generated by the adaptive notch filter (solid line). Fig. 5(b) presented the error between them.
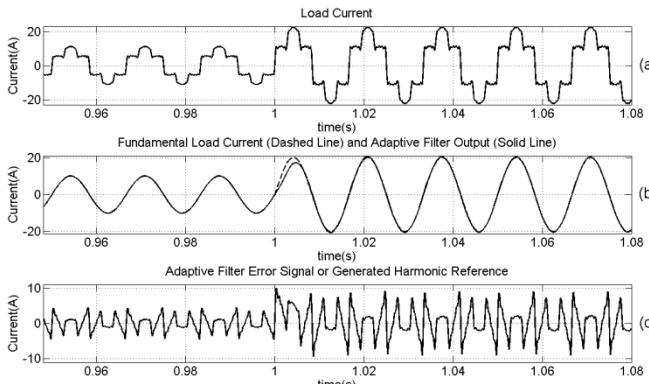

Fig. 4. Simulation results of adaptive notch filter with LMS algorithm. (a) Load current with 100% increase. (b) Fundamental load current (dashed line) and adaptive notch filter output (solid line). (c) Adaptive notch filter error signal or generated harmonic reference.
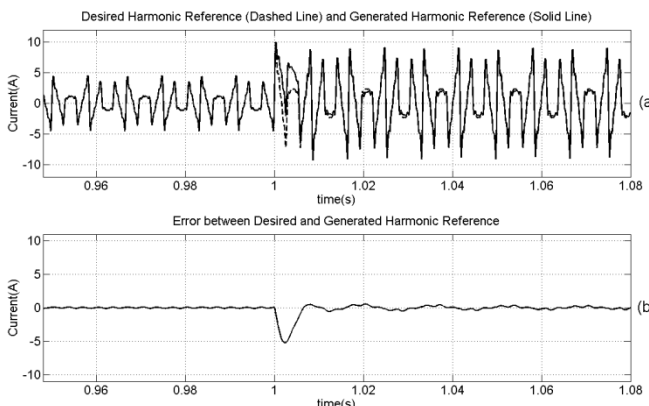

Fig. 5. (a) Desired harmonic reference (dashed line) and generated harmonic reference (solid line). (b) Error between desired and generated harmonic reference.

The transient behavior of the adaptive notch filter with RLS algorithm, for a 100% load current variation, is presented in Figs. 6 and 7. Fig. 6(a) shows load current $d(n)$. The fundamental of the load current (dashed line) and the adaptive notch filter output $y(n)$ (solid line) are presented in Fig. 6(b). The Fig. 6(c) shows the harmonic current reference $e(n)$. Fig. 7(a) shows the desired harmonic reference and the harmonic reference generated by the adaptive notch filter. The error between them in the second graphic is presented in Fig. 7(b).
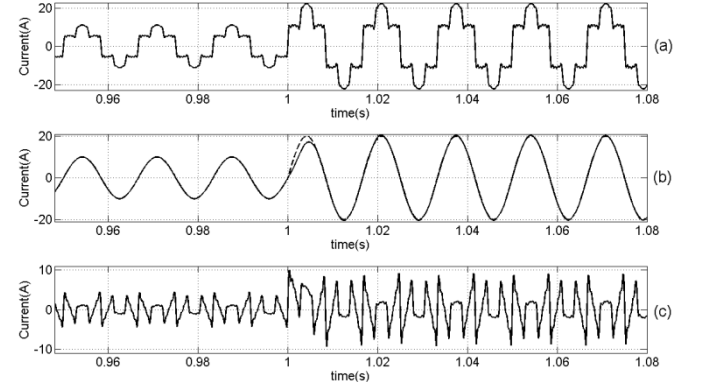
Fig. 6. Simulation results of adaptive notch filter with RLS algorithm. (a) Load current with 100% increase. (b) Fundamental load current (dashed line) and adaptive filter output (solid line). (c) Adaptive filter error signal or generated harmonic reference.
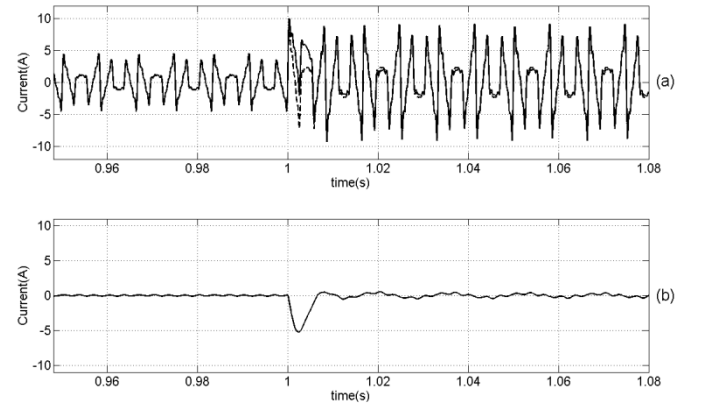
Fig. 7. (a) Desired harmonic reference (dashed line) and generated harmonic reference (solid line). (b) Error between desired and generated harmonic reference.

The simulations demonstrate that the adaptive notch filter with LMS or RLS algorithm produces a convergence less than half cycle of fundamental frequency. These results confirm an improvement of convergence time over the results presented in the literature for adaptive filters techniques applied to harmonic detection [4]-[12].

V. EXPERIMENTAL RESULTS

Experimental results are obtained from the application of the proposed technique in a shunt active power filter (SAPF) composed of three single-phase full H-bridges voltage source inverter (VSI) type, rated 15kVA, working in 40kHz switching frequency. The DC link voltage is adjusted to 500V. The smooth inductor used to connect the SAPF to

power system is rated 5mH. The harmonic current injection is controlled by a VSI PWM. The power system voltage is 220V line to line. The load, rated 20kVA, is a 6 pulse rectifier, CSI type. The shunt active power filter diagram is shown in Fig. 8. In these experimental results, a feedback configuration of SAPF was used, as illustrated in Fig. 8. Three Hall current sensors measure the three-phase source current. The control algorithm was implemented in a Texas DSP TMS320F2812.

The Fig. 9 shows the load current (IL_A) of 19A, the compensation current (Ic_A) and the source current (Is_A) of phase A after compensation, using an adaptive notch filter with LMS algorithm to extract the harmonic content. In Fig.10, the harmonic spectrum of source current before and after compensation is shown; the Total Harmonic Distortion (THDi) of the current Is_A is reduced from 28.9% to 8.29%.
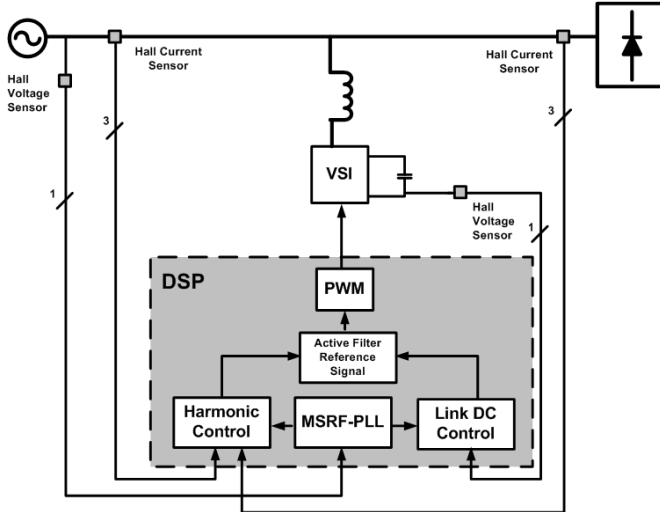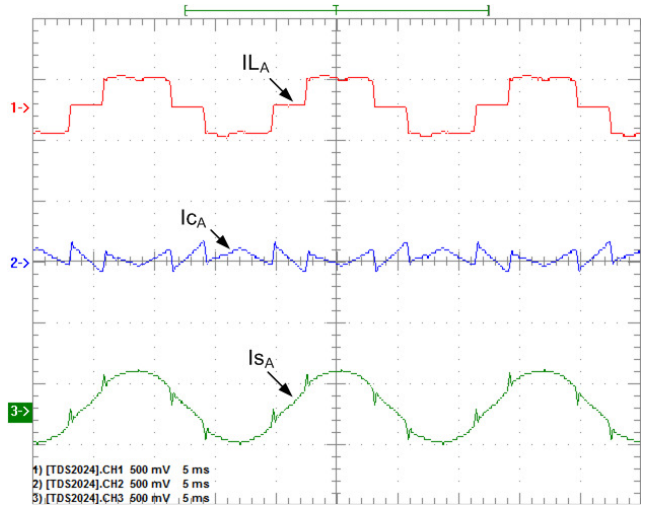
Fig. 10. Source current harmonic spectrum of the adaptive notch filter LMS algorithm.

Fig. 8. Shunt Active Power Filter Block Diagram.

Fig. 11. Experimental results: 100% load current increase with adaptive notch filter LMS algorithm.

Fig. 12 presents IL_A, Ic_A and Is_A after compensation, using an adaptive notch filter with RLS algorithm for a load current of 19A. The Fig. 13 shows the harmonic spectrum of the source current; the THDi of Is_A is reduced from 28.9% to 8.56%.
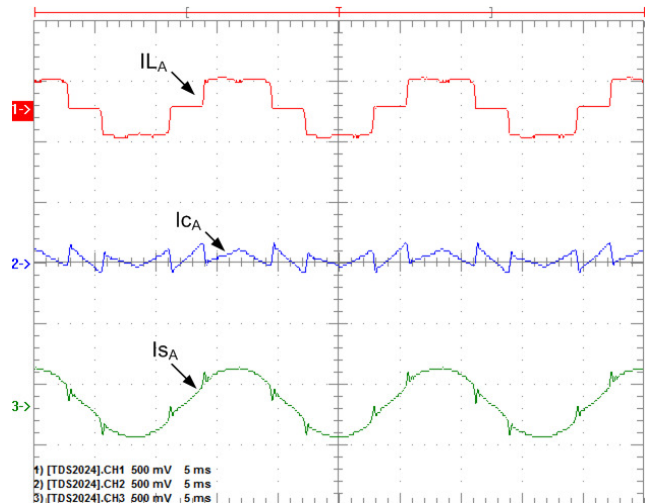
Fig. 9. Experimental results of adaptive notch filter LMS algorithm with a load current of 19A.

The Fig. 11 shows the transient behavior of the adaptive notch filter with LMS algorithm for a 100% load current variation. The result illustrates the convergence time Tc less than half cycle (~8ms).


Fig. 12. Experimental results of adaptive notch filter RLS algorithm with a load current of 19A.

The Fig. 14 shows the transient behavior of the adaptive notch filter with RLS algorithm for a 100% load current

variation. In the results the convergence time Tc is less than half cycle.

The results, with LMS or RLS algorithms, also confirm that obtained by simulations and is a important improvement over the results of the adaptive filters presented in literature.
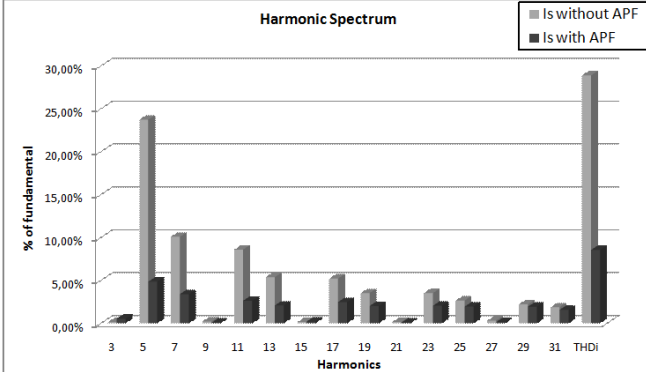

Fig. 13. Source current harmonic spectrum of the adaptive notch filter RLS algorithm.
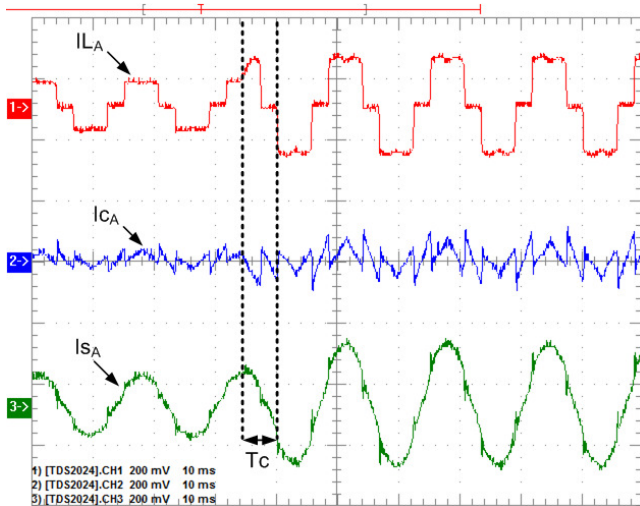
Fig. 14. Experimental results: 100% load current increase with adaptive notch filter RLS algorithm.

VI. CONCLUSION

In real time applications of active power filters, the calculation time, the speed of convergence and the steady-state error are critical matters to be taken into consideration during the design process. The proposed strategy with adaptive notch filters using LMS or RLS algorithms demonstrated good results concerning speed of convergence and steady-state error. The adaptive notch filter presented here is a very good choice, with respect to calculation time, because just two coefficients are needed to be adjusted.

The results of the strategy presented in this work demonstrated a convergence time faster than the results reported in the literature. The simulations and the experimental results show that the convergence time is less than half cycle (~8ms) of the fundamental frequency. Much faster than the 1 and 2 cycles of convergence time reported in

the literature for application of adaptive filters techniques to harmonic detection.

Another advantage of this strategy is the absence of a PLL to generate the input for the adaptive filter. In this case, the input orthogonal signals are obtained by the Clarke transformation of the three-phase load currents. Using the DSP TMS320F2812 running at 150MHz the entire algorithm takes 16μs to be completed. The strategy proposed here also is robust concerning the noise in the measurements, something very important in this kind of application.

ACKNOWLEDGMENT

REFERENCES

[1] S. Bhattacharya, D. M.Divan, T. M.Frank, B. Banerje – "Active filter system implementation", IEEE Ind. Appl. Mag., vol. 4, no. 5, pp 47-63, Set/Oct 1998.

[2] L. Asiminoaei, F. Blaabjerg, and S. Hansen, "Detection is key - Harmonic detection methods for active power filter applications," IEEE Ind.Appl. Mag., vol. 13, no. 4, pp. 22–33, Jul/Aug 2007.

[3] L. Asiminoaei, F. Blaabjerg, S. Hansen and P. Thogersen, "Adaptive compensation of reactive power with shunt active power filters," IEEE Trans. Ind. Appl., vol. 44, no. 3, pp. 867–877, May/Jun 2008.

[4] F. D. Freijedo, J. Doval-Gandoy, O. Lopez, P. Fernández-Comesaña and C. Martinez-Peñalver, "A signal-processing adaptive algorithm for selective current harmonic cancellation in active power filters," IEEE Trans. Ind. Electron., v. 56, n. 8, pp. 2829–2840, Aug. 2009.

[5] B.Singh, and J. Solanki, "An implementation of an adaptive control algorithm for a three-phase shunt active filter," IEEE Trans. Ind. Electron., v. 56, n. 8, pp. 2811–2820, Aug. 2009.

[6] M. Cirrincione, M. Pucci, G. Vitale, S. Scordato, and A. Miraoui, "Current harmonic compensation by a single-phase shunt active aower filter controlled by adaptive neural filtering," IEEE Trans. Ind. Electron., v. 56, n. 8, pp. 3128–3143, Aug. 2009.

[7] S. Välviita, S. J. Ovaska – "Delayless method to generate current reference for active filters". IEEE Trans. Ind. Electron., v. 45, n. 4, 1998.

[8] L. Qian, D. Cartes, and H. Li – "An improved adaptive detection method for power quality improvement". IEEE Trans. Ind. Appl., v. 44, n. 2, pp. 525–533, March/April 2008.

[9] M. H. Byung, Y. B. Byung, S. J. Ovaska – "Reference signal generator for active power filters using improved adaptive predictive filter". IEEE Trans. Ind. Electron., v. 52, n. 2, 2005.

[10] Mu Longhua, Jiangzi – "Application of adaptive filtering in harmonic analysis and detection", Transmission and Distribution Conference and Exhibition: Asia and Pacific, 2005 IEEE/PES, Dalian, 2005.

[11] Y. Qu, W. Tan, Y. Dong, and Y. Yang – "Harmonic detection using fuzzy LMS algorithm for active power filter", IEEE IPEC 2007, Singapore, 2007.

[12] H. Li, Z. Wu, F. Liu – "A novel variable step-size adaptive harmonic detecting algorithm applied to active power filter", IEEE ICIT 2006, Mumbai, 2006.

[13] B. Widrow, et al. – "Adaptive noise cancelling: principles and applications", Proceedings of the IEEE, v. 63, n. 12, p. 1692, 1975.

[14] R. H. Kwong, E. W. Johnston – "A variable step-size LMS algorithm", IEEE Trans. Signal Processing, 1992, 40(7), pp. 1633-1642.

[15] R. R. Pereira, C.H. da Silva, L.E.Borges da Silva, G.L.Torres, "A new strategy to step-size control of adaptive filters in the harmonic detection for shunt active power filter", IEEE IAS09, Houston, 2009.

[16] B. Farhang-Boroujeny, "Adaptive Filters: Theory and Applications". Chichester: John Wiley and Sons, 1998, ch. 12.

A Hybrid Active Var Compensator (HAVarC)

Carlos Henrique da Silva, Rondineli R. Pereira, Luiz E. Borges da Silva, Germano L. Torres, Robson B. Gonzatti

UNIFEI , Federal University of Itajuba

Itajuba, Brazil

Email: carloschedas@unifei.edu.br, leborges@unifei.edu.br, germano@unifei.edu.br

Abstract- **This paper proposes a modification on the Hybrid Active Series Filter (HASF) creating a topology named Hybrid Active Var Compensator (HAVarC) suitable to manipulate, in continuous way, the displacement power factor or voltage regulation. The HAVarC is composed by a small rating Active Power Filter (APF) in series with a capacitor bank. The main objective of this topology is to control the reactive power injected by the capacitor into the system by controlling the voltage applied on its terminals. The system automatically compensates the reactive power flow in order to guarantee the desired displacement power factor (DPF) or rated voltage and no power system parameters knowledge are necessary to the correct operation of the topology. Also the system guaranties the absence of inrush current or voltage surge in the power system at all operation modes.**

I. INTRODUCTION

As a variation of the Hybrid Active Series Filter (HASF), already described in the literature [2][3], the HAVarC is composed by a small rating Active Power Filter (APF) in series with a capacitor bank. This topology, shown in Fig.1, is able to control the reactive power injected by the capacitor into the system by controlling the voltage applied on its terminals. Differently from the Hybrid Active Series Filter (HASF), the active impedance created by the APF appears as an open-circuit to the harmonics frequencies and variable active impedance at fundamental frequency. The system automatically compensates the reactive power flow in order to guaranty the desired displacement power factor (DPF) or the voltage regulation independent of the power system parameters.

When the HAVarC system is working as a power factor controller it calculates the actual displacement power factor and controls the imposing capacitor voltage. This is done through the APF inverter, where a voltage with appropriated phase and amplitude, is imposed in series with the capacitor bank in order to increase or decrease the amount of reactive power injected into the mains.

The HAVarC works well even under voltage or current harmonic distortion without any special action. It is important to notice the power rate of the Active Power Filter, in the proposed configuration, is just 10% of the total reactive power provided by the capacitor bank. The reactive power flow can be controlled continuously from 20% to 120% of the capacitor bank power rating, limited only by the maximum voltage accepted by the capacitor bank.

The control strategy as well as the details of the implementation will be described and the practical results show the effectiveness of the proposed technique. The methodology was tested for a single-phase prototype using the DSP TMS320F2812 as real time calculator.

II. HYBRID ACTIVE VAR COMPENSATOR DESCRIPTION

The proposed structure, shown in Fig.1, named Hybrid Active Var Compensator (HAVarC), combines an Active Power Filter (APF) with a single capacitor bank where the series inductor was eliminated.
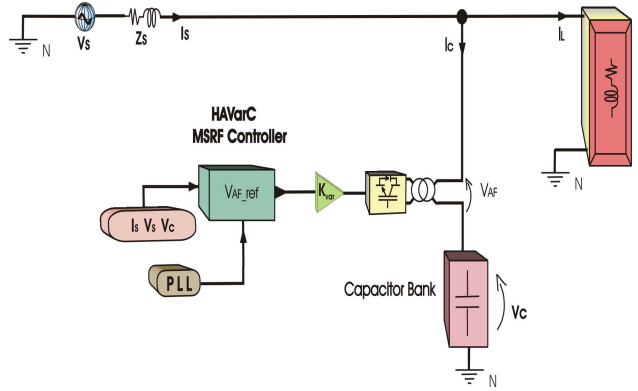
Fig. 1. Hybrid Active Var Compensator

The Active Power Filter (APF) is a controllable voltage source and it is controlled in such way to guaranty zero voltage for harmonics frequencies (open circuit) and a non-zero voltage at fundamental frequency.

The command for the instantaneous AC voltage, at fundamental frequency, is calculated based on the voltage across the capacitor bank and also proportional to the displacement power factor, given by equation (1).

$$\overrightarrow{V_{af}} = K_{var} \cdot \vec{V}_c \qquad (1)$$

The control strategy is based in the equation (2).

$$\vec{V}_s = \vec{V}_{AF} + \vec{V}_c \qquad (2)$$

Where V_S is the source voltage, V_{AF} is the imposed Active Power Filter voltage and V_C is the capacitor bank voltage.

The imposed V_{AF} is given by (3):

$$V_{AF} = \left(Z_{transf} \cdot I_c \right) + \left(V_{DC} \cdot \frac{N_1}{N_2} \cdot V_{REF} \right) \quad (3)$$

Where:

$Z_{transf} = R_{transf} + jX_{transf}$ (coupling transformer impedance), V_{DC} (APF DC link voltage), N1/N2 (transformer turn ratio), I_C (capacitor current) and V_{REF} (controller reference voltage).

III.   THE HAVArC IMPLEMENTATION

The testes were performed using as load a full-bridge single-phase rectifier and a variable RL load. The line to ground voltage is 127 Vrms. The Active Power Filter coupling transformer has a turn ratio of 4:1, 440/110 V, connected in series with a 400μF capacitor bank. The inverter switching frequency is 20kHz. The Active power Filter DC link voltage is regulated to 440 Vcc.

The strategy used to extract the source fundamental components of the voltage and the current is called Modified Synchronous Reference Frame MSRF, an adaptation of the standard three-phase Synchronous Reference Frame (SRF), applied to single-phase systems proposed on [11, 12].

The Fig.2 summarizes the technique.
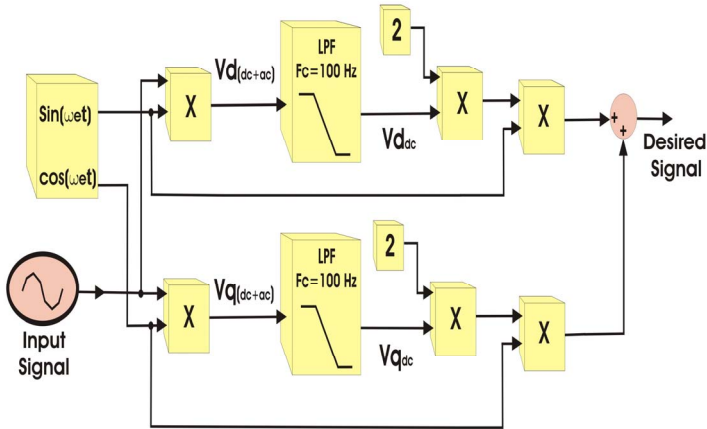
Fig. 2. MSRF to filter out the fundamental current wave form.

To guaranty the correct control action, the hybrid active power conditioner uses a double PLL arrangement. The first synchronizes the control system to the source voltage and the second synchronizes with capacitor bank voltage. At the beginning, before the HAVarC starts compensation, the voltage across the capacitor bank terminals is almost null, because the APF impedance is almost infinity (open circuit) and all source voltage is placed on coupling transformer. The control unit, in this operation instant, has to be synchronized with the source voltage to initiate charging APF DC link. As soon as the voltage of the APF DC link start increasing, the output voltage

of the APF start diminishing, at the limit it goes to be just the voltage drop across the transformer impedance. So, the capacitor bank voltage tends to be almost equal the source voltage Vs. After charging the DC link capacitor, for a pre-established value (440V), the voltage of the capacitor bank has a phase shifting related to the source voltage, due the non-negligible value of the transformer resistance. So, the capacitor bank current is not leading 90 degrees the source voltage (shown in Fig.7). It means, part of the power flowing in the HAVarC branch is active power and has to be drain from the source.

To avoid this active power consumption, undesirable for this kind of equipment, a new reference has to be chosen. Then, the control system switches the PLL reference from the source voltage to the capacitor bank voltage. This action is very important, because during the normal operation of the HAVarC the voltage across the capacitor bank change its phase according the value of the reactive power to be injected in the mains.   In order to cope with the abrupt phase variation, harmonic distortions and amplitude variations, inherent of this kind of application, this implementation uses a PLL algorithm called Modified Synchronous Reference Frame PLL (MSRF_PLL), explained in detail in [12].

The Fig.3 shows the block diagram of the MSRF_PLL.
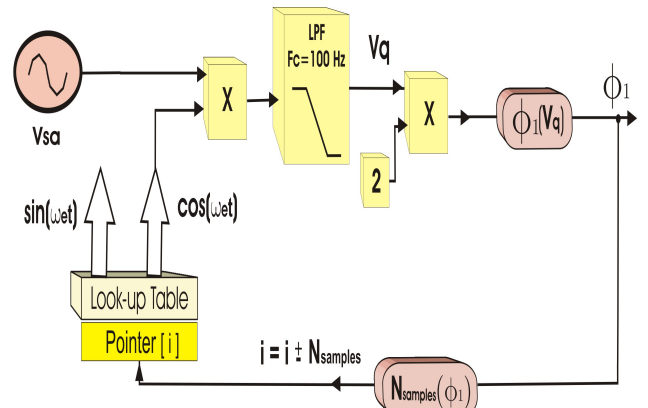
Fig. 3.   Block diagram of actual MSRF-PLL.

IV.   THE HAVArC REAL TIME REACTIVE POWER FLOW CONTROL

The amount of reactive power manipulated by the HAVarC is determined by the capacitor size and the voltage applied to it. In the proposed topology, the reactive power injected in the mains is controlled by controlling the voltage applied to capacitors terminals. Although the capacitor terminal voltage is designed to be the source voltage, the HAVarC adjust the capacitor voltage changing the reactive power delivery by the entire system continuously.

The proposed topology allows three well defined operation regions.

The OVERQ, where the reactive power Q, delivery by the capacitor bank, is bigger than the nominal rate; this is obtained applying to the capacitor a voltage bigger than 1.0 pu. This can be achieved respecting the acceptable voltage limit of the capacitor bank.

The STDQ, when the reactive power Q, delivery by the capacitor bank, is the nominal and the voltage applied to the capacitor is equal to 1.0pu.

The SUBQ, where the applied voltage varies between 0.2 to 1 pu.

Summarizing, the strategy proposed here, copes with the manipulation of the equivalent impedance of the entire branch (APF plus capacitor bank) in order to reach a desired displacement power factor. The Figures 4, 5, 6 and 7 show the measured source voltage, capacitor voltage, source current and load current to the each HAVarC operating region operating with a linear RL load.

The figures show the control of the reactive power flow, according the load variation, keeping the displacement power factor close to one.

The Fig.4 shows the OVERQ region. Here, the capacitor voltage is bigger than source voltage.
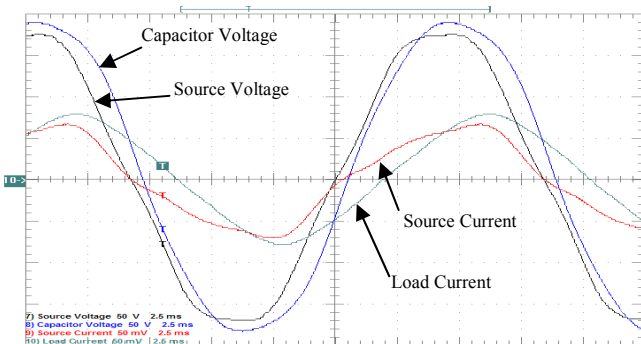
Fig. 4. Hybrid Active Var Compensator at OVERQ Region.

The Fig.5 shows STDQ region, where the capacitor voltage is equal to source voltage.
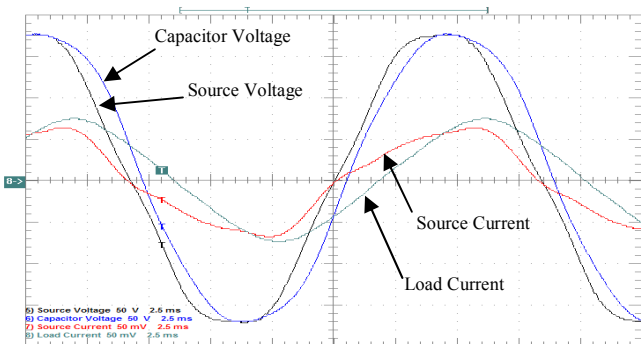
Fig. 5. Hybrid Active Var Compensator at STDQ Region.

It is important to notice there is neither transient current nor voltage surge occurrence during transitions between reactive power operating regions.

The Fig.6 shows the SUBQ region. The capacitor voltage is smaller than source voltage.
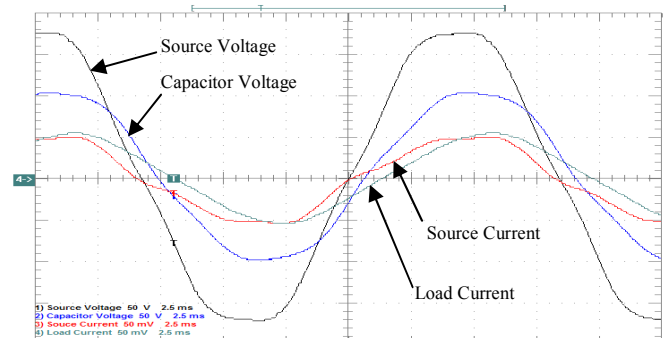
Fig. 6. Hybrid Active Var Compensator at SUBQ Region.

The Fig.7 shows the capacitor current to the SUBQ region.
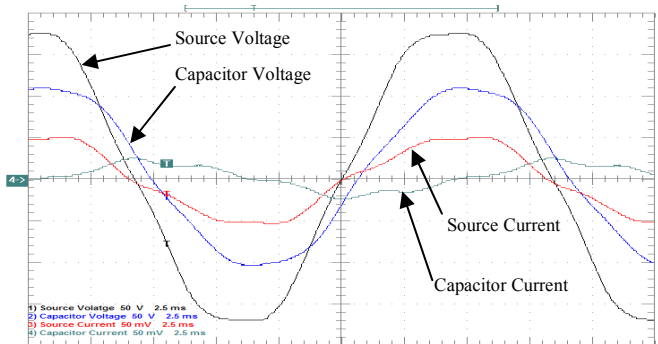
Fig. 7. Capacitor Current at SUBQ Region.

The table 1 presents the values for the variables related to each operation point.

TABLE I
VARIABLES SYSTEM PARAMETERS WITH THE HYBRID ACTIVE VAR COMPENSATOR

	HAVarC Regions		
	OVERQ	STDQ	SUBQ
Source voltage and Load Current phase shift	41.03°	39.3°	29.37°
Load displacement power factor	0.754	0.774	0.87
Source displacement power factor	0.995	1	1
Source voltage (Vrms)	127	127	127
Capacitor voltage (Vrms)	141	127	75.6
Source and Capacitor voltage shift	10.8°	11.23°	14.7°

The figures 8, 9, 10 shows the measured source voltage, capacitor voltage, source current and load current to the each HAVarC operating region. Now it operates under a non-linear load, a full-controlled single phase rectifier.

The figures show the control of the reactive power flow, according the load variation, keeping the displacement power factor close to one. The load variation has been obtained by stepping the converter firing angle.

The Fig.8 shows the OVERQ region. Here, the capacitor voltage is bigger than source voltage, 149 and 130 Vrms respectively. The firing angle was set to 55°.
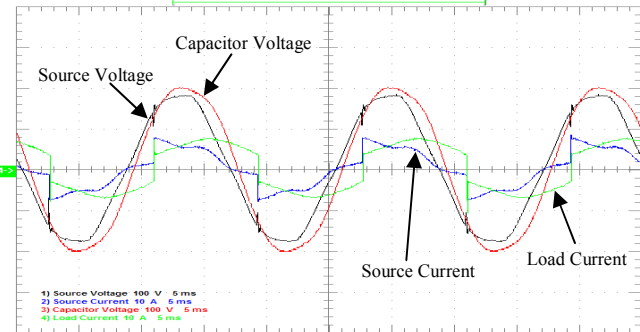
Fig. 8. Hybrid Active Var Compensator at OVERQ Region. Converter firing angle set to 55°.

The Fig.9 shows STDQ region, where the capacitor voltage is equal to source voltage, 130 Vrms. The firing angle was set to 45°.
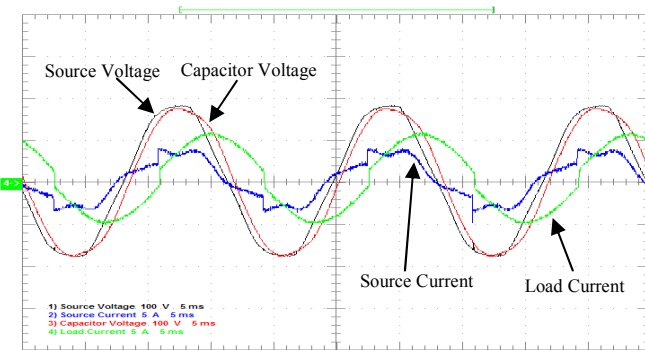
Fig. 9. Hybrid Active Var Compensator at STDQ Region. Converter firing angle set to 45°.

The Fig.10 shows the SUBQ region. Here, the capacitor voltage is smaller than source voltage, 53 and 130 Vrms respectively. The firing angle was set to 15°.

Note as the fire angle have been reduced the APF imposed voltage have been increased, reducing the applied voltage trough the capacitor bank.

In the latest three conditions presented above, where the HAVarC is operating with non-linear load, the reactive power demanded form the load is 422, 368 and 85 Var respectively.

Expressed in per unit terms, based on the capacitor bank nominal rate, the reactive power managed is 1.16 pu, 1 pu and 0.23 pu, to the OVERQ, STDQ and SUBQ operation mode respectively.
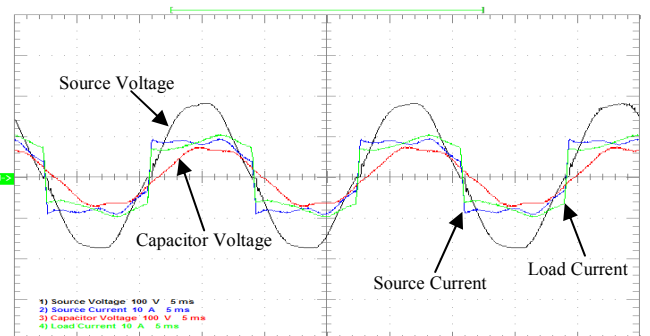

Fig. 10. Hybrid Active Var Compensator at SUBQ Region. Converter firing angle set to 15°.

V. CONCLUSION

The proposed topology is able to control the displacement power factor of the system in a real time mode. Using just a capacitor unit, the reactive power is controlled in a wide range, from 0.2 to 1.2 pu. Neither inrush current nor voltage surge is observed in whole HAVarC operation range. The voltage applied to the capacitor bank is free form harmonic, characteristic added due the HAVarC transformer. In order to change the HAVarC operation from displacement power factor control to voltage regulation, one has just to change the control variable from displacement factor to source voltage. The HAVarC proposed topology improves the well known static switch topology in two ways. The first is the continuous control of the power factor the second is related with the smaller power rate of the power electronics used in this topology. Therefore, it represents also a suitable alternative to the STATCON topology.

REFERENCES

[1] S.Bhattacharya, D.M.Divan, B.Banerjee, "Synchronous Frame Harmonic Isolator Using Active Series Filter" EPE Conf. Record,1991, Vol 3,pp 30-35.

[2] S.Bhattacharya, D.M.Divan "Synchronous Frame Based Controller Implementation for Hybrid Series Active Filter System" IEEE/IAS Conf. Record,1995, pp 2531-2540.

[3] H. Akagi, H. Fujita, "A New Power Line Conditioner for Harmonic Compensation in Power Systems" IEEE Trans. Power Del. Vol.10, No 3, pp 1570-1575, 1995.

[4] T.Thomas, K.Haddad, G.Joós, A.Jaafari, "Performance Evaluation of Three Phase Three and Four Wire Active Filters" IEEE/IAS Conf. Record, pp 1016- 1023, 1996.

[5] S.Bhattacharya, D.M.Divan, T.M.Frank, B.Banerje "Active Filter System Implementation" IEEE Trans. Ind. Appl. Set/Oct 1998, pp 47-63.

[6] F.Z.Peng, H. Akagi, "A New Aproach to Harmonic Compensation in Power System – A combined of Shunt Passive and Series Active Filter" IEEE/IAS ,Annual Meeting, pp 874-880, 1988.

[7] H. Fujita, H. Akagi, "A Pratical Aproach to Harmonic Compensation in Power System – Series Connection of Passive and Active Filter" IEEE/IAS ,Annual Meeting, pp 1107-1112, 1990.

[8] S. Tnani, M. Mazaudier, A.Berthon, S.Diop, "Comparison Between Different Real-Time Harmonic Analysis Methods for Control of Electrical Machines" PEVD94, pp. 4946-4951. 1994.

[9] J.Dixon, L.Moran, J.Rodriguez, R.Domke, "Reactive Power Compensation Technologies: State-of-the-Art Review", Proceedings of IEEE, vol.93, no.12, December 2005.

[10] S.Bhattacharya, D.M. Divan, B.B.Banerjee, "Control and Reduction of Terminal Voltage Harmonic Distortion (THD) in a Hybrid Series and Parallel Passive Filter System", IEEE PESC record, Seattle, 1993, pp.779-785. 1993.

[11] C.H. da Silva, V.F.da Silva, L.E.Borges da Silva, G.L.Torres, "Optimizing the Active Series Filters under Unbalanced Conditions Acting in the Neutral Current", IEEE ISIE2007, Vigo, Spain, June, 2007.

[12] C.H. da Silva, V.F.da Silva, L.E.Borges da Silva, G.L.Torres, R.R.Pereira, "DSP Implementation of Three-Phase PLL using Modified Synchronous Reference Frame", IEEE IECON07, Taiwan, 2007.

[13] Annabelle van Zyl, Johan H.R. Einslin and René Spée, " A new Unified Approach to Power Quality Management" IEEE Trans. Power Electronics, Vol. 11, N° 5, pp. 691-697, 1996.

[14] da Silva, C.H.; Pereira, R.R.; da Silva, L.; Lambert-Torres, G.; Pinto, J.; Takauti, E.H.; "Modified Synchronous Reference Frame strategy for single phase hybrid active power filter" 13th IEEE ICHQP, 2008.

[15] da Silva, C.H.; Pereira, R.R.; da Silva, L.E.B.; Lambert-Torres, G.; Bose, B.K.; " Improving the dynamic response of shunt active power filter using modified Synchronous Reference Frame PLL" 34th IEEE IECON 2008, 2008 .

Charging and Regulating the DC Link Voltage of Hybrid Active Series Power Filters

Carlos Henrique da Silva, Rondineli R. Pereira, Luiz E. Borges da Silva, Germano L. Torres, Robson B. Gonzatti

UNIFEI, Federal University of Itajuba
Itajuba, Brazil
Email: carloschedas@unifei.edu.br, leborges@unifei.edu.br, germano@unifei.edu.br

*Abstrac--*This paper describes the technique developed to charge and to regulate the hybrid active power filter link DC. The developed strategy is based on the Modified Synchronous Reference Frame Controller. The ability of the hybrid topology in charging and regulating its own Link DC without external sources connection is analyzed. The accuracy and the dynamics are presented, and the measurements of active power demand to perform the task are evaluated. Practical results exhibits the non-active power demanded to charge the Link DC capacitor and the absence of ripple in DC capacitor Voltage. The algorithm is executed in the DSP TMS320F2812 and the inverter switching frequency is 20 kHz.

I. INTRODUCTION

Although the concept of active hybrid filter has been widely discussed [1][2][3], the problem concerning the energy stored in the DC link is still weakly described in the literature [4]. Usually when dealing with hybrid active power filters, authors assume an ideal condition related to the energy storage. In practical terms, this assumption might be equivocated, once the DC link voltage charging and regulation model is far from the battery model representation, interfering in the dynamic of harmonic mitigation, and power factor regulation. This paper describes in detail the phenomenon of charging and regulating the DC link voltage. These actions of charging and regulating the DC link voltage are achieved by a modified step-up chopper circuit working with an AC input voltage producing a DC output voltage (DC link voltage).

II. HYBRID SERIES ACTIVE FILTER: PRINCIPLE OF OPERATION

An equivalent Hybrid Active Series Filter circuit which combines active filter AF and passive filter PF is shown in Fig. 1. The active filter is assumed as a controllable voltage source manipulated in order to present zero voltage when looking from the grid, at the fundamental frequency, and a harmonic voltage at specific harmonic frequency. The Active Power Filter (APF) has the ability to cancel the harmonic voltage which appears due the non-negligible impedance of passive filter (PF), thus providing a low impedance branch of that specific harmonic current.

The Fig. 2 shows the equivalent circuit taking in account just the impedances used during the DC link capacitor charging, i.e., the impedances at the fundamental frequency. The Passive Filter (PF) inductor is not considered because at fundamental frequency the passive filter inductive reactance is almost null comparing with the passive filter capacitive reactance, that is, $X_L << X_C$.
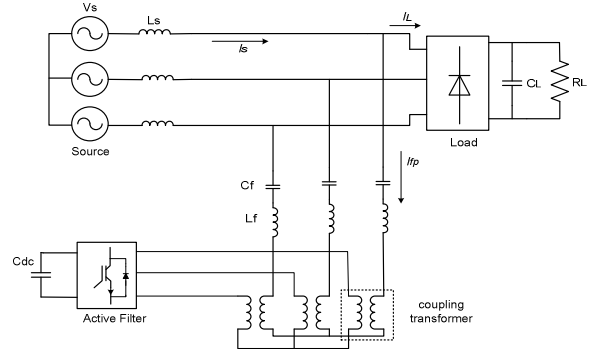
Fig. 1. Hybrid active power filter circuit
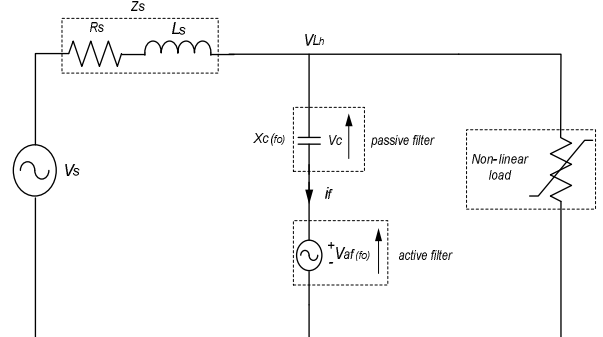
Fig. 2. Equivalent circuit during Link DC charging and Voltage regulation

III. CIRCUIT OPERATION

The active filter Coupling Transformer (CT) connected in series with the AC capacitor, works in a different manner than usual converters transformers. Its primary energy source V_{Lt} (low voltage side) mainly is obtained through an imposed current source, at fundamental frequency, function of the reactive power exchanged by the AC capacitor. This capacitive current I_C, flowing through the primary windings of the coupling transformer, produces a voltage drop, at fundamental frequency, across the CT primary impedance,

Z_{CT}. This primary side voltage source V_{Lt} depends on the primary impedance and the magnitude of capacitor current. The primary voltage drop usually is a small value, this is due to the low impedance (Z%) of the coupling transformer (CT). This low impedance is one of the most important specifications of the CT used in Hybrid Active Power Filter. Although the CT primary voltage presents a small value, the magnetic flux established into CT core is function of the current flowing across its windings. The correct choice of the transformer turn ratio is important to accomplish the necessary secondary voltage (V_{Ht}) in order to achieve the desirable DC link voltage charge and regulation. In fact, the V_{Ht} voltage still is far from the minimum desirable AC voltage level, so, an AC step-up chopper (AC-CHP) has to be implemented to guaranty the charge and regulation of the DC link voltage.

IV.   THE AC STEP-UP CHOPPER OPERATION

As mentioned above, the CT primary, connected in series, imposes a magnetic flux into CT core which is dependent of reactive power exchanged between the capacitor bank and the mains. This effect leads to a small voltage induced in the secondary, not big enough to start the Hybrid Active power Filter operation. A special procedure has to be done, i.e., increase the DC Link Voltage to a desirable value. Widely studied in literature, the DC-DC converters usually works with a continuous DC input voltage. In this application, the step-up configured chopper try to place in the DC link voltage a value as high as demanded, but using an input voltage coming from the secondary of the CT, i.e., an AC voltage. Looking deep inside this chopper topology, one can say that it is, in fact, a mix between a DC-DC step-up chopper and an active rectifier, because the converter input voltage can change the value along with the working period. The duty cycle of the chopper has to be modulated along with the voltage input signal in order to keep constant the chopper output voltage; it means the DC link voltage. This action is accomplished by a sinusoidal PWM technique commanding the IGBT switches, at fixed frequency of 20 kHz.   The Fig. 3 shows the circuit of the step-up AC chopper, which is in fact the actual Hybrid Active Power Filter converter circuit.
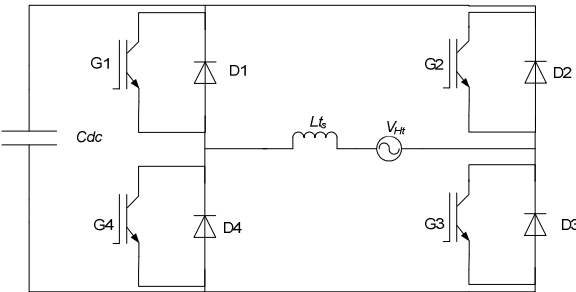

Fig. 3. Step-up AC chopper

V.   THE DYNAMICS OF DC LINK VOLTAGE CHARGING AND REGULATION

The analysis that follows describes the chopper dynamics during the charging process of DC link capacitor. This analysis was performed here just in positive semi-cycle of the input voltage. The same happens at the negative semi-cycle, but is not shown here. The equivalent inductance, reflected to the secondary side (L_{ts}), of the coupling transformer is responsible for the inductive energy storage element and energy transfer component of the AC step-up chopper. During the positive semi-cycle of the input voltage (V_{Ht}), the chopper algorithm commands only the IGBTs (G2) and (G4), according to the PWM output signal (while G1 and G3 are commanded to switch on during the negative semi-cycle of V_{Ht}. When G2 and G4 are switch on (ton), the energy (W_{Lpos}) is stored in the equivalent inductor (L_{ts}). The amount of energy depend on the circulating current (It_{sec}), which is dependent of the input voltage (V_{Ht}) and the inductance (L_{ts}), shown in Fig. 4.
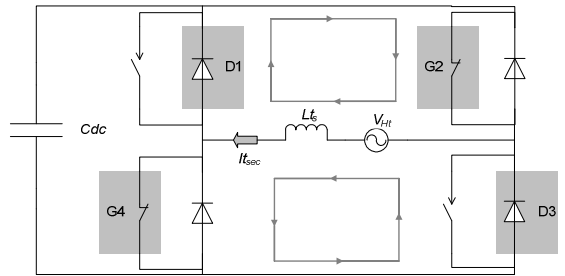
Fig. 4. Energy store equivalent circuit during positive semi-cycle IGBTs switch-on

One has to notice that a suddenly short-circuit occurs at the source terminals, determined by (t_{on}), which imply in a certain amount of energy stored (W_{Lpos}), expressed by (1).

$$w_{L_{pos}} = \int_0^t P dt = \int_0^t V_l I_l dt = L_t \cdot \int_0^{ton} \left(I_{t_{sec}} \right) dt \qquad (1)$$

As soon as G2 and G4 are switched off (t_{off}), the inductance counter-electromotive force (V_{Ltsec}) appears. This voltage is added to instantaneous source voltage effectively increasing the rectified DC capacitor voltage (V_C). It happens until the DC link voltage (V_{DC}) becomes equal to the source peak voltage (V_{Ht}), shown in Fig. 5.
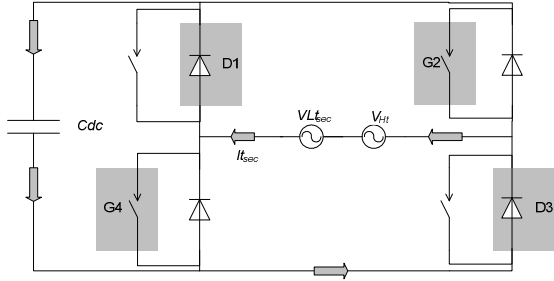
Fig. 5. Energy transfer equivalent circuit during positive semi-cycle IGBTs switch-off

When the DC link capacitor voltage (V_{DC}) equals to the source peak value (V_{Ht}) the rectifier process ends up, then the step-up chopper operation takes the task. To reach the predetermined DC Link voltage value, much bigger than the rectified voltage (V_{Ht}), the additional energy transferred to the DC capacitor is provided by the energy stored (W_{Lpos}) in the inductance (L_t). The instantaneous source voltage (V_{Ht}) keeps contributing to the capacitor charge, but now according to (2).

$$V_C - V_{Ht} = L_t \frac{di_{tsec}}{dt};$$
$$V_C > V_{Ht} \qquad (2)$$

The energy transfer between L_t and the DC link capacitor continuous until the desired DC link voltage equals to the step-up chopper output voltage ($V_{Ht} + V_{Ltsec}$), established by the PWM Modulation index. In other words, when the desired DC link voltage is achieved, the energy transfer stops.

VI. THE DC LINK VOLTAGE CHARGING AND REGULATION POWER DEMAND

A very important effect is the fact that there is no active power demand from the grid during this operation. The current flowing through the coupling transformer has capacitive nature because it is generated by the filter capacitor, so it leads the grid voltage by 90°. Setting the AC reference voltage of the converter in phase with the current flowing through Hybrid Active Power Filter branch, it results that all energy drain from the grid is in phase with this capacitive current, so the grid sees it as a reactive power. In other words, the voltage across the coupling transform and the current flowing through it lead 90° the grid voltage. Then, during the DC link charge, a pseudo-active power is drained from the grid. In fact the grid sees just a reactive power demand.

The equation (3) describes this pseudo-active power demanded by the grid to charge the DC link capacitor.

$$S_{HASPF} = V_{AF_{fo}} \sin\left(\omega t + \frac{\pi}{2}\right) \cdot I_{PF_{fo}} \sin\left(\omega t + \frac{\pi}{2}\right) \quad (3)$$

From the grid point of view, the power demand is given by (4).

$$S_{grid} = V_{grid_{fo}} \sin(\omega t) \cdot I_{PF_{fo}} \sin\left(\omega t + \frac{\pi}{2}\right) = S_{HASPF} \quad (4)$$

To achieve this control actions a double PLL arrangement is used. The first synchronizes with the source voltage and the other synchronizes with capacitor bank voltage. After charging the DC link capacitor, the voltage across the capacitor bank has a phase shifting related to the source voltage, due the non-negligible value of the transformer resistance. So, the capacitor bank current is not leading 90 degrees the source voltage (shown in Fig. 9 and Fig. 10). This means, part of the apparent power flowing in the filter branch is active power and has to be drain from the source. To keep the DC link capacitor charging continuing using only the reactive power drained from the grid, the control system switches the PLL reference from the source voltage to the capacitor bank voltage.

VII. THE DC LINK VOLTAGE CHARGE AND REGULATION RESULTS

The implementation setup, Fig. 6, is composed by a single phase H-bridge IGBT inverter plugged to a coupling transformer with turn ratio of 4:1 (440/110V) connected in series with a 50μF capacitor. The inverter switching frequency is 20kHz, the DC link voltage is regulated to 440 V_{DC} and the system voltage is 127 V.
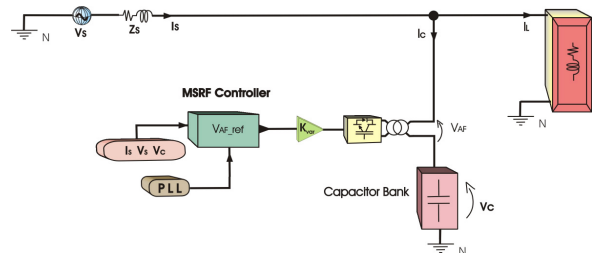

Fig. 6. Hybrid active power filter implementation Set-up

Fig. 7 shows the link DC voltage regulation under three different PWM modulation index.
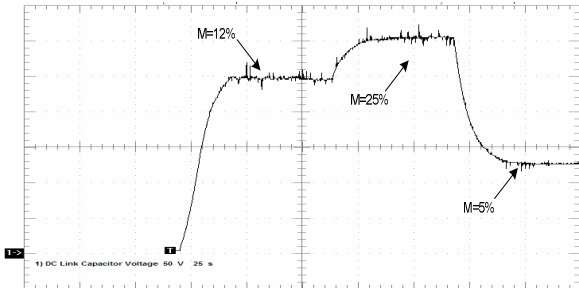
Fig.7. Link DC Voltage: Charging and Regulation under 3 different modulations indexes

Fig. 8 shows the power system variables under free-wheeling diodes conduction, and DC regulation to 160 V.
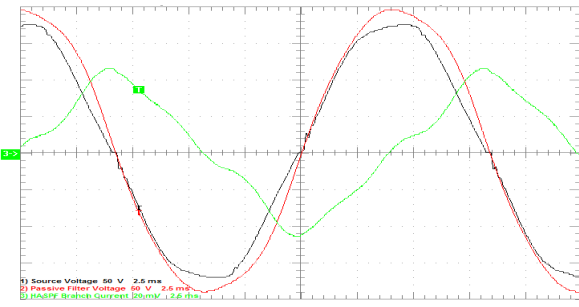

Fig. 8. Charging the DC ling using only the freewheeling diodes rectifier - DC link Voltage (160V)

Fig. 9 and Fig. 10 shows the DC link regulation to 440 and 540 V respectively. The voltage phase shift between source and passive filter are evidenced.
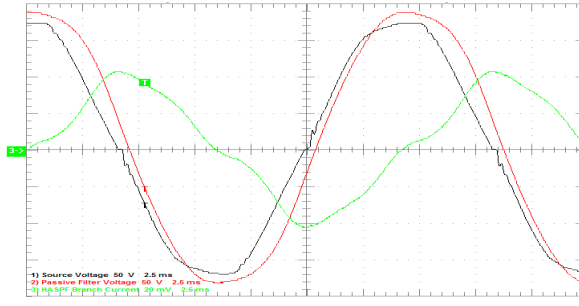

Fig. 9. System Variables to Step-up Chopper standing alone Operation - DC link Voltage (440v)
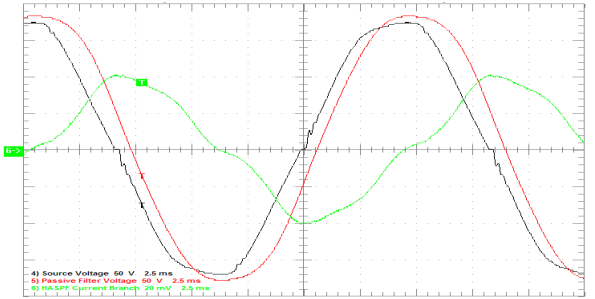

Fig. 10. System Variables to Step-up Chopper standing alone Operation - DC link Voltage (540v)

VIII. CONCLUSION

The methodology applied to charge and regulate the link DC voltage of Hybrid Series Active Power Filters (HSAPF) are presented and discussed in details. The fundamental concepts, strategies and procedures to implement the charge and regulation of the DC link voltage using only the hybrid active filter structure is shown. The power demanded during the process of voltage regulation is modeled and measured. The technique is shown in details and helps for practical implementation guideline.

REFERENCES

[1] S.Bhattacharya, D.M.Divan, B.Banerjee, "Synchronous Frame Harmonic Isolator Using Active Series Filter" EPE Conf. Record,1991, Vol 3,pp 30-35.

[2] S.Bhattacharya, D.M.Divan "Synchronous Frame Based Controller Implementation for Hybrid Series Active Filter System" IEEE/IAS Conf. Record,1995, pp 2531-2540.

[3] H. Akagi, H. Fujita, "A New Power Line Conditioner for Harmonic Compensation in Power Systems" IEEE Trans. Power Del. Vol.10, No 3, pp 1570-1575, 1995.

[4] J. Turunen, M. Salo and H. Tusa, "Comparison of three series Hybrid Active Power Filter Topologies" Proceedings of 11th IEEE/ICHQP , pp. 324-329, 2004

[5] C. H. Silva, V. F. Silva, L. E. B. Silva, Germano L Torres, E. H.Takauti, "Optimizing the Series Active Filters under Unbalanced Conditions Acting in the Neutral Current " Proceedings of International Conference on Industrial Electronics IEEE/ISIE, 2007.

[6] C.H. da Silva, V.F.da Silva, L.E.Borges da Silva, G.L.Torres, R.R.Pereira, "DSP Implementation of Three-Phase PLL using Modified Synchronous Reference Frame", IEEE IECON07, Taiwan, 2007.

[7] C.H. da Silva, R.R.Pereira, L.E.Borges da Silva, G.L.Torres, Joao Onofre Pereira Pinto and Edson Hideki Takauti "Modified Synchronous Reference Frame Strategy for Single Phase Hybrid Active Power Filter", Proceedings of 13th IEEE /ICHQP, Australia, 2008.

[8] S. Tnani, M. Mazaudier, A.Berthon, S.Diop, "Comparison Between Different Real-Time Harmonic Analysis Methods for Control of Electrical Machines" PEVD94, pp. 4946-4951.

[9] C.H. da Silva, R.R.Pereira, L.E.Borges da Silva, G.L.Torres, Joao Onofre Pereira Pinto "Modified Synchronous Reference Frame Strategy for Selective-Tuned Single Phase Hybrid Active Power Filte" Proceedings of IEEE/ IAS 2009.

[10] Annabelle van Zyl, Johan H.R. Einslin and René Spée, " A new Unified Approach to Power Quality Management" IEEE Trans. Power Electronics, Vol. 11, N° 5, pp. 691-697, 1996.

Unified Hybrid Power Quality Conditioner (UHPQC)

Carlos Henrique da Silva [1], Rondineli R. Pereira [1], Luiz E. Borges da Silva [1], Germano L. Torres [1], J. O. P. Pinto [2]
UNIFEI , Federal University of Itajuba   UFMS, Federal University of Mato Grosso do Sul
Itajuba, Brazil   Campo Grande, Brazil
Email: carloschedas@unifei.edu.br [1], leborges@ unifei.edu.br [1], germano@unifei.edu.br [1], jpinto@nin.ufms.br [2]

Abstract- **This paper proposes the Unified Hybrid Power Quality Conditioner (UHPQC). The proposed topology manipulates, at the same time and in continuous way, the displacement power factor and also it mitigates the dominant harmonic component of the line current. The structure is composed by a small rating Active Power Filter (APF) in series with a single passive filter. The main objective of this topology is to control the reactive power injected by the passive filter into the system by controlling the voltage applied on its terminals and simultaneously to compensate the dominant harmonic of the line current. The system automatically compensates the reactive and dominant harmonic power flow in order to guarantee the desired displacement power factor (DPF) and a low harmonic distortion. No information about power system parameters is necessary to the correct operation of the topology. Single phase practical results are presented and discussed.**

I. INTRODUCTION

The proposed topology unifies two already tested structures, the Selective-Tuned Hybrid Active Series Filter (ST-HASF) [1] and the HAVarC [2][3]. The proposed conditioner is composed by a small rating Active Power Filter (APF) in series with a passive filter. This topology, shown in Fig.1, is able to control the reactive power injected by the Passive Filter into the system by controlling the voltage applied on its terminals and also can tune the passive filter for the dominant harmonic current. The fundamental idea behind the proposed Unified Hybrid Power Quality Conditioner (UHPQC) topology is to implement a series active impedances, one at the fundamental frequency and the other at the dominant harmonic current frequency, using only one power converter. One has to notice that the classical Unified power Quality Conditioner (UPQC) is implemented using two power converters [4][5].

The UHPQC creates a variable active impedance at fundamental frequency and an harmonic sort-circuit to the dominant harmonic frequency, remaining as an open-circuit to the non-dominant harmonics frequencies. The system automatically compensates the reactive power flow in order to guaranty the desired displacement power factor (DPF) and eliminate completely the source dominant harmonic current, independent of the power system parameters.

When the Unified Hybrid Power Quality Conditioner (UHPQC) is working as a power factor controller it calculates the actual source displacement power factor and controls the fundamental voltage imposed to the passive filter. This action is performed by the APF inverter witch apply, in series with the Passive filter, a voltage with appropriated amplitude and phase, in order to increase or decrease the amount of reactive power injected into the mains.

Further, the UHPQC also imposes a harmonic voltage with appropriated phase and amplitude, related to the measured dominant harmonic source current, in series with the passive filter, in order to adjust it's Quality and the Tuned factor. Therefore, the passive filter reaches the absolute filter characteristics in that dominant harmonic frequency, i.e., zero impedance at this frequency. For the remaining harmonic content, the compensator acts as an open circuit

It is important to notice the power rate of the Active Power Filter, in the proposed configuration, is just 10% of the total reactive power provided by the passive filter. The reactive power flow can be controlled continuously from 20% to 120% of the equivalent capacitor bank power rating, limited only by the maximum voltage accepted by the capacitor bank.

The control strategy as well as details of the implementation will be described. Practical results showing the effectiveness of the proposed technique also will be presented. The methodology was tested for a single-phase prototype using the DSP TMS320F2812 as real time calculator.

II.   HYBRID ACTIVE VAR COMPENSATOR DESCRIPTION

The Fig.1 shows the Unified Hybrid Power Quality Conditioner which combines the active filter and the passive filter.
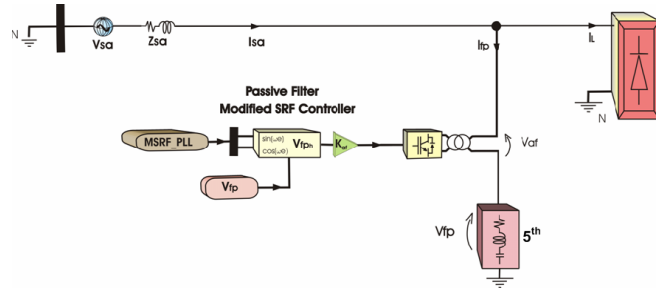

Fig. 1. Unified Hybrid Power Quality Conditioner

The Active Power Filter (APF) works as two independent controllable voltage sources. These sources are controlled in such way it's guaranty an appropriate voltage at fundamental frequency plus the necessary voltage at the dominant harmonic frequency.

The command for the instantaneous AC voltage, at fundamental frequency, is calculated based on the voltage across the passive filter bank and also proportional to the displacement power factor, given by equation (1).

$$\overrightarrow{V_{af}}_{fo} = K_{var} \cdot \overrightarrow{V_{pf}}_{fo} \tag{1}$$

The control strategy is based in the equation (2).

$$\vec{V}_s = \vec{V}_{af} + \vec{V}_{pf} \tag{2}$$

Where V_S is the source voltage, V_{af} is the imposed Active Power Filter voltage, V_{pf} is the passive filter voltage and *fo* is index indicating the fundamental frequency.

For the dominant source current harmonic frequency, the command for the instantaneous AC voltage, calculated based on the harmonic voltage across the passive filter bank, is given by equation (3).

$$\overrightarrow{V_{af}}_{fdh} = -K_{af} \cdot \overrightarrow{V_{pf}}_{fdh} \tag{3}$$

The constants K_{var} (1) and K_{af} (3) are the active filter gains to fundamental and dominant harmonic frequency respectively.

If K_{af} is unity, in an ideal control condition, the harmonic voltage which appears due the non-negligible impedance of passive filter (PF) is cancelled, thus providing a low impedance branch for dominant harmonic current.

In a passive filter, the tuned factor δ defines the magnitude in which the passive filter resonant frequency changes due to the variations in the power system frequency and in the passive filter parameters L_f and C_f. The values of C_f and L_f can change due to aging, temperature, or design tolerances. The tuned factor δ can be defined in terms of frequency and parameter variation , such as

$$\delta = \frac{\Delta f}{f_n} + \frac{1}{2}\left(\frac{\Delta L}{L_n} + \frac{\Delta C}{C_n}\right) \tag{4}$$

where:

Δf is the frequency variation around the nominal value f_n;

ΔL is the inductance variation around the nominal value L_n and

ΔC is the capacitance variation around the nominal value C_n.

An additional important parameter that must be considered in the passive filter design, which has a strong influence in the hybrid scheme compensation, is the quality factor Q. The quality factor of a passive filter is defined by

$$Q = \frac{1}{R_f}\sqrt{\frac{L_f}{C_f}} \tag{5}$$

where R_f, L_f, and C_f are the resistor, inductor and capacitor values of the passive filter.

A low value in the quality factor and/or a large value in the tuned factor increase the passive filter impedance at the desired harmonic frequency. This effect increases the amplitude of the required active filter voltage necessary to keep the compensation effectiveness.

The equivalent compensation circuit of the proposed UHPQC is shown in the Fig. 3.

The two controlled voltage frequencies and its respective impedances are represented.
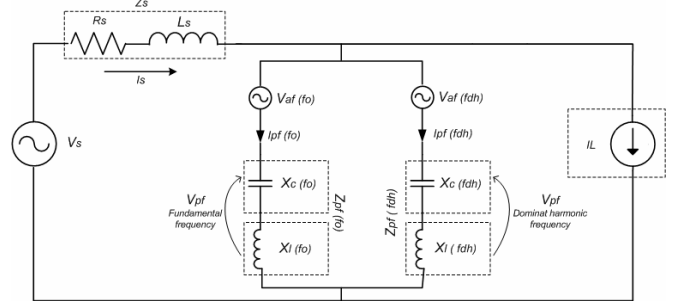

Fig. 2. UHPQC equivalent compensation circuit.

If the resonance frequency of the passive LC filter deviates from the desired value, the UHPQC can electronically re-tuned the filter to the original resonance frequency, or even to another chosen frequency [1].

The electronically re-tuning of the LC shunt circuit is done by generating an active inductance L_a. The resonance frequency of the passive filter can be tuned by controlling this active inductance as follows:

$$f_f = \frac{1}{2\pi\sqrt{C_f\left(L_f + L_a\right)}} \tag{6}$$

In this way, the passive filter can be re-tuned for any desired frequency by choosing the appropriate active inductance [1].

The active filter gain K_{af}, is then re-nominated Active Impedance (extending the Akagi/Fujita concept [6]). The Active impedance K_{af} is composed by an active resistance $k = -R_f$ and by an active inductance $k = j2\pi f_h L_a$, generating $k_{af} = -R_f \pm j2\pi f_h L_a$.

III. THE UHPQC IMPLEMENTATION

The setup were built as shown in Fig.1 where, the line to ground voltage is 127 Vrms, the Active Power Filter coupling transformer turn ratio 4:1 (440/110 V) connected in series with a fifth harmonic tuned passive filter (L_f=4.7mH and C_f=60μF). The inverter switching frequency is 20kHz. The Active power Filter DC link voltage is regulated to 440 Vcc. The non-linear load is implemented using a full-controlled single phase rectifier.

The information about the voltages and currents needed in the UHPQC control strategy is extract, from the system, using the Modified Synchronous Reference Frame MSRF, which is an adaptation of the standard three-phase Synchronous Reference Frame (SRF) [7][8].

The Fig.3 summarizes the technique.
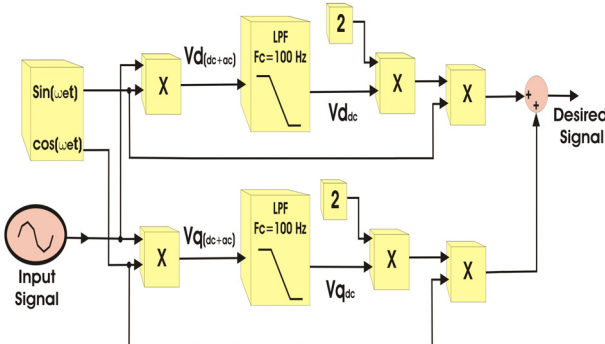
Fig. 3. MSRF block diagram.

To guaranty the correct control action, the hybrid active power conditioner uses a double PLL arrangement. The first synchronizes the control system to the source voltage and the second synchronizes with passive filter voltage.

The UHPQC uses the PLL algorithm called Modified Synchronous Reference Frame PLL (MSRF_PLL)[8]. This PLL algorithm manipulates very well abrupt phase variations, harmonic distortions, amplitude variations and noise, inherent in this kind of application.

The Fig.4 shows the block diagram of the MSRF_PLL.
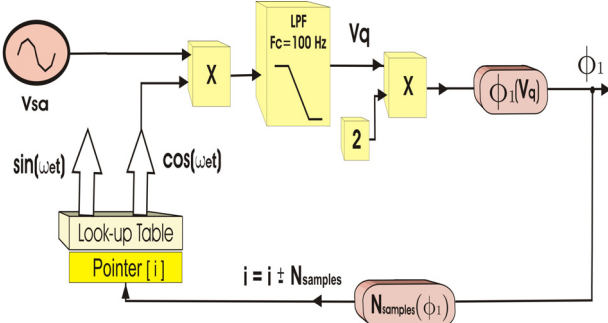
Fig. 4. MSRF-PLL block diagram.

IV. THE UHPQC REACTIVE POWER FLOW CONTROL

The amount of reactive power manipulated by the UHPQC is determined by the passive filter size and the voltage applied to it. In the proposed topology, the reactive power injected into the mains is controlled by controlling the voltage applied to passive filter. Although the voltage across the passive filter was designed to be the source voltage, the UHPQC manipulates that voltage in order to continuously control the total reactive power delivery by the entire system.

The topology has three well defined operation regions.

OVERQ: the reactive power Q delivery by the passive filter is bigger than the nominal rate. This situation is achieved applying to the passive filter a voltage bigger than 1.0 pu.

STDQ: the reactive power Q delivery by the passive filter is the nominal rate and the voltage applied to the passive filter is equal to 1.0pu.

SUBQ: the reactive power Q delivery by the passive filter is below the nominal rate and the voltage applied to the passive filter varies between 0.2 to 1 pu.

Summarizing, the UHPQC under fundamental frequency operation manipulates the equivalent impedance of the entire branch (APF plus passive filter) in order to reach a desired displacement power factor.

The figures 5, 6 and 7 show the source voltage, capacitor voltage, source current and load current to the each UHPQC operating region.

The figures show the reactive power flow control, under the load variations, always keeping the displacement power factor close to one.

The Fig.5 shows the OVERQ region. Here, the passive filter voltage is bigger than source voltage, 149V and 130V respectively. The load firing angle was set to 55 degrees.
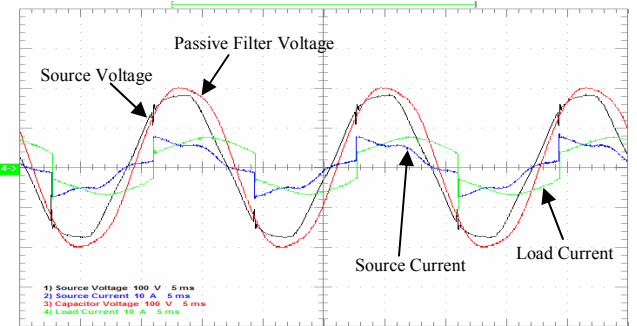

Fig. 5. Hybrid Active Var Compensator at OVERQ Region. Converter firing angle set to 55 degrees.

The Fig.6 shows STDQ region, the passive filter voltage is equal to source voltage, 130V. The load firing angle was set to 45 degrees.

Fig. 6. Hybrid Active Var Compensator at STDQ Region.
Converter firing angle set to 45 degrees.
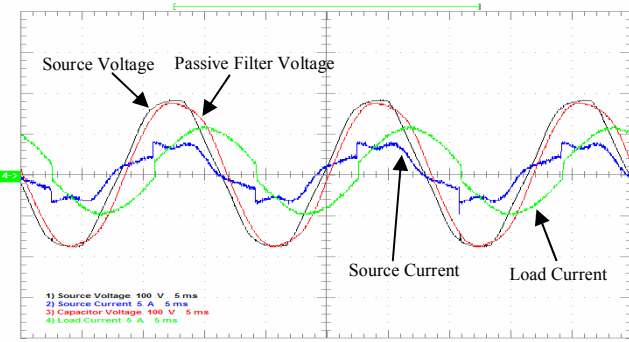
The Fig.7 shows the SUBQ region. Here, the capacitor voltage is smaller than source voltage, 53V and 130V respectively. The load firing angle was set to 15 degrees.

When the load fire angle goes down, the imposed APF voltage has to go up, then reducing the applied voltage trough the passive filter.

Expressed in per unit (pu) terms, based on the passive filter nominal rate, the OVERQ, STDQ and SUBQ operation modes are delivering reactive power of 1.16 pu, 1 pu and 0.23 pu respectively.


Fig. 7. Hybrid Active Var Compensator at SUBQ Region.
Converter firing angle set to 15 degrees.
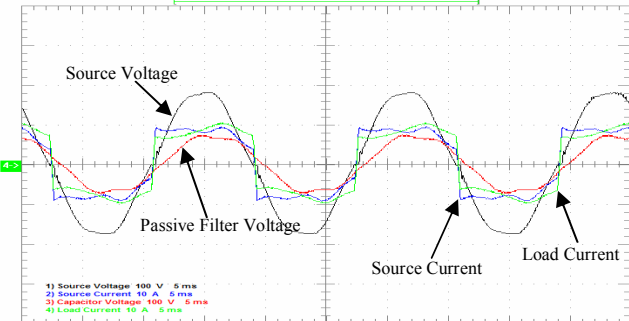
V. THE UHPQC HARMONIC POWER FLOW CONTROL

In addition to the quality factor improvement, the resonance frequency of the passive filter can be electronically changed by a complementary active inductance L_a. Based on that action, the proposed UHPQC strategy can determine the dominant harmonic in the source current and then compensate it.

The entire process of dominant harmonic mitigation is performed simultaneously with Var compensation.

The Fig. 8 shows the source current spectrum where the third harmonic is dominant.


Fig. 8. Source current with third harmonic dominant frequency.
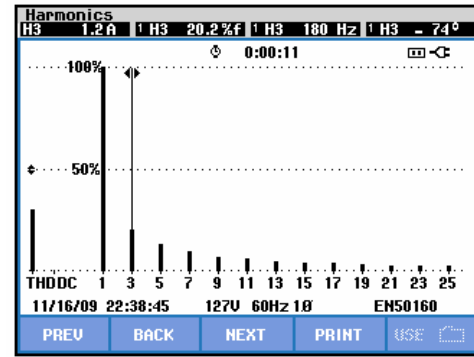
At this operation point, the fifth harmonic amplitude is 0.8A against the 1.2A of third harmonic component. The fundamental current is 5.8A.

Fig. 9 shows the source voltage and current, load current and passive filter terminal voltage without UHPQC dominant harmonic compensation.
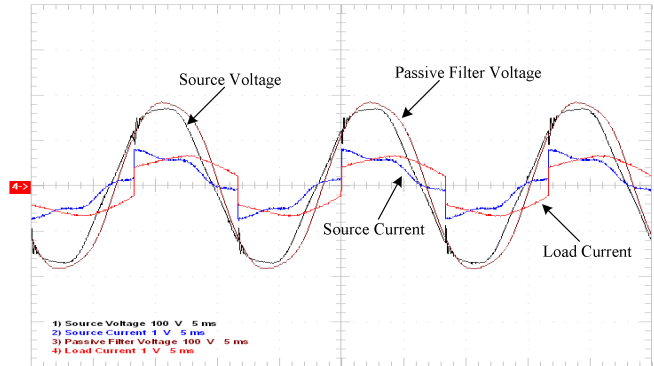

Fig. 9. System variables without UHPQC harmonic dominant mitigation.
.

At this operation point, the load rectifier demands 325Var from the source adequately compensating by the UHPQC as shown in Fig 10, where (cosΦ=1) .

Fig. 10. Displacement power factor compensation before UHPQC harmonic dominant mitigation.
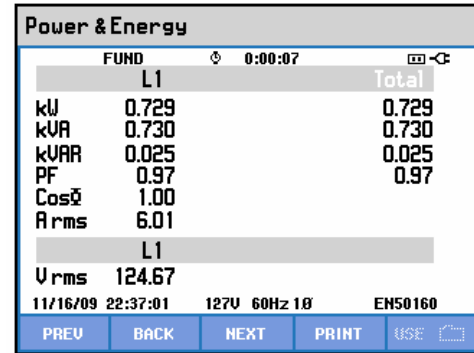
The Fig.11 shows the source current and voltages, the load current and the passive filter voltage, after the UHPQC starting the dominant harmonic compensation.
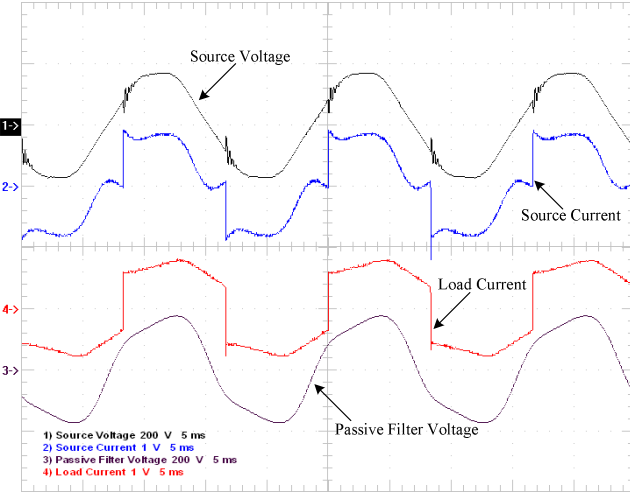

Fig. 11. System variables with UHPQC harmonic dominant mitigation.

The source current spectrum, shown in Fig. 12, confirms the dominant harmonic mitigation by harmonic active impedance implementation associated to Var compensation.

It has to be notice that, the third harmonic current has fallen from 20.2% to 0.4%, even thought the passive filter was design to mitigate the fifth harmonic .
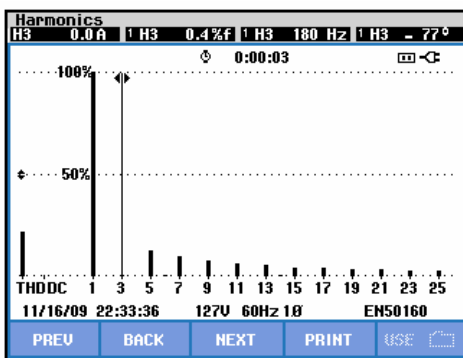

Fig. 12. Source Current under UHPQC harmonic dominant mitigation.

VI. CONCLUSION

The proposed topology is able to control, at the same time, the displacement power factor of the system and the dominant harmonic of the line current using only one power converter. The compensation characteristic can also electronically retune the passive filter independently of the pre-built passive filter tuned frequency. Therefore, the Unified Hybrid Power Quality Conditioner (UHPQC), after playing with all the variables discussed in details before, it can compensate de displacement power factor, harmonic mitigation and consequently it does voltage regulation.

Also, the drawbacks inherent to passive filter compensation are eliminated and the compensation characteristics of already installed passive filter can be significantly improved and even changed. The DSP as control unit is essential.

REFERENCES

[1] da Silva, C.H., Pereira, R.R., da Silva, L.E.B., Lambert-Torres, G., Pinto, J.O.P. "Modified Synchronous Reference Frame Strategy for Selective-Tuned Single Phase Hybrid Active Power Filter" IEEE/IAS ,Annual Meeting, 2009.

[2] da Silva, C.H., Pereira, R.R., da Silva, L.E.B., Lambert-Torres, G. "A Hybrid Active Var Compensator (HAVarC)" IEEE/IECON 2009, 2009 .

[3] Annabelle van Zyl, Johan H.R. Einslin and René Spée, " A new Unified Approach to Power Quality Management" IEEE Trans. Power Electronics, Vol. 11, N° 5, pp. 691-697, 1996.

[4] H. Fujita, H. Akagi, "A New Power Line Conditioner for Harmonic Compensation in Power Systems" IEEE Trans. Power Eletronics. Vol.13, No 2, pp 315-322, 1998.

[5] V. Khadkikar, A. Chandra, A. 0. Barry, T. D. Nguyen, "Conceptual Study of Unified Power Quality Conditioner (UPQC)", IEEE ISIE2006, Montreal, Canada, July, 2006.

[6] H. Akagi, H. Fujita, "A New Power Line Conditioner for Harmonic Compensation in Power Systems" IEEE Trans. Power Del. Vol.10, No 3, pp 1570-1575, 1995.

[7] C.H. da Silva, V.F.da Silva, L.E.Borges da Silva, G.L.Torres, "Optimizing the Active Series Filters under Unbalanced Conditions Acting in the Neutral Current", ISIE2007, Vigo, Spain, June, 2007.

[8] C.H. da Silva, V.F.da Silva, L.E.Borges da Silva, G.L.Torres, R.R.Pereira, "DSP Implementation of Three-Phase PLL using Modified Synchronous Reference Frame", IECON07, Taiwan, 2007.

[9] S.Bhattacharya, D.M.Divan "Synchronous Frame Based Controller Implementation for Hybrid Series Active Filter System" IEEE/IAS Conf. Record,1995, pp 2531-2540.

[10] S.Bhattacharya, D.M.Divan, B.Banerjee, "Synchronous Frame Harmonic Isolator Using Active Series Filter" EPE Conf. Record,1991, Vol 3,pp 30-35.

[11] T.Thomas, K.Haddad, G.Joós, A.Jaafari, "Performance Evaluation of Three Phase Three and Four Wire Active Filters" IEEE/IAS Conf. Record, pp 1016- 1023, 1996.

[12] S.Bhattacharya, D.M.Divan, T.M.Frank, B.Banerje "Active Filter System Implementation" IEEE Trans. Ind. Appl. Set/Oct 1998, pp 47-63.

[13] F.Z.Peng, H. Akagi, "A New Aproach to Harmonic Compensation in Power System – A combined of Shunt Passive and Series Active Filter" IEEE/IAS ,Annual Meeting, pp 874-880, 1988.

[14] H. Fujita, H. Akagi, "A Pratical Aproach to Harmonic Compensation in Power System – Series Connection of Passive and Active Filter" IEEE/IAS ,Annual Meeting, pp 1107-1112, 1990.

[15] S. Tnani, M. Mazaudier, A.Berthon, S.Diop, "Comparison Between Different Real-Time Harmonic Analysis Methods for Control of Electrical Machines" PEVD94, pp. 4946-4951. 1994.

[16] S.Bhattacharya, D.M. Divan, B.B.Banerjee, "Control and Reduction of Terminal Voltage Harmonic Distortion (THD) in a Hybrid Series and Parallel Passive Filter System", IEEE PESC record, Seattle, 1993, pp.779-785. 1993.

[17] da Silva, C.H.; Pereira, R.R.; da Silva, L.; Lambert-Torres, G.; Pinto, J.; Takauti, E.H.; "Modified Synchronous Reference Frame strategy for single phase hybrid active power filter" 13th IEEE ICHQP, 2008.

[18] da Silva, C.H.; Pereira, R.R.; da Silva, L.E.B.; Lambert-Torres, G.; Bose, B.K.; " Improving the dynamic response of shunt active power filter using modified Synchronous Reference Frame PLL" IEEE IECON 2008, 2008 .

APPLICATION OF ADAPTIVE FILTERS IN ACTIVE POWER FILTERS

R.R. Pereira   C.H. da Silva   L.E. Borges da Silva   G. Lambert-Torres

Federal University of Itajubá - UNIFEI

Itajubá, Brazil

rondi@unifei.edu.br, carloschedas@unifei.edu.br, leborges@unifei.edu.br, germano@unifei.edu.br

Abstract – **This paper presents a new idea applied to adaptive filters for harmonic detection in shunt active power filters. Improve the speed of convergence of the adaptive filter and reduces the steady-state error are the finals objectives of the strategy. Two cases are presented and discussed, one with a Finite Impulse Response (FIR) adaptive filter with 32 coefficients and another with an adaptive notch filter. The Least Mean Square (LMS) algorithm was used to adjust the coefficients in the both cases. An algorithm based on Coulon oscillator principle was used to determine the load current amplitude and then modify the step-size value. Simulations using Matlab are presented to clarify the algorithm. Also practical implementation is performed using the DSP Texas Instruments TMS320F2812 and the experimental results depicted.**

Keywords – **Adaptive filters, active power filter, adaptive FIR filter, adaptive notch filter, harmonic compensation.**

I. INTRODUCTION

The compensation for harmonic currents, generated by power electronic equipments, has become important as its growing use in the industrial applications. In this context, more and more, new techniques are developed in order to improve the effectiveness of active power filters (APF) in harmonic mitigation. The performance of active power filters basically depend on the extraction method used to generate the current reference signal, the control method used to generate the compensation harmonic current and the dynamic characteristic of the entire filter [1].

In power system, the current can be described as

$$i(t) = \sum_{n=1}^{N} A_n \sin(n\omega t + \theta_n) \tag{1}$$

The fundamental current is denoted by $i_1(t)$ and harmonic current as

$$i_h(t) = \sum_{n=2}^{N} A_n \sin(n\omega t + \theta_n) \tag{2}$$

The harmonics can be obtained just eliminating the fundamental components. The problem arisen is how to extract the sinusoidal waveform, separating the harmonic components.

Actually the synchronous reference frame and the instantaneous power theory are the two methods of harmonic extraction more used in active power filters control. In recent years the use of Adaptive Filters has shown a powerful technique to perform this job.

II. HARMONIC DETECTION WITH ADAPTIVE FILTERS

The adaptive noise canceling technique based on the Wiener theory has been widely used in many signal processing applications [2]. It can maintain the system in the best operating state by continuously self-adjusting its parameters. According to the adaptive noise canceling theory, the principle of adaptive harmonic detecting method is that illustrated in Fig 1.


Fig. 1. The principle of adaptive detecting of harmonics.

In this basic structure of adaptive filter (Fig. 1) applied to current harmonic detection, $d(n)$ represents the current $i(t)$ blurred with harmonics and $x(n)$ represents the sinusoidal waveform $v_{sin}(t)$ in phase with the source voltage. The reference input signal $x(n)$ is processed by adaptive filter producing the output signal $y(n)$ that tracks the variation of fundamental signal of the load current. The objective of adaptive filter is approximates $y(n)$, in both amplitude and phase, to the fundamental signal $i_1(n)$. So, the desired harmonics content $i_h(n)$ can be directly obtained from the error signal $e(n)$ given by the subtracting of $y(n)$ from $d(n)$. The coefficients of the adaptive filter are adjusted using the Least Mean Square (LMS) algorithm. The recursion formula of LMS algorithm is given by the equations:

$$e(n) = d(n) - y(n) = d(n) - \boldsymbol{X}^T(n)\boldsymbol{W}(n) \tag{3}$$

$$\boldsymbol{W}(n+1) = \boldsymbol{W}(n) + \mu e(n)\boldsymbol{X}(n) \tag{4}$$

Where:
$X(n)$ - input vector.
$W(n)$ - coefficient vector.
μ - step-size.

The parameter μ controls the rate of convergence of the algorithm to the optimum solution.

In this work a Finite Impulse Response (FIR) adaptive filter [2-4] with 32 coefficients and an adaptive notch filter [2][5-7] were tested. The adaptive FIR filter structure uses the general structure of adaptive filter shown in Fig.1. The adaptive notch filter is shown in Fig. 2. This structure (Fig. 2) uses two orthogonal signals as input, one for the input $x(n)$ and other 90° phase shifted. In this way only two coefficients are needed to be adapted. The adaptation procedure is the same as used in the general structure of adaptive filters.


Fig. 2. Adaptive notch filter principle.

To overcome the problems with the speed of convergence, several approaches based on a variable step-size method were proposed in recent years [5-8]. The approach proposed in this work also plays with the step-size to speed-up the adaptation algorithm. But, instead of looking to the error signal, which is polluted with noise complicating the adaptation algorithm behavior, it looks directly to the load current value searching for significative transients. Once the transient in the load current is detected the algorithm starts the step-size adjustments. That shows up to improve the adaptation algorithm behavior. In the simulations the convergence speed reaches the maximum of 1.5 cycles for both cases, the adaptive FIR filter and the adaptive notch filter, against the minimum of 2 cycles reported in the literature [4][6-7]. The amplitude of the load current is determined with a simple algorithm described in [9], based on Coulon oscillator principle. This algorithm is illustrated in Fig. 3.
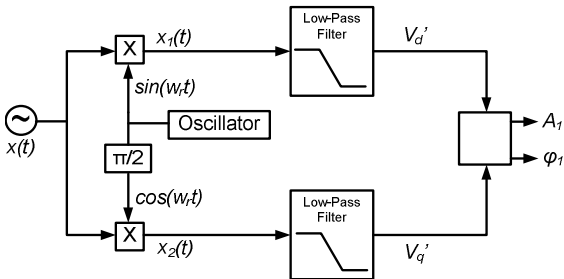

Fig. 3. Coulon oscillator principle.

The oscillator frequency w_r is defined in 60Hz and the load current is used as the signal $x(t)$. In this way, the amplitude of the load current fundamental component can be detected with the algorithm.

With an IIR low-pass filter the components V_d' and V_q' can be extracted as shown in (5) and (6):

$$V_d' = \frac{A_1}{2}\cos(\varphi_1) \tag{5}$$

$$V_q' = \frac{A_1}{2}\sin(\varphi_1) \tag{6}$$

Various filters configurations were designed and tested. A second order elliptic filter with a 30Hz cutoff frequency was chose. With this filter was obtained a fast response of the algorithm presented in the Fig. 3. The frequency response of this filter is presented in the Fig. 4.
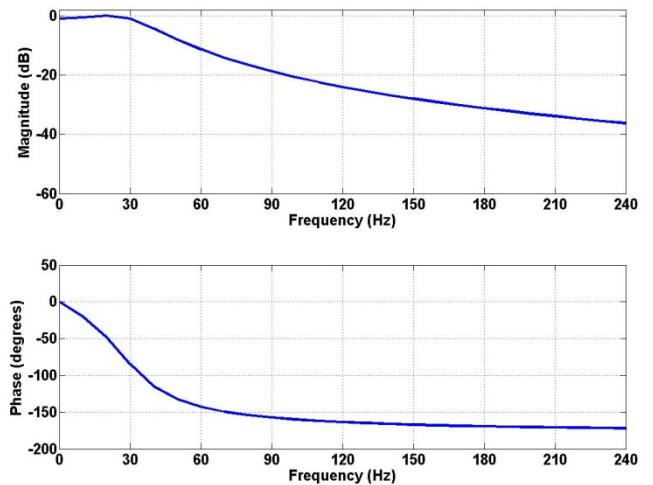

Fig. 4: Frequency response of second order elliptic filter with cutoff frequency of 30Hz.

The amplitude of the load current fundamental component is calculated as demonstrated in (7):

$$A_1 = \sqrt{(2V_d')^2 + \left(2V_q'\right)^2} \tag{7}$$

When any significant changes happen in the load current value, it is detected and the step-size is immediately increased to a certain value (μ_{max}). After 8.45 ms the step-size is decreased to a medium value (μ_{med}). Finally, after 16.7 ms, μ is modified to a minimum or steady-state value (μ_{min}) and stay with this value until next transient in the load current. The values of μ are defined as

$$\mu_{min} < \mu_{med} < \mu_{max} \tag{8}$$

This procedure guaranties a fast transient response to adaptive filter action.

III. SIMULATION RESULTS

The simulation results are shown in Figs. 5, 6, 7 and 8. The transient behavior of the adaptive FIR filter strategy, for a 100% load current variation, is presented in Fig. 5 and Fig. 6. The Fig. 5 shows the signals: the load current $d(n)$ in the first graphic, the fundamental of the load current (in blue) and the adaptive FIR filter output $y(n)$ (in red) in the second graphic and the harmonic current reference $e(n)$ in the third graphic. The Fig. 6 shows the desired harmonic reference and the harmonic reference generated by the adaptive FIR filter in the first graphic and the error between them in the second graphic.
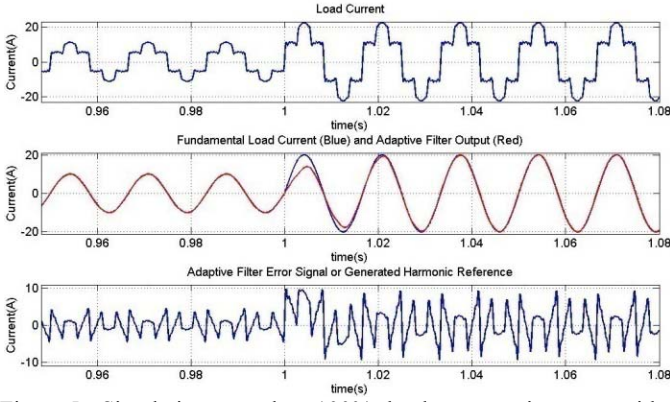

Fig. 5. Simulations results: 100% load current increase with adaptive FIR filter.
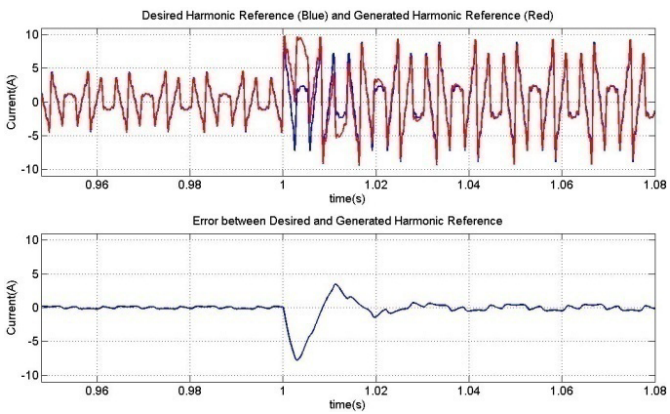

Fig. 6. Error between desired harmonic reference and generated harmonic reference by adaptive FIR filter with load current transient.

The transient behavior of the adaptive notch filter strategy, for a 100% load current variation, is presented in Fig. 7 and Fig. 8. The Fig. 7 shows the signals: the load current $d(n)$ in the first graphic, the fundamental of the load current (in blue) and the adaptive notch filter output $y(n)$ (in red) in the second graphic and the harmonic current reference $e(n)$ in the third graphic. The Fig. 8 shows the desired harmonic reference and the harmonic reference generated by the adaptive notch filter in the first graphic and the error between them in the second graphic.
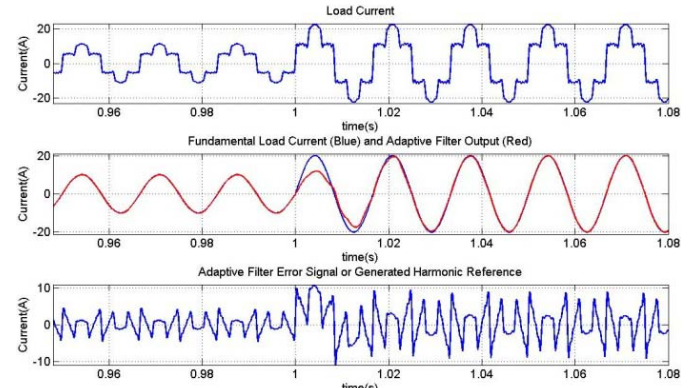

Fig. 7. Simulations results: 100% load current increase with adaptive notch filter.
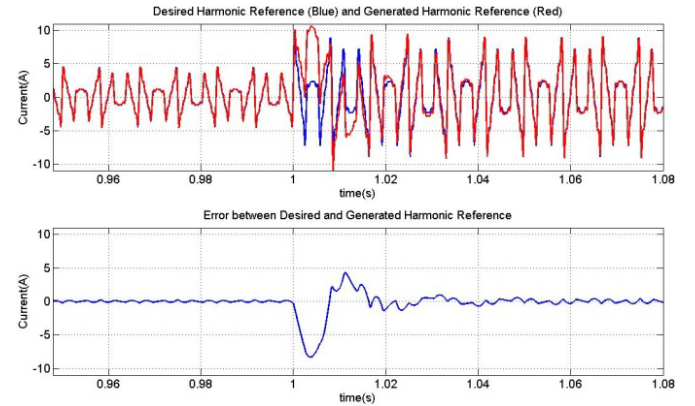
Fig. 8. Error between desired harmonic reference and generated harmonic reference by adaptive notch filter with load current transient.

The simulations demonstrate that there is a slightly difference between the steady-state error for the two strategies. The adaptive FIR filter presents an error a little bit bigger than for adaptive notch filter. The proposed algorithm for the step-size adjusts produces the same speed of convergence in both cases.

IV. EXPERIMENTAL RESULTS

The practical results are obtained from a shunt active power filter (SAPF) composed by three single-phase full H-bridges voltage source inverter (VSI) type, rated 35kVA, working in 40kHz switching frequency. The DC link voltage is adjusted in 500V. The smooth inductor used to connect the SAPF to power system is rated 5mH. The harmonic current injection is controlled by a VSI PWM. The power system voltage is 220V line to line. The load is a rated 100kVA, 6 pulse rectifier, CSI type. The shunt active power filter diagram is shown in the Fig. 9. In these experimental results a feedback configuration of SAPF was used, as illustrated in Fig. 8 three Hall current sensor measure the three phase source current. But the feedforward configuration, with the sensors measuring the three phase load current, can also be

used. The control algorithm was implemented in a Texas DSP TMS320F2812.
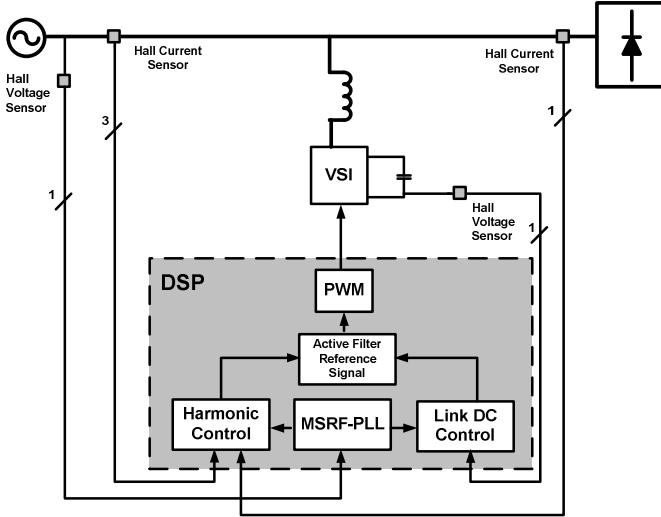
Fig. 9. Shunt Active Power Filter Block Diagram.

The Fig. 10 presents the load current (IL_A) of 27A, the compensation current (Ic_A) and the source current (Is_A) of phase A after compensation using an adaptive FIR filter strategy to extract the harmonic content. In Fig. 11 the harmonic spectrum of source current before and after compensation is shown, the current Total Harmonic Distortion (THDi) of Is_A is reduced from 28.9% to 7.56%.

The Fig. 12 presents IL_A, Ic_A and Is_A after compensation using an adaptive notch filter for a load current of 27A. The Fig. 13 shows the harmonic spectrum of source current, the THDi of Is_A is reduced from 28.9% to 8.29%.
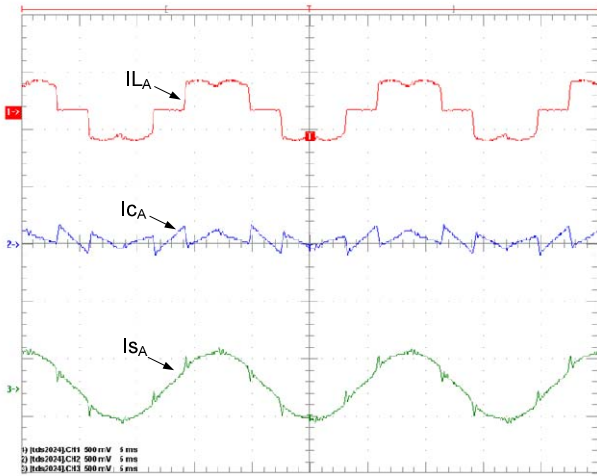

Fig. 10. Experimental results of adaptive FIR filter with a load current of 27A.
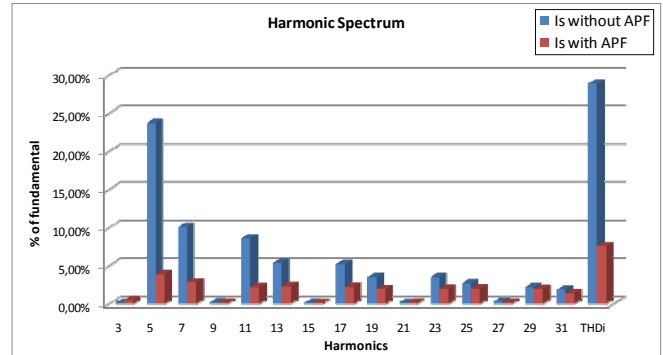
Fig. 11. Source current harmonic spectrum of the adaptive FIR filter.
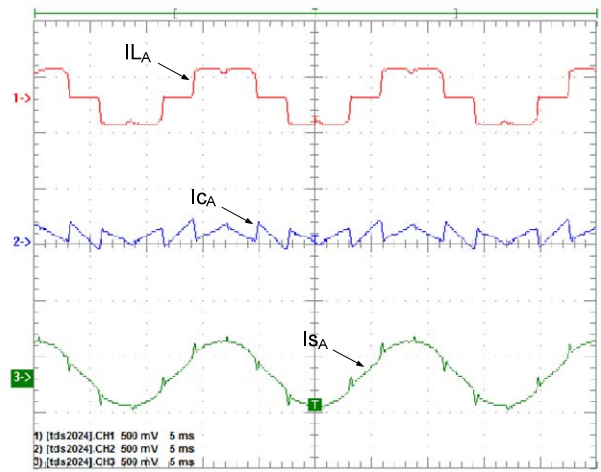
Fig. 12. Experimental results of adaptive notch filter with a load current of 27A.
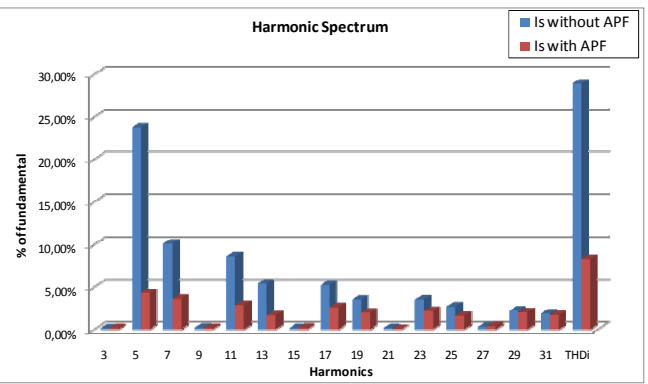
Fig. 13. Source current harmonic spectrum of the adaptive notch filter.

The Fig. 14 shows the adaptive notch filter transient behavior for a 100% load current variation. The result illustrates the convergence time Tc of 1.5 cycles. This result confirms that obtained by simulations.

The reduction of THDi in the two types of adaptive filter implemented has a small difference, the result for a FIR structure is a little better than adaptive notch filter. But the

773

calculation time of the adaptive FIR filter and adaptive notch filter are completely different. The adaptive notch filter has just two coefficients to be adjusted, so its calculation time is significantly smaller than adaptive FIR filter that uses 32 coefficients for the same task.

Fig. 14. Experimental results: 100% load current increase with adaptive notch filter.

V. CONCLUSION

In real time applications, as active power filters, the calculation time, the speed of convergence and steady-state error are critical matters to be taken in consideration during the design process. The proposed step-size adjustments algorithm, for the two types of adaptive filters, demonstrates good results concerning speed of convergence and steady-state error. The implementation with adaptive notch filter demonstrated to be the best choice related to calculation time, because adaptive notch filter has just two coefficients to be adjusted.

The results of the new strategy were faster than the results reported in the literature. The simulations and experimental results showed that the convergence time last 1.5 cycles of the fundamental, against the minimum of 2 cycles reported in the literature.

The adaptive notch filter algorithm has shown to be more interesting in terms of computational burden and steady-state error.

REFERENCES

[1] S. Bhattacharya, D. M.Divan, T. M.Frank, B. Banerje – "Active filter system implementation", IEEE Trans. Ind. Appl. Set/Oct 1998, pp 47-63.

[2] B. Widrow, et al. – "Adaptive noise cancelling: principles and applications", Proceedings of the IEEE, v. 63, n. 12, p. 1692, 1975.

[3] S. Välviita, S. J. Ovaska – "Delayless method to generate current reference for active filters". IEEE Transactions on Industrial Electronics, v. 45, n. 4, 1998.

[4] M. H. Byung, Y. B. Byung, S. J. Ovaska – "Reference signal generator for active power filters using improved adaptive predictive filter". IEEE Transactions on Industrial Electronics, v. 52, n. 2, 2005.

[5] Mu Longhua, Jiangzi – "Application of adaptive filtering in harmonic analysis and detection", Transmission and Distribution Conference and Exhibition: Asia and Pacific, 2005 IEEE/PES, Dalian, 2005.

[6] Y. Qu, W. Tan, Y. Dong, and Y. Yang – "Harmonic detection using fuzzy LMS algorithm for active power filter", IEEE IPEC 2007, Singapore, 2007.

[7] H. Li, Z. Wu, F. Liu – "A Novel Variable Step Size Adaptive Harmonic Detecting Algorithm Applied to Active Power Filter", IEEE ICIT 2006, Mumbai, 2006.

[8] R. H. Kwong, E. W. Johnston – "A variable step-size LMS algorithm", IEEE Trans. Signal Processing, 1992, 40(7), pp. 1633-1642.

[9] C.H. da Silva, V.F.da Silva, L.E.Borges da Silva, G.L.Torres, R.R.Pereira, "DSP implementation of three-phase PLL using modified synchronous reference frame", IEEE IECON07, Taiwan, 2007.

MODIFIED SYNCHRONOUS REFERENCE FRAME STRATEGY FOR SELECTIVE-TUNED SINGLE PHASE HYBRID ACTIVE POWER FILTER

Carlos Henrique da Silva, Rondineli R. Pereira,
Luiz E. Borges da Silva, Germano L. Torres
UNIFEI, Federal University of Itajuba
Itajuba, Brazil
Email: carloschedas@unifei.edu.br, leborges@unifei.edu.br,
germano@unifei.edu.br

João Onofre Pereira Pinto
Federal University of Mato Grosso do Sul - UFMS
Campo Grande, Brazil

Abstract--**This paper shows the behavior of same structure of an hybrid active series power filter (HASPF) tuned in three different frequencies. The developed strategy is based on the Modified Synchronous Reference Frame Controller. The initial structure of the passive filter was chosen to be tuned for the fifth harmonic. The performance of the system is compared with and without the active compensation. The ability of the hybrid topology in changing the resonant frequency is shown. The active hybrid structure is first tuned for the fifth harmonic, further it is electronically re-tuned to the third and finally to the seventh harmonic. Practical results exhibits these tuning changes showing as close as the passive filter can approach the absolutely compensation for a chosen frequency. The algorithm of the HASPF is executed in the DSP TMS320F2812 and the inverter switching frequency is 20 kHz.**

Keywords – **Hybrid active power filter, selective harmonic compensation, modified synchronous reference frame, non-linear loads.**

I. INTRODUCTION

The Hybrid Active Series Power Filters (HASPF) are generally composed by one Active filter (AF) associated in series with a tuned passive filter (PF), [1][2][3]. These active filters have the ability to cancel the harmonic voltage produced due the non-negligible impedance of passive filter (PF), thus providing a low impedance branch for harmonic currents. It is well known that tuned passive filters efficiency is dependent of source equivalent impedance and by its Quality Factor. In this way, the active filter associated with passive one improves the passive filter action, creating an ideal harmonic impedance to load harmonics current. In other words, a severe harmonic short circuit created by the active resistance implementation.

As the quality factor, the tuned factor of the passive filter affects the passive filtering performance, and in consequence the hybrid active filter behavior. To deal with tuned factor deviation, the fine-tuning of the LC shunt circuit can be done by a electronically implementation of a complementary inductance. Therefore, the resonance frequency of the passive filter can be adjusted by controlling this active inductance [3.1].

To achieve the ideal passive filter tuning the control strategy is crucial, in other words, the hybrid filter performance depended on it.

A new control strategy, using the Modified Synchronous Reference Frame (MSRF), is proposed in this work to control the hybrid active series filter. The harmonic frequency tuning improvement is done, at the first moment, for that specific harmonic of the passive filter, the fifth harmonic. After, by an active re-tuning of the passive filter, the filter resonance frequency was adjusted to compensate the third and finally for the seventh harmonic current. The result of this proposed methodology is the absolute filter for any chosen frequency.

The strategy is developed and the practical results are confirmed on a single-phase prototype using the DSP TMS320F2812 as control unit.

II. HYBRID SERIES ACTIVE FILTER PRINCIPLE

The Fig.1 shows an equivalent Hybrid Active Series Filter circuit which combines active filter and passive filter.
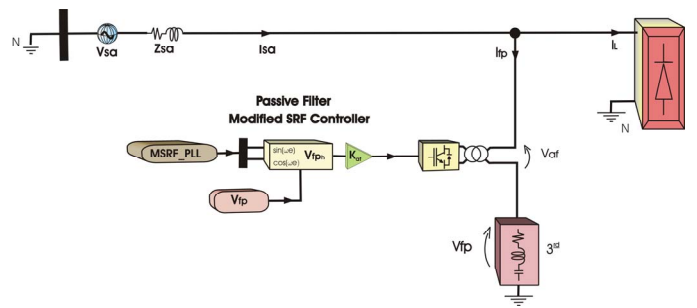

Fig. 1 . Hybrid Active Series Power Filter

The Active filter AF1 is assumed as a controllable voltage source, invisible at the fundamental frequency, but providing the adequate voltage at specific harmonics frequency. The command of instantaneous voltage of active filter AF1, Vaf, is given by

$$V_{af} = -K_{af} \cdot V_{fh} \qquad (1)$$

Here, Kaf is a gain and Vfh is the harmonic voltage across the passive filter. The total equivalent impedance (Zaf) is the passive filter (Zpf) plus the active filter (kaf) connected in series each other, calculated by (2).

$$Z_{af} = (1 - k_{af}) \cdot Z_{pf} \qquad (2)$$

The active filter (AF) has the ability to cancel the harmonic voltage which appears due the non-negligible impedance of passive filter (PF), thus providing a low impedance branch for harmonic currents. Since kaf is unity under an ideal control condition, Vaf is given by

$$V_{af} = V_{sh} \cdot (Z_f / Z_s) + Z_{fh} \cdot I_{lh} \qquad (3)$$

The tuned factor δ defines the magnitude in which the passive filter resonant frequency changes due to the variations in the power system frequency and in the passive filter parameters Lf and Cf . The values of Cf and Lf can change due to aging, temperature, or design tolerances. The tuned factor δ can also be defined in terms of frequency and parameter variation [5.7], such as

$$\delta = \frac{\Delta f}{f_n} + \frac{1}{2} \left(\frac{\Delta L}{L_n} + \frac{\Delta C}{C_n} \right)$$

where Δf is the frequency variation around the nominal value f_n, ΔL is the inductance variation around the nominal value L_n , and ΔC is the capacitance variation around the nominal value C_n .

An important parameter that must be considered in the passive filter design, which has a strong influence in the hybrid scheme compensation, is the quality factor Q. The quality factor of a passive filter is defined by

$$Q = \frac{1}{r_f} \sqrt{\frac{L_f}{C_f}}$$

where rf, Lf, and Cf are the resistor, inductor and capacitor values of the passive filter.

On the other hand, a low value in the quality factor and/or a large value in the tuned factor reduces the passive filter bandwidth and increases the impedance at the resonant frequency. That effect increases the amplitude of the required active filter voltage necessary to keep the same compensation effectiveness, and therefore increasing the active power filter rated power.

Moreover, since the tuned factor and the quality factor modify the filter bandwidth and the passive filter harmonic equivalent impedance, at the resonant frequency, their values must be carefully selected in order to maintain the compensation effectiveness of the hybrid topology.

In case the hybrid active filter be implemented with only one tuned LC shunt passive filter and the resonance frequency of this filter deviates from the desired value, the SAPF can performer the task of electronically re-tune the resonance frequency of the LC shunt circuit. A better hybrid

filter bandwidth can be achieved by modifying the active power filter gain.

The electronic tuning of the LC shunt circuit is done by generating an active inductance La. The resonance frequency of the passive filter can be tuned by controlling this active inductance as follows:

$$f_f = \frac{1}{2\pi \sqrt{C_f \left(L_f + L_a \right)}}$$

In this way, the passive filter can be re-tuned for any desired frequency by choosing the appropriate active inductance.

The active filter gain Kaf, is then re-nominated Active Impedance (extending the Akagi/Fujita concept [3.3]). The Active impedance Kaf is composed by an active resistance $k = -r_f$ and by an active inductance $k = j2\pi f_h L_a$, generating $k_{af} = -r_f \pm j2\pi f_h L_a$.

III. THE SINGLE PHASE HYBRID SERIES ACTIVE FILTER

The system under test is built with a full-bridge single-phase rectifier as load, connected to a 30Ω resistance and 100mH inductance fed by a 127Vrms phase-neutral voltage. The hybrid active filter transformer turn ratio is 1:4 (110/440V), series connected to fifth harmonic passive filter (L5 = 8mH and C5 = 35µF). The inverter switching frequency is 20kHz. The active filter DC link voltage is regulated to 440 Vdc.

The strategy, called Modified Synchronous Reference Frame MSRF, used to extract the harmonic components from the passive filter voltage (Vpf), is an adaptation of the standard three-phase Synchronous Reference Frame (SRF) applied to single-phase systems. All details about this technique is described in [4][5]. The Fig.2 summarizes the technique.
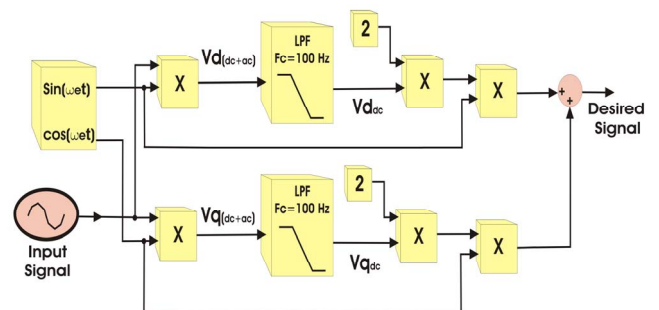

Fig. 2 . MSRF to filter out the fundamental current wave form

The method consists in multiply the measured signal, simultaneously, by the functions sine and cosine in a chosen frequency [7]. This strategy reaches the same effect of transforming a component, in a certain frequency, in a DC

component letting the others as AC quantities. After the resulting signal pass trough a low-pass filter, it is inversely transformed to provide the desired harmonic component. Those modules, transformations and filtrations, can be used to extract a specific harmonic component. So, the outputs for each specific frequency must be added to produce the current harmonic reference to the active filter [4].

The fifth harmonic voltage across the passive filter terminal is obtained using the MSRF. It has to be notice that, the extracted harmonic component corresponds to the characteristic frequency of passive filter.

The Hybrid Active Series Power Filter (HASPF) uses a double PLL arrangement. The first one is synchronized to source voltage (Vs), and the second synchronized to capacitor Cf voltage (Vcf). It is justified due occurrence of phase displacement between Vs and Vpf.

Before the hybrid active power filter starts compensation, the voltage through passive filter terminals is null and the HASPF has to be synchronized to source voltage. Once initiated the charge of HASPF DC link, the voltage through the passive filter (Vpf) tends to be equal the source voltage Vs. In order to avoid active power consumption due phase displacement between Vs and Vpf, the compensation algorithm must be re-synchronized to Vpf, which justify the double PLL. The PLL algorithm, used on this development, called Modified Synchronous Reference Frame PLL (MSRF_PLL), is well explained in [6].

IV. PRACTICAL RESULTS ON HASPF IMPLEMENTATION

The Fig.4 shows the power system signals (voltage and current) before the HASPF starts compensating. The THD of load current is 36.85%. When the fifth harmonic passive filter is connected, the THD drops to 29.5% (depicted in Fig.4).
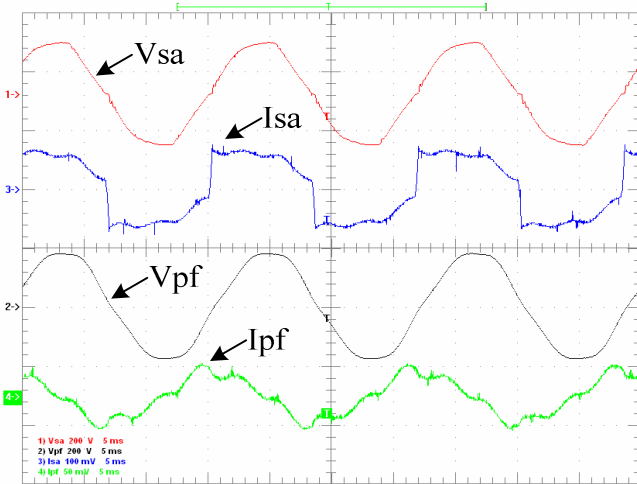

Fig. 4 . Power System waveforms without active compensation

The Fig.5 shows the current source harmonic spectrum (Isa) before the active compensation.
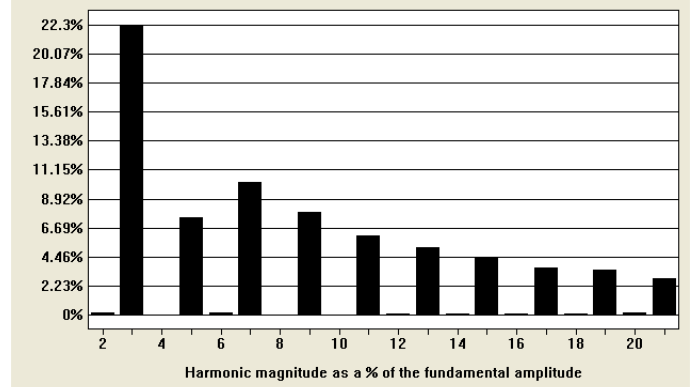

Fig.5 . Source Current Spectrum under fifth harmonic passive filtering

Under passive filtering, the residual harmonic current components related to 300 Hz, 420 Hz and 180 Hz are 7.27%, 10.3% and 22.74% respectively.

The Fig.6 shows the passive filter current spectrum before active compensation. The THD of passive filter current is 23,4%. The passive filter operation reduces the THD of source harmonic current (Isa) in 7.4%.
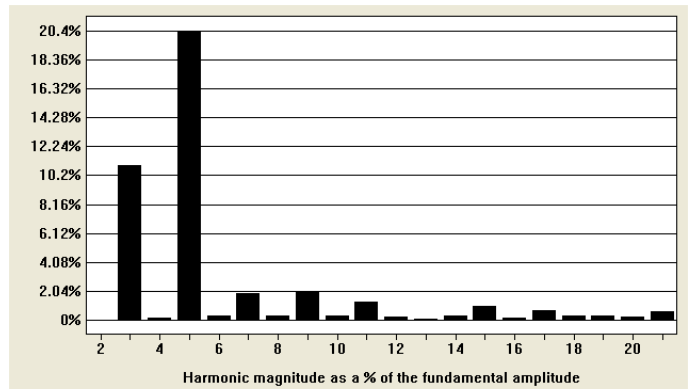

Fig. 6 . 5th Harmonic passive filter current spectrum

The HASPF tries to increase the efficiency of the fifth harmonic passive filter providing, for the 300Hz current signal, a low impedance branch. This is done by acting in the quality factor of passive filter, that is, creating an active resistance $k_{af} = -r_f$.

The Fig.8 shows the system voltages and currents after HASPF turned on.
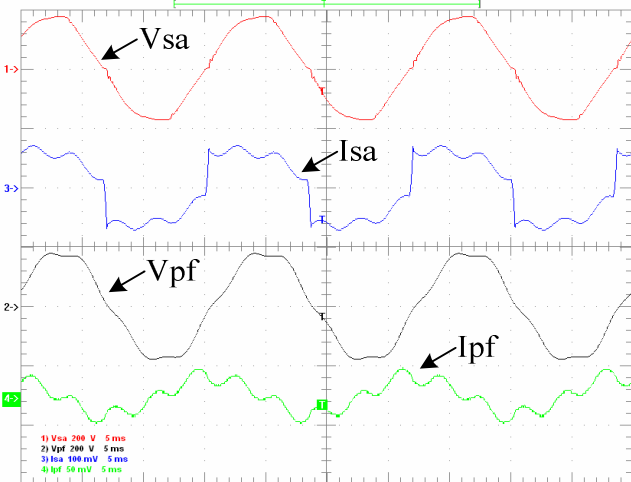
Fig. 8 . Power System waveforms with active compensation

The Fig.9 shows the source current spectrum behavior before and after the active compensation of fifth harmonic. It has be notice the reduction, from 7.27% to 0.46%, of fifth harmonic amplitude after active compensation.


Before Active Compensation   After Active Compensation
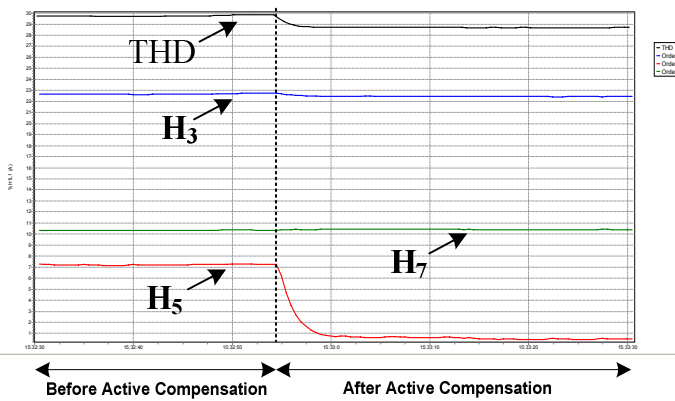
Fig.9 . Source Current Spectrum under fifth active filtering

V. PRACTICAL RESULTS ON HASPF SELECTIVE TUNE IMPLEMENTATION

Added to the quality factor improvement, the resonance frequency of the passive filter, or the tuned factor, can be electronically changed by a complementary active inductance, La.

The Fig.10 shows the system voltages and currents, after re-tuning the passive filter from 300Hz to 420Hz. One has to notice that the current in active filter branch increases and become more distorted. The seventh harmonic source current amplitude is reduced from 10.3% to 0.55% and the fifth harmonic source current returns to its initial value, i.e., the passive filter characteristic.
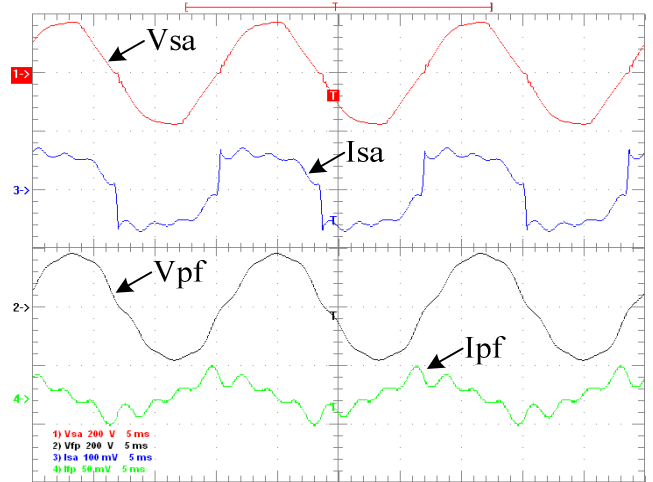

Fig.10 . System Currents during HASPF filtering

The Fig.11 shows the source current spectrum behavior during the tuning factor changing. After the transient, for the seventh harmonic, the hybrid active filter branch goes as close as possible to short-circuit.

300Hz Active Compensation   420Hz Active Compensation
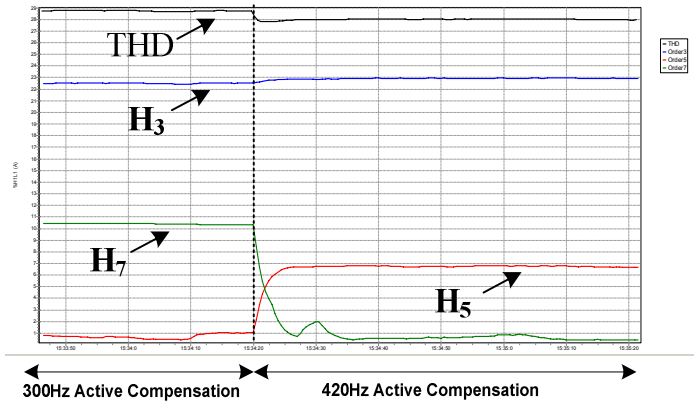
Fig. 11. 7th Active Harmonic current selective Tune.

The system voltage and current, with the hybrid active filter re-tuning to 180Hz, are shown in Fig.12 during the active compensation change.
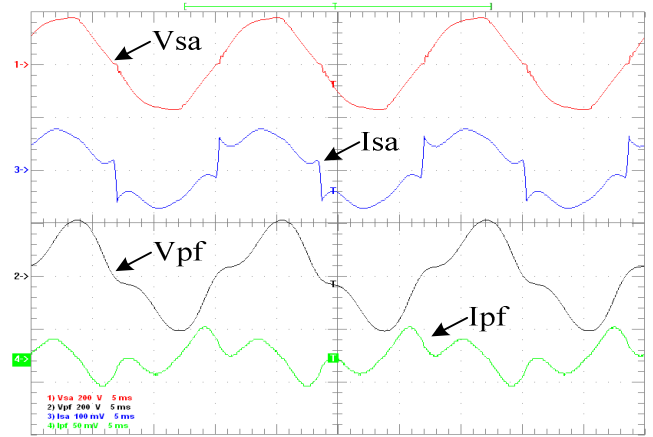

Fig.12 . Voltage and Current under 3rd harmonic active mitigation

The 180Hz source current amplitude drops from 1.2A to 0.1A rms., in other words, the third harmonic current distortion drops from 22.74% to 0.9%. The THD of source harmonic current is reduced to 18.7%.

The Fig.13 shows the source current spectrum behavior before and after the active compensation from 420Hz (seventh harmonic) to 180Hz (third harmonic).
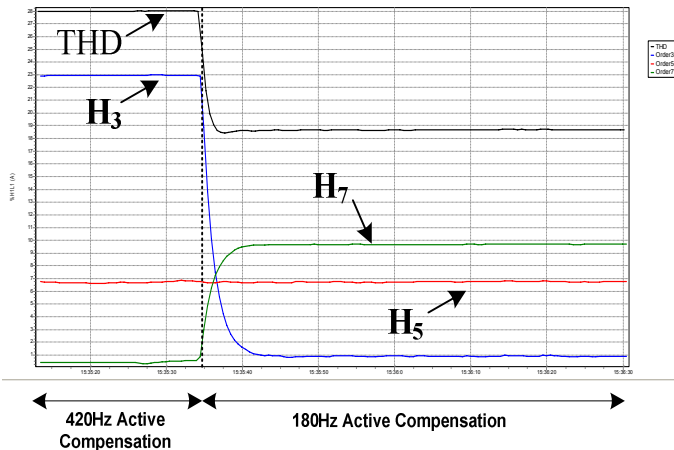

Fig. 13 . Source Current Spectrum - Active Mitigation

The Fig.14 shows the harmonic spectrum of the HASPF current during the 180Hz active compensation.
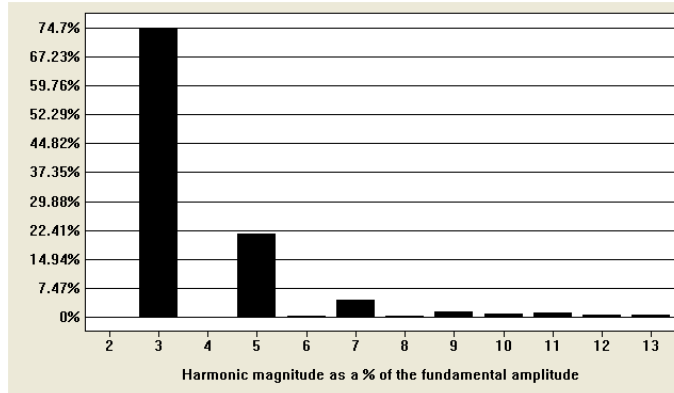

Fig. 14 . Passive Filter Current Spectrum –Active Mitigation

The Fig.15 shows harmonic source current spectrum when the hybrid active filter returns to its initial state, i.e., just improving the fifth harmonic compensation, evidencing the active harmonic selective tuning.

VI. CONCLUSION

The developed technique, applied to the hybrid active series filter, shows the excellent performance to harmonic current compensation issue. Improving the standard principle of passive filter quality factor or, as demonstrated, allowing the selective frequency tune choice, creating the active impedance. The drawbacks inherent to passive filter compensation are eliminated and the compensation characteristics of already installed passive filter can be significantly improved and even changed. The DSP as control unit is essential. The strategy also can be extended to three-phase systems.
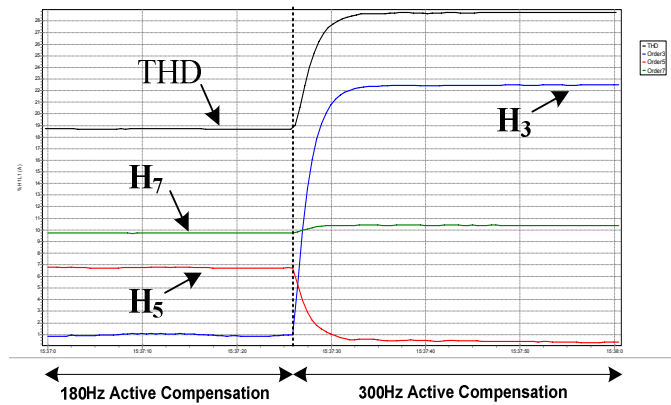

Fig. 15. Source Current Spectrum – Retuning to Initial HASPF Tune of 300Hz

VII. REREFENCE

[1] S.Bhattacharya, D.M.Divan, B.Banerjee, "Synchronous Frame Harmonic Isolator Using Active Series Filter" EPE Conf. Record,1991, Vol 3,pp 30-35.

[2] S.Bhattacharya, D.M.Divan "Synchronous Frame Based Controller Implementation for Hybrid Series Active Filter System" IEEE/IAS Conf. Record,1995, pp 2531-2540.

[3] H. Akagi, H. Fujita, "A New Power Line Conditioner for Harmonic Compensation in Power Systems" IEEE Trans. Power Del. Vol.10, No 3, pp 1570-1575, 1995.

[4] Darwin rivas, Luiz Moran, Juan W. Dixon and José R. Espinoza "Improving Passive Filter Compensation Performance With Active Techniques" IEEE Trans. Industrial Electronics, Vol. 50, N° 1, pp. 161-170, 2003.

[5] J. Turunen, M. Salo and H. Tusa, "Comparison of three series Hybrid Active Power Filter Topologies" Proceedings of 11th IEEE/ICHQP , pp. 324-329, 2004

[6] C. H. Silva, V. F. Silva, L. E. B. Silva, Germano L Torres, E. H.Takauti, "Optimizing the Series Active Filters under Unbalanced Conditions Acting in the Neutral Current " Proceedings of International Conference on Industrial Electronics IEEE/ISIE, 2007.

[7] C. H. Silva, V. F. Silva, L. E. B. Silva, "Synchronous Frame Based Controller Improvement for Active Series Filters under Unbalanced Conditions in Three Phase - Four Wire Systems" Proceedings of 7th International Conference on Industrial Applications IEEE/INDUSCON, 2006.

[8] C.H. da Silva, V.F.da Silva, L.E.Borges da Silva, G.L.Torres, R.R.Pereira, "DSP Implementation of Three-Phase PLL using Modified Synchronous Reference Frame", IEEE IECON07, Taiwan, 2007.

[9] C.H. da Silva, R.R.Pereira, L.E.Borges da Silva, G.L.Torres, Joao Onofre Pereira Pinto and Edson Hideki Takauti "Modified Synchronous Reference Frame Strategy for Single Phase Hybrid Active Power Filter", Proceedings of 13th IEEE /ICHQP, Australia, 2008.

[10] S. Tnani, M. Mazaudier, A.Berthon, S.Diop, "Comparison Between Different Real-Time Harmonic Analysis Methods for Control of Electrical Machines" PEVD94, pp. 4946-4951.

[11] Annabelle van Zyl, Johan H.R. Einslin and René Spée, " A new Unified Approach to Power Quality Management" IEEE Trans. Power Electronics, Vol. 11, N° 5, pp. 691-697, 1996.

DETECTION OF PARTIAL DISCHARGE IN POWER TRANSFORMERS USING ROGOWSKI COIL AND MULTIRESOLUTION ANALYSIS

Giscard F. C. Veloso[1], L.E. Borges da Silva[1], I. Noronha[1], G. Lambert Torres[1], J. Haddad[1]
Rondineli R. Pereira[1], Se Un Ahn[2]
[1]Group of Artificial Intelligence Applications - UNFEI
Av. BPS, 1303 – Pinheirinho – Itajubá MG
{gveloso, leborges, ismael, germano, jamil}@unifei.edu.br   rondinelipereira@yahoo.com.br
[2]CPFL Paulista
Campinas, Brasil

Abstract – **Partial discharge detection in power transformers is discussed using a new approach that exploit the broad band of the Rogowski coils and the potential of two signal processing tools: discrete wavelet transform and empirical mode decomposition. Detecting and analyzing incipient activities of partial discharge can provide useful information to diagnostics and prognostics about transformer insulation. So, partial discharge signals embedded in the electric current at ground conductor are measured using the Rogowski coil. These signals are submitted to noise suppression and the partial discharges waveforms are extracted through different ways: using discrete wavelet transform and using empirical mode decomposition. These two methods are compared and their advantages discussed.**

Keywords – **Discrete Wavelet Transform, Empirical Mode Decomposition, Partial Discharge, Power Transformer, Rogowski coil.**

I. INTRODUCTION

The power transformers are the most expensive equipment in the electric power systems. A replacement due an unexpected fail can cause huge troubles and enormous financial losses. A permanent monitoring in this kind of equipment can detect incipient flaws and avoid its unconstrained evolution that certainly would lead to an abrupt failure. So, a predictive maintenance of these transformers can assure reliability to the electric system and lower costs in its conservation.

A common problem in this context of inconspicuous flaws is the partial discharge. If its activities are not monitored and constrained, the transformer insulation system can be deteriorated until a disruption lead to a catastrophic fail. There are several techniques to detect partial discharges, but the greater part requires the transformer cut out, making them high-cost and impractical. These difficulties lead to a search for methods sufficiently non-invasive and safety to be applied at the equipment in normal operation.

Another problem concerned to partial discharge monitoring is the susceptibility to noise. There are cases where it is impossible to distinguish between noise and signal of partial discharge, what requires the implementation of a signal processing to extract the correct information. Among the possibilities in digital signal processing tools, the Discrete Wavelet Transform and the Empirical Mode Decomposition can be very useful in the solution of problems with partial discharge signal detection. Theirs multiresolution characteristics allows not only the noise reduction, but the detection of transient signals related to partial discharge activities.

In this work, a technique that take advantage of the characteristics of Rogowski coils and the power of the Discrete Wavelet Transform and of the Empirical Mode Decomposition to detect partial discharge pulses shall be described and compared using simulations and a real case.

II. PARTIAL DISCHARGE CHARACTERISTICS IN POWER TRANSFORMERS

Partial discharge is an electric arc that can occurs inside bubbles immersed in liquid insulations [1] [2]. This arc partially completes the circuit between electric conductors or between it and ground through transformer core or tank [1]. It manifests itself in the form of electrical pulses of high frequency [3] that travel through the insulation and transformer structure until the electrical terminals suffering attenuations that substantially distort its original waveform [2]. To this small amplitude pulses are summed the electrical noise. In a substation, there are several noise sources like radio waves, electrostatic discharges, corona, lightning and thermal noise [4]. The data acquisition equipment itself can contribute with random noise because its broadband characteristic to detect high frequency pulses. So, a simple visual analysis of sample signal can not reveal anything related to partial discharge. It is indispensable a more accurate analysis using digital signal processing techniques.

III. PARTIAL DISCHARGE DETECTION USING ROGOWSKI COIL

Taking into account the transformer grounding attachment as a way through which partial discharge pulses flow to the earth, its detection can be made measuring the electric current in this place. This task must be accomplished using a sensor capable to detect high frequencies electric current and provide a strong insulation. The device suitable to perform such a measurement is the Rogowski coil.

The Rogowski coil (fig. 1) is a circular plastic mold with a winding mounted in order to have a uniformly distributed density of turns [5]. The crosswise sections must have uniform areas. It is used mounting the coil around the conductor where the alternating current must be measured. A voltage signal proportional to the variations in time (t) of the electrical current I appears at the terminals of the winding

according to the eq. (1), where H is related to the coil sensitivity. Therefore, integrating this voltage signal, the electric current signal can be obtained.

$$E = H \frac{dI}{dt} \quad (1)$$
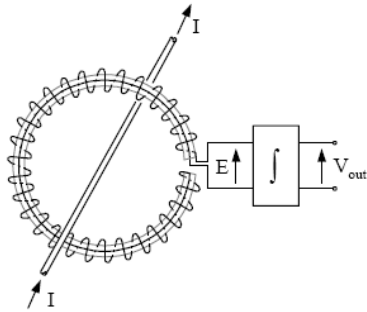
Fig. 1: Rogowski coil schematic [5].

The Rogowski coil exhibit a great sensitivity in high frequencies and your structure provide good electrical insulation. It is also capable to measure high levels of electric currents, varying since some hundreds of miliamperes to hundreds of thousands of amperes.

The electrical current in the ground terminal of the transformer can be monitored using a Rogowski coil mounted in that place. The using of appropriate signal processing techniques allows the extraction of partial discharge pulses eventually flowing through this path.

IV. SIGNAL PROCESSING

A. Overview

Taking into account the characteristics of the partial discharge pulses, a suitable signal processing strategy must be defined (fig. 2). There are two mathematical tools used in this strategy with the same capabilities, but different in precision and computational efficiency. The Discrete Wavelet Transform has an efficient algorithm, simple and fast, but its precision in frequency resolution is restricted. The Empirical Mode Decomposition can be adjusted to be very precise in time and frequency resolution, however its implementation in a computer is hard, slow and exhibit some difficult to configure. In that strategy, both was used to perform the same tasks and their results are compared.
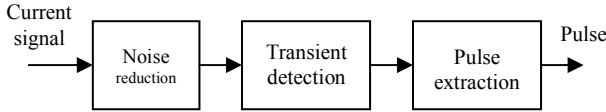

Fig. 2: Signal processing strategy used in this work.

B. Discrete Wavelet Transform and Multiresolution

Multi-resolution relates to the capacity to visualize a signal in different resolutions, i.e., to analyze a signal at different detail levels and determine what is relevant at each level. The decomposition of a signal to different resolutions can be accomplished with the Discrete Wavelet Transform. The importance of seeing the signal at different detail levels relies on the fact that the characteristics of a signal can be distributed into such levels. By separating the levels, the characteristics of the wave at each level are also separated.

Discrete wavelet transform is a type of signal expansion [6]. In this case, the expanding set is made up of wavelet and scaling functions. The expression is written as

$$f(t) = \sum_{k=-\infty}^{\infty} c_{j_0,k} \cdot \varphi_{j_0,k}(t) + \sum_{j=j_0}^{\infty} \sum_{k=-\infty}^{\infty} d_{j,k} \cdot \psi_{j,k}(t) \quad (2)$$

Where:

$c_{j0,k}$ - Coefficients related to the scaling functions called approximation coefficients.
$d_{j,k}$ - Coefficients related to the wavelet functions called detail coefficients.
$\varphi_{j0,k}$ - The scaling functions' expanding set.
$\psi_{j,k}$ - The wavelet functions' expanding set.
j - The scale index.
k - The time index.

The coefficients in the Discrete Wavelet Transform are referenced using two variables covering the frequency and time content of the signals. These coefficients are organized into levels defined by the variable j and are related to the concept of scale. Scale is a parameter related to the frequency and can be thought of as the inverse of the frequency. The time information is represented by variation in k. Thus, the Discrete Wavelet Transform is the process to calculate the coefficients $c_{j0,k}$ e $d_{j,k}$.

When the signal is decomposed with the Discrete Wavelet Transform, it is broken into levels related to a particular frequency band (fig. 3). The number of levels is a parameter during this process. Therefore, the Discrete Wavelet Transform of a signal results in several levels of detail coefficients and one level of approximation coefficients that retain the lower frequency content. The frequency information is preserved at the levels of decomposition and the time information is preserved through the variation of the coefficients. In this work, the information separated in the decomposition with the Discrete Wavelet Transform is used to noise reduction and to pulse extraction.
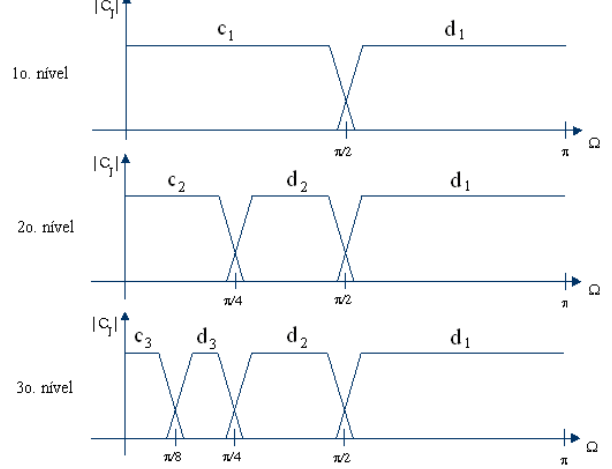

Fig. 3: Decomposition with Discrete Wavelet Transform visualized in the frequency domain.

C. Empirical Mode Decomposition

The Empirical Mode Decomposition (EMD) reduces a signal in components from which is possible to calculate valid instantaneous frequencies through the Hilbert Transform. These components are called Intrinsic Mode Functions (IMF) and they are narrow band signals which means: (i) its DC level must be zero, and (ii) it must has local symmetry related to its mean value.

The EMD is not an analytical decomposition and, therefore, it is not defined through mathematical equations. Indeed, the EMD is defined by an algorithm with adaptive characteristics [7] [8]. The IMFs produced by the EMD can be visualized as a multiresolution analysis because their spectral content has frequencies gradually smaller, starting from the highest frequencies until reach the lowest spectral component. The EMD is therefore an alternative for Discrete Wavelet Transform.

The EMD algorithm is based on a recursive structure called sifting. The careful application of the sifting produces physically plausible IMFs. The algorithm can be synthesized as following. Given a signal x(t):

1. Let $r(t) = d_1(t) = x(t)$;
2. Identify the extrema (local maxima and local minima) of $d_1(t)$;
3. Calculate the superior envelope (using local maxima) and the inferior envelope (using local minima). These envelopes can be obtained through polynomials or cubic splines;
4. Calculate the mean signal $m(t)$ for the envelopes;
5. Subtract the mean $m(t)$ from $d_1(t)$ to obtain the first candidate to IMF $d_1(t)$: $d_1(t) = d_1(t) - m(t)$;
6. Verify if $d_1(t)$ is an IMF; if not, restart the algorithm from the step 2;
7. If $d_1(t)$ is an IMF, verify if the number of IMFs already extracted meets a stop criteria; if not, let $d_2(t) = r(t) - d_1(t)$ followed by $r(t) = d_2(t)$; restart the algorithm from the step 2 replacing $d_1(t)$ by $d_2(t)$; the signal $r(t)$ is called residue;
8. If the stop criteria is satisfied for n IMFs, let $r(t) = r(t) - d_n(t)$; this final residue is not necessarily an IMF.

The criterion for a signal being an IMF is related to the possibility to calculate plausible instantaneous frequency from it, which is extensively discussed in [7]. Essentially, there are two conditions for a signal being an IMF: (i) the number of zero crossings and the number of extrema must be equal or differ at most by one; (ii) it must have a symmetry related to the local mean, i.e., the mean value defined by the envelopes must be zero, which is difficult to achieve. The second condition can be a source of convergence problems for the algorithm, allowing some numerical variations to accomplish it. There are good suggestions in [7] and in [8] to numerically satisfy the idea contained in condition (ii).

The stop criterion for the EMD algorithm is based on the objective to extract all the oscillatory modes from the residue. Thus, the final residue must be a monotonic signal or it contains so reduced samples that can be considered negligible. Therefore, the decomposition results can be synthesized in the eq. (3), which shows that is possible to reconstruct the original signal from the IMFs and the final residue.

$$x(t) = \sum_{i=1}^{n} d_i + r \tag{3}$$

Where:
$x(t)$ - Original signal.
d_i - IMFs.
r - Final residue.

D. Noise Reduction

The partitioning of features in frequency bands can be useful to reduce the signal noise [9][10][11]. The Inverse Discrete Wavelet Transform can reconstruct the original signal by summing the components. However, those components can be modified before the reconstruction, allowing the noise reduction. If some decomposition levels are strong related to noise, they can be modified or simply discarded and the reconstruction with the Inverse Discrete Wavelet Transform will result in a signal without the noisy components. This concept is formally demonstrated in [12].

The process of noise reduction consists in decompose the signal with the Discrete Wavelet Transform and inspect the levels of decomposition. For each level, a value of threshold can be defined in a way that every sample below this value will be replaced by zero. Such a threshold can be calculated using eq. (4) [12].

$$t = \sigma \cdot \sqrt{2 \cdot \log_{10}(N)} \tag{4}$$

Where:
σ - Standard deviation of the component samples.
N - Number of samples.

After modify each level of decomposition, the reconstruction using the Inverse Discrete Wavelet Transform can be made to produce a signal with reduced noise.

E. Transient Detection and Pulse Extraction

Applying a multiresolution analysis like EMD or Discrete Wavelet Transform in a signal with high frequency transients, it will be decomposed in several levels detaching the stationary component (low frequency) from the transient component (high frequency), like partial discharge pulses. To extract the transient, the reconstruction of the signal must be made using only the components related to the pulses, discarding the others.

Therefore, the method for extract partial discharge signals is realized applying a multiresolution analysis on the current signal captured at the grounding terminal of the power transformer. First, a noise reduction using Discrete Wavelet Transform is made. Then, the pulses are extracted reconstructing the signal using only the components related to them. This procedure allows the analysis of the pulses, its duration and distribution in a cycle of the main frequency.

V. EXPERIMENTS AND RESULTS

The method was tested at TERMOPE in 223MVA power transformers. Several signals were captured, but only one example is showed in this work (fig. 4). At a glance, there are not significant pulses or noise content in that signal.
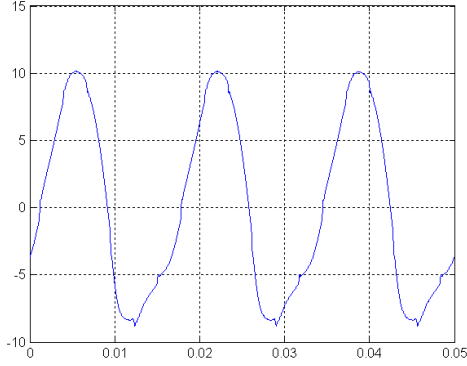

Fig. 4: Current signal at a 223MVA power transformer grounding terminal.

The noise reduction process using the Discrete Wavelet Transform is illustrated in the figure 5. It is possible to visualize the noise content and the pulses properly separated.
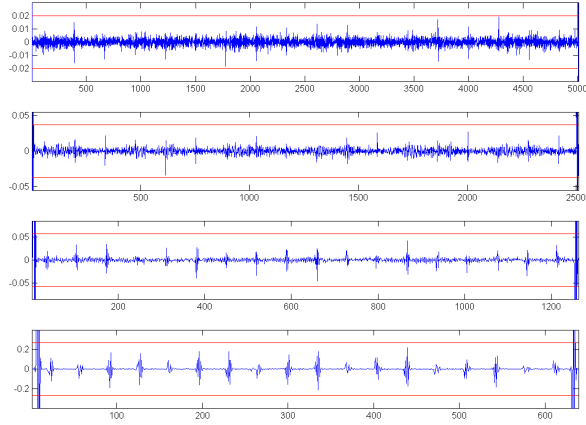
Fig. 5: Noise reduction in the current signal.

The pulse extraction resulted in signals like those showed in figures 6 and 7.
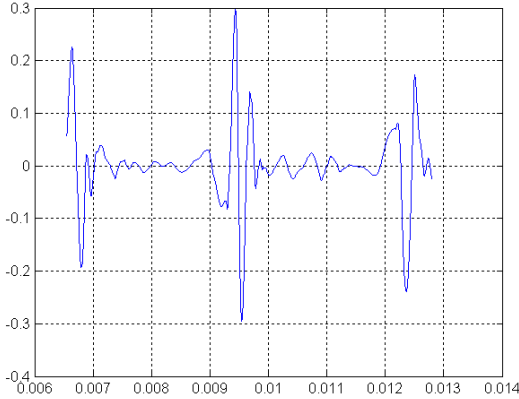
Fig. 6: Fist pulses found in current signal.
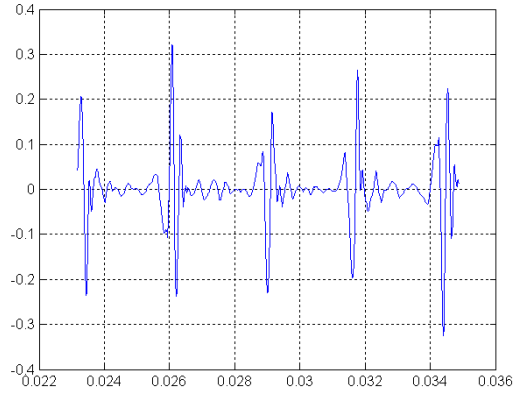
Fig. 7: A sequence of pulses extracted from the current signal.

Applying the EMD to the signal without noise result in the decomposition showed in figure 8.
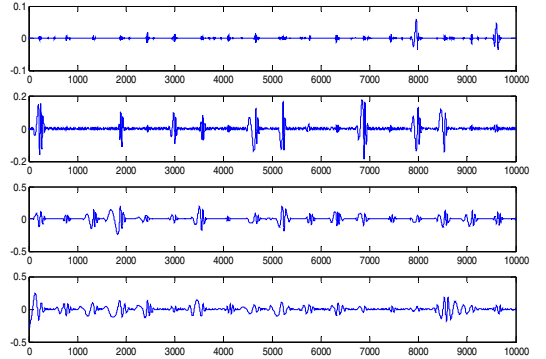
Fig. 8: EMD applied to the signal without noise.

Using the first two IMFs to extract the pulses results in signals like that showed in figure 9 and 10.

VI. CONCLUSIONS

The technique to detect partial discharge using Rogowski coil and multiresolution analysis is effective in the extract of small amplitude pulses in the presence of noise. Some tests will be made to confirm the partial discharge activity with the pulses showed in this work, but that is a promising method. It can be applied with the transformer in normal operation, avoid interruption and being not invasible.

The differences in the results presented by the EMD and the Discrete Wavelet Transform are in the waveforms of the pulses extracted. The pulses extracted with Discrete Wavelet Transform seem to be artificial. Indeed, this transformation depends of the choice of a wavelet which will induce a waveform. Therefore, the Discrete Wavelet Transform will produce different results according to each wavelet used. This problem does not appear if EMD is used because its adaptive characteristic. However, the algorithm configuration is difficult and incorrect parameters can produce misleading results.
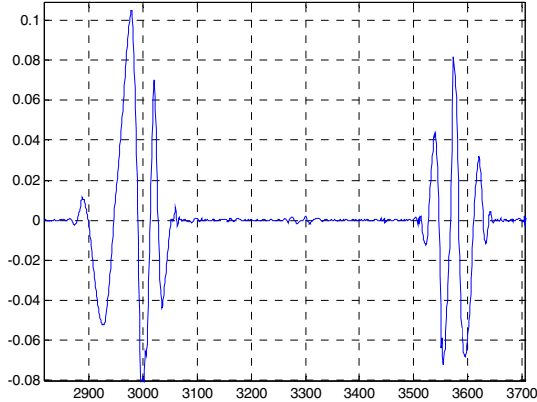
Fig. 9: Some pulses extracted with EMD.
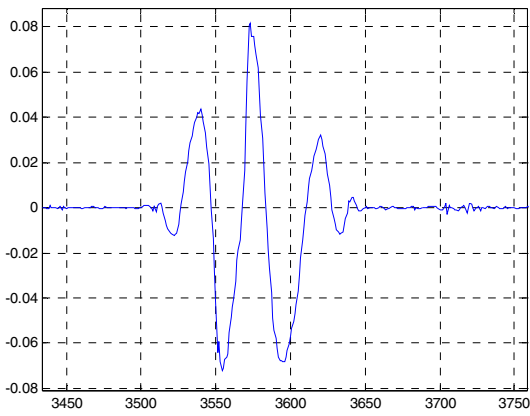
Fig. 10: Pulse extracted with EMD.

ACKNOWLEDGEMENT

REFERENCES

[1] G.J. Paoletti, A. Golubev, "Partial discharge theory and technologies related to medium-voltage electrical equipment", IEEE Transactions on Industry Applications, vol. 37, no. 1, pp. 90-103, January/February 2001.

[2] S.A. Boggs, "Partial discharge: overview and signal generation", IEEE Electrical Insulation Magazine, vol. 6, no. 4, pp. 33-39, July/August 1990.

[3] R. Bartnikas, "Partial discharges: their mechanism, detection and measurement", IEEE Transactions on Dielectrics and Electrical Insulation, vol. 9, no. 5, pp. 763-808, October 2002.

[4] I. Shim, J.J. Soraghan, W. H. Siew, "Digital signal processing applied to the detection of partial discharge: an overview", IEEE Electrical Insulation Magazine, vol. 16, pp. 06-12, May/June 2000.

[5] W. F. Ray, C. R. Hewson, "High performance rogowski current transducers", in *Conference Record of the 2000 IEEE Industry Applications Conference*, Rome, Italy, October 2000.

[6] C.S. Burrus, R. A. Gopinath, H. Guo, Introduction to wavelets and wavelet transforms. New Jersey: Prentice Hall, 1998.

[7] N.E. Huang, Z. Shen, S.R. Long, M.L. Wu, H.H. Shih, Q. Zheng, N.C. Yen, C.C. Tung, H.H. Liu, "The empirical mode decomposition and Hilbert spectrum for nonlinear and nonstationary time series analysis," *Proc. Roy. Soc. London A*, vol. 454, pp. 903–995, 1998.

[8] G. Rilling, P. Flandrin, and P. Gonçalves, "On empirical mode decomposition and its algorithms," in *Proceedings of 6th IEEE-EURASIP Workshop on Nonlinear Signal and Image Processing* (NSIP '03), Grado, Italy, June 2003.

[9] H. Borsi, "A pd measuring and evaluation system based on digital signal processing", IEEE Transactions on Dielectrics and Electrical Insulation, vol. 7, no. 1, pp. 21-29, February 2000.

[10] X. Ma, C. Zhou, I.J. Kemp, "Automated wavelet selection and thresholding for partial discharge detection", IEEE Electrical Insulation Magazine, vol. 18, no. 2, April 2002.

[11] I. Shim, J.J. Soraghan, W. H. Siew, "Detection on pd utilizing digital signal processing methods part 3: open-loop noise reduction", IEEE Electrical Insulation Magazine, vol. 17, no. 1, pp. 06-13, January/February 2001.

[12] D.L. Donoho, "De-noising by soft-thresholding", IEEE Transactions on Information Theory, vol. 41, no. 3, pp. 613-627, May 1995.